Reduced Order Modeling and Substructuring

Applications in Nonlinear Structural Dynamics

Andersson, Linus

2024

Document Version:
Publisher's PDF, also known as Version of record

LUND UNIVERSITY

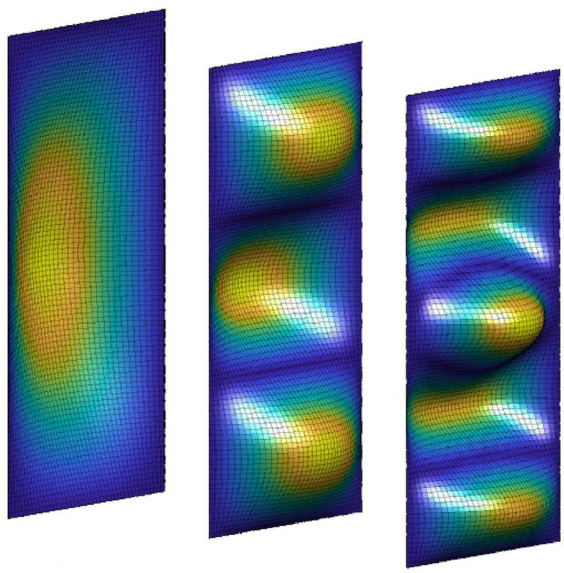

REDUCED ORDER MODELING AND SUBSTRUCTURING

Applications in Nonlinear Structural Dynamics

LINUS ANDERSSON

Structural Mechanics

Doctoral Thesis

DEPARTMENT OF CONSTRUCTION SCIENCES
DIVISION OF STRUCTURAL MECHANICS

ISRN LUTVDG/TVSM--24/1034--SE (1-242) | ISSN 0281-6679
ISBN 978-91-7895-996-9 (print) | ISBN 978-91-7895-997-6 (electronic)
DOCTORAL THESIS

REDUCED ORDER MODELING AND SUBSTRUCTURING

Applications in Nonlinear Structural Dynamics

LINUS ANDERSSON

Printed by V-husets tryckeri LTH, Lund, Sweden, March 2024 *(PI)*.

For information, address:
Division of Structural Mechanics,
Faculty of Engineering LTH, Lund University, Box 118, SE-221 00 Lund, Sweden.
Homepage: www.byggmek.lth.se

Acknowledgements

The work presented in this dissertation was carried out at the Division of Structural Mechanics at the Faculty of Engineering LTH, Lund University.

I would like to express my sincere gratitude towards my main supervisor Prof. Kent Persson and co-supervisors Dr. Peter Persson and Prof. Per-Erik Austrell for their guidance, support and encouragement. Thanks also to Dr. Marcin Kozłowski from Silesian University of Technology for his helpful advice and assistance regarding the experimental studies of soft-body impact tests. Bo Zadig is gratefully acknowledged for his excellent work on many of the illustrations. I would also like to thank the rest of the staff at the Division of Structural Mechanics for providing an inspiring workplace.

I would furthermore like to thank my good friend Jens Malmborg for good company while sharing the office room as well as moral support, valuable advice and encouraging discussions.

Finally, I thank my fiancée Frida and our wonderful children Hugo, Oskar and Vera for bringing lots of joy to my life and reminding me of what is truly important.

March 2024
Linus Andersson

Abstract

A structural design process typically involves various load cases for which a sufficient load-bearing capacity must be demonstrated. In addition to static load cases, a verification of dynamic loads, such as blast and impact loading, may be required. To this end, the response can be estimated using computational models representing an idealized structure, often formulated using the finite element method. In contrast to static analyses, a dynamic response analysis generally requires some form of time (or frequency) discretization. Furthermore, to properly capture the structural behavior, it can be necessary to consider nonlinear effects, e.g., due to contact conditions, nonlinear material behaviors, or geometrically nonlinear effects. The repeated solution in time of large nonlinear finite element models can be computationally expensive and time-consuming. Consequently, there is a need for computationally efficient modeling approaches, allowing for an interactive design process where alternative designs may be tested in a time-efficient manner.

By generating a reduced order model, the aim is to reduce the system size while maintaining sufficient accuracy of important output quantities. Hence, the computational cost can be reduced by analyzing a smaller, approximate system. For continuous structural dynamics problems discretized using the finite element method, reduced order models can be obtained by introducing a reduction basis. More specifically, the response is approximated using a set of time-independent displacement fields, referred to as mode shapes, which constitute the basis vectors of the modal basis. This approach is well-established and frequently used within linear structural dynamics. In the context of nonlinear structural dynamics, modal methods for reduced order modeling have gained more prominence during the last decades and is still an active area of research.

In the dissertation, strategies for nonlinear reduced order modeling are developed on the basis of structural engineering applications within two different areas; namely, concerning concrete structures subjected to blast loading and glass structures subjected to impact loading. Some of the challenges with regard to structural dynamics modeling are similar. In particular, brittle failure modes are often critical, why the response of higher order modes can be of particular importance. Moreover, an accurate representation of the structural behavior typically necessitates models considering nonlinear behaviors. More specifically, the dynamic problems involve localized nonlinearities in the form of contact conditions and joints, as well as geometric nonlinearity which, in contrast, is a distributed nonlinearity where degrees of freedoms throughout the structure are nonlinearly coupled.

Impact loading is a fundamental load case in design of glazed barriers, such as full-height facades and balustrades, which often governs the design. In this work, modeling strategies were developed for predicting the pre-failure elastic response of flat glass panels subjected to a standardized impactor, which represent a human body falling towards the glass panel. The

response of glass panels, having a small thickness compared to the span width, are typically characterized by bending-stretching coupling effects. To consider these effects, which result in a geometrically nonlinear behavior, reduction bases were generated using bending modes and the associated static modal derivatives, corresponding to the second order terms in a Taylor's expansion of the quasi-static displacement field. Moreover, approximate techniques for modeling contact were proposed, and a nonlinear viscous single-degree-of-freedom model was developed for reduced modeling of the impacting body. The response was evaluated based on experimental data and detailed finite element models. For the studied load cases, the proposed model was shown to predict important output quantities, such as the glass principal stresses, with high accuracy.

Furthermore, computationally efficient analysis techniques were developed for analysis of concrete structures subjected to blast loading. Specifically, reduced models including pre-defined plastic joints were developed by means of dynamic substructuring. A comparison to commonly used modeling strategies, which uses equivalent single-degree-of-freedom systems, suggests that the developed models provide a significantly improved accuracy of shear forces. This can be critical in a verification of brittle failure modes, such as diagonal and direct shear failure.

Finally, a review of various reduced order modeling techniques is presented which, in a broader perspective, provide a basis for developing reduced order models in various structural dynamics applications.

Sammanfattning

Vid utformning och dimensionering av såväl anläggningskonstruktioner som enskilda byggnadsdelar måste vanligtvis ett flertal olika belastningssituationer analyseras. Utöver statiska lastfall kan det vara nödvändigt att beakta dynamiska laster, såsom explosions- eller stötlast. För att påvisa tillräcklig bärförmåga används i allmänhet datorbaserade beräkningsmodeller, ofta framtagna med finita elementmetoden. Vid beräkning av dynamisk respons krävs då, till skillnad från statisk analys, en uppdelning av beräkningarna i antingen tids- eller frekvenssteg, vilket medför upprepade beräkningar. Vidare kan det vara väsentligt att beakta olinjära effekter för att säkerställa en beräkningsmodell som representerar ett korrekt strukturbeteende och ger resultat med tillräcklig noggrannhet. Sådana effekter kan exempelvis uppstå till följd av interaktion mellan strukturdelar, olinjärt materialbeteende eller geometrisk olinjäritet. Sammantaget medför detta ofta beräkningsmässigt kostsamma och tidskrävande analyser. För att möjliggöra en tidseffektiv designprocess, där olika utformningsalternativ och dimensioner kan utvärderas, finns således behov av beräkningseffektiva modellerings- och analystekniker. I detta avseende utgör också balansen mellan prestanda och noggrannhet en central aspekt.

Genom att upprätta en reducerad beräkningsmodell är målet att minska antalet systemvariabler samtidigt som viktiga utdataparameterar kan predikteras med tillräcklig noggrannhet. Reducerade beräkningsmodeller kan exempelvis genereras utifrån finita elementmodeller. Mer specifikt kan responsen approximeras som en summa av ett antal tidsoberoende utböjningsformer, så kallade modformer. På detta sätt kan de fysiska frihetsgrader som vanligtvis används vid formulering av finita elementmodeller ersättas med ett reducerat antal generella frihetsgrader som representerar modala amplituder. Denna metodik används regelbundet och är väletablerad inom linjär strukturdynamik. Under de senaste decennierna har liknande metoder även föreslagits för reducerad modellering av olinjära strukturdynamiska problem. Detta utgör däremot fortfarande ett aktivt forskningsområde.

Utifrån samma principer som vid reducering av linjära system kan geometriskt olinjära modeller reduceras genom att responsen uttrycks i modala amplituder. Till skillnad från linjärdynamiska tillämpningar, där relevanta modformer ofta har låga egenfrekvenser, kan det vara väsentligt att beakta högfrekventa moder, som typiskt har egenfrekvenser avsevärt högre än lastens frekvensinnehåll. Ett systematiskt val av modformer utgör därför en av svårigheterna vid reducerad modellering av geometriskt olinjära strukturer. De modala responserna blir även olinjärt kopplade. För att möjliggöra en tidseffektiv dynamisk analys finns därför behov av tekniker för effektiv tidsintegrering.

Beräkningsmodeller som inkluderar lokalt begränsade olinjäriteter kan reduceras genom dynamisk substrukturering. Med detta angreppsätt kan exempelvis substrukturer som förblir linjärelastiska modelleras effektivt utifrån modformer, medan förfinande modeller kan användas för

delar med olinjär respons. För att möjliggöra beräkningseffektiva modeller krävs dock tekniker för att begränsa antalet frihetsgrader i gränssnitt mellan olika substrukturer.

I avhandlingen undersöks strategier för reducerad modellering av olinjära strukturdynamiska problem, med fokus på tillämpningar gällande betongkonstruktioner belastade av explosionslast samt glasstrukturer belastade av stötlast. I båda dessa tillämpningar är spröda brott ofta kritiska, varför det blir speciellt viktigt att etablera beräkningsmodeller med god noggrannhet. Vidare är det, för att säkerställa ett korrekt strukturbeteende, väsentligt att ta hänsyn till olinjära effekter.

Vid dimensionering av glasbarriärer, såsom glasfasader och glasräcken, utgör stötlast ofta ett kritiskt lastfall. I detta arbete har modelleringsstrategier tagits fram för beräkning av elastisk respons för plana glaspaneler belastade av standardiserade stötlaster, vilka representerar en människa som faller mot glaset. Eftersom glasets tjocklek vanligtvis är liten i förhållande till spännvidd påverkas strukturresponsen i hög grad av andra ordningens effekter. För att hantera dessa effekter formulerades geometriskt olinjära reducerade modeller. Mer specifikt approximerades responsen utifrån böjmoder och en uppsättning tillhörande membranmoder. Vidare utvecklades en olinjär en-frihetsgradsmodell för impaktorn samt tekniker för effektiv modellering av interaktion mellan impaktor och glaspanel. Beräknad respons utvärderades utifrån experimentella data och detaljerade finita elementmodeller. Framtagen reducerad modell visades prediktera viktiga resultat, såsom största huvudspänningar i glaspanel, med god noggrannhet.

Modelleringsstrategier har även utvecklats för analys av betongkonstruktioner belastade av explosionslast. Mer specifikt användes dynamisk substrukturering för att formulera reducerade modeller med flytleder i fördefinierade positioner. Föreslagen modelleringsmetod möjliggör effektiva beräkningar med god precision, vilket kan vara särskilt viktigt vid dimensionering med hänsyn till spröda brott.

Slutligen presenteras en översikt av olika tekniker för reducerad modellering, vilket i ett bredare perspektiv utgör en grund för vidare utveckling av beräkningseffektiva modeller inom olika strukturdynamiska tillämpningar.

Contents

Paper C
Reduced order modeling of soft-body impact on glass panels.
L. Andersson, M. Kozłowski, P. Persson, P.-E. Austrell, K. Persson
Engineering Structures, Volume 256, 1 April 2022, 113988.

Paper D
Efficient nonlinear reduced order modeling for dynamic analysis of flat structures.
Linus Andersson, Peter Persson, Kent Persson
Mechanical Systems and Signal Processing, Volume 191, 15 May 2023, 110143.

Paper E
Nonlinear reduced order modeling of glass panels subjected to soft-body impact.
Linus Andersson, Peter Persson, Kent Persson
Submitted for publication.

Part I

Introduction and Overview

1 Introduction

1.1 BACKGROUND

A structural design process typically involves various load cases for which a sufficient load-bearing capacity must be demonstrated. To this end, the response may be estimated using a computational model representing an idealized structure. Developing a suitable analytical model by means of modeling abstractions is, therefore, an important step in a structural design process; the model should capture the structural behavior and provide a sufficiently accurate prediction of important output quantities. Furthermore, in many engineering applications, a space discretization of the continuous analytical model is typically required, e.g., using the finite element (FE) method [1].

In addition to static load cases, a verification of dynamic loads may be required. In contrast to static analyses, a dynamic response analysis generally involves some form of time (or frequency) discretization. Furthermore, to properly capture the structural behavior, it can be necessary to consider nonlinear effects, e.g., due to contact conditions, nonlinear material behaviors, or geometrically nonlinear effects. However, the repeated solution in time of nonlinear FE models can be computationally expensive and time-consuming. Consequently, there is a need for computationally efficient modeling approaches, allowing for an interactive design process where design parameters can be evaluated in a time-efficient manner.

A detailed high-fidelity analysis, aiming to mimic the response of the real structure, may be useful for analyzing complex structures, and can provide further insight into the structural behavior. On the other hand, a simplified, approximate model can be beneficial for analyzing the governing structural behavior or evaluating assumed failure modes. Particularly in the conceptual design phase, a time-efficient and straightforward modeling approach can be of great utility. Furthermore, an approach using a so-called reduced order model may be considered, which is generated based on a detailed numerical model, e.g., formulated using the FE method. The aim is to reduce the system size while maintaining sufficient accuracy of important output quantities, i.e., the computational cost can be reduced by analyzing a smaller, approximate system.

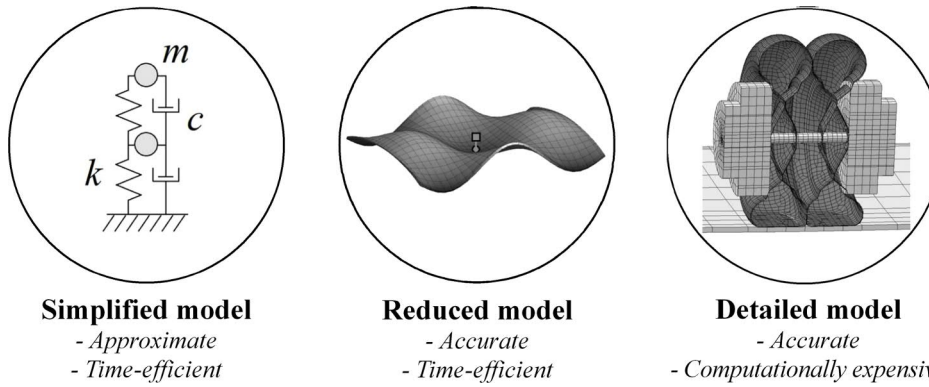

Figure 1.1: Principal differences between models for structural dynamics analysis.

The concept is illustrated in Figure 1.1. A *simplified model* typically considers the governing structural behavior and provide a rough estimate of the response in a time-efficient manner, whereas a *detailed model* provides a "best estimate" representation of the structural response. In contrast, by using a detailed numerical model as a starting point, an approximate *reduced model* may be formed, which is computationally efficient, while providing a sufficiently accurate response prediction. Moreover, by developing a reduced model, the essential dynamics are extracted from the underlying detailed model, which can enable a more thorough understanding of the dynamic problem at hand.

For structural dynamics problems discretized using the FE method, reduced order models can be obtained by introducing a modal basis. More specifically, the response is approximated as a linear combination of a set of time-invariant displacement fields, referred to as mode shapes, which constitute the basis vectors of the modal basis. For instance, a modal basis can be constructed using a set of low-frequency normal modes. The approach is well-established and frequently used within linear structural dynamics. In the context of nonlinear structural dynamics, modal methods for reduced order modeling have gained more prominence during the last decades and is still an active area of research.

Reduced order models considering geometrically nonlinear effects, such as bending-stretching coupling, can be established in a manner similar to modal reduction in linear dynamics (e.g., see [2, 3]). However, in contrast to linear systems, the response generally involves high-frequency modes, with eigenfrequencies far above the frequency content of the loading. Consequently, the basis selection procedure constitutes one of the main challenges here. Moreover, to effectively determine the transient dynamic response using direct time-integration, specialized methods are needed for evaluating the system restoring forces and tangent stiffness.

Dynamic substructuring (DS) is a key concept for handling localized nonlinearities [4]. Hence, by subdividing the structure into substructures, the modeling approach and the level of accuracy can be effectively adjusted for different parts of the structure. For example, substructures that remain linear elastic may be modeled using mode-superposition methods whereas sub-

structures involving nonlinear behavior can be represented by refined FE submodels.

In the dissertation, strategies for nonlinear reduced order modeling are developed on the basis of structural engineering applications within two different areas; namely, concerning concrete structures subjected to blast loading and glass structures subjected to impact loading. Some of the challenges with regard to structural dynamics modeling are similar. In particular, brittle failure modes are often critical, why the response of higher order modes can be of particular importance. Moreover, an accurate representation of the structural behavior typically necessitates models considering nonlinear behaviors. More specifically, the dynamic problems involve localized nonlinearities in the form of contact conditions and joints, as well as geometric nonlinearity which, in contrast, is a distributed nonlinearity where degrees of freedoms throughout the structure are nonlinearly coupled.

The developed modeling strategies are suitable for implementation in design tools, specialized for specific applications. For instance, the model developed for analyzing impact loading is intended to be implemented in ClearSight [5], which is a user-friendly FE tool, specialized for design of glass structures.

1.2 AIMS AND OBJECTIVES

The aim of this research is to facilitate a broadened use of interactive structural design processes, where different designs can be tested in a time-efficient and convenient manner, and, in particular, that methods are available that can be used in accurate and computationally efficient design tools for structural dynamic applications, suitable for such design processes. Furthermore, by enabling accurate and efficient numerical models, too conservative designs can be avoided, thus, leading to reduced costs as well as environmental benefits.

The objectives are to develop accurate and computationally efficient modeling strategies appropriate for implementation in such specialized design tools. In particular, various reduced order modeling techniques are evaluated and exemplified on the basis of the aforementioned structural engineering applications. In the broader perspective, a review of the available reduced order modeling methods provides a basis for further investigations. Apart from various numerical studies, the objectives include investigations of experimental methodologies for validating reduced order models employed for analyzing glass structures subjected to soft-body impact.

1.3 LIMITATIONS

In this work, focus is on investigating computationally efficient modeling techniques, appropriate for use in a structural design process. Accordingly, the models are evaluated based on output quantities typically used in a structural verification. However, a detailed investigation

with regard to design code requirements, e.g. related to the reinforcement arrangement in concrete structures or allowable stress levels in glass structures, are not within the scope of this dissertation.

On the basis of the aforementioned applications, various reduced order modeling techniques and DS methods are investigated. However, the presented review is by no means exhaustive. In particular, focus is on reduced order modeling techniques in structural dynamics, applied in time domain analyses. Similar methods have been developed in other fields, e.g. system and control, where focus often is on single input–output relations. Here, however, a structural dynamics approach is considered where typically output for the whole structure is of interest.

Numerical models in structural dynamics applications are often established by means of the FE method. However, using the reduction methods studied herein, a numerical model is typically the starting point, which is then further modified to obtain a computational efficient reduced order model. Therefore, only a brief review of the FE method is presented. Thus, details regarding numerical methods for discretizing continuous dynamic problems are not within the scope of this dissertation.

The geometrically nonlinear reduced order models are established using modal methods. In particular, reduction methods using time-invariant reduction bases are considered. Other so-called nonlinear reduction methods have been developed, where the full-order solution subspace is approximated using time-invariant submanifolds rather than linear reduction bases. This concept is however not further studied in this work. Moreover, the geometric nonlinearity considered here is based on the assumption of small strains and large displacements. Further, focus is on nonintrusive methods, which do not require access to the source code of an FE software.

1.4 OUTLINE OF DISSERTATION

This dissertation is divided into two parts:

Part I contains an introduction to structural dynamics modeling, reduced order modeling, DS, and the applications further investigated in the appended papers. Starting with the equations of motion, Chapter 2 introduces various modeling methods for structural dynamics applications. Furthermore, a brief overview of damping models for time domain analyses and solution techniques are presented. In Chapters 3 and 4, reviews of reduced order modeling techniques for linear and geometrically nonlinear systems, respectively, are presented. In Chapter 5, dynamic substructuring is introduced; in particular, various assembly methods and component mode synthesis methods are presented. Moreover, some aspects regarding geometrically nonlinear substructures are discussed. In Chapter 6, civil engineering applications using the concepts introduced in Chapters 2 to 5 are discussed. In particular, an overview of reduced order modeling techniques applied to concrete and glass structures subjected to blast and impact loading, respectively, is presented.

Part II contains the appended papers. Papers A and B consider concrete structures subjected to blast loading, and Papers C to E consider glass structures subjected to soft-body impact. In Paper A, reduced order models are developed providing an improved response accuracy as compared to the simplified models commonly used for design of concrete beams and slabs subjected to blast loading. Paper B presents strategies for analyzing concrete frame structures subjected to blast loading in a computationally efficient manner. In Paper C, reduced order models for verifying glass panels subjected to impact loading are presented. In particular, the models are validated using a detailed reference model as well as experimental tests. Paper D investigates modeling strategies for efficient reduced order modeling of geometrically nonlinear flat structures. The methods developed in Paper D are then utilized in Paper E, where a nonlinear reduced order model is presented for analyzing glass panels subjected to impact loading.

2 Structural dynamics and modeling methods

A structural dynamics analysis differs from the corresponding static analysis in some important aspects. Firstly, the accelerations of the structure give rise to inertia forces. Consequently, both the stiffness and mass distribution of the structure affect the structural dynamic behavior. Secondly, the frequency content of the loading, not only the load magnitude, affect the dynamic response. In particular, structural vibrations may arise from an initial disturbance (e.g., impact excitation), and/or from time-varying excitations. Here, the former type of excitation, which typically is wide in the frequency domain and very short in the time domain, result in free vibrations. In contrast, harmonic loading for selected frequencies result in forced vibrations.

A distinction between dynamic and static loading can be made based on how quickly the load varies in time, as compared to the natural dynamics of the structure. For dynamic loading, the frequency range of the loading is in the range of the natural frequencies of the structure. On the other hand, if the forcing frequency is far below the natural frequencies of the structure, the loading can be considered static or quasi-static, where the latter implies that the load varies through time, while it varies slowly compared to the structure's natural dynamics. Accordingly, both the loading characteristics and the properties of the structure must be considered to determine if a structural verification necessitates a dynamic response analysis.

In a structural verification, the real structure (or design) must generally be idealized to obtain a suitable analytical model. An analytical model representing a continuous system theoretically has an infinite number of degrees-of-freedom. In general, the analytical model must be discretized in some manner, e.g., by means of the finite element (FE) method or by an assumed-mode approach [6]. The resulting discretized model should provide a sufficiently accurate response prediction and be computationally efficient, both aspects being particularly important in a structural dynamics analysis.

In this chapter, basic terminology and some fundamental modeling methods for structural dynamics applications are presented. First, in Section 2.1, various applications of single-degree-of-freedom (SDOF) systems are discussed. In Section 2.2, the FE method is introduced which allows for a space discretization of general continuous dynamic problems, leading to the formu-

lation of multi-degree-of-freedom (MDOF) systems. In Section 2.3, modal expansion techniques for MDOF systems are introduced, and, finally, damping models and solution methods for time history analysis are presented in Sections 2.4 and 2.5.

The semi-discretized equations of motion (i.e., discretized in space and continuous in time), obtained using an appropriate modeling method, constitute the starting point in both the linear and nonlinear reduced order modeling techniques considered in this work, which are described in detail in Chapters 3, 4, and 5. In Chapter 6, the reduction methods are then employed for developing reduced order models in various engineering applications.

2.1 SINGLE-DEGREE-OF-FREEDOM MODELS

The simplest possible model is a lumped mass system with a massless supporting structure. Such a system can be modeled by a single-degree-of-freedom (SDOF) model having only one system variable, a degree-of-freedom (DOF), representing the movement of the lumped mass. The equation of motion for an SDOF system can be derived from Newton's second law of motion. Hence, the inertia force acting in the opposite direction of the acceleration is balanced by the external load and the force imposed by the supporting structure, e.g., expressed as

$$p(t) - f_S(t,u) - f_D(t,\dot{u}) = m\ddot{u}(t) \tag{2.1}$$

where u is the displacement, m is the lumped mass, p is the external force, f_S is the linear (or nonlinear) restoring force and f_D is the damping force (dot notation is used for differentiation with respect to time). If assuming linear elastic behavior and linear viscous damping, Eq. 2.1 can be rewritten to obtain the equation of motion for a linear elastic SDOF system, a second-order differential equation of the form:

$$m\ddot{u}(t) + c\dot{u}(t) + ku(t) = p(t) \tag{2.2}$$

where c is the damping coefficient and k is the linear spring stiffness (see Figure 2.1). Furthermore, in many applications it is convenient to rewrite Eq. 2.2 such that:

$$\ddot{u}(t) + 2\zeta\omega_n\dot{u}(t) + \omega_n^2 u(t) = \frac{p(t)}{m} \tag{2.3}$$

where

$$\omega_n = \sqrt{\frac{k}{m}} \tag{2.4}$$

is the natural angular frequency, $f_n = \frac{\omega_n}{2\pi}$ is the natural frequency, or eigenfrequency, and

$$\zeta = \frac{c}{2m\omega_n} \tag{2.5}$$

is the damping ratio.

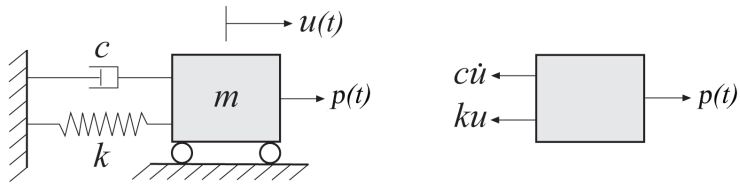

Figure 2.1: Single-degree-of-freedom system.

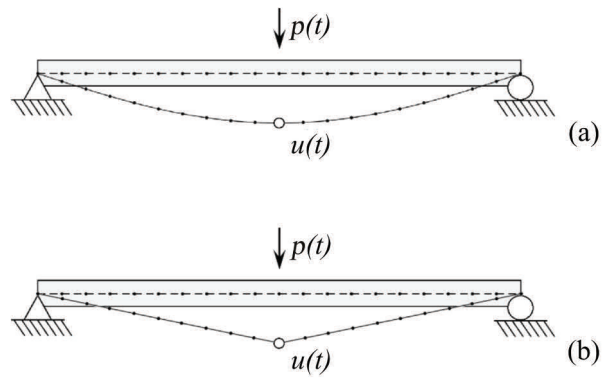

Figure 2.2: Example of approximate, generalized SDOF systems for an elastic (a) and elasto-plastic (b) response. $p(t)$ is the external force and $u(t)$ is the vertical displacement at midspan.

Despite its simple form, the SDOF system turns out to be useful in several structural dynamic applications. Apart from a wide range of applications in which the governing structural behavior can be well-represented by an SDOF system it is the basis in response analysis methods based on modal expansion techniques (see further Sections 2.3 and 2.5).

Furthermore, in some applications, continuous structures may be well-represented by a so-called *generalized* SDOF system. For example, consider a simply supported beam subjected to an external point load, as shown in Figure 2.2a. The vertical displacement at midspan may be considered a degree-of-freedom. A linear spring stiffness representing the load–displacement relation at midspan can readily by derived using standard static load cases found in textbooks (see e.g. [7]). The mass associated to the vertical displacement may be determined based on the assumed mode shape or, as a rough estimate, say 50% of the beam mass, which is referred to as a lumped mass model. The beam's dynamic response, in terms of the midspan displacement, is thus represented by a generalized SDOF system. More specifically, the SDOF system represents the motion of both the midspan displacement and the amplitude of the mode, corresponding to the static deflection of the external force. It should be emphasized that the mode *shape* is constant whereas the mode amplitude varies through time.

In more general form, the generalized mass and stiffness for a linear elastic beam, assuming

small displacements, can be written as [6]:

$$k = \int_0^L EI \left(\frac{d^2\psi}{dx^2} \right)^2 dx \tag{2.6a}$$

$$m = \int_0^L \rho A \psi^2 dx \tag{2.6b}$$

where L is the beam length, E is Young's modulus, I is the area moment of inertia, ρ is the mass per unit volume, A is the cross-sectional area, and $\psi(x)$ is an *admissible function*, meaning that it is continuous, satisfies geometric boundary conditions, and possesses derivatives of sufficient order [6]. Further, ψ is in general normalized such that a value of one is provided in a suitable position (e.g. at midspan).

In the specific case of a linear elastic simply supported beam, it turns out that a lumped mass model can be employed for a fairly accurate prediction of the fundamental natural frequency. However, the accuracy of this simplified model can be expected to decrease with an increasing forcing frequency, because the response of higher order modes is neglected. Nonetheless, the approach using assumed mode shapes (also referred to as basis or shape functions) is, in principle, employed also in more advanced space discretization methods, such as the FE method (see Section 2.2).

Moreover, note that a generalized SDOF system may also be utilized for modeling the nonlinear response of a structure, at least in an approximate manner. Consider, for example, a simply supported beam where a plastic hinge may develop at midspan, modeled by means of the assumed mode shape shown in Figure 2.2b. This model can e.g. be employed for estimating the inelastic dynamic response of a concrete beam—a commonly used approach in blast loading design of concrete structures [8] (see also Paper A).

2.2 FINITE ELEMENT METHOD

To compute the response of complex structures some form of discretization is generally required, e.g., by means of the FE method [1, 9, 10]. The structure is then idealized as an assemblage of elements representing subsystems, e.g., bars, beams, shells, or a continuum, for which the stiffness and mass distribution are easier to define.

In this section, the FE formulation is introduced by first establishing the strong and weak form of the continuous balance equation, being valid for linear as well as nonlinear dynamic problems. Next, a space discretization is obtained by using element shape functions. Here, solid continuum elements are considered, which allows for analyzing the deformations of an arbitrary body. For details regarding the FE formulation of structural elements, such as beams or shells, see e.g. [9].

2.2.1 Strong and weak form of continuous dynamic problems

The equation of motion for an infinitesimal cube within a continuum in the current configuration can be expressed as (henceforth, the time dependence of variables may be omitted to simplify the notation):

$$\frac{\partial \sigma_{ij}}{\partial x_j} + b_i - \rho \ddot{\bar{u}}_i = 0 \tag{2.7}$$

where $\sigma_{ij}(x_1, x_2, x_3, t)$ is the Cauchy stress tensor, $b_i(x_1, x_2, x_3, t)$ is the body force per unit volume in direction i, and $\bar{u}_i(x_1, x_2, x_3, t)$ is the displacement in direction i ($i = 1, 2, 3$). Further, $\rho(x_1, x_2, x_3)$ is the material density and x_i is the coordinate in direction i. Eq. 2.7, which is referred to as Cauchy's equation of motion, can be derived either from Newton's second law or the balance of linear momentum [10,11].

For a (deformed) body V with surface boundary S, Eq. 2.7 can be rewritten as:

$$\tilde{\boldsymbol{\nabla}}^{\mathrm{T}} \boldsymbol{\sigma} + \mathbf{b} - \rho \ddot{\bar{\mathbf{u}}} = \mathbf{0} \quad \bar{\mathbf{u}} \in V \tag{2.8}$$

where

$$\tilde{\boldsymbol{\nabla}}^{\mathrm{T}} = \begin{bmatrix} \frac{\partial}{\partial x_1} & 0 & 0 & \frac{\partial}{\partial x_2} & \frac{\partial}{\partial x_3} & 0 \\ 0 & \frac{\partial}{\partial x_2} & 0 & \frac{\partial}{\partial x_1} & 0 & \frac{\partial}{\partial x_3} \\ 0 & 0 & \frac{\partial}{\partial x_3} & 0 & \frac{\partial}{\partial x_1} & \frac{\partial}{\partial x_2} \end{bmatrix} \tag{2.9}$$

$$\boldsymbol{\sigma}^{\mathrm{T}} = \begin{bmatrix} \sigma_{11} & \sigma_{22} & \sigma_{33} & \sigma_{12} & \sigma_{13} & \sigma_{23} \end{bmatrix} \tag{2.10}$$

$$\mathbf{b}^{\mathrm{T}} = \begin{bmatrix} b_1 & b_2 & b_3 \end{bmatrix} \tag{2.11}$$

$$\bar{\mathbf{u}}^{\mathrm{T}} = \begin{bmatrix} \bar{u}_1 & \bar{u}_2 & \bar{u}_3 \end{bmatrix} \tag{2.12}$$

and the necessary boundary conditions can be expressed as:

$$\begin{cases} \boldsymbol{\Sigma}\mathbf{n} = \tilde{\mathbf{t}} \quad \bar{\mathbf{u}} \in S_\sigma & \text{(2.13a)} \\ \bar{\mathbf{u}} = \tilde{\mathbf{u}} \quad \bar{\mathbf{u}} \in S_u & \text{(2.13b)} \end{cases}$$

where $\boldsymbol{\Sigma}$ is the 3×3 matrix representation of the Cauchy stress tensor, $\mathbf{n}$ is the outward unit normal vector at the boundary, $\tilde{\mathbf{t}}$ is the traction vector (i.e., force per unit current surface area), and $\tilde{\mathbf{u}}$ are prescribed displacements (which are typically zero in structural dynamics applications). Here, the boundary conditions $\tilde{\mathbf{t}}$ and $\tilde{\mathbf{u}}$ are prescribed on complementary parts of the surface boundary, i.e., $S = S_\sigma \cup S_u$. Moreover, the initial conditions at the initial time $t = 0$ must be specified for the dynamic problem, namely, in the form of the initial velocity field $\dot{\bar{\mathbf{u}}}(t = 0) = \dot{\bar{\mathbf{u}}}_0$ and the initial displacement field $\bar{\mathbf{u}}(t = 0) = \bar{\mathbf{u}}_0$. Together with Eqs. 2.8–2.13, this is known as the strong form of the problem.

The weak form of the problem can be obtained by multiplying Eq. 2.8 by an arbitrary weight function $\mathbf{v}$, which is a smooth function being zero on the surface boundary S_u, and integrating over the region V [11]. In the context of structural dynamics, the weight function is typically considered to be the kinematically admissible virtual displacements $\delta\bar{\mathbf{u}}$. Then, by use

of Green–Gauss divergence theorem, the weak form (or virtual work) in the current, deformed, configuration can be written as (e.g., see [10,11]):

$$\int_V \left(\tilde{\boldsymbol{\nabla}}\delta\bar{\mathbf{u}}\right)^{\mathrm{T}} \boldsymbol{\sigma}\, dV + \int_V \rho\delta\bar{\mathbf{u}}^{\mathrm{T}}\ddot{\bar{\mathbf{u}}}\, dV - \int_V \delta\bar{\mathbf{u}}^{\mathrm{T}}\mathbf{b}\, dV - \int_S \delta\bar{\mathbf{u}}^{\mathrm{T}}\mathbf{t}\, dS = 0. \tag{2.14}$$

Note that Eq. 2.14 is valid for linear and nonlinear problems using materials with arbitrary stress–strain relations.

Here, the virtual work has been written in the deformed configuration. As will be further discussed in Chapter 4, an alternative is to express the balance relation and virtual work in the reference configuration. In an iterative solution process, the reference configuration and the deformed configuration constitute the computational domain in the total and updated Lagrangian formulation, respectively [1].

2.2.2 Finite element discretization

Using the FE method, the body is then idealized as an assemblage of smaller parts, finite elements, representing subregions, which are interconnected through a set of nodal points. Specifically, to obtain the FE formulation, the continuous displacement field is approximated using nodal displacements and shape functions, as

$$\bar{\mathbf{u}}(t) = \mathbf{N}\mathbf{u}(t) \tag{2.15}$$

where $\mathbf{u}$ is a $n \times 1$ vector containing nodal displacements, and $\mathbf{N}$ is a matrix containing time-independent shape functions. If considering continuum solid elements having three global displacement DOFs per node, the shape function matrix can be expressed as:

$$\mathbf{N}(x_1, x_2, x_3) = \begin{bmatrix} N_1 & 0 & 0 & N_2 & 0 & 0 & \cdots & N_{\tilde{n}} & 0 & 0 \\ 0 & N_1 & 0 & 0 & N_2 & 0 & 0 & \cdots & N_{\tilde{n}} & 0 \\ 0 & 0 & N_1 & 0 & 0 & N_2 & 0 & 0 & \cdots & N_{\tilde{n}} \end{bmatrix} \tag{2.16}$$

where N_k ($k = 1, \ldots, \tilde{n}$) is the shape function associated to the kth global node, and $\tilde{n}$ is the total number of nodes. Thus, for continuum solid elements, we note that $n = 3\tilde{n}$, where, again, n is the number of DOFs of the discretized model.

The shape functions are commonly constructed as low-order polynomial functions. Further, the shape functions N_k are nonzero only within subregions, or elements, containing the global nodal point k. In particular, at the nodal points, the shape functions are defined such that:

$$\begin{cases} N_k(\mathbf{x}_p) = 1 & \text{if} \quad k = p \qquad (2.17a) \\ N_k(\mathbf{x}_p) = 0 & \text{if} \quad k \neq p \qquad (2.17b) \end{cases}$$

where $k, p = 1, \ldots, \tilde{n}$, and $\mathbf{x}_p = (x_{1,p}, x_{2,p}, x_{3,p})$ is the coordinate vector for nodal point p. The displacement field within the body is thus expressed in terms of the nodal displacements $\mathbf{u}$,

which can be viewed as generalized coordinates having a physical meaningful interpretation as the displacements in the nodal DOFs. Accordingly, the model is sometimes said to be formulated in the *physical* domain. Furthermore, a global assembly can be formed by interconnecting the element DOFs in the nodal points (cf. Section 5.1).

By introducing the Galerkin method, the virtual displacements are expressed using the same shape functions, i.e., $\delta\bar{\mathbf{u}} = \mathbf{N}\delta\mathbf{u}$. By inserting these approximations into Eq. 2.14, and noting that the virtual displacements $\delta\bar{\mathbf{u}}$ are arbitrary, expressions for the mass matrix, the internal (or restoring) force vector, and the external force vector can be written, respectively, as:

$$\mathbf{M} = \int_V \rho \mathbf{N}^{\mathrm{T}} \mathbf{N} \, dV \tag{2.18}$$

$$\mathbf{f} = \int_V \left(\tilde{\boldsymbol{\nabla}} \mathbf{N} \right)^{\mathrm{T}} \boldsymbol{\sigma} \, dV \tag{2.19}$$

$$\mathbf{p} = \int_V \mathbf{N}^{\mathrm{T}} \mathbf{b} \, dV + \int_S \mathbf{N}^{\mathrm{T}} \mathbf{t} \, dS. \tag{2.20}$$

Thus, in accordance with Eq. 2.14, it follows that the semi-discretized equations of motion can be written as:

$$\mathbf{M}\ddot{\mathbf{u}} + \mathbf{C}\dot{\mathbf{u}} + \mathbf{f} = \mathbf{p} \tag{2.21}$$

where the $n \times n$ mass matrix $\mathbf{M}$, and the $n \times 1$ restoring force and external force vectors $\mathbf{f}$ and $\mathbf{g}$ are given by Eqs. 2.18–2.20. Further, to consider energy dissipation, the $n \times n$ viscous damping matrix $\mathbf{C}$ is included in the equations of motion, which is typically expressed as a weighted sum of the mass and tangent stiffness matrices (see further Section 2.3).

According to above, the FE method was introduced using global shape functions N_k, being defined over the whole body. An alternative but equivalent approach, which is often encountered in the literature, is to employ element shape functions, being defined only within each subregion/element. However, by using global shape functions, the similarity between the FE method and projective reduced order modeling procedures can be clearly illustrated, as will be further described in Chapter 3.

Next, by assuming small displacements and adopting a linear elastic constitutive law, the Cauchy stress can be expressed in terms of the engineering strain $\boldsymbol{\epsilon}$:

$$\boldsymbol{\sigma} = \mathbf{D}\boldsymbol{\epsilon} \tag{2.22}$$

where

$$\mathbf{D} = \frac{E}{(1+\nu)(1-2\nu)} \begin{bmatrix} 1-\nu & \nu & \nu & 0 & 0 & 0 \\ \nu & 1-\nu & \nu & 0 & 0 & 0 \\ \nu & \nu & 1-\nu & 0 & 0 & 0 \\ 0 & 0 & 0 & \frac{1}{2}(1-2\nu) & 0 & 0 \\ 0 & 0 & 0 & 0 & \frac{1}{2}(1-2\nu) & 0 \\ 0 & 0 & 0 & 0 & 0 & \frac{1}{2}(1-2\nu) \end{bmatrix} \tag{2.23}$$

is the constitutive matrix for isotropic elasticity, where E and ν are the Young's modulus and Poisson's ratio, respectively.

By substituting Eq. 2.22 into Eq. 2.19, and introducing the relation $\boldsymbol{\sigma} = \mathbf{D}\boldsymbol{\epsilon} = \mathbf{D}\tilde{\boldsymbol{\nabla}}\mathbf{N}\mathbf{u}$, it follows that the linearized stiffness matrix can be expressed as:

$$\mathbf{K} = \int_{V^o} \left(\tilde{\boldsymbol{\nabla}}\mathbf{N}\right)^{\mathrm{T}} \mathbf{D} \left(\tilde{\boldsymbol{\nabla}}\mathbf{N}\right) \, dV^o \tag{2.24}$$

where the superscript o of a quantity indicate that it is evaluated in the reference configuration. Thus, the linearized equations of motion for the MDOF system can be written as:

$$\mathbf{M}\ddot{\mathbf{u}} + \mathbf{C}\dot{\mathbf{u}} + \mathbf{K}\mathbf{u} = \mathbf{p} \tag{2.25}$$

where the mass matrix and the external force vector can be obtained by evaluating Eqs. 2.18 and 2.20 in the reference configuration. Notice the similarity between the equations of motion for the linear MDOF system (Eq. 2.25) and the SDOF system (Eq. 2.2). In fact, as will be demonstrated in the next section, the response of linearized MDOF systems can be decomposed into a set of generalized SDOF system responses, which can be solved independently and superimposed to recover the MDOF system response.

2.3 MODAL EXPANSION

The equations of motion for free vibration of a linearized undamped MDOF system, e.g. established using the FE method, is given by:

$$\mathbf{M}\ddot{\mathbf{u}} + \mathbf{K}\mathbf{u} = \mathbf{0} \tag{2.26}$$

where, again, $\mathbf{M}$ and $\mathbf{K}$ are the $n \times n$ mass and linearized stiffness matrices, respectively, and $\mathbf{u}$ is an $n \times 1$ displacement vector, which may include generalized and/or physical displacement coordinates.

By assuming harmonic motion, $\mathbf{u} = \boldsymbol{\phi}\cos(\omega t - \theta)$, where $\boldsymbol{\phi}$ is a vector constant through time and θ is the phase angle, and substituting into Eq. 2.26, the following nth-order generalized eigenvalue problem is obtained [6]:

$$\left(\mathbf{K} - \omega_j^2\mathbf{M}\right)\boldsymbol{\phi}_j = 0 \quad j = 1, 2, \ldots, n. \tag{2.27}$$

where $\boldsymbol{\phi}_j$ is the jth eigenmode and ω_j is the corresponding eigenfrequency. The eigenmodes are ordered increasingly, such that $\omega_1 < \omega_2 < \ldots < \omega_n$. Further, in the literature, the system eigenmodes, as introduced above, are also referred to as *normal modes*, *natural modes* or *vibration modes*. As will be demonstrated throughout this thesis, the eigenmodes are fundamental in structural dynamics as well as in model order reduction.

The amplitudes of the eigenmodes are arbitrary, thus, the modes may be scaled in any suitable manner. For example, in many applications it is convenient to scale the eigenmodes such that the modal mass is one unit of mass, i.e.

$$\boldsymbol{\phi}_j^{\mathrm{T}}\mathbf{M}\boldsymbol{\phi}_j = 1. \tag{2.28}$$

By pre-multiplying with $\boldsymbol{\phi}_j^{\mathrm{T}}$ in Eq. 2.27, it follows that the corresponding modal stiffness is given by

$$\boldsymbol{\phi}_j^{\mathrm{T}}\mathbf{K}\boldsymbol{\phi}_j = \omega_j^2. \tag{2.29}$$

Furthermore, an important property of the eigenmodes is the orthogonality property, namely that

$$\boldsymbol{\phi}_i^{\mathrm{T}}\mathbf{M}\boldsymbol{\phi}_j = 0 \quad \text{if} \quad i \neq j \tag{2.30}$$

$$\boldsymbol{\phi}_i^{\mathrm{T}}\mathbf{K}\boldsymbol{\phi}_j = 0 \quad \text{if} \quad i \neq j. \tag{2.31}$$

Thus, by adopting the scaling introduced in Eq. 2.28, the eigenmodes are mass-orthonormal and stiffness-orthogonal.

The physical displacements of the semi-discretized problem can be expressed in terms of the modal responses, as:

$$\mathbf{u} = \boldsymbol{\Phi}\mathbf{q} \tag{2.32}$$

where $\boldsymbol{\Phi} = \begin{bmatrix} \boldsymbol{\phi}_1 & \boldsymbol{\phi}_2 & \dots & \boldsymbol{\phi}_n \end{bmatrix}$ is the *modal matrix* and $\mathbf{q} = \begin{bmatrix} q_1 & q_2 & \dots & q_n \end{bmatrix}^{\mathrm{T}}$ is the corresponding modal coordinates.

Further, by using the modal matrix, the linearized system equations (Eq. 2.25) can be transformed into modal coordinates. The transformed system equations are then given as:

$$\tilde{\mathbf{M}}\ddot{\mathbf{q}} + \tilde{\mathbf{K}}\mathbf{q} = \tilde{\mathbf{p}} \tag{2.33}$$

where

$$\tilde{\mathbf{M}} = \boldsymbol{\Phi}^{\mathrm{T}}\mathbf{M}\boldsymbol{\Phi}, \quad \tilde{\mathbf{K}} = \boldsymbol{\Phi}^{\mathrm{T}}\mathbf{K}\boldsymbol{\Phi}, \quad \tilde{\mathbf{p}} = \boldsymbol{\Phi}^{\mathrm{T}}\mathbf{p}.$$

Here, $\tilde{\mathbf{M}}$, and $\tilde{\mathbf{K}}$ are the $n \times n$ *modal mass matrix* and *modal stiffness matrix*, respectively, and $\tilde{\mathbf{p}}$ is the $n \times 1$ modal load vector. The orthogonality property of the eigenmodes implies that the modal mass and stiffness matrices are diagonal:

$$\tilde{\mathbf{M}} = \boldsymbol{\Phi}^{\mathrm{T}}\mathbf{M}\boldsymbol{\Phi} = \mathbf{I} \tag{2.34}$$

$$\tilde{\mathbf{K}} = \boldsymbol{\Phi}^{\mathrm{T}}\mathbf{K}\boldsymbol{\Phi} = \boldsymbol{\Lambda} = \mathrm{diag}(\omega_1^2, \omega_2^2, \dots, \omega_n^2). \tag{2.35}$$

Hence, a set of n uncoupled second-order differential equations, which can be solved independently, is obtained, e.g. expressed as:

$$\ddot{q}_j + \omega_j^2 q_j = \boldsymbol{\phi}_j^{\mathrm{T}}\mathbf{p} \quad j = 1, 2, \dots, n. \tag{2.36}$$

If using a modal basis including all n eigenmodes, a pure transformation from physical to modal coordinates is obtained. Hence, the systems expressed in terms of modal and physical

coordinates, respectively, are equivalent. However, the full set of n eigenmodes is rarely used in practice. Instead, a reduced system is commonly established using a truncated modal basis, as will be further discussed in Section 3.2. The benefit of using modal coordinates is thus two-fold—the orthogonality property of the modes enables a set of uncoupled differential equations, and the number of system variables are decreased.

The eigenmodes are determined from a linearized system. However, as will be further described in Chapter 4, eigenmodes can be used also for approximating the response of geometrically nonlinear systems. In this case, however, the modal responses are no longer decoupled and specialized techniques for calculating the transient dynamic response are needed (cf. Section 2.5.2).

2.4 DAMPING MODELS FOR TIME DOMAIN ANALYSIS

For structures subjected to free vibration, a steadily diminishing displacement amplitude is observed. Hence, energy is dissipated due to various mechanisms, such as opening/closing of small cracks, friction between structural members etc., which is referred to as *damping* [12]. It turns out that a viscous damping model is convenient in linear analyses because it enables analytical solutions. However, it should be emphasized that, in many structural engineering applications, this model is unphysical. Thus, it is merely a mathematical model that can be calibrated to mimic the damping of the real structure. In particular, a viscous damping model is frequency dependent as indicated by Eq. 2.2; i.e., the damping force correspond to the damping coefficient c multiplied with the velocity. Nonetheless, the viscous damping model has several benefits regarding computational aspects that, in most engineering applications, far outweighs the gain of using a more realistic and complicated damping model.

2.4.1 Rayleigh damping

Because both the modal mass and stiffness matrix are diagonal, one way to ensure that also the viscous damping matrix $\mathbf{C}$ can be diagonalized is to construct the damping matrix as a weighted sum of the mass and stiffness matrix, thus:

$$\mathbf{C} = \alpha\mathbf{M} + \beta\mathbf{K}. \tag{2.37}$$

This damping model is referred to as *Rayleigh damping* or *proportional damping* [12]. The damping coefficients α and β, thus, determine the contribution of mass- and stiffness-proportional damping, respectively.

If the eigenmodes are mass normalized, the set of uncoupled differential equations including viscous damping can be expressed as:

$$\ddot{q} + 2\zeta_j\omega_j\dot{q} + \omega_j^2 q = \boldsymbol{\phi}_j^{\mathrm{T}}\mathbf{p} \quad j = 1, 2, \ldots, n. \tag{2.38}$$

It follows that the Rayleigh damping coefficients can be expressed as:

$$2\zeta_j\omega_j = \alpha + \omega_j^2\beta \Rightarrow \zeta_j = \frac{1}{2}\left(\frac{\alpha}{\omega_j} + \omega_j\beta\right) \quad j = 1, 2, \ldots, n \tag{2.39}$$

where ζ_j is the *modal damping ratio* for mode j.

In structural engineering applications, experimental data typically suggests that the damping ratio for many materials is frequency-independent [12]. Nonetheless, a viscous damping model where the amount of damping increases linearly with the forcing frequency is often employed due to its utility in time domain analyses of linear systems. However, a useful property of the Rayleigh damping model is that the mass-proportional damping is inversely proportional to the eigenfrequency, whereas the stiffness-proportional damping is linearly proportional to the eigenfrequency. Hence, the coefficients α and β can be adjusted such that the desired modal damping ratio is fulfilled for two eigenfrequencies [12]. Furthermore, if the desired damping ratio is equal for all modes, frequencies in-between the selected eigenfrequencies will then be slightly underdamped whereas frequencies below and above the selected eigenfrequencies will be overdamped, as shown in Figure 2.3. Thus, to ensure that the damping is not overestimated, the set of eigenmodes used for calibrating the Rayleigh coefficients may be chosen such that the frequency of important eigenmodes lies in-between the eigenfrequencies of the selected modes.

The implication of prescribing a mass- and stiffness-proportional damping is shown in Figure 2.4 [12]. Clearly, the mass-proportional part, corresponding to dashpots connected to ground, is unphysical. For example, a mass-proportional damping associates damping to rigid body modes. Nonetheless, a pure stiffness-proportional viscous damping being linearly pro-

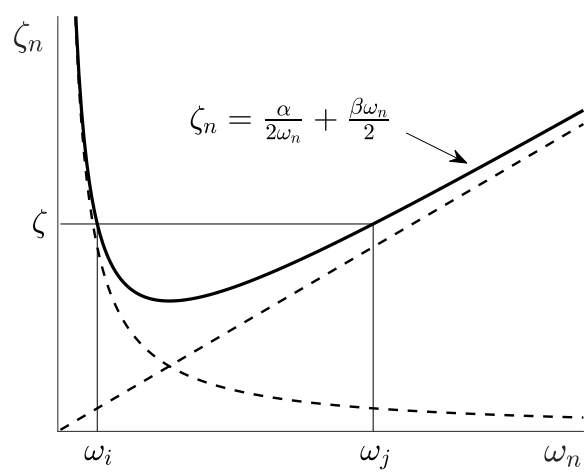

Figure 2.3: Rayleigh damping: variation of modal damping ratios ζ_n with natural frequency ω_n. (Figure based on [12].)

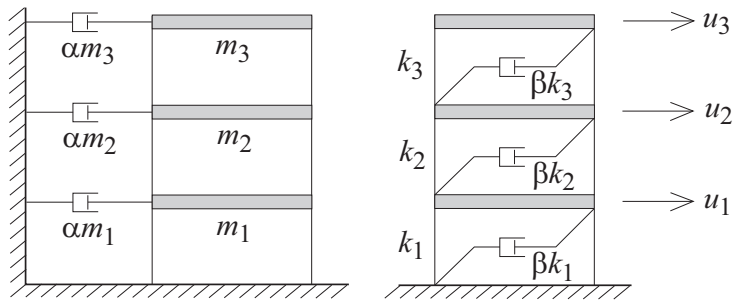

Figure 2.4: Mass-proportional (left) and stiffness-proportional damping (right). (Figure based on [12].)

portional to the forcing frequency is in general not appropriate. Thus, a mass-proportional part is useful in practical applications. For structures having an irregular mass distribution, however, a mass-proportional damping model might not be appropriate and should be used with care.

Finally, it should be noted that the Rayleigh damping model is applicable in mode superposition methods, as well as in direct time-integration of linear or nonlinear systems expressed in terms of physical DOFs. This is one of the main advantages using this damping model.

2.4.2 Modal damping

As discussed in Section 2.4.1, the frequency dependency of a viscous damping model can be somewhat controlled by combining a mass- and stiffness proportional damping. An alternative, however, is to explicitly prescribe modal damping in the modal domain [12].

Recall that a modal transformation decouples the modal responses, as shown in Eqs. 2.34 and 2.35. Thus, the desired *modal damping ratio* may be prescribed explicitly in Eq. 2.38. In a modal analysis, this approach is obviously advantageous compared to Rayleigh damping. The drawback, however, is that this damping model is in principle only applicable in modal domain analyses, whereas the Rayleigh damping model can also be employed for systems expressed in terms of physical DOFs.

It should be mentioned, however, that it is actually possible to expand the modal damping matrix to obtain a corresponding damping matrix in the physical domain [12]. Such an approach should be used with great care, however—in general the resulting damping matrix will be full and, moreover, may be physically impossible requiring external as well as negative damping elements. Thus, the Rayleigh damping model is in general the preferred choice in time domain analyses of systems formulated in the physical domain.

2.4.3 Modal strain energy method

An approach using modal damping requires proportional, also referred to as *classical*, damping. However, in several practical applications the damping is non-proportional, e.g., in models representing buildings having a lower part made of concrete and an upper part made of steel, or rubber components interacting with steel or glass structures (cf. Paper C). A Rayleigh damping model can be employed for such systems. Then, the Rayleigh damping coefficients are derived for each subsystem, respectively, by means of the global undamped eigenfrequencies and the desired damping ratios [12].

However, because the damping matrix is not proportional, the corresponding modal damping matrix may not be diagonal. For determining the linearized response of such MDOF systems either a direct time-integration of the coupled equations of motion or a mode superposition method using the complex eigenmodes of the damped system is generally required (e.g., see [13]). However, for lightly damped structures, non-proportional MDOF systems can be analyzed using an approximate approach, which is sometimes referred to as the modal strain energy (MSE) method [14]. The concept can be described as follows.

The damping ratio of an SDOF system representing a modal coordinate can be expressed as [12]:

$$\zeta = \frac{E_D}{4\pi E_S} \tag{2.40}$$

where E_D is the one-cycle modal energy loss due to viscous damping and E_S is the modal strain energy amplitude, given by:

$$E_S = \frac{1}{2}\boldsymbol{\phi}_j^{\mathrm{T}}\mathbf{K}\boldsymbol{\phi}_j \tag{2.41}$$

where $\mathbf{K}$ is the global stiffness matrix for a structure with non-proportional damping, and $\boldsymbol{\phi}_j$ is the jth global eigenmode.

In the MSE method, the modal energy loss is determined as:

$$E_D = \pi\omega_j\boldsymbol{\phi}_j^{\mathrm{T}}\mathbf{C}\boldsymbol{\phi}_j \tag{2.42}$$

where ω_j is the eigenfrequency of mode j and $\mathbf{C}$ is the global damping matrix containing the damping submatrices for substructures having different levels of damping. Assuming that the modal basis is mass-normalized, it follows that the modal damping ratio for mode j can be estimated as:

$$\zeta_j = \frac{\boldsymbol{\phi}_j^{\mathrm{T}}\mathbf{C}\boldsymbol{\phi}_j}{2\omega_j}. \tag{2.43}$$

Using the above procedure, systems with non-proportional damping can be effectively analyzed using a modal superposition of the undamped eigenmodes, as will be further discussed in Section 2.4.2. As indicated by Eq. 2.43, the method implies that possible off-diagonal terms in the modal damping matrix are ignored, i.e., $\boldsymbol{\phi}_i^{\mathrm{T}}\mathbf{C}\boldsymbol{\phi}_j = 0$ if $i \neq j$. As, e.g., demonstrated in [15], this is, however, a reasonable approximation for lightly damped structures.

2.5 SOLUTION TECHNIQUES

In general, the following strategies may be employed for solving for the response of MDOF systems in the time domain:

- mode superposition using the undamped eigenmodes,
- mode superposition using the complex damped eigenmodes, or
- by direct time-integration of the coupled system equations.

Here, only the first and third methods are considered. The damping levels for the structures considered (see further Chapter 6) are fairly low, hence, an approximate mode-superposition approach using the undamped eigenmodes are sufficiently accurate for analyzing the linearized response (see Section 2.5.1). Systems including localized nonlinearities as well as geometric nonlinearity are solved using direct time-integration (see Section 2.5.2). Moreover, although time history analysis methods are the focus of this work, it should be mentioned that the response can also be determined using frequency domain approaches, by establishing complex frequency response functions (FRFs) (see further [12]).

2.5.1 Mode superposition methods

For linear (or linearized) systems, each modal response can be represented by a corresponding SDOF system, i.e., Eqs. 2.3 and Eq. 2.38 are equivalent. It follows that the methods available for computing the dynamic response of SDOF systems can be utilized for computing the modal responses. In particular, a closed-form solution can be established for computing the damped free vibration response:

$$q_j(t) = e^{-\zeta_j \omega_j t} \left(q_j(0) \cos(\omega_{jD} t) + \frac{\dot{q_j}(0) + \zeta_j \omega_j q_j(0)}{\omega_{jD}} \sin(\omega_{jD} t) \right) \tag{2.44}$$

where $\omega_{jD} = \omega_j \sqrt{1 - \zeta_j^2}$ is the jth damped natural frequency [12].

A time discretization is clearly needed to consider a load varying arbitrary through time. Nonetheless, for such load cases, highly efficient numerical procedures are available that provide the "exact" response of a load varying linearly between a range of time increments, i.e., the accuracy merely depend on the time discretization of the dynamic problem. Moreover, a closed-form solution can be established for certain pulse loads, periodic loads and, in particular, harmonic loads, which in turn may be utilized for solving for arbitrary loading by means of frequency domain methods [12].

2.5.2 Direct time-integration methods

The computationally efficient analytical solution methods discussed in Section 2.5.1 require that the system equations are linear (cf. Eq. 2.25). For nonlinear problems, however, a direct time-integration of the equations of motion is generally required. Several time-stepping methods can be found in the literature (see e.g. [15]), which can be divided into one-step and multi-step methods, where the former implies that only two time points are involved in the computations at a given time, whereas the latter may include several time increments. In structural dynamics applications the most common time-integration methods are one-step methods.

Furthermore, a time-stepping scheme may be *implicit*, which implies knowledge of the accelerations in the computation of the velocity and displacements at a given time step, or *explicit*, if the displacements and velocities are computed without prior knowledge of the accelerations.

One of the most important time-stepping methods is Newmark's method—a one-step method based on the following equations [15]:

$$\dot{\mathbf{u}}_{n+1} = \dot{\mathbf{u}}_n + (1-\gamma)\, h\ddot{\mathbf{u}}_n + \gamma h \ddot{\mathbf{u}}_{n+1} \tag{2.45a}$$

$$\mathbf{u}_{n+1} = \mathbf{u}_n + h\dot{\mathbf{u}}_n + h^2 \left(\frac{1}{2} - \beta\right) \ddot{\mathbf{u}}_n + h^2 \beta \ddot{\mathbf{u}}_{n+1} \tag{2.45b}$$

where h is the time increment (i.e. $t_{n+1} = t_n + h$), and γ and β are parameters that defines the variation of the acceleration within time increments. In particular, setting $\gamma = \frac{1}{2}$ and $\beta = \frac{1}{4}$ correspond to constant average acceleration within time increments, i.e., $\ddot{\mathbf{u}}(\tau) = \frac{\ddot{\mathbf{u}}_{n+1} + \ddot{\mathbf{u}}_n}{2}$ where $t_n < \tau < t_{n+1}$. This result in an unconditionally stable scheme, meaning that the time increment size is always stable and need only be adjusted to ensure that the transient dynamic response can be adequately resolved [15].

For nonlinear systems, where the tangent stiffness is amplitude dependent, the stable time increment size will generally not be constant. Consequently, an unconditionally stable time-integration scheme, such as Newmark's method assuming constant average acceleration, is particularly convenient. However, because it is an implicit time-stepping method, iterative solution techniques are generally required to enforce equilibrium of the equations of motion (see e.g. [12]). Specifically, using Newmark's method, equilibrium is enforced at each time point t_{n+1}.

The residual, which should be minimized, can be expressed as:

$$\mathbf{r}(\mathbf{u}_{n+1}) = \mathbf{M}\ddot{\mathbf{u}}_{n+1} + \mathbf{C}\dot{\mathbf{u}}_{n+1} + \mathbf{f}(\mathbf{u}_{n+1}) - \mathbf{p}_{n+1}. \tag{2.46}$$

An iterative solution procedure is commonly established using the Newton–Raphson method. The iteration, which is carried out for each time point t_{n+1}, is initialized by setting the accelerations $\ddot{\mathbf{u}}_{n+1}$ to zero. Accordingly, an initial prediction of the displacements $\mathbf{u}_{n+1}$ and velocities $\dot{\mathbf{u}}_{n+1}$ can be determined from Eq. 2.45 using the results from the previous time

point t_n. Then, the residual is updated in subsequent iteration steps. Namely, in the ith iteration, the corrected displacements can be expressed as:

$$\mathbf{u}_{n+1}^{i+1} = \mathbf{u}_{n+1}^{i} + \Delta\mathbf{u}_{n+1}^{i} \tag{2.47}$$

where the corrections $\Delta\mathbf{u}_{n+1}^{i}$ are determined as [15]:

$$\Delta\mathbf{u}_{n+1}^{i} = -\mathbf{S}^{-1}\mathbf{r}(\mathbf{u}_{n+1}^{i}). \tag{2.48}$$

Here, $\mathbf{S}$ is the iteration (or Jacobian) matrix, given as:

$$\mathbf{S} = \left[\frac{\partial \mathbf{r}}{\partial \mathbf{u}}\right]_{\mathbf{u}_{n+1}^{i}} = \frac{1}{h^2\beta}\mathbf{M} + \frac{\gamma}{h\beta}\mathbf{C} + \mathbf{K}^t(\mathbf{u}_{n+1}^{i}) \tag{2.49}$$

where, again, $\mathbf{M}$ and $\mathbf{C}$ are the mass and damping matrix, and $\mathbf{K}^t = \left[\frac{\partial \mathbf{f}}{\partial \mathbf{u}}\right]_{\mathbf{u}_{n+1}^{i}}$ is the tangent stiffness evaluated at $\mathbf{u} = \mathbf{u}_{n+1}^{i}$. The updated acceleration and velocity vectors can then be computed from the displacement correction, as:

$$\dot{\mathbf{u}}_{n+1}^{i+1} = \dot{\mathbf{u}}_{n+1}^{i} + \frac{\gamma}{h\beta}\Delta\mathbf{u}_{n+1}^{i} \tag{2.50a}$$

$$\ddot{\mathbf{u}}_{n+1}^{i+1} = \ddot{\mathbf{u}}_{n+1}^{i} + \frac{1}{h^2\beta}\Delta\mathbf{u}_{n+1}^{i}. \tag{2.50b}$$

The iterative procedure is repeated until convergence is achieved and the residual is sufficiently small, i.e., $||\mathbf{r}(\mathbf{u}_{n+1})|| \approx 0$. Further, it should be noted that the damping matrix may be amplitude dependent, although any dependencies have been left out in Eqs. 2.46 and 2.49 to simplify the notation. For instance, Rayleigh damping may be adopted, such that $\mathbf{C}(\mathbf{u}_{n+1}) = \alpha\mathbf{M} + \beta\mathbf{K}^t(\mathbf{u}_{n+1})$.

If using the Newton–Raphson method to enforce equilibrium for a nonlinear system, the Jacobian matrix has to be updated in each iteration, namely, because the tangent stiffness (and possibly the damping matrix) is amplitude dependent. However, an alternative is to keep the Jacobian matrix constant during the equilibrium iterations, such that it is only generated ones for each time point. This approach is referred to as the modified Newton–Raphson method. Although it typically results in more iterations to reach equilibrium, it can be computationally less expensive since the Jacobian matrix is only constructed ones in the iterative process [12].

Another important time-stepping technique, a two-step method, is the central difference method (CDM), where the velocity and accelerations are expressed as (e.g., see [12,15]):

$$\dot{\mathbf{u}}_n = \frac{\mathbf{u}_{n+1} - \mathbf{u}_{n-1}}{2h} \tag{2.51a}$$

$$\ddot{\mathbf{u}}_n = \frac{\mathbf{u}_{n+1} - 2\mathbf{u}_n + \mathbf{u}_{n-1}}{h^2}. \tag{2.51b}$$

In fact, the above expressions can be derived from Newmark's formula by setting $\gamma = \frac{1}{2}$ and $\beta = 0$. The CDM method is a second order accurate explicit scheme, i.e., it can be formulated

such that the displacements and velocities can be computed without prior knowledge of the accelerations. In particular, a computationally efficient implementation of the CDM method can be achieved for undamped systems having a diagonal lumped mass matrix, an approach commonly employed in highly nonlinear and transient problems, such as crash simulations and impact loading. Further, using an explicit time-stepping scheme, such as the CDM method, for solving nonlinear systems is straightforward, because the nonlinear forces may be computed explicitly.

The CDM method is conditionally stable, however, requiring that $\omega_{cr} h \leq 2$, where ω_{cr} is the highest eigenfrequency of the system [15]. For large FE models this typically result in a very small stable time increment. Furthermore, for nonlinear systems, the stable time increment is not constant, which follows from the fact that the tangent stiffness matrix is amplitude dependent. For this reason, the nonlinear systems considered in this work are generally solved using Newmark's method with $\gamma = \frac{1}{2}$ and $\beta = \frac{1}{4}$, resulting in an unconditionally stable implicit time-integration scheme. Further, equilibrium is enforced using Newton-Raphson iterations.

For completeness, it should also be mentioned that enhanced versions of the Newmark time-stepping scheme has been developed, such as the HHT (Hilber-Hughes-Taylor) method [16] and the Generalized-α method [17], that introduces numerical damping for high frequencies. These methods can be beneficial in the process of solving large FE models, where unphysical high frequency modes can occur due to the use of small elements. Hence, it is desired to add an appropriate amount of numerical damping for high frequencies, while the frequency band of interested is undamped.

3 Reduced order modeling of linear systems

This chapter presents methods for reduced order modeling of linear systems. The linearized, semi-discretized equations of motion (cf. Eq. 2.25) constitute the starting point in the process of generating the reduced order models. Although linear systems are considered here, many of the procedures will be useful also in the context of reduced order modeling of nonlinear systems, as further discussed in Chapter 4.

By generating a reduced order model, the aim is to reduce the system size while maintaining sufficient accuracy of important output quantities. Hence, the computational cost can be reduced by analyzing a smaller, approximate model. In an FE framework, the continuous displacement field is typically discretized using a substantial number of physical DOFs, i.e., which represent the displacements (or rotations) at a set of nodal points. By introducing a reduced order model, the size of the numerical model is reduced by instead representing the displacement field using a reduced set of modal coordinates, representing the amplitude of a set of global mode shapes, also referred to as reduction basis vectors or Ritz-vectors.

In an evaluation of the reduction methods, it is useful to distinguish between the computational *offline* cost, referring to the computational effort for generating the reduced order system matrices, and the *online* cost, related to the computational cost for calculating the dynamic response of the reduced order model. In particular, to obtain an efficient reduction method, the sum of the offline and online cost should be smaller than the computational cost required for solving the full-order model, while ensuring a reduced order model with adequate accuracy. In this regard, the reduced order models are often particularly efficient for analyzing long time-records or in situations where several load cases is to be analyzed using the same model.

3.1 RAYLEIGH–RITZ METHOD

As described in Section 2.1, a continuous structure may be represented by an assumed mode shape to form a generalized SDOF system. Using the Rayleigh–Ritz method, this approach can be extended further such that the displacements are approximated by a superposition of k

linearly independent mode shapes, satisfying the geometric boundary conditions [12]. Thus, the structure displacements can be expressed as:

$$\mathbf{u}(t) = \sum_{j=1}^{k} \boldsymbol{\psi}_j q_j(t) \tag{3.1}$$

where q_j is the generalized coordinate corresponding to the amplitude of mode shape $\boldsymbol{\psi}_j$ and k is the number of mode shapes, e.g., generated using a set of assumed load patterns. The Rayleigh-Ritz method was originally developed for continuous systems. Here, however, the method is applied to discretized MDOF systems, e.g., formulated using the FE method.

Similar to the procedure using normal modes (cf. Section 2.3), the relation between the generalized coordinates and the physical DOFs can be expressed as a transformation (for clarity, explicit time dependence is henceforth omitted):

$$\mathbf{u} = \boldsymbol{\Psi}\mathbf{q} \tag{3.2}$$

where $\boldsymbol{\Psi} = \begin{bmatrix} \boldsymbol{\psi}_1 & \boldsymbol{\psi}_2 & \dots & \boldsymbol{\psi}_k \end{bmatrix}$ is a transformation matrix constructed using the Ritz-vectors, and $\mathbf{q} = \begin{bmatrix} q_1 & q_2 & \dots & q_k \end{bmatrix}^{\mathrm{T}}$ are the corresponding set of generalized coordinates. Further, it is assumed that the number of assumed modes is less than the number of physical DOFs, thus, $k \ll n$. Accordingly, the system size is reduced by replacing the physical DOFs by a reduced set of generalized coordinates.

By substituting Eq. 3.2 into Eq. 2.25 and pre-multiplying with $\boldsymbol{\Psi}^{\mathrm{T}}$ the reduced system is given by:

$$\tilde{\mathbf{M}}\ddot{\mathbf{q}} + \tilde{\mathbf{C}}\dot{\mathbf{q}} + \tilde{\mathbf{K}}\mathbf{q} = \tilde{\mathbf{p}} \tag{3.3}$$

where

$$\tilde{\mathbf{M}} = \boldsymbol{\Psi}^{\mathrm{T}}\mathbf{M}\boldsymbol{\Psi}, \quad \tilde{\mathbf{C}} = \boldsymbol{\Psi}^{\mathrm{T}}\mathbf{C}\boldsymbol{\Psi}, \quad \tilde{\mathbf{K}} = \boldsymbol{\Psi}^{\mathrm{T}}\mathbf{K}\boldsymbol{\Psi}, \quad \tilde{\mathbf{p}} = \boldsymbol{\Psi}^{\mathrm{T}}\mathbf{p}.$$

Here, $\tilde{\mathbf{M}}$, $\tilde{\mathbf{C}}$, and $\tilde{\mathbf{K}}$ are the $k \times k$ reduced system matrices and $\tilde{\mathbf{p}}$ is the $k \times 1$ reduced load vector. The linearly independent mode shapes form a reduction basis, in which the response, i.e. the modal amplitudes, are represented by generalized (or modal) coordinates. Hence, the reduction can be interpreted as a projection of the system equations onto a subspace, thus, a reduction is achieved be means of a *subspace projection*. This projective reduced order modeling technique is the basis in many of the methods considered in this work.

The reduced system matrices, as introduced above, are generally not diagonal, i.e., in contrast to the modal mass and stiffness matrices introduced in Section 2.3. This follows from the fact that the reduction basis is not constructed using eigenmodes of the full-order system (cf. Eq. 2.27). However, the eigenmodes can be approximated by means of a reduced eigenvalue problem in the space of the assumed modes, given as:

$$\tilde{\mathbf{K}}\mathbf{Z} = \tilde{\mathbf{M}}\mathbf{Z}\boldsymbol{\Lambda} \tag{3.4}$$

where $\boldsymbol{\Lambda}$ is a diagonal matrix containing pseudo-frequencies, and $\mathbf{Z}$ contains the associated eigenvectors (or pseudo-modes), being normalized in order that $\mathbf{Z}^{\mathrm{T}}\tilde{\mathbf{M}}\mathbf{Z} = \mathbf{I}$. Then, a set

of reduction basis vectors being stiffness-orthogonal and mass-orthonormal is given by $\tilde{\mathbf{\Psi}} = \mathbf{\Psi}\mathbf{Z}$. The approximate pseudo-frequencies are usually upper bound eigenfrequencies, and approaches the exact value when k is increased [12].

The orthogonal basis vectors $\tilde{\mathbf{\Psi}}$, which are linear combinations of the assumed Ritz-vectors $\mathbf{\Psi}$, can be employed to form a reduced order system, in accordance with Eq. 3.3. Because the reduction basis is orthogonal, the reduced system can be analyzed using any of the mode superposition methods discussed in Section 2.5.1.

The procedure using assumed mode shapes may not be feasible for analyzing general structures. Particularly for complex FE models, it is difficult to select appropriate mode shapes. This problem is further addressed in the following sections, where various techniques for generating reduction bases are discussed.

Finally, it is of interest to compare Eqs. 2.15 and 3.2, which illustrate the similarity between the projective reduced order modeling approach, as introduced above, and the FE method. Thus, in the FE framework, the infinite solution space is approximated using a finite set of shape functions, leading to a semi-discretized MDOF system. On the other hand, by introducing the transformation Eq. 3.2, the number of DOFs is reduced by assuming that the solution can be represented in a subspace of the solution space of the full-order MDOF system. Two observations can be made. Firstly, the approaches are similar in that an approximate solution is introduced by projecting the system onto a subspace, and, secondly, that the reduced order modeling technique can theoretically be applied directly on the infinite solution space. However, to avoid evaluating integrals (cf. Eqs. 2.18–2.20) involving complicated global shape functions, it is convenient to first establish a space discretization by means of an FE model, which is then reduced in a subsequent step by applying a reduction basis. In particular, as will be further described in Sections 3.2–3.6, the FE model can then be used both for identifying the reduction basis vectors as well as determining the reduced order system matrices.

3.2 MODAL TRUNCATION

The modal expansion of linear MDOF systems was introduced in Section 2.3. As mentioned previously, this allows for diagonalizing the system matrices enabling the use of highly efficient solution methods. Furthermore, by use of a modal truncation, the dynamic response can be approximated by considering a reduced set of low-frequency eigenmodes, i.e., the displacements are approximated as:

$$\mathbf{u} \approx \sum_{j=1}^{k} \boldsymbol{\phi}_j q_j. \tag{3.5}$$

Hence, the responses of the discarded modes $\boldsymbol{\phi}_j$ ($j = k+1, k+2, \ldots, n$) are neglected. This approach is sometimes also referred to as the modal displacement method (MDM). As will be shown next, the accuracy of the MDM can be further improved by use of the mode acceleration (MA) method.

Furthermore, it should be noted that, for large FE models, solving the full-order eigenvalue problem can be computationally expensive. Then, an alternative is to adopt the Rayleigh–Ritz method for approximating the eigenmodes, as described in Section 3.1. Moreover, in Section 3.5, alternative approaches using Krylov-subspaces are introduced, which can be utilized for reducing the computational effort, as well as improving the model accuracy.

3.3 MODE ACCELERATION METHOD

If the eigenfrequencies of the discarded modes ω_j are significantly higher than the forcing frequency ω, which in general is the case, it is reasonable to assume that the responses of these modes are essentially static. Hence, if $\omega_j \gg \omega$ the dynamic response of mode j can be approximated based on the corresponding quasi-static response (for comparison, consider an SDOF system subjected to a forcing frequency much lower than the natural frequency). This is the essence of the mode-acceleration (MA) method [12]. The concept can be described as follows.

The equation of motion for an undamped system may be written as:

$$\mathbf{M}\ddot{\mathbf{u}} + \mathbf{K}\mathbf{u} = \mathbf{M}\boldsymbol{\Phi}\ddot{\mathbf{q}} + \mathbf{K}\mathbf{u} = \mathbf{p} \tag{3.6}$$

where $\ddot{\mathbf{q}}$ contains the complete set of n modal accelerations. Further, Eq. 3.6 may be rewritten as:

$$\mathbf{u}(t) = \mathbf{K}^{-1}\left(\mathbf{p} - \mathbf{M}\boldsymbol{\Phi}\ddot{\mathbf{q}}\right). \tag{3.7}$$

If the eigenmodes are mass-normalized, the spectral expansion of the inverse stiffness matrix is given by:

$$\mathbf{K}^{-1} = \boldsymbol{\Phi}\tilde{\mathbf{K}}^{-1}\boldsymbol{\Phi}^{\mathrm{T}} = \sum_{j=1}^{n} \frac{\boldsymbol{\phi}_j \boldsymbol{\phi}_j^{\mathrm{T}}}{\omega_j^2}. \tag{3.8}$$

(This expression will be useful in the derivation of the MA method, according to below, as well as in the methodologies investigated in Sections 3.4 and 3.6.)

Substituting Eq. 3.8 into Eq. 3.7 and rearranging the terms yields:

$$\mathbf{u}(t) = \mathbf{K}^{-1}\mathbf{p} - \boldsymbol{\Phi}\tilde{\mathbf{K}}^{-1}\boldsymbol{\Phi}^{\mathrm{T}}\mathbf{M}\boldsymbol{\Phi}\ddot{\mathbf{q}} = \mathbf{K}^{-1}\mathbf{p} - \boldsymbol{\Phi}\tilde{\mathbf{K}}^{-1}\ddot{\mathbf{q}} = \mathbf{K}^{-1}\mathbf{p} - \sum_{j=1}^{n} \frac{\ddot{q}_j}{\omega_j^2}\boldsymbol{\phi}_j. \tag{3.9}$$

Now, assume that the dynamic response is only computed for the first k modes, then

$$\mathbf{u}(t) \approx \mathbf{K}^{-1}\mathbf{p} - \sum_{j=1}^{k} \frac{\ddot{q}_j}{\omega_j^2}\boldsymbol{\phi}_j. \tag{3.10}$$

The above expression is thus employed in the MA method, where the first term in Eq. 3.10 can be interpreted as the pseudo-static response modified by the second term to obtain the dynamic response.

The mode-acceleration method may be derived in a slightly different manner using an approach referred to as the *static correction method*. Even though both methods are referred to in the literature, the MA method and the static correction method are in fact equivalent, i.e., both methods provide the exact same results [12]. The only difference lies in how the expressions are derived (except for, possibly, differences due to numerical round-off errors in a numerical implementation). Here, however, the alternative formulation employed in the static correction method will be useful in Sections 3.4 and 3.6, namely, in a derivation of the (generalized) modal truncation augmentation method as well as certain DS methods discussed in Chapter 5.

In the static correction method, the displacements are expressed as:

$$\mathbf{u}(t) \approx \sum_{j=1}^{k} (\boldsymbol{\phi}_j q_j) + \mathbf{u}_{\text{cor}} \tag{3.11}$$

where $\mathbf{u}_{\text{cor}}$ is a static correction vector. Furthermore, by substituting the inverse stiffness matrix in Eq. 3.10 with its spectral expansion (Eq. 3.8), and separating the summation, the following expression is obtained:

$$\mathbf{u}(t) \approx \left(\sum_{j=1}^{k} \frac{\boldsymbol{\phi}_j \boldsymbol{\phi}_j^{\mathrm{T}}}{\omega_j^2} + \sum_{j=k+1}^{n} \frac{\boldsymbol{\phi}_j \boldsymbol{\phi}_j^{\mathrm{T}}}{\omega_j^2} \right) \mathbf{p} - \sum_{j=1}^{k} \frac{\ddot{q}_j}{\omega_j^2} \boldsymbol{\phi}_j. \tag{3.12}$$

Further, recall that $\ddot{q}_j + q_j \omega_j^2 = \boldsymbol{\phi}_j^{\mathrm{T}} \mathbf{p}$ (cf. Eq. 2.36), thus:

$$\sum_{j=1}^{k} \boldsymbol{\phi}_j q_j = \sum_{j=1}^{k} \frac{\boldsymbol{\phi}_j \boldsymbol{\phi}_j^{\mathrm{T}}}{\omega_j^2} \mathbf{p} - \sum_{j=1}^{k} \frac{\ddot{q}_j(t)}{\omega_j^2} \boldsymbol{\phi}_j. \tag{3.13}$$

Substituting Eq. 3.13 into Eq. 3.12 yields:

$$\mathbf{u}(t) \approx \sum_{j=1}^{k} \boldsymbol{\phi}_j q_j + \sum_{j=k+1}^{n} \frac{\boldsymbol{\phi}_j \boldsymbol{\phi}_j^{\mathrm{T}}}{\omega_j^2} \mathbf{p} \tag{3.14}$$

Thus, by comparing Eq. 3.14 and Eq. 3.11, it follows that the correction vector is given by:

$$\mathbf{u}_{\text{cor}} = \sum_{j=k+1}^{n} \frac{\boldsymbol{\phi}_j \boldsymbol{\phi}_j^{\mathrm{T}}}{\omega_j^2} \mathbf{p}. \tag{3.15}$$

However, the above expression can rarely be used in practice, because a computation of all n eigenmodes is generally not feasible. Therefore, using Eq. 3.8, the following alternative expression may be utilized:

$$\mathbf{u}_{\text{cor}} = \left(\mathbf{K}^{-1} - \sum_{j=1}^{k} \frac{\boldsymbol{\phi}_j \boldsymbol{\phi}_j^{\mathrm{T}}}{\omega_j^2} \right) \mathbf{p}. \tag{3.16}$$

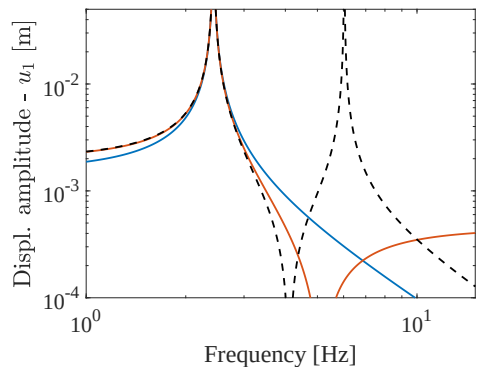

(a)

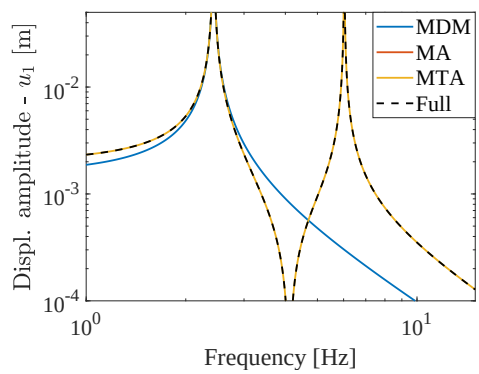

(b)

Figure 3.1: Example of harmonic response (sine sweep) for an undamped two-DOF model, as shown in Figure 3.2a. The stiffness and mass are set to $k = 1000$ N/m and $m = 1$ kg, respectively, and the external force is $p_0 = 1$ N (cf. Figure 3.2a). The displacement amplitude in DOF 1 is shown for the MA method (a), and the MTA method (b) (cf. Section 3.4). The first normal mode is considered. For comparison, the response is presented for the full model and the MDM method (cf. Section 3.2). Notice that, in this case, the response provided by the MTA method is identical to the full order response; thus the MTA basis span the full solution.

In Figure 3.1a, the response of the undamped two-DOF model, shown in Figure 3.2a, due to harmonic loading (sine sweep) is presented for the MA method and the MDM method, respectively. The dynamic response of the first normal mode is considered. For comparison, the response is also presented for the full model. As manifested by the results, the quasi-static response is fully captured if adopting the MA method. The same is not true for the MDM method, which follows from the fact that the static displacements cannot be fully resolved by a single eigenmode. Further, as shown in the figure, the second resonance is neither captured by the MDM method nor the MA method.

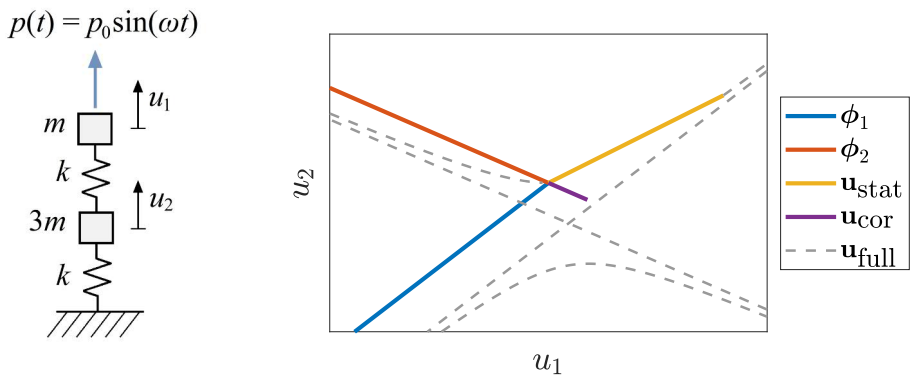

Figure 3.2: Two-DOF system (a) and example of a static correction vector $\mathbf{u}_{\text{cor}}$ (b). The vectors ϕ_1 and ϕ_2 indicate the directions of the normal modes, and $\mathbf{u}_{\text{static}}$ and $\mathbf{u}_{\text{cor}}$ are the static displacement and static correction vectors, respectively. The dashed line indicate the displacement response of the full model, given by $\mathbf{u}_{\text{full}}(\omega) = \left(\mathbf{K} - \omega^2\mathbf{M}\right)^{-1}\mathbf{p}_0$.

The static correction vector $\mathbf{u}_{\text{cor}}$ is illustrated in Figure 3.2b. The dashed gray line corresponds to the full order solution, i.e., where both eigenmodes are considered. Note that the response of the second mode is indeed essentially static for a forcing frequency close to the first resonance. As indicated by the figure, both eigenmodes are needed in the MDM approach to fully resolve the static displacements.

3.4 MODAL TRUNCATION AUGMENTATION

In the MA method, the quasi-static response of the discarded modes are considered in the dynamic analysis. An alternative is to employ the modal truncation augmentation (MTA) method [18], where the eigenmodes are augmented by additional modes generated based on the spatial distribution of the external force.

The MTA method is useful if the external load can be decomposed into a set of m time-independent spatial load vectors, which usually is the case. Thus, the external force vector is then expressed as:

$$\mathbf{p}(t) = \sum_{j=1}^{m} \mathbf{p}_j \alpha_j(t) = \mathbf{P}\alpha(t) \tag{3.17}$$

where $\mathbf{P}$ is a $n \times m$ matrix containing the spatial load vectors and $\alpha(t)$ contains the corresponding time functions. Then, similar to the static correction method (cf. Eq. 3.16), a set of

correction modes can be generated as:

$$\mathbf{X}_{\text{cor}} = \left(\mathbf{K}^{-1} - \sum_{j=1}^{k} \frac{\boldsymbol{\phi}_j \boldsymbol{\phi}_j^{\text{T}}}{\omega_j^2} \right) \mathbf{P}. \tag{3.18}$$

which are mass- and stiffness orthogonal with respect to the retained eigenmodes. Further, the additional basis vectors $\mathbf{X}_{\text{cor}}$ can be made mutually orthogonal by use of a reduced eigenvalue problem, expressed as (cf. Eq. 3.4):

$$\left(\mathbf{X}_{\text{cor}}^{\text{T}} \mathbf{K} \mathbf{X}_{\text{cor}} \right) \mathbf{Z} = \left(\mathbf{X}_{\text{cor}}^{\text{T}} \mathbf{M} \mathbf{X}_{\text{cor}} \right) \mathbf{Z} \boldsymbol{\Lambda} \tag{3.19}$$

where, again, $\boldsymbol{\Lambda}$ and $\mathbf{Z}$ contain pseudo-frequencies and pseudo-modes of the reduced eigenvalue problem. Thus, an orthogonal basis, which span the original correction modes, can be determined as $\tilde{\mathbf{X}}_{\text{cor}} = \mathbf{X}_{\text{cor}} \mathbf{Z}$. A reduction basis including eigenmodes and correction modes can then be constructed as:

$$\boldsymbol{\Psi}_{\text{MTA}} = \begin{bmatrix} \boldsymbol{\Phi} & \tilde{\mathbf{X}}_{\text{cor}} \end{bmatrix} \tag{3.20}$$

which can be applied in a standard fashion to obtain a reduced order model (cf. Eq. 3.3). Orthogonalizing the basis improves the numerical robustness. Furthermore, the reduced system will be fully decoupled. Thus, for linear models, the dynamic response can be obtained using the mode superpositions methods described in Section 2.5.1.

The MTA is similar to the MA method in that it considers the quasi-static response of the discarded modes. However, in the MTA method, the modal basis is enriched by additional Ritz-vectors. Hence, additional generalized coordinates are considered in the dynamic response analysis. For instance, if a single eigenmode is considered for the two-DOF system illustrated in Figure 3.2a, the MTA method result in an additional basis vector that coincides with the direction of the static correction vector $\mathbf{u}_{\text{cor}}$. Accordingly, as manifested by the results presented in Figure 3.2b, the response of the two-DOF model is fully captured; i.e., the MTA basis span the full order solution. The MTA method is, thus, more accurate than the MA method, which is also demonstrated by the numerical investigations in [19]. However, because additional coordinates are introduced, the computational online cost can be expected to be somewhat larger. Furthermore, in contrast to the MA method, the MTA method is restricted to load cases where the external force can be decomposed into time-independent spatial load vectors (cf. Eq. 3.17).

3.5 KRYLOV-SUBSPACE METHODS

Despite the great utility of modal expansion techniques and the wide range of applications, there are some drawbacks when employed for reducing the number of system variables. Firstly, solving the full-order eigenvalue problem for large systems can be computationally expensive and, secondly, information related to the spatial distribution of the load is not considered (i.e., if not adopting the MA or MTA methods). Furthermore, a basis constructed using modal

truncation may include eigenmodes that are not important for the specific load case. For example, consider again the simply supported beam in Figure 2.2a. Indeed, anti-symmetric eigenmodes, having zero displacement at midspan, cannot be excited by the external pressure and, consequently, the solution accuracy will not be improved by including these eigenmodes in the reduction basis.

An alternative to a reduction using a truncated set of full-order eigenmodes is the so-called Krylov-subspace methods, which do consider the spatial distribution of the load and, moreover, are computationally efficient. As shown in the derivation below, the basis vectors can be computed by matrix–vector multiplications. In contrast, an eigenvalue problem must be solved for determining the eigenmodes.

In a structural dynamics context, the Krylov-vectors can be interpreted as the displacements due to quasi-static loads and, accordingly, the modes are sometimes referred to as *static correction modes* [20]. This naming convention is also useful in an attempt to demonstrate how the Krylov-subspace methods are related to the MA and MTA method, as described in Sections 3.3 and 3.4, as well as the generalized MTA method, which will be introduced in Section 3.6. In the following, the static correction modes are derived based on the approach presented in [21].

Neglecting damping, the equation of motion can be written as:

$$\mathbf{M}\ddot{\mathbf{u}} + \mathbf{K}\mathbf{u} = \mathbf{p}. \tag{3.21}$$

Further, the displacement can be split into a static and dynamic part:

$$\mathbf{u} = \mathbf{u}_{\text{stat}} + \mathbf{y}. \tag{3.22}$$

By setting the acceleration to zero in Eq. 3.21, the static response is given by $\mathbf{u}_{\text{stat}} = \mathbf{K}^{-1}\mathbf{p}$. Further, substituting Eq. 3.22 into Eq. 3.21, an expression similar to Eq. 3.22 is obtained for $\mathbf{y}$, namely

$$\mathbf{M}\ddot{\mathbf{y}} + \mathbf{K}\mathbf{y} = -\mathbf{M}\mathbf{K}^{-1}\ddot{\mathbf{p}}. \tag{3.23}$$

This procedure can be continued by splitting $\mathbf{y}$ into a static and dynamic part $\mathbf{z}$, i.e.

$$\mathbf{y} = \mathbf{y}_{\text{stat}} + \mathbf{z}. \tag{3.24}$$

The quasi-static solution is then given by

$$\mathbf{y}_{\text{stat}} = \mathbf{K}^{-1}\left(-\mathbf{M}\mathbf{K}^{-1}\right)\ddot{\mathbf{p}}. \tag{3.25}$$

In a similar manner, substituting Eq. 3.24 into Eq. 3.23 yields:

$$\mathbf{M}\ddot{\mathbf{z}} + \mathbf{K}\mathbf{z} = \left(-\mathbf{M}\mathbf{K}^{-1}\right)^2 \frac{\mathrm{d}^4\mathbf{p}}{\mathrm{d}t^4}. \tag{3.26}$$

Thus, the response is given by a sequence of quasi-static solutions:

$$\mathbf{u} = \mathbf{u}_{\text{stat}} + \mathbf{y}_{\text{stat}} + \mathbf{z}_{\text{stat}} + \dots \tag{3.27}$$

Hence, a recursive procedure is obtained, indicating that the dynamic response can be approximated as

$$\mathbf{u} \approx \sum_{j=1}^{k} \mathbf{K}^{-1} \left(-\mathbf{M}\mathbf{K}^{-1}\right)^{j-1} \frac{\mathrm{d}^{2(j-1)}\mathbf{p}}{\mathrm{d}t^{2(j-1)}} \tag{3.28}$$

where k is the number of static corrections. Furthermore, the higher order derivatives can be treated as separate DOFs. Hence, instead of computing a sequence of static corrections, a dynamic response analysis is conducted by means of generalized coordinates representing the amplitudes of quasi-static modes. However, for this technique to be meaningful, the spatial variation of the load must be time-independent in some manner. Hence, such that the external load can be decomposed into a set of m spatial load vectors in accordance with Eq. 3.17.

Then, the set of j-th order static correction modes are given by:

$$\mathbf{X}_{\mathrm{cor},j} = \mathbf{K}^{-1} \left(\mathbf{M}\mathbf{K}^{-1}\right)^{j-1} \mathbf{P}. \tag{3.29}$$

where, again, the columns of $\mathbf{P}$ are a set of spatial load vectors. Further, the generated correction modes can be collected in a matrix:

$$\mathbf{\Psi}_{\mathrm{cor}} = \begin{bmatrix} \mathbf{X}_{\mathrm{cor},1} & \mathbf{X}_{\mathrm{cor},2} & \dots & \mathbf{X}_{\mathrm{cor},k} \end{bmatrix} \tag{3.30}$$

where $\mathbf{\Psi}_{\mathrm{cor}}$ is a $n \times (k \cdot m)$ matrix including static correction modes. Due to the consideration of the external force in the derivation, the static correction modes are often referred to as load-dependent vectors. Further, to avoid numerical round-off errors, the correction modes may be generated using the modified Gram–Schmidt orthogonalization procedure [12,22]. Moreover, by solving a small eigenvalue problem, the basis $\mathbf{\Psi}_{\mathrm{cor}}$ can be replaced by a corresponding set of mass- and stiffness-orthogonal basis vectors. Thus, by using Eq. 3.4, the orthogonal basis is given as $\tilde{\mathbf{\Psi}}_{\mathrm{cor}} = \mathbf{\Psi}_{\mathrm{cor}}\mathbf{Z}$, where $\mathbf{Z}$ contains the pseudo-modes of the reduced eigenvalue problem.

Now, by introducing a transformation in a standard manner, the physical displacements are approximated as:

$$\mathbf{u} \approx \tilde{\mathbf{\Psi}}_{\mathrm{cor}}\boldsymbol{\eta} \tag{3.31}$$

where $\boldsymbol{\eta} = \begin{bmatrix} \eta_1 & \eta_2 & \dots & \eta_k \end{bmatrix}^{\mathrm{T}}$ are the generalized coordinates, corresponding to the correction mode amplitudes. Finally, a reduced system is obtained by setting $\mathbf{\Psi} = \tilde{\mathbf{\Psi}}_{\mathrm{cor}}$ in Eq. 3.3.

The first order correction modes simply correspond to the static displacement of the external force patterns. As indicated by Eq. 3.29, the jth-order static modes can be interpreted as displacements due to inertia forces associated to the set of $(j-1)$th-order static modes (cf. Figure 3.3). Furthermore, note that the sequence of correction vectors form a so-called block-Krylov subspace, given by:

$$\mathcal{K}_r(\mathbf{K}^{-1}\mathbf{M}; \mathbf{K}^{-1}\mathbf{P}) = \mathrm{span}\left(\mathbf{K}^{-1}\mathbf{P}, (\mathbf{K}^{-1}\mathbf{M})\mathbf{K}^{-1}\mathbf{P}, \dots, (\mathbf{K}^{-1}\mathbf{M})^{r-1}\mathbf{K}^{-1}\mathbf{P}\right). \tag{3.32}$$

Krylov subspace methods originating from system and control (e.g., see [23, 24]) are thus closely related to the technique using higher-order static corrections, as introduced above.

(a) 1st static correction mode (b) 2nd static correction mode

Figure 3.3: Example of static correction modes and corresponding load distributions, derived from an uniform external pressure.

3.6 GENERALIZED MODAL TRUNCATION AUGMENTATION

The MA method can be generalized to include higher order corrections, referred to as the *generalized* MA method [20]. In fact, the higher order corrections can be derived in a manner similar to the force-dependent Krylov vectors discussed in Section 3.5. Notice that setting $k = 1$ in Eq. 3.28 correspond to the pseudo-static solution, which in turn is equal to the static correction provided by Eq. 3.16 if the modal responses are neglected. Furthermore, if including k modal responses, it follows that the higher order corrections can be computed as:

$$\mathbf{u}_{\text{cor},\,j} = \left(\mathbf{K}^{-1} - \sum_{j=1}^{k} \frac{\boldsymbol{\phi}_j \boldsymbol{\phi}_j^{\mathrm{T}}}{\omega_j^2} \right) \left(-\mathbf{M}\mathbf{K}^{-1} \right)^{j-1} \frac{\mathrm{d}^{2(j-1)}\mathbf{p}}{\mathrm{d}t^{2(j-1)}}. \tag{3.33}$$

Hence, the response is approximated as

$$\mathbf{u}(t) \approx \sum_{s}^{k} \boldsymbol{\phi}_s q_s(t) + \sum_{j}^{l} \mathbf{u}_{\text{cor},\,j} \tag{3.34}$$

where l is the static correction order. Note that setting $l = 1$ in Eq. 3.34 indeed provides an expression equivalent to the static correction method.

Calculating the higher order derivatives of the forcing, included in Eq. 3.33, might be inconvenient (or not even possible). However, instead of computing the higher order derivatives, the truncated modal matrix can be augmented by higher order correction modes, i.e., similar to the procedure used in the MTA method as well as the Krylov-subspace method (cf. Sections 3.4 and 3.5). Hence, the idea is to utilize higher order correction vectors as additional Ritz-vectors. This approach is known as generalized Modal Truncation Augmentation (g-MTA) [20].

The set of jth-order correction modes are then given by:

$$\mathbf{X}_{\text{cor},j} = \left(\mathbf{K}^{-1} - \sum_{j=1}^{k} \left(\frac{\boldsymbol{\phi}_j \boldsymbol{\phi}_j^{\mathrm{T}}}{\omega_j^2} \right) \right) \left(\mathbf{M}\mathbf{K}^{-1} \right)^{j-1} \mathbf{P} \tag{3.35}$$

which are both mass- and stiffness-orthogonal to the retained eigenmodes. Further, to avoid numerical round-off errors, the correction vectors may be generated using the modified Gram–Schmidt orthogonalization procedure, as discussed in Section 3.5.

The generated correction vectors can be collected in a matrix:

$$\bar{\mathbf{X}}_{\text{cor}} = \begin{bmatrix} \mathbf{X}_{\text{cor},1} & \mathbf{X}_{\text{cor},2} & \dots & \mathbf{X}_{\text{cor},l} \end{bmatrix}. \tag{3.36}$$

Then, the set of correction vectors can be further orthogonalized by means of a reduced eigenvalue problem, i.e., in a manner similar to the procedure in Sections 3.4 (also see [20, 21]). Hence, by replacing $\mathbf{X}_{\text{cor}}$ with $\bar{\mathbf{X}}_{\text{cor}}$ in Eq. 3.19, the orthogonalized vectors are given as $\hat{\mathbf{X}}_{\text{cor}} = \bar{\mathbf{X}}_{\text{cor}}\mathbf{Z}$, where, again, $\mathbf{Z}$ contains the pseudo-modes of the reduced eigenvalue problem.

A reduction basis can now be constructed using the retained eigenmodes and the orthogonalized higher order correction modes, as:

$$\boldsymbol{\Psi}_{\text{g-MTA}} = \begin{bmatrix} \boldsymbol{\Phi} & \hat{\mathbf{X}}_{\text{cor}} \end{bmatrix}. \tag{3.37}$$

Finally, a reduced system can be generated by replacing $\boldsymbol{\Psi}$ with $\boldsymbol{\Psi}_{\text{g-MTA}}$ in Eq. 3.3. Note that, due to the orthogonality properties of the basis, the reduced system will be fully decoupled. Thus, as for the basis generation methods discussed previously, the dynamic response of linear systems can be obtained using any of the mode superposition methods described in Section 2.5.1.

4 Reduced order modeling of geometrically nonlinear systems

In Chapter 3, linear systems were considered, and, accordingly, the reduced order models were developed based on the linear semi-discretized equations of motion, which assumes small displacements and linear elastic materials. However, if the deformations can no longer be considered small, due to the internal stresses being rotated with respect to the undeformed configuration, it can be necessary to consider geometric nonlinearity. Hence, the discretized dynamic problem is then expressed in terms of the nonlinear equations of motion, Eq. 2.21.

In the following, focus is on geometric nonlinearity due to large displacements and small strains. Further, it is assumed that linear elastic constitutive laws can be adopted. In this regard, thin-walled structures are critical, where the response is typically influenced by bending–stretching coupling effects resulting in a geometrically nonlinear behavior.

4.1 EQUATIONS OF MOTION FOR GEOMETRICALLY NONLINEAR SYSTEMS

The nonlinear semi-discretized equations of motion for an MDOF system, e.g., formulated using the FE method are given by Eq. 2.21 (restated here for convenience):

$$\mathbf{M}\ddot{\mathbf{u}}(t) + \mathbf{C}\dot{\mathbf{u}}(t) + \mathbf{f}(\mathbf{u}(t)) = \mathbf{p}(t). \tag{4.1}$$

Similar to the modal techniques commonly used in linear structural dynamics (cf. Chapter 3), a reduced order model can be formulated by projecting the system equations onto a reduction basis. Hence, the physical displacements can be approximated as:

$$\mathbf{u}(t) \approx \mathbf{V}\boldsymbol{\eta}(t) \tag{4.2}$$

where $\mathbf{V}$ is a $n \times m$ reduction basis and $\boldsymbol{\eta}$ is a $m \times 1$ vector containing the associated generalized coordinates, and where $m \ll n$. Thus, the physical displacement field is approximated as a linear combination of the reduction basis vectors, which constitute the columns of $\mathbf{V}$.

Now, substituting Eq. 4.2 into Eq. 4.1 gives (henceforth, time-dependencies are left out for compactness):

$$\mathbf{M}\mathbf{V}\ddot{\boldsymbol{\eta}} + \mathbf{C}\mathbf{V}\dot{\boldsymbol{\eta}} + \mathbf{f}(\mathbf{V}\ddot{\boldsymbol{\eta}}) = \mathbf{p} + \mathbf{r} \tag{4.3}$$

where $\mathbf{r}$ is the residual force vector, compensating for the discrepancy between the full-order solution and the approximate response spanned by the reduction basis vectors.

Next, a Galerkin projection may be considered where the error is forced to be orthogonal to the reduction basis, i.e., similar to the approach employed in the FE discretization described in Section 2.2, thus (e.g., see [2, 3]):

$$\mathbf{V}^{\mathrm{T}}\mathbf{r} = \mathbf{0}. \tag{4.4}$$

Hence, by pre-multiplying with the transpose of the reduction basis, Eq. 4.3 can be rewritten as:

$$\tilde{\mathbf{M}}\ddot{\boldsymbol{\eta}} + \tilde{\mathbf{C}}\dot{\boldsymbol{\eta}} + \tilde{\mathbf{f}} = \tilde{\mathbf{p}} \tag{4.5}$$

where

$$\tilde{\mathbf{M}} = \mathbf{V}^{\mathrm{T}}\mathbf{M}\mathbf{V}, \quad \tilde{\mathbf{C}} = \mathbf{V}^{\mathrm{T}}\mathbf{C}\mathbf{V}, \quad \tilde{\mathbf{f}} = \mathbf{V}^{\mathrm{T}}\mathbf{f}(\mathbf{V}\boldsymbol{\eta}), \quad \tilde{\mathbf{p}} = \mathbf{V}^{\mathrm{T}}\mathbf{p}.$$

Here, $\tilde{\mathbf{M}}$ and $\tilde{\mathbf{C}}$ are the $m \times m$ reduced mass and damping matrices. Further, $\tilde{\mathbf{f}}$ and $\tilde{\mathbf{p}}$ are the $m \times 1$ reduced restoring force and external force vectors, respectively. A nonlinear reduced order model, given by Eq. 4.5, can thus be established. Nevertheless, in order to achieve a model that is both accurate and computationally efficient, two main challenges still exist, as will be described as follows.

Firstly, an appropriate basis selection technique is needed. In particular, the geometrically nonlinear response generally involves modes with eigenfrequencies far above the frequency content of the forcing. For instance, in an analysis of the geometrically nonlinear response of flat structures, the reduction basis typically has to be enriched by in-plane (membrane) modes, as exemplified for a cantilever beam in Figure 4.1. Here, it should be emphasized that, to ensure sufficient accuracy of the basis, additional in-plane modes is required regardless of the forcing frequency; i.e., the in-plane motion must be adequately resolved in both static and dynamic analyses. This is thus a fundamental difference to the requirements of reduction bases applied in linear dynamics applications. Hence, for static loading, the linear response can be fully resolved by a single mode shape, namely, corresponding to the static displacement field $\mathbf{u} = \mathbf{K}^{-1}\mathbf{p}$. On the other hand, the geometrically nonlinear displacement field due to static loading is amplitude dependent, why several modes might be needed to obtain a sufficiently accurate approximation. Thus, in contrast to linear dynamics applications, bases constructed using a few low-frequency normal modes is generally not appropriate. This issue will be further discussed in Section 4.3, where various basis generation techniques are discussed.

The second problem concerns the evaluation of the reduced restoring force vector $\tilde{\mathbf{f}}$ (cf. Eq. 4.5). The transient dynamic response of the nonlinear system has to be solved using direct time-integration. Then, as described in Section 2.5.2, a time discretization is introduced, where equilibrium at each time point is typically enforced using Newton–Raphson iterations.

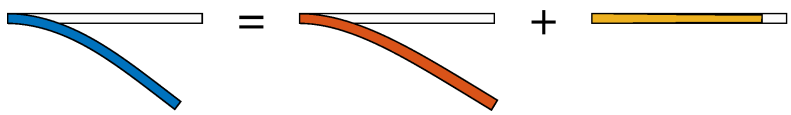

Figure 4.1: Example of approximation of the geometrically nonlinear deformation of a cantilever beam using a bending and membrane mode.

Consequently, the reduced restoring force vector (as well as the reduced tangent stiffness matrix) has to be constructed in several iterations, for each time point. As indicated by Eq. 4.5, this implies that the full-order internal forces must be generated and then projected onto the reduction subspace, i.e., the reduced restoring forces are computed based on the expression $\tilde{\mathbf{f}} = \mathbf{V}^{\mathrm{T}}\mathbf{f}(\mathbf{V}\boldsymbol{\eta})$. Hence, with regard to computational efficiency, a new bottleneck emerges due to that the internal force vector has to be generated based on the full-order displacement field. One way to address this issue is to utilize the polynomial structure of the nonlinear restoring forces, which is the approach adopted in this work. This concept will be further described in the next section. For the sake of completeness, it should be mentioned that other techniques have also been proposed for approximating the reduced internal forces, e.g., see [2, 3].

4.1.1 Polynomial structure of nonlinear internal forces

The reduced nonlinear restoring forces can be expressed by means of a Taylor series expansion around the point of equilibrium (e.g., $\boldsymbol{\eta} = \mathbf{0}$). In particular, if considering three terms, the following approximate expression is obtained:

$$\tilde{\mathbf{f}}(\boldsymbol{\eta}) \approx \frac{\partial \tilde{\mathbf{f}}}{\partial \boldsymbol{\eta}}\boldsymbol{\eta} + \frac{1}{2}\frac{\partial^2 \tilde{\mathbf{f}}}{\partial \boldsymbol{\eta}^2}\boldsymbol{\eta}\boldsymbol{\eta} + \frac{1}{6}\frac{\partial^3 \tilde{\mathbf{f}}}{\partial \boldsymbol{\eta}^3}\boldsymbol{\eta}\boldsymbol{\eta}\boldsymbol{\eta} = \mathbf{K}^{(1)}\boldsymbol{\eta} + \mathbf{K}^{(2)}\boldsymbol{\eta}\boldsymbol{\eta} + \mathbf{K}^{(3)}\boldsymbol{\eta}\boldsymbol{\eta}\boldsymbol{\eta} \tag{4.6}$$

where the compact tensor notation e.g. employed in [2, 25] is used. Further, $\mathbf{K}^{(1)} = \mathbf{V}^{\mathrm{T}}\mathbf{K}\mathbf{V}$ is the $m \times m$ reduced linear stiffness matrix, which can be obtained in a standard manner from the $n \times n$ linearized stiffness matrix $\mathbf{K} = \frac{\partial \mathbf{f}}{\partial \mathbf{u}}\Big|_{\mathbf{0}}$. Thus, if using the FE method for space discretization, the linear stiffness matrix can be determined from Eq. 2.24. In addition, $\mathbf{K}^{(2)}$ and $\mathbf{K}^{(3)}$, having sizes $m \times m \times m$ and $m \times m \times m \times m$, respectively, are higher order stiffness tensors which consider the nonlinear part of the reduced restoring forces. Methods for determining the coefficients of the higher order tensors, henceforth referred to as nonlinear stiffness coefficients (NSCs), are discussed in Section 4.2. (Note that the term *tensor* used here simply refers to a multidimensional array, i.e., in contrast to the tensors used in continuum mechanics, e.g., representing stresses and strains.)

By substituting Eq. 4.6 into Eq. 4.5, it follows that the reduced nonlinear equations of motion can be expressed, using index notation, as:

$$M_{r,ij}\ddot{\eta}_j + C_{r,ij}\dot{\eta}_j + K^{(1)}_{ij}\eta_j + K^{(2)}_{ijk}\eta_j\eta_k + K^{(3)}_{ijkl}\eta_j\eta_k\eta_l = g_{r,i}. \tag{4.7}$$

Hence, an NLROM is obtained that only involves the reduced set of generalized coordinates, and thus avoids evaluations of the nonlinear restoring forces based on the full-order displacement field. The tensors are fully symmetric, i.e., the indices i, j, k, l are fully interchangeable and in an numerical implementation only the unique values has to be considered.

The reduced nonlinear restoring forces can thus be approximated using a Taylor series in accordance with Eq. 4.6. Furthermore, if considering large displacements, while restricting the analysis to small strains and assuming a linear elastic constitutive law, it turns out that the approximation using multivariate cubic polynomials is "exact".

This property can be shown by expressing the continuous balance equations (cf. Section 2.2) in the undeformed (reference) configuration, as [11]:

$$\mathrm{div}(\mathbf{FS}) + \mathbf{b}^o - \rho^o\ddot{\bar{\mathbf{u}}} = \mathbf{0} \tag{4.8}$$

where $\mathbf{b}^o$ is the body force per unit volume and ρ^o is the material density in the undeformed configuration. Further, div is the divergence operator; specifically, the divergence of a tensor field $\mathbf{A}$ is given as $[\mathrm{div}(\mathbf{A})]_i = \sum_j \frac{\partial A_{ij}}{\partial x^o_j}$ $(i, j = 1, 2, 3)$. Moreover, $\mathbf{F}$ is the *deformation gradient*, given by:

$$\mathbf{F} = \mathbf{I} + \boldsymbol{\nabla}\bar{\mathbf{u}} \tag{4.9}$$

where $\mathbf{I}$ is the 3×3 identity matrix and $[\boldsymbol{\nabla}\bar{\mathbf{u}}]_{ij} = \frac{\partial \bar{u}_i}{\partial x^o_j}$ is the *displacement gradient*. Further, $\mathbf{S}$ is the second Piola–Kirchhoff stress tensor, which is related to the Cauchy stress as $\boldsymbol{\sigma} = \frac{\rho}{\rho^o}\mathbf{FSF}^T$. Hence, $\boldsymbol{\sigma}$ and $\mathbf{S}$ coincide for small displacements, since $\rho^o \approx \rho$ and $\mathbf{F} \approx \mathbf{I}$. The second Piola–Kirchhoff stress measure is conjugated with the Green–Lagrange strain. The Green–Lagrange strain tensor can be expressed in terms of the displacement gradient, as:

$$\mathbf{E} = \frac{1}{2}\left(\boldsymbol{\nabla}\bar{\mathbf{u}} + \boldsymbol{\nabla}^{\mathrm{T}}\bar{\mathbf{u}} + \boldsymbol{\nabla}^{\mathrm{T}}\bar{\mathbf{u}}\boldsymbol{\nabla}\bar{\mathbf{u}}\right). \tag{4.10}$$

Consider now a linear elastic constitutive law, given as:

$$\mathbf{S}_v = \mathbf{D}\mathbf{E}_v \tag{4.11}$$

where the constitutive matrix for isotropic elasticity $\mathbf{D}$ is given by Eq. 2.23, and the subscript v indicate the vector form of the stress and strain tensors (also known as the Voigt notation), i.e.:

$$\mathbf{S}_v^{\mathrm{T}} = \begin{bmatrix} S_{11} & S_{22} & S_{33} & S_{12} & S_{13} & S_{23} \end{bmatrix} \tag{4.12}$$

$$\mathbf{E}_v^{\mathrm{T}} = \begin{bmatrix} E_{11} & E_{22} & E_{33} & 2E_{12} & 2E_{13} & 2E_{23} \end{bmatrix}. \tag{4.13}$$

This is known as a St. Venant–Kirchhoff material which can be interpreted as a hyperelastic representation of a linear elastic material.

Next, assume that the continuous displacement field $\bar{\mathbf{u}}$ is discretized using the FE method (cf. Eq. 2.15). Then, by considering the constitutive law Eq. 4.11 and the expression for the Green–Lagrange strain Eq. 4.10, it can be shown that the second Piola–Kirchhoff stresses can be expressed as quadratic functions of the nodal displacements, i.e., $\mathbf{S} = \mathcal{O}(\mathbf{u}^2)$ (e.g., see [2, 26, 27]). Further, in accordance with Eq. 4.9, the deformation gradient can be expressed as a linear function of the nodal displacements, i.e., $\mathbf{F} = \mathcal{O}(\mathbf{u})$. By considering the balance relation Eq. 4.8, and noting that the nodal displacements $\mathbf{u}$ are linear functions of the generalized coordinates $\boldsymbol{\eta}$ (cf. Eq. 4.2), it follows that the reduced internal forces can be fully represented by cubic polynomials in the generalized coordinates $\boldsymbol{\eta}$, and, accordingly, the Taylor series (Eq. 4.6) is fully converged.

Note that the reduction basis is constructed using modes which are determined in the undeformed configuration. Thus, the reduced order model is indeed formulated using a total Lagrangian framework. Further, it should be emphasized that the cubic polynomials are exact in the sense that the reduced order response can be fully resolved, thus, the equations of motion given by Eqs. 4.5 and 4.7 are equivalent (if using the constitutive law Eq. 4.11). However, if the full order solution is not properly spanned by the reduction basis, i.e., if the residual $\mathbf{r}$ is not negligible, the reduced order model might still not be accurate.

The nonlinear equations of motion, as stated in Eq. 4.7, consider large displacements. However, because a St. Venant–Krichhoff material is assumed, the model can only be expected to be valid for small or medium strain levels. Thus, large rigid body rotations and translations are considered, whereas large strains is not. Furthermore, it should be noted that the size of the higher order stiffness tensors grows exponentially. Therefore, to ensure a computational efficient model, it is particularly important to keep the size of the reduction basis as small as possible. In this regard, it is crucial to employ a basis selection technique which excludes any redundant modes. Furthermore, for flat structures, several of the polynomial coefficients can be ignored, thus, leading to a more computationally efficient model. This will be further discussed in the next section.

4.1.2 Simplified form for flat structures

For transversely loaded flat structures, which are symmetric with respect to the middle plane, a simplified form of the polynomial expressions for the reduced restoring forces can be established, as will be demonstrated as follows.

First, note that the reduction basis for a flat structure can be divided into a set of out-of-plane and in-plane modes. In particular, a flat structure modeled using an FE shell model may be formulated such that the physical in-plane and out-of-plane displacements are fully decoupled (e.g., see [9]). Thus, the reduction basis can be written in partitioned form, as:

$$\mathbf{V} = \begin{bmatrix} \mathbf{V}_b & \mathbf{V}_m \end{bmatrix} \tag{4.14}$$

where subscripts b and m refer to out-of-plane *bending* and in-plane *membrane* modes, respectively. Here, the sizes of the matrices $\mathbf{V}_b$ and $\mathbf{V}_m$ are $n \times m_b$ and $n \times m_m$, respectively.

It follows that the generalized coordinate vector may be partitioned accordingly, as:

$$\boldsymbol{\eta} = \left[\begin{array}{cc} \mathbf{q}^{\mathrm{T}} & \mathbf{p}^{\mathrm{T}} \end{array} \right]^{\mathrm{T}} \tag{4.15}$$

where $\mathbf{q}$ and $\mathbf{p}$ are vectors including the associated bending and membrane coordinates, having sizes $m_b \times 1$ and $m_m \times 1$, respectively (notice the difference between the membrane coordinate vector $\mathbf{p}$ and the reduced external force vector $\tilde{\mathbf{p}}$).

In structural dynamics applications of transversely loaded thin structures, the membrane modes typically have resonance frequencies far above the frequency content of the forcing. Furthermore, the membrane modes are not explicitly excited by the transverse load. Thus, the external modal forcing on the in-plane coordinates is zero, and, accordingly, the membrane modes are only excited due to the nonlinear coupling between bending and membrane coordinates (cf. Eq. 4.7). Therefore, as demonstrated in [25, 28, 29], it can be reasonable to neglect the higher order stiffness coefficients of the in-plane coordinates. Furthermore, due to the symmetry of the restoring forces, all quadratic coefficients involving three bending coordinates are zero [29]. Thus, for flat structures $K^{(2)}_{ijk} = 0$ for all $i, j, k = 1, \ldots, m_b$.

It follows that the equations of motion for the bending coordinates can be expressed, using index notation, as:

$$\tilde{M}_{b,ij}\ddot{q}_j + \tilde{C}_{b,ij}\dot{q}_j + K^{(1)}_{b,ij}q_j + K^{(2)}_{bm,ijk}q_j p_k + K^{(3)}_{b,ijkl}q_j q_k q_l = \tilde{p}_{b,i} \tag{4.16}$$

and for the membrane coordinates:

$$\tilde{M}_{m,ij}\ddot{p}_j + \tilde{C}_{m,ij}\dot{p}_j + K^{(1)}_{m,ij}p_j + K^{(2)}_{mb,ijk}q_j q_k = 0 \tag{4.17}$$

where it is assumed that the membrane and bending modes are mass- and stiffness-orthogonal.

Similarly, if using the compact tensor notation, the equations of motion can be expressed schematically as:

$$\left[\begin{array}{cc} \tilde{\mathbf{M}}_b & \mathbf{0} \\ \mathbf{0} & \tilde{\mathbf{M}}_m \end{array} \right] \left[\begin{array}{c} \ddot{\mathbf{q}} \\ \ddot{\mathbf{p}} \end{array} \right] + \left[\begin{array}{cc} \mathbf{K}^{(1)}_b & \mathbf{0} \\ \mathbf{0} & \mathbf{K}^{(1)}_m \end{array} \right] \left[\begin{array}{c} \mathbf{q} \\ \mathbf{p} \end{array} \right] + \left[\begin{array}{c} \mathbf{K}^{(2)}_{bm}\mathbf{qp} + \mathbf{K}^{(3)}_b\mathbf{qqq} \\ \mathbf{K}^{(2)}_{mb}\mathbf{qq} \end{array} \right] = \left[\begin{array}{c} \tilde{\mathbf{p}}_b \\ \mathbf{0} \end{array} \right] \tag{4.18}$$

where the viscous damping has been excluded to simplify the notation. Here, the system matrices for the bending coordinates $\tilde{\mathbf{M}}_b$ and $\mathbf{K}^{(1)}_b$ have sizes $m_b \times m_b$. Further, $\mathbf{K}^{(2)}_{bm}$ have size $m_b \times m_b \times m_m$, and $\mathbf{K}^{(3)}_b$ have size $m_b \times m_b \times m_b \times m_b$. For the membrane coordinates, $\mathbf{M}_m$ and $\mathbf{K}^{(1)}_m$ have sizes $m_m \times m_m$, and $\mathbf{K}^{(2)}_{mb}$ have size $m_m \times m_b \times m_b$. Moreover, transverse loading is considered, i.e, the modal forcing on the membrane coordinates is zero.

4.1.3 Static condensation of membrane coordinates

As mentioned previously, the eigenfrequencies of the membrane modes are often significantly higher than the frequency content of the forcing. Therefore, it can be reasonable to neglect

inertia terms associated to the membrane coordinates (see e.g. [25, 28, 29]). Hence, the idea is similar to the concept used in the mode acceleration method, where the discarded modal responses are approximated based on the quasi-static response (cf. Section 3.3).

By neglecting the inertia terms in Eq. 4.17, it follows that the membrane coordinates can be expressed in terms of the bending coordinates:

$$p_j = -\left[K_m^{(1)}\right]_{jr}^{-1} K_{mb,rkl}^{(2)} q_k q_l. \tag{4.19}$$

Then, by substituting Eq. 4.19 into Eq. 4.16, the *condensed* equations of motion can be expressed as:

$$\tilde{M}_{b,ij}\ddot{q}_j + \tilde{C}_{b,ij}\dot{q}_j + K_{b,ij}^{(1)} q_j + \bar{K}_{b,ijkl}^{(3)} q_j q_k q_l = \tilde{p}_{b,i} \tag{4.20}$$

where

$$\bar{K}_{b,ijkl}^{(3)} = K_{b,ijkl}^{(3)} - K_{bm,ijr}^{(2)} \left[K_m^{(1)}\right]_{rs}^{-1} K_{mb,skl}^{(2)} \tag{4.21}$$

are the condensed stiffness coefficients. Note that the dynamic response of the condensed system is expressed solely in terms of the bending coordinates. However, the structure is not constrained in the in-plane direction, namely, the condensed stiffness coefficients are adjusted such that the quasi-static response of the membrane coordinates is considered implicitly.

As e.g. demonstrated in Papers D and E, the condensed system equations can, e.g., be used to accurately predict the response of flat plates supported on four sides. However, for cantilevered structures, the in-plane inertia generally affects the dynamic response, and, consequently, an analysis based on the condensed equations of motion can lead to erroneous results (on the other hand, an approach using the simplified form, Eq. 4.18, including the in-plane inertia terms, typically provide satisfactory results, e.g., see [29] and Paper D).

Finally, it should be noted that the procedure using static condensation of membrane coordinates, as introduced above, theoretically can be applied to any of the modes included in the reduction basis. Thus, the reason for restricting the static condensation to membrane coordinates is that this is motivated by the structural characteristics observed for transversely loaded flat structures. This aspect, and a generalization of the concept to consider slightly curved structures, is further discussed in Paper D, where reduction bases enriched by so-called static modal derivatives are investigated.

4.2 NONINTRUSIVE IDENTIFICATION OF NONLINEAR STIFFNESS COEFFICIENTS

As shown in Section 4.1, the reduced nonlinear restoring forces can be fully represented by multivariate cubic polynomials in modal coordinates. In fact, as e.g. demonstrated in [26,30], closed form expressions can be derived for the higher order stiffness tensors. However, this approach requires a space discretization using, e.g., the FE method, where expressions for the

higher order tensors are implemented on the element level. Therefore, the so-called *direct* approach for determining the NSCs can be cumbersome, especially if the FE model includes various element types, or if the source code of the FE program is not available.

An alternative is to identify the NSCs using a *nonintrusive* (or *in-direct*) method. The idea is to identify the NSCs by evaluating an FE model on the global level, namely, by solving a series of static problems. In particular, the nonintrusive approaches do not require detailed knowledge of the FE implementation, and, therefore, any commercial FE software which allows for solving geometrically nonlinear static problems can be used. Furthermore, the nonintrusive approaches can be used for identifying the NSCs of FE models where the nonlinearity may not be fully described by cubic polynomials. Thus, for such models, the Taylor series Eq. 4.6 is, in general, an approximation. For instance, this would be the case if the FE model is not formulated using St. Venant–Kirchhoff materials, or if the FE code uses an updated Lagrangian framework.

Several nonintrusive NSC identification techniques have been developed, which can be divided into so-called enforced displacement (ED) and applied force (AF) methods (e.g., see [31, 32]). The ED method, which is also referred to as stiffness evaluation procedure (STEP), was first proposed by Muravyov and Rizzi [33]. Using the ED method, the NSCs are identified by imposing a series of static displacement fields onto the FE model, as further described in Section 4.2.1. Moreover, an enhanced version of the ED method, the enhanced enforced displacement (EED) method, was proposed by Perez et al. [34], which reduces the number of static evaluations in the identification process. The EED method is briefly described in Section 4.2.2. Specialized techniques for determining the condensed NSCs of flat structures, which are based upon the ED method, are discussed in Section 4.2.3. Finally, an overview of the implicit condensation and expansion (ICE) method, which was proposed by McEwan et al. [35] and later improved by Hollkamp and Gordon [36], is provided in Section 4.2.4. The ICE method is an AF method which, in contrast to the ED/EED method, is based upon a series of static problems where external forces are applied on the FE model. Compared to the ED methods, the ICE method is generally computationally more expensive. However, in contrast to the ED methods, the ICE method allows for extracting additional basis vectors from the results provided by the static problems (see further Section 4.2.4).

4.2.1 Enforced displacement method

In the ED method [33], the NSCs are determined based on a series of static problems where prescribed displacement fields are imposed onto the underlying FE model. The idea is to utilize that the polynomial structure of the nonlinear restoring forces is known. Specifically, the reduced order restoring force vector can be determined by projecting the full-order restoring force vector onto the reduction basis, as:

$$\tilde{\mathbf{f}}(\boldsymbol{\eta}) = \mathbf{V}^{\mathrm{T}}\mathbf{f}(\mathbf{u}) \tag{4.22}$$

where $\mathbf{V}$ is an orthogonal reduction basis, $\mathbf{u}$ is the physical displacement vector of the FE model, and $\tilde{\mathbf{f}}$ and $\mathbf{f}$ are the reduced and full-order restoring force vectors, respectively. Further, by using the polynomial expression, Eq. 4.6, the ith component of the reduced restoring force vector can be expressed as:

$$\tilde{f}_i(\boldsymbol{\eta}) = K_{ij}^{(1)}\eta_j + K_{ijk}^{(2)}\eta_j\eta_k + K_{ijkl}^{(3)}\eta_j\eta_k\eta_l. \tag{4.23}$$

The reduced restoring force vector can thus be expressed using either Eq. 4.22 or Eq. 4.23. Then, assume that the full-order restoring force vector has been determined from the FE model by prescribing the displacement fields $\alpha_1\mathbf{v}_j$ and $\alpha_2\mathbf{v}_j$, respectively, where $\mathbf{v}_j$ is a reduction basis vector and α_1 and α_2 are arbitrary scalars. By using Eq. 4.22, the corresponding reduced restoring force vectors can be determined by projecting the full-order restoring forces onto the reduction basis. Now, by considering the orthogonality properties of the basis, the following set of equations can be established (no summation over repeated indices):

$$\begin{cases} \tilde{f}_i(\boldsymbol{\eta} = \mathbf{e}_j\alpha_1) = K_{ij}^{(1)}\alpha_1 + K_{ijj}^{(2)}\alpha_1^2 + K_{ijjj}^{(3)}\alpha_1^3 \\ \tilde{f}_i(\boldsymbol{\eta} = \mathbf{e}_j\alpha_2) = K_{ij}^{(1)}\alpha_2 + K_{ijj}^{(2)}\alpha_2^2 + K_{ijjj}^{(3)}\alpha_2^3 \end{cases} \tag{4.24}$$

where $\mathbf{e}_j$ is a unit vector in the jth direction. Hence, because the prescribed displacement field is composed of a single reduction basis vector, the orthogonality properties of the basis implies that $\eta_j = \alpha$ and $\eta_i = 0$ for all $i \neq j$. By repeating this process for each of the m basis vectors, and noting the linear stiffness coefficients $K_{ij}^{(1)}$ are known, it follows that all the NSCs of the form $K_{ijj}^{(2)}$ and $K_{ijjj}^{(3)}$ can be solved from algebraic systems of equations, i.e., given by Eq 4.24.

Next, by prescribing displacement fields composed of two different basis vectors, stiffness coefficients having three different indices (i.e. $K_{ijk}^{(2)}$, $K_{ijjk}^{(3)}$, and $K_{ijkk}^{(3)}$) can be identified. Here, the displacement fields must be prescribed using three different amplitudes. Furthermore, the symmetry of the stiffness tensors is considered, e.g. $K_{ijk}^{(2)} = K_{ikj}^{(2)}$ and $K_{ijjk}^{(3)} = K_{ijkj}^{(3)} = K_{ikjj}^{(3)}$.

In the final step, NSCs having four different indices ($K_{ijkl}^{(3)}$) are determined by prescribing displacement fields composed of three different basis vectors. In total, $2N + 3N(N-1) + N(N-1)(N-2)/6$ static problems are required for determining all the NSCs [34]. For FE models generated using St-Venant–Kirchhoff materials, the displacement fields can theoretically be prescribed using an arbitrary amplitude [2]. However, the amplitude can affect the influence of numerical round-off errors. In the general case, the magnitude should be sufficiently small to ensure convergence, but large enough such that the nonlinear regime is entered. For instance, in [25, 37], it is suggested that displacement fields for flat structures are prescribed using an amplitude of $t/20$, where t is the structure thickness.

4.2.2 Enhanced enforced displacement method

In many applications, the ED method can be used effectively for determining the NSCs. In particular, if the underlying FE model is built up using hyperelastic "memoryless" materials

(e.g., St. Venant–Kirchhoff materials), the nonlinear restoring forces of the static problems can be obtained by merely evaluating the restoring force vector for the prescribed displacement field. Thus, the full-order nonlinear problems need not be solved using iterative techniques, such as the Newton–Raphson method (cf. Section 2.5.2). However, for large reduction bases, the number of static problems can become immense. Particularly if using commercial FE tools, which typically are not optimized for analyzing a large series of static problems, the cost of evaluating the prescribed displacement field can become unmanageable.

The EED method, which was proposed in [34], significantly reduces the number of static cases needed for determining the NSCs. The method relies on the same concept as the ED method. However, instead of using the restoring force vector the EED method is based upon evaluations of the tangent stiffness matrix. The method is briefly described as follows.

The reduced tangent stiffness matrix can be obtained by projecting the full-order tangent stiffness matrix onto the associated reduction basis, as:

$$\tilde{\mathbf{K}}(\boldsymbol{\eta}) = \mathbf{V}^{\mathrm{T}}\mathbf{K}^{t}(\mathbf{V}\boldsymbol{\eta})\mathbf{V}. \tag{4.25}$$

On the other hand, the reduced tangent stiffness matrix can be determined from the polynomial expression of the reduced nonlinear restoring forces, as (see e.g. [31, 34]):

$$\begin{aligned} \tilde{K}_{iu} &= \tfrac{\partial}{\partial \eta_u}\left[K^{(1)}_{ij}\eta_j + K^{(2)}_{ijl}\eta_j\eta_l + K^{(3)}_{ijlp}\eta_j\eta_l\eta_p\right] \\ &= K^{(1)}_{iu} + \left[K^{(2)}_{iju} + K^{(2)}_{iuj}\right]\eta_j + \left[K^{(3)}_{ijlu} + K^{(3)}_{ijul} + K^{(3)}_{iujl}\right]\eta_j\eta_l. \end{aligned} \tag{4.26}$$

Hence, the reduced tangent stiffness can be determined using either Eq. 4.25 or Eq. 4.26. Now, similar to the ED method, static problems are defined in terms of prescribed displacement fields. In the first step, displacement fields composed of a single basis vector, scaled by α_1 and α_2, respectively, are imposed onto the FE model. Then, by using Eqs. 4.25 and 4.26, the following set of equations can be established (no summation over repeated indices):

$$\begin{cases} \tilde{K}_{iu}(\boldsymbol{\eta} = \mathbf{e}_j\alpha_1) = K^{(1)}_{iu} + \left[K^{(2)}_{iju} + K^{(2)}_{iuj}\right]\alpha_1 + \left[K^{(3)}_{ijju} + K^{(3)}_{ijuj} + K^{(3)}_{iujj}\right]\alpha_1^2 \\ \tilde{K}_{iu}(\boldsymbol{\eta} = \mathbf{e}_j\alpha_2) = K^{(1)}_{iu} + \left[K^{(2)}_{iju} + K^{(2)}_{iuj}\right]\alpha_2 + \left[K^{(3)}_{ijju} + K^{(3)}_{ijuj} + K^{(3)}_{iujj}\right]\alpha_2^2. \end{cases} \tag{4.27}$$

Then, by assuming that the linear stiffness coefficients $K^{(1)}_{iu}$ are known, and noting that the stiffness tensors are fully symmetric, it follows that all NSCs of the form $K^{(2)}_{iuj}$, $K^{(2)}_{ijj}$, $K^{(3)}_{iujj}$, $K^{(3)}_{ijju}$, and $K^{(3)}_{ijjj}$ can be determined. Finally, by enforcing displacement fields composed of two different basis vectors, the coefficients of the form $K^{(3)}_{ijlu}$ can be determined. Thus, in contrast to the ED method, displacement fields composed of three different basis vectors need not be evaluated in the identification procedure. Therefore, all the NSCs can be determined by evaluating $2N + N(N-1)/2$ static cases, i.e., significantly less than in the ED method. However, the method necessitates an FE program which releases the tangent stiffness matrix. Furthermore, in the numerical investigations presented in Paper D, convergence issues was sometimes encountered for models generated using the EED method. This was also observed

in [31, 34]. Therefore, in certain applications, the standard ED method may be the preferred choice, even though the computational offline cost is larger.

4.2.3 Identification of condensed stiffness coefficients

The condensed system equations, Eq. 4.20, were introduced in Section 4.1.3. Further, the condensed stiffness coefficients $\bar{K}^{(3)}_{b,ijkl}$ can be determined from Eq. 4.21, i.e., based on the linear stiffness coefficients $K^{(1)}_{ij}$, and the nonlinear coefficients $K^{(2)}_{ijk}$ and $K^{(3)}_{ijkl}$, which in turn can be determined using, e.g., the ED or EED method. However, for flat structures, the condensed NSCs can be determined explicitly by applying the ED method on the out-of-plane DOFs, as demonstrated in [28].

First, consider an FE shell model representing a flat structure, and, furthermore, assume that a reduction basis $\mathbf{V}$ is constructed using pure bending and membrane modes. Then, the physical displacements of the FE model can be expressed as:

$$\underbrace{\begin{bmatrix} \mathbf{u}_b \\ \mathbf{u}_m \end{bmatrix}}_{\mathbf{u}} = \underbrace{\begin{bmatrix} \mathbf{V}_{bb} & \mathbf{0} \\ \mathbf{0} & \mathbf{V}_{mm} \end{bmatrix}}_{\mathbf{V}} \underbrace{\begin{bmatrix} \mathbf{q} \\ \mathbf{p} \end{bmatrix}}_{\boldsymbol{\eta}} \tag{4.28}$$

where the matrices $\mathbf{V}_{bb}$ and $\mathbf{V}_{mm}$ have sizes $n_b \times m_b$ and $n_m \times m_m$, respectively, and thus contain the entries of the reduction basis vectors corresponding to physical out-of-plane and in-plane displacement DOFs. Hence, the total number of DOFs of the FE model is $n = n_b + n_m$ and the size of the reduced order model is $m = m_b + m_m$.

Next, the displacement fields, as defined in the ED method, are enforced onto the out-of-plane DOFs $\mathbf{u}_b$, while the in-plane displacement DOFs $\mathbf{u}_m$ are allowed to move freely. Thus, the modal forcing on the in-plane coordinates is zero, and the static problems involving a single out-of-plane basis vector are given as:

$$\begin{cases} \mathbf{u}_b = \alpha \mathbf{v}_{bb,j} \\ \mathbf{g}_m = \mathbf{0} \end{cases} \tag{4.29}$$

where $\mathbf{v}_{bb,j}$ is a $n_b \times 1$ vector containing the out-of-plane displacements of a bending mode, α is a scaling coefficient, and $\mathbf{g}_m$ is the external forces associated to in-plane DOFs.

Recall that the reduction basis vectors are mutually orthogonal. Consequently, the load cases, as defined by Eq. 4.29, implies that $q_j = \alpha$ and $q_i = 0$ for all $i \neq j$ ($i = 1, \ldots, m_b$). However, the membrane coordinates are generally nonzero, i.e., $p_i \neq 0$ for all $i = 1, \ldots, m_m$, which is due to the nonlinear coupling between the bending and membrane modes. Then, by using Eqs. 4.20 and 4.22, and assuming that the linear stiffness coefficients are known, it follows that the condensed NSCs of the form $\bar{K}^{(3)}_{ijjj}$ can be determined from the equation (no summation over repeated indices):

$$f_{r,i}(\mathbf{q} = \alpha \mathbf{e}_j) = K^{(1)}_{ij}\alpha + \bar{K}^{(3)}_{ijjj}\alpha^3. \tag{4.30}$$

By following the procedure in the standard ED method, the condensed NSCs of the form $\bar{K}^{(3)}_{ijjk}$, $\bar{K}^{(3)}_{ijkk}$ can be identified by prescribing displacement fields composed of two out-of-plane basis vectors. The static problems are then given as:

$$\begin{cases} \mathbf{u}_b = \alpha(\mathbf{v}_{bb,j} + \mathbf{v}_{bb,k}) \\ \mathbf{g}_m = \mathbf{0} \end{cases} . \tag{4.31}$$

Finally, coefficients of the form $\bar{K}^{(3)}_{ijkl}$ can be determined based on static problems defined using out-of-plane displacement fields composed of three out-of-plane basis vectors; i.e., the static cases are defined such that:

$$\begin{cases} \mathbf{u}_b = \alpha(\mathbf{v}_{bb,j} + \mathbf{v}_{bb,k} + \mathbf{v}_{bb,l}) \\ \mathbf{g}_m = \mathbf{0} \end{cases} . \tag{4.32}$$

Note that the membrane modes are not included in the identification procedure. Hence, the condensed NSCs can be generated without knowledge of the in-plane basis. Further, the number of static problems is reduced compared to the standard ED method, i.e., since the load cases are defined solely in terms of the n_b out-of-plane bending modes. However, because the in-plane DOFs are allowed to move freely, the static problems must be solved using iterative techniques, such as the Newton–Raphson method. As will be further described in Sections 4.2.4 and 4.3.1, it turns out that the number of membrane basis vectors required to properly resolve the in-plane response is, in general, quadratically proportional to the number of bending coordinates. Therefore, the computational cost can still be reduced using the explicit procedure for identifying the condensed NSCs, i.e., which only involves the bending modes.

A similar procedure for estimating the condensed NSCs of flat structures (or straight beams) modeled using solid elements was proposed by Vizzaccaro et al. [25], which is referred to as the modified-STEP (M-STEP) method. Thus, the above approach, where FE shell models were considered, is generalized to flat FE models implemented using solid elements. However, the geometrical and material distribution of the structure, as well as boundary conditions must be symmetric with respect to the middle line/plane of the structure.

In this generalized case, the membrane modes are replaced by *non-bending* modes, which generally involve longitudinal and thickness displacements. Furthermore, as for the approach using shell (or beam) elements, all quadratic coefficients involving three bending coordinates can be assumed zero, i.e., $K^{(2)}_{ijk} = 0$ for all $i, j, k = 1, \ldots, m_b$. In particular, this allows for defining the non-bending modes as the set of modes for which this condition is not fulfilled.

By adopting a procedure similar to the standard ED method, the bending modes $\mathbf{v}_{b,i}$ ($i = 1 \ldots m_b$) are enforced on a subset of the FE model physical DOFs, referred to as master DOFs $\mathbf{u}_M$, which correspond to the out-of-plane DOFs along the middle line/surface. Thus, the remaining DOFs, referred to as slave DOFs $\mathbf{u}_S$, are allowed to move freely. Accordingly, the

physical displacements can be expressed in terms of the generalized coordinates, as:

$$\underbrace{\begin{bmatrix} \mathbf{u}_M \\ \mathbf{u}_S \end{bmatrix}}_{\mathbf{u}} = \underbrace{\begin{bmatrix} \mathbf{V}_b^M & \mathbf{0} \\ \mathbf{V}_b^S & \mathbf{V}_m^S \end{bmatrix}}_{\mathbf{V}} \underbrace{\begin{bmatrix} \mathbf{q} \\ \mathbf{p} \end{bmatrix}}_{\boldsymbol{\eta}} \tag{4.33}$$

where superscripts M and S refers to master and slave DOFs, respectively. Because the displacements are enforced solely on the $\mathbf{u}_M$ DOFs in the identification process, it can be shown that the modal forcing on the non-bending coordinates is zero [25]. Hence, for displacement fields composed of one basis vector, the static problems are defined such that:

$$\begin{cases} \mathbf{u}_M = \alpha \mathbf{v}_{b,i}^M \\ \mathbf{g}_S = \mathbf{0} \end{cases} \tag{4.34}$$

where $i = 1, \ldots, m_b$, α is an arbitrary scalar, and $\mathbf{g}_S$ is the external force vector associated to the slave DOFs. Furthermore, it is assumed that the slave DOFs are not involved in the orthogonality relations of the bending modes. Thus, as in the standard ED method, the orthogonality of the bending modes implies that $q_j = 0$ if $j \neq i$ ($j = 1, \ldots, m_b$) for load cases defined according to Eq. 4.34. However, the coordinates representing non-bending modes $\mathbf{p}$ are generally not zero and depend on their nonlinear coupling with the prescribed modal coordinate.

Although the conceptual framework is more complicated, the M-STEP method can be implemented in a similar manner as the standard ED method; thus, instead of prescribing the modal displacement fields on the full set of DOFs, the displacements are enforced solely on the master DOFs. Furthermore, it should be noted that the M-STEP approach implies that the external load in the reduced order dynamic analysis is applied on the master DOFs, i.e. the external forcing on the non-bending coordinates is assumed zero. A detail description of the M-STEP method can be found in [25].

4.2.4 Implicit condensation and expansion

The ICE method [35, 36, 38] allows for generating reduced order models of flat as well as slightly curved structures. In its original form, a set of low-frequency normal modes are used as a starting point, which would typically be used for analyzing the corresponding linearized system. Thus, additional modes, such as high-frequency membrane modes, are not required. Instead, the statically condensed response of modes not included in the basis are considered implicitly. In this regard, the method is similar to the approaches using the condensed system equations, discussed in Sections 4.1.3 and 4.2.3. An overview of the method is presented as follows.

By ignoring the inertia terms in Eq. 2.21, the nonlinear static problem for a full-order FE model can be expressed as:

$$\mathbf{f}(\mathbf{u}) = \mathbf{p}. \tag{4.35}$$

Further, let $\mathbf{p}$ be a prescribed external force vector. Then, the unknown displacement field $\mathbf{u}$ can be determined using any appropriate FE code capable of solving geometrically nonlinear static problems. Further, the computed displacements and the associated external loads can be projected onto a mass-orthogonal reduction basis $\mathbf{V}_b$, as [6]:

$$\mathbf{q} = \mathbf{V}_b^{\mathrm{T}}\mathbf{M}\mathbf{u}, \quad \tilde{\mathbf{p}} = \mathbf{V}_b^{\mathrm{T}}\mathbf{p} \tag{4.36}$$

where, again, $\mathbf{q}$ is the generalized coordinate vector and $\tilde{\mathbf{p}}$ are the associated modal force vector. For flat structures, $\mathbf{V}_b$ is typically constructed using pure out-of-plane bending modes, why the subscript b is employed here. However, for slightly curved structures, the set of low-frequency modes included in $\mathbf{V}_b$ would rather be transverse-dominated modes, involving out-of-plane as well as in-plane displacements.

Next, by adopting the polynomial form of the nonlinear restoring forces, the corresponding reduced order static problem can be written as:

$$K_{ij}^{(1)}q_j + K_{ijk}^{(2)}q_j q_k + K_{ijkl}^{(3)}q_j q_k q_l = \tilde{p}_i \tag{4.37}$$

where all quantities are known, except for the NSCs $K_{ijk}^{(2)}$ and $K_{ijkl}^{(3)}$ (again, we assume that the linear stiffness coefficients are available). Now, according to the procedure suggested in [38], external force patterns are defined using permutations of one, two, and three basis vectors, such that the external force is given by:

$$\mathbf{p} = \mathbf{K}\left(\pm\alpha_i\mathbf{v}_{b,i} \pm \alpha_j\mathbf{v}_{b,j} \pm \alpha_k\mathbf{v}_{b,k}\right) \tag{4.38}$$

where $\mathbf{v}_{b,i}$, $\mathbf{v}_{b,j}$, $\mathbf{v}_{b,k}$ are basis vectors with the associated scaling coefficients α_i, α_j, α_k, respectively, and $i, j, k = 0, \ldots, m_b$, $i \neq j \neq k$, with index zero implying that a term is omitted (e.g., see [3]). It follows that the total number of static cases to be analyzed is $n_p = 2m_b + 2m_b(m_b - 1) + 4m_b(m_b - 1)(m_b - 2)/3$ [38].

Similar to the ED/EED method, the scaling coefficients α (cf. Eq. 4.38) should be sufficiently large to ensure that geometric nonlinearities are activated [36, 38]. Then, based on the results from the series of static analyses, i.e., the set of n_p pairs of modal coordinate vectors $\mathbf{q}$ and modal forces $\tilde{\mathbf{p}}$, the NSCs can be determined in a least-squares sense, as described in detail in [38].

It should be emphasized that the basis can be constructed using the same modes as would be used for the corresponding linearized system. Hence, for a flat transversely loaded structure, it is sufficient to consider solely the out-of-plane bending modes. The condensed response of the membrane modes is considered implicitly, which follows from the fact that the in-plane displacements are not constrained in the static load cases. Consequently, the number of load cases can, in practice, be smaller than for the standard ED method (cf. Section 4.2.1) which involves $m = m_b + m_m$ basis vectors. On the other hand, in contrast to the ED method, the nonlinear static problems must be solved using iterative techniques, e.g., the Newton–Raphson method.

The NSC identification procedure, as introduced above, is referred to as the implicit condensation (IC) method, and was originally proposed in [35]. In [36], an additional step was suggested for identifying modes using an expansion process. The procedure, where both the NSCs are determined and additional modes are generated, is referred to as the implicit condensation and expansion (ICE) method. The expansion process is briefly described below.

According to [36], the physical displacements of the full-order FE model are approximated as:

$$\mathbf{u} \approx \mathbf{V}_b\mathbf{q} + \mathbf{T}\mathbf{r} \tag{4.39}$$

where, again, $\mathbf{V}_b$ contains the reduction basis vectors considered in the IC procedure, and $\mathbf{q}$ is the associated coordinate vector. The $n \times m_m$ matrix $\mathbf{T}$ contains a set of m_m unknown basis vectors, which are assumed to be orthogonal to $\mathbf{V}_b$ (here, the subscript m is used since the additional modes are generally membrane-dominated). Further, $\mathbf{r}$ is a $m_m \times 1$ vector containing the corresponding modal coordinates, which, thus, are currently unknown.

By using Eq. 4.39, it follows that the set of n_p nonlinear static solutions generated in the IC procedure can be written in matrix form, such that:

$$\mathbf{U} \approx \mathbf{V}_b\mathbf{Q} + \mathbf{T}\mathbf{R} \tag{4.40}$$

where the columns of the $n \times n_p$ matrix $\mathbf{U} = \left[\begin{array}{ccc} \mathbf{u}^{(1)} & \dots & \mathbf{u}^{(n_p)} \end{array} \right]$ are the displacement fields calculated based on the static cases, and the $m_b \times n_p$ matrix $\mathbf{Q} = \left[\begin{array}{ccc} \mathbf{q}^{(1)} & \dots & \mathbf{q}^{(n_p)} \end{array} \right]$ contains the generalized coordinate vectors obtained by projecting the static solutions onto $\mathbf{V}_b$ (cf. Eq. 4.36). Further, the modal coordinates associated to $\mathbf{T}$ are stored in the $m_m \times n_p$ matrix $\mathbf{R} = \left[\begin{array}{ccc} \mathbf{r}^{(1)} & \dots & \mathbf{r}^{(n_p)} \end{array} \right]$.

Then, a quadratic relationship between the generalized coordinates $\mathbf{q}$ and the coordinates of the unknown basis vectors $\mathbf{r}$ is assumed. Specifically, these are defined such that:

$$\mathbf{r} = \left[\begin{array}{ccccccccccc} q_1^2 & q_1q_2 & \dots & q_1q_{m_b} & q_2^2 & q_2q_3 & \dots & q_2q_{m_b} & \dots & q_{m_b-1}^2 & q_{m_b-1}q_{m_b} & q_{m_b}^2 \end{array} \right]^{\mathrm{T}}. \tag{4.41}$$

Hence, the number of modal coordinates associated to the basis $\mathbf{T}$ is $n_m = m_b + m_b(m_b - 1)/2$. It follows that the n_m unknown basis vectors can be determined in a least squares sense, as:

$$\mathbf{T} = (\mathbf{U} - \mathbf{V}_b\mathbf{Q})\,\mathbf{R}^+ \tag{4.42}$$

where $\mathbf{R}^+$ is the pseudo-inverse of $\mathbf{R}$.

According to the procedure suggested in [36], the additional basis vectors obtained in the expansion process are used for generating the displacements of the full-order models in the post-processing stage. Thus, the time-integration is performed using m_b bending coordinates, while the time-histories for the m_m membrane coordinates are generated after the dynamic response analysis has been completed. Accordingly, only the quasi-static responses of the additional membrane coordinates are considered. However, the membrane coordinates can be used for generating physical displacement fields including out-of-plane as well as in-plane displacements, e.g., needed for determining the stress distribution.

The ICE method, as introduce above, can thus be employed for both identifying the condensed NSC of the transverse-dominated basis $\mathbf{V}_b$ as well as generating additional mode shapes. Other techniques for generating reduction bases appropriate for geometrically nonlinear structures will be further discussed in the next section.

4.3 REDUCTION BASIS GENERATION

The reduction basis is a key aspect in the process of developing accurate reduced order models. A proper reduction basis should capture the dynamic characteristics of the system, or put differently, it should (approximately) span the full-order solution subspace. Furthermore, an important aspect is the computational effort for generating the reduction basis, i.e., which affect the computational offline cost. In particular, for the reduction method to be meaningful, the sum of the computational offline and online cost of the reduced model should be smaller than the computational cost for solving the full-order dynamic problem.

In Chapter 3, various methods for generating modes based on the linearized system were discussed. This type of modes, e.g., normal modes and modes generated using Krylov-subspace methods, are sometimes referred to as linear modes (e.g., see [31, 32]). In contrast to linear dynamics applications, a substantial number of linear modes are generally required to ensure a basis that adequately spans the solution of geometrically nonlinear problems (e.g., see [25]). As discussed previously, this is due to the influence of high-frequency modes, such as membrane modes, which need not be considered in the corresponding linear analysis.

Various basis generation techniques have been proposed to approach the problem (see, e.g., [2, 30, 34]). In principle, these can be divided into data-driven methods, where the basis generation procedure involves training data (see, e.g., [39]), and *simulation-free* methods, which can be employed without prior knowledge of the full-order solution [2, 30, 31, 34].

Reviews of basis generation methods can, e.g., be found in [3, 32]. Here, an overview of basis generation techniques employed in this work is presented. In Section 4.3.1, the concept of static modal derivatives is introduced. Static modal derivatives are derived based on an associated linear basis and correspond to the second order terms in a Taylor's expansion of the quasi-static displacement field. The basis generation procedure is simulation-free in the sense that results from the full-order dynamic solution are not required. In Section 4.3.2, a data-driven technique, often referred to as proper orthogonal decomposition (POD), is briefly described which, in contrast, is based on time-history data from the full-order solution.

4.3.1 Static modal derivatives

Reduction bases generated using linear modes can be used effectively for analyzing the linearized response of a structure. However, as the deformations increases and the structure enters the nonlinear regime, a set of low-frequency linear modes may no longer capture the struc-

tural behavior. To approach this problem, the linear basis can be enriched by so-called *modal derivatives*, which was first proposed in [40, 41]. The modal derivatives, as defined in [40] are mode shapes which are calculated based on a perturbation of the generalized eigenvalue problem (cf. Eq. 2.27). Here, however, the so-called *static* modal derivatives are considered, where the inertial contribution is neglected [42]. As, e.g., demonstrated in [2, 42], the computation of the static modal derivatives is more straightforward. Moreover, the numerical investigations presented in [2, 31] indicate that reduction bases enriched by modal derivatives and static modal derivatives, respectively, result in a response prediction of similar accuracy. Further, the static modal derivatives can be computed nonintrusively, as further described below.

Let $\mathbf{V}_b$ be an $n \times m_b$ linear basis, with the associated modal coordinates $\mathbf{q}$, being generated using any of the techniques discussed in Chapter 3. Here, the subscript b is used to indicate that, for flat structures, the basis would typically be constructed using low-frequency bending modes.

Then, as e.g. shown in [43], a Taylor series expansion of $\mathbf{u}(\mathbf{q})$ around $\mathbf{q} = \mathbf{0}$ including two terms can be expressed as:

$$\mathbf{u}(\mathbf{q}) \approx \sum_{i=1}^{m_b} \left.\frac{\partial \mathbf{u}}{\partial q_i}\right|_{\mathbf{0}} q_i + \frac{1}{2} \sum_{i=1}^{m_b} \sum_{j=1}^{m_b} \left.\frac{\partial^2 \mathbf{u}}{\partial q_j \partial q_i}\right|_{\mathbf{0}} q_i q_j. \tag{4.43}$$

It can be shown that the terms $\left.\frac{\partial \mathbf{u}}{\partial q_i}\right|_{\mathbf{0}}$ is equal to the linear basis vectors $\mathbf{v}_{b,i}$, $i = 1, \ldots, m_b$ (e.g., see [43]). Moreover, as demonstrated in [42, 43], the static modal derivatives associated to $\mathbf{V}_b$ can be expressed as:

$$\boldsymbol{\theta}_{ij} = \left.\frac{\partial^2 \mathbf{u}_{\mathrm{g}}}{\partial q_i \partial q_j}\right|_{\mathbf{0}} = -\mathbf{K}^{-1} \left.\frac{\partial \mathbf{K}^t}{\partial q_j}\right|_{\mathbf{0}} \mathbf{v}_{b,i} \tag{4.44}$$

where $\mathbf{K}$ is the linear stiffness matrix of the full-order model (linearized around $\mathbf{u} = \mathbf{0}$), and $\mathbf{v}_{b,i}$ is a reduction basis vector. Further, $\left.\frac{\partial \mathbf{K}^t}{\partial q_j}\right|_{\mathbf{0}}$ is the directional derivative of the tangent stiffness matrix along the mode $\mathbf{v}_{b,j}$.

It then follows that the nonlinear static response can be approximated as:

$$\mathbf{u}(\mathbf{q}) \approx \sum_{i=1}^{m_b} \mathbf{v}_{b,i} q_i + \frac{1}{2} \sum_{i=1}^{m_b} \sum_{j=1}^{m_b} \boldsymbol{\theta}_{ij} q_i q_j. \tag{4.45}$$

Thus, if the second term is neglected, this result in an approximation using a standard modal truncation including m_b linear modes, being appropriate in linear dynamics applications. However, by considering the second term including the static modal derivatives, an approximation suitable for geometrically nonlinear structures is obtained. Furthermore, note that the static modal derivatives are symmetric with respect to the indices i and j, i.e. $\boldsymbol{\theta}_{ij} = \boldsymbol{\theta}_{ji}$, which can be utilized in a numerical implementation (this is, however, not the case for modal derivatives defined based on a perturbation of the generalized eigenvalue, e.g., see [42]). In

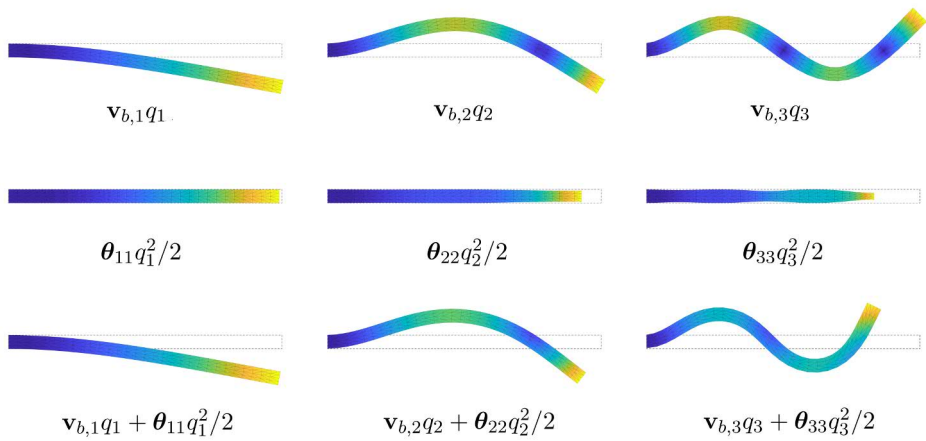

Figure 4.2: Example of bending modes and the associated static modal derivatives for a cantilever beam.

Figure 4.2, linear bending modes and the associated static modal derivatives are exemplified for a cantilever beam, modeled using two-dimensional continuum elements. As shown in the figure, the static modal derivatives include displacements in the thickness direction as well as the longitudinal direction of the beam, which are not considered by the bending modes.

If using an FE code which releases the tangent stiffness matrix, the directional derivative of the tangent stiffness matrix can be calculated in a nonintrusive manner, as [31]:

$$\left.\frac{\partial \mathbf{K}^t}{\partial q_i}\right|_{\mathbf{0}} = \frac{\mathbf{K}^t(\mathbf{v}_{b,i}h) - \mathbf{K}^t(-\mathbf{v}_{b,i}h)}{2h} \tag{4.46}$$

where h is a small value, and $\mathbf{K}^t$ is the full-order tangent stiffness matrix, which can be determined by imposing the displacement fields ($\pm\mathbf{v}_{b,i}h$) onto the full-order FE-model. Accordingly, the static modal derivatives can be calculated nonintrusively using Eq. 4.44. In situations where the FE software does not support the generation of tangent stiffness matrices for prescribed displacement fields, the directional derivative of the tangent stiffness matrix can be calculated using numerical differentiation based on the reaction forces from prescribed displacement fields, as shown in [25, 31]. This approach is, however, computationally more expensive.

A reduction basis can thus be formed using linear modes and the associated static modal derivatives, determined from Eq. 4.44. For numerical robustness, the basis should be reorthogonalized using the procedures discussed in Chapter 3. Further, the NSCs of the enriched basis can be determined in a nonintrusive manner using, e.g., the ED method (cf. Section 4.2.1). However, as indicated by Eq. 4.45, the number of modal derivatives is quad-

ratically proportional to the number of linear modes. Thus, for large or moderate linear bases, the size of the enriched basis can become substantial, which in turn may result in an unacceptable offline and online computational cost.

To mitigate this issue, techniques for reducing the size of the enriched basis have been proposed, e.g., see [30, 44]. For flat structures, an alternative is to employ the condensed system equations, which is the approach generally adopted in this work (e.g., see Paper E). In fact, as shown in [25], the static modal derivatives associated to out-of-plane bending modes of flat FE models, which are symmetric with respect to the middle plane, are pure in-plane modes which are orthogonal to the bending modes. Thus, similar to the ICE method, the static modal derivatives can be used for recovering the quasi-static in-plane displacements in the post-processing stage.

Another approach to reduce the computational effort for analyzing flat structures is to adopt the simplified form, Eq. 4.18 (e.g., see [26]). More specifically, the higher order stiffness coefficients are omitted for coordinates representing static modal derivatives. It should be emphasized that, in contrast to the approach using the condensed system equations, inertia effects are in this case considered for the bending modes as well as the associated static modal derivatives, which are thus represented by additional coordinates in the dynamic analysis. Further, the static modal derivatives should be made mutually orthogonal for numerical robustness. As manifested by the numerical investigations in Paper D, this approach results in a significant reduction of both the offline and online cost, as compared to an approach using the full set of NSCs. Furthermore, the numerical studies in Paper D suggests that this approach is reasonably accurate for cantilevered structures, which cannot be properly modeled using the condensed system equations [29].

For linear bases constructed using normal modes, this modeling strategy can be generalized to non-flat structures; namely, by computing the static modal derivatives using the residual flexibility (cf. Eq. 3.16), i.e.:

$$\tilde{\boldsymbol{\theta}}_{ij} = -\left(\mathbf{K}^{-1} - \sum_{l=1}^{m_b} \frac{\mathbf{v}_{b,l}\mathbf{v}_{b,l}^{\mathrm{T}}}{\omega_l^2}\right) \frac{\partial \mathbf{K}^t}{\partial q_j}\bigg|_{\mathbf{0}} \mathbf{v}_{b,i} = \left(\mathbf{I} - \mathbf{V}_b\mathbf{V}_b^{\mathrm{T}}\mathbf{M}\right)\boldsymbol{\theta}_{ij} \tag{4.47}$$

where $\mathbf{V}_b$ contains (out-of-plane) normal modes with eigenfrequencies ω_l. Hence, the subspace spanned by the linear basis $\mathbf{V}_b$ is removed from the static modal derivatives. Moreover, for numerical robustness, the vectors $\tilde{\boldsymbol{\theta}}_{ij}$ can be made mutually orthogonal.

It follows that the simplified form, Eqs. 4.16–4.18, can be adopted, where coordinates representing the subspace spanned by the vectors $\tilde{\boldsymbol{\theta}}_{ij}$ can be treated as membrane coordinates. The numerical investigation presented in Paper D indicates that the method provides satisfactory results for slightly curved structures. How this technique performs for structures with arbitrary geometry is, however, an open question.

4.3.2 Proper orthogonal decomposition

By means of a proper orthogonal decomposition (POD), a reduction basis can be generated based on time-history data from full-order dynamic solutions (e.g., see [2, 32, 39, 45]). In contrast to the approach using modal derivatives, the POD is a purely data-driven method; thus, knowledge of system properties (e.g., mass and stiffness matrices) are not needed in the basis generation procedure. The concept is briefly described as follows.

The displacement time–histories from a full-order dynamic analysis can be organized in a snapshot matrix, as:

$$\mathbf{S} = \begin{bmatrix} \mathbf{u}(t_1) & \mathbf{u}(t_2) & \cdots & \mathbf{u}(t_k) \end{bmatrix} \tag{4.48}$$

where $\mathbf{u}(t_i)$ is a $n \times 1$ vector containing the nodal displacements at time point t_i.

In the POD, a reductions basis $\mathbf{V}$ is determined by considering the minimization problem $\min \sum_{i=1}^{k} ||\mathbf{u}(t_i) - \mathbf{V}\boldsymbol{\eta}(t_i)||_2$, where $\boldsymbol{\eta}$ are generalized coordinates associated to the reduction basis vectors. Specifically, this can be accomplished by means of a singular value decomposition (SVD) of the snapshot matrix, such that (for further details on the SVD, see [22]):

$$\mathbf{S} = \mathbf{U}_{\text{svd}} \boldsymbol{\Sigma} \mathbf{V}_{\text{svd}}^{\mathrm{T}} \tag{4.49}$$

where the columns of the orthogonal matrices $\mathbf{U}_{\text{svd}}$ and $\mathbf{V}_{\text{svd}}$ are the left- and right singular vectors, respectively. Further, $\boldsymbol{\Sigma} = \text{diag}(\sigma_1, \sigma_2, \ldots, \sigma_n)$ is a diagonal matrix containing the singular values, which are ordered decreasingly such that $\sigma_i \geq \sigma_{i+1}$. The left singular vectors $\mathbf{u}_{\text{svd},i}$ contain the spatial information of the displacement fields, and the importance of a left singular vector is associated to the magnitude of the corresponding singular value σ_i. Furthermore, as indicated by Eq. 4.49, the right singular vectors $\mathbf{v}_{\text{svd},i}$ provide information of the variation of the displacements through time.

It follows that the displacement time-histories included in the snapshot matrix can be approximated by a truncated set of singular vectors, as:

$$\mathbf{u}(t) \approx \sum_{i=1}^{r} \sigma_i \mathbf{u}_{\text{svd},i} \mathbf{v}_{\text{svd},i}^{\mathrm{T}} \tag{4.50}$$

where r is the number of retained singular vectors. Here, the left singular vectors represent an approximation of the full-order solution subspace. Accordingly, a reduction basis may be constructed using the first r left singular vectors. Further, the basis may be orthogonalized using the procedure discussed in Section 3.1.

For FE models that uses both translational and rotational DOFs, or models with irregular meshes, it can be beneficial to introduce a weighted POD, where the mass norm is used instead of the Euclidean norm (e.g., see [2]). For flat FE models, the in-plane and out-of-plane DOFs may also be separated into different snapshot matrices. Hence, a POD is then applied on the in-plane and out-of-plane displacement fields, i.e., resulting in an in-plane and out-of-plane basis, respectively [32]. By using this approach, the difference of the in-plane and out-of-plane

response amplitude is also somewhat accounted for. Thus, in a POD of the total displacement field, the resulting basis can be expected to be transverse-dominated and important membrane modes might not be identified.

Reduction bases generated using a POD can be viewed as the best possible basis for approximating the full-order solution considered in the snapshot matrix. However, a significant drawback in the approach using a POD is that the accuracy of the basis is strongly dependent on the data included in the snapshot matrix. Thus, in contrast to the approach using static modal derivatives, which is load-independent, the reduction basis cannot be expected to be suitable for load cases not considered in the training data.

Finally, it should be mentioned that the POD can also be used for approximating other quantities. For instance, in Paper E, the POD is employed for approximating a time-dependent pressure distribution. In particular, this can be useful in basis generation procedures, such as Krylov subspace methods (see 3.5), where time-independent load patterns are considered (cf. Eq. 3.17).

5 Dynamic substructuring

The dynamic response of linear systems can be efficiently computed by use of modal dynamics; the system matrices are diagonalized and reduced by projecting the system equations onto a truncated modal basis (cf. Chapters 2 and 3). However, for large systems it can be beneficial to divide the system into substructures and employ DS to perform a reduction on the substructure level, e.g. as a preconditioning in the process of computing the global eigenmodes. Solving several substructures can be computationally less expensive than solving one large system.

Moreover, DS can be used for reducing nonlinear structures. For instance, it allows for reducing linear substructures interacting with nonlinear subsystems. In particular, reduced models considering local nonlinearities, such as plastic hinges in concrete structures or local contact interactions, can be established, as illustrated by various applications in Chapter 6. The parts of the structure that remain linear elastic are then modeled using a reduced set of generalized coordinates, while the nonlinear submodels may be expressed in terms of physical displacement DOFs. In contrast, geometric nonlinearity is a distributed nonlinearity where degrees of freedoms throughout the structure are nonlinearly coupled (cf. Chapter 4). Nonetheless, an approach using DS can still be useful, e.g., in cases where geometrically nonlinear affects need not be considered for the whole structure.

Several DS methods have been developed since the late 1960s, extensive reviews of existing methods are e.g. presented in [4,6,46]. In particular, DS may be applied in both time domain and frequency domain analyses. Here, however, focus is on DS for time domain analysis.

Section 5.1 presents assembly methods, which is an important aspect of DS. To this end, the fundamental equilibrium and compatibility conditions are introduced, as formulated in [4], which then provide a basis in a derivation of various assembly techniques. In particular, a global assembly may be formed such that a unique set of DOFs or, in contrast, dual DOFs are retained at interfaces.

In most DS methods a reduction is performed on the substructure level using some form of modal method. Hence, the substructure response is expressed in terms of generalized coordinates representing the amplitudes of a specific set of *component modes* (in the following, the terms *substructure* and *component* are used interchangeably). This class of DS approaches are often referred to as component-mode synthesis (CMS) and is further discussed in Section 5.2.

In particular, CMS methods may be formulated using a so-called free- or fixed-interface approach.

In Sections 5.1 and 5.2, assembly methods and common CMS techniques are introduced for systems composed of linear (or linearized) substructures. Aspects regarding CMS for structures including geometrically nonlinear substructures are discussed in Section 5.3.

5.1 ASSEMBLY METHODS

The equations of motion for a linear structure consisting of N substructures and the associated compatibility and equilibrium conditions may be written as [4]:

$$\begin{cases} \mathbf{M}\ddot{\mathbf{u}} + \mathbf{C}\dot{\mathbf{u}} + \mathbf{K}\mathbf{u} = \mathbf{p} + \mathbf{g} & \text{(5.1a)} \\ \mathbf{B}\mathbf{u} = \mathbf{0} & \text{(5.1b)} \\ \mathbf{L}^{\mathrm{T}}\mathbf{g} = \mathbf{0} & \text{(5.1c)} \end{cases}$$

where

$$\begin{aligned} \mathbf{M} &= \operatorname{diag}\left(\mathbf{M}^{(1)}, \mathbf{M}^{(2)}, \ldots, \mathbf{M}^{(N)}\right) \\ \mathbf{C} &= \operatorname{diag}\left(\mathbf{C}^{(1)}, \mathbf{C}^{(2)}, \ldots, \mathbf{C}^{(N)}\right) \\ \mathbf{K} &= \operatorname{diag}\left(\mathbf{K}^{(1)}, \mathbf{K}^{(2)}, \ldots, \mathbf{K}^{(N)}\right) \\ \mathbf{u} &= \begin{bmatrix} \mathbf{u}^{(1)\mathrm{T}} & \mathbf{u}^{(2)\mathrm{T}} & \ldots & \mathbf{u}^{(N)\mathrm{T}} \end{bmatrix}^{\mathrm{T}} \\ \mathbf{p} &= \begin{bmatrix} \mathbf{p}^{(1)\mathrm{T}} & \mathbf{p}^{(2)\mathrm{T}} & \ldots & \mathbf{p}^{(N)\mathrm{T}} \end{bmatrix}^{\mathrm{T}} \\ \mathbf{g} &= \begin{bmatrix} \mathbf{g}^{(1)\mathrm{T}} & \mathbf{g}^{(2)\mathrm{T}} & \ldots & \mathbf{g}^{(N)\mathrm{T}} \end{bmatrix}^{\mathrm{T}}. \end{aligned}$$

Here, $\mathbf{M}$, $\mathbf{C}$, and $\mathbf{K}$ are the global mass, damping and stiffness matrices, respectively, $\mathbf{u}$ is the global displacement vector and $\mathbf{p}$ and $\mathbf{g}$ are the external and interface force vectors, respectively. Furthermore, note that the global system equations (Eq. 5.1a) are written in block-diagonal form which implies that dual DOFs are present at interfaces between substructures.

Eq. 5.1b concerns the compatibility condition. More specifically, it includes equations describing how DOFs are constrained. For example, consider the constraint equation $u_i - u_j = 0$, i.e., the displacement in DOF i is equal to the displacement in DOFj. This correspond to $\mathbf{B}$ being a row vector of the form:

$$\mathbf{B} = \begin{bmatrix} 0 \cdots\cdots 1 \cdots\cdots -1 \cdots\cdots 0 \end{bmatrix} \qquad \text{(5.3)}$$
$$\qquad\qquad\quad u_i \qquad\quad u_j$$

Hence, if assuming a conforming discretization on interfaces, $\mathbf{B}$ will be a signed $n_c \times n$ Boolean matrix, where n_c is the number of constraints and n is the number of DOFs in the dually assembled global system.

Eq. 5.1c represents the equilibrium condition where, in the case of a conforming interface discretization, $\mathbf{L}$ is a Boolean localization matrix. For example, consider again the constraint equation $u_i - u_j = 0$ and the associated equilibrium condition $g_i + g_j = 0$. This correspond to $\mathbf{L}$ being a $n \times (n-1)$ matrix given by (with blank entries being zero):

$$\mathbf{L} = \begin{bmatrix} 1 & & & & \\ & \ddots & & & \\ & & 1 & & \\ & & & 1 & \\ & & & & \ddots \\ & & & & & 1 \end{bmatrix} \begin{matrix} \\ \\ \\ u_i \\ \\ u_j \end{matrix} \tag{5.4}$$

The global displacement vector may be partitioned into a set of unique $\mathbf{u}_u$ and redundant $\mathbf{u}_r$ DOFs. Hence, the unique DOFs include one set of interface DOFs and, possibly, internal DOFs being substructure DOFs that are not part of the substructure boundary (a selection of interface DOFs is thus required). Then, the compatibility condition can be expressed as:

$$\begin{bmatrix} \mathbf{B}_{rr} & \mathbf{B}_{ru} \end{bmatrix} \begin{bmatrix} \mathbf{u}_r \\ \mathbf{u}_u \end{bmatrix} = \mathbf{0}. \tag{5.5}$$

Further, by rewriting Eq. 5.5, the redundant DOFs can be expressed in terms of the unique DOFs:

$$\mathbf{u}_r = -\mathbf{B}_{rr}^{-1}\mathbf{B}_{ru}\mathbf{u}_u. \tag{5.6}$$

Hence, the following transformation may be defined:

$$\mathbf{u} = \mathbf{L}\mathbf{u}_u = \begin{bmatrix} -\mathbf{B}_{rr}^{-1}\mathbf{B}_{ru} \\ \mathbf{I}_{uu} \end{bmatrix} \mathbf{u}_u. \tag{5.7}$$

Thus, the Boolean localization matrix $\mathbf{L}$, that transforms the unique set of DOFs to dual form, can readily be obtained if $\mathbf{B}$ is available.

Furthermore, substituting Eq. 5.7 into Eq. 5.1a and pre-multiplying with $\mathbf{L}^{\mathrm{T}}$ gives:

$$\mathbf{M}_P\ddot{\mathbf{u}}_u + \mathbf{C}_P\dot{\mathbf{u}}_u + \mathbf{K}_P\mathbf{u}_u = \mathbf{p}_P \tag{5.8}$$

where

$$\mathbf{M}_P = \mathbf{L}^{\mathrm{T}}\mathbf{M}\mathbf{L}, \quad \mathbf{C}_P = \mathbf{L}^{\mathrm{T}}\mathbf{C}\mathbf{L}, \quad \mathbf{K}_P = \mathbf{L}^{\mathrm{T}}\mathbf{K}\mathbf{L}, \quad \mathbf{p}_P = \mathbf{L}^{\mathrm{T}}\mathbf{p}.$$

Here, $\mathbf{M}_P$, $\mathbf{C}_P$ and $\mathbf{K}_P$ are $n_P \times n_P$ system matrices and $\mathbf{p}_P$ is a $n_P \times 1$ external force vector, where n_P is the number of unique DOFs in a so-called *primal* formulation. Notice that this primal approach correspond to the assembly procedure commonly employed in standard FE

modeling, i.e., the global displacement vector $\mathbf{u}$ is replaced by a set of unique displacements $\mathbf{u}_u$. Moreover, substituting Eq. 5.7 into the compatibility condition yields $\mathbf{Bu} = \mathbf{BLu}_u = \mathbf{0}$. Hence, by noting that $\mathbf{u}_u$ is arbitrary, it follows that the Boolean localization matrix $\mathbf{L}$ represents the null-space of $\mathbf{B}$, i.e., $\mathbf{BL} = \mathbf{0}$ [4]. Accordingly, a primal assembly is actually obtained by projecting the system equations onto the null-space of $\mathbf{B}$ (cf. Eqs. 3.3 and 5.8). Furthermore, it follows that $(\mathbf{BL})^{\mathrm{T}} = \mathbf{L}^{\mathrm{T}}\mathbf{B}^{\mathrm{T}} = \mathbf{0}$, i.e. $\mathbf{B}^{\mathrm{T}}$ is the null-space of $\mathbf{L}^{\mathrm{T}}$.

Instead of using a primal formulation, the compatibility and equilibrium conditions (Eqs. 5.1b and 5.1c) can be enforced such that dual DOFs are retained at interfaces, e.g., by means of Lagrange multipliers [4]. Then, the interface forces may be selected such that:

$$\mathbf{g} = -\mathbf{B}^{\mathrm{T}}\lambda \tag{5.9}$$

where λ is a $n_c \times 1$ vector containing Lagrange multipliers. Further, by substituting Eq. 5.9 into the equilibrium equation (Eq. 5.1b) one obtains:

$$\mathbf{L}^{\mathrm{T}}\mathbf{g} = -\mathbf{L}^{\mathrm{T}}\mathbf{B}^{\mathrm{T}}\lambda = \mathbf{0}. \tag{5.10}$$

Hence, because $\mathbf{B}^{\mathrm{T}}$ is the null-space of $\mathbf{L}^{\mathrm{T}}$ the equilibrium condition is always satisfied. It then remains to enforce the compatibility condition, i.e. $\mathbf{Bu} = \mathbf{0}$. In matrix form, the dually assembled system can thus be written as:

$$\begin{bmatrix} \mathbf{M} & \mathbf{0} \\ \mathbf{0} & \mathbf{0} \end{bmatrix} \begin{bmatrix} \ddot{\mathbf{u}} \\ \lambda \end{bmatrix} + \begin{bmatrix} \mathbf{C} & \mathbf{0} \\ \mathbf{0} & \mathbf{0} \end{bmatrix} \begin{bmatrix} \dot{\mathbf{u}} \\ \lambda \end{bmatrix} + \begin{bmatrix} \mathbf{K} & \mathbf{B}^{\mathrm{T}} \\ \mathbf{B} & \mathbf{0} \end{bmatrix} \begin{bmatrix} \mathbf{u} \\ \lambda \end{bmatrix} = \begin{bmatrix} \mathbf{p} \\ \mathbf{0} \end{bmatrix} \tag{5.11}$$

where both the equilibrium and compatibility conditions are satisfied.

Furthermore, a dually assembled system can be enforced in an approximate manner using a penalty formulation, e.g. expressed as:

$$\mathbf{M}\ddot{\mathbf{u}} + \mathbf{C}\dot{\mathbf{u}} + \left(\mathbf{K} + \alpha\mathbf{B}^{\mathrm{T}}\mathbf{B}\right)\mathbf{u} = \mathbf{p} \tag{5.12}$$

where α is a penalty stiffness being sufficiently large such that $\mathbf{Bu} \approx \mathbf{0}$ [1]. Again, consider the constraint equation $u_i - u_j = 0$ and the corresponding signed Boolean matrix $\mathbf{B}$ (cf. Eq. 5.3). It follows that:

$$\alpha\mathbf{B}^{\mathrm{T}}\mathbf{B} = \begin{bmatrix} & 0 & & 0 & \\ & \vdots & & \vdots & \\ 0 & \cdots\cdots & \alpha & \cdots\cdots & -\alpha & \cdots\cdots & 0 & u_i \\ & \vdots & & \vdots & \\ 0 & \cdots\cdots & -\alpha & \cdots\cdots & \alpha & \cdots\cdots & 0 & u_j \\ & \vdots & & \vdots & \\ & 0 & & 0 & \\ & u_i & & u_j & \end{bmatrix} \tag{5.13}$$

Hence, using the penalty formulation, the constraint is indeed enforced by means of a spring element having stiffness α.

The preferred assembly method depends on the specific application. A primal formulation where the number of global DOFs are reduced can be cumbersome in some applications. On the contrary, it can be problematic to ensure stability in direct time-integration schemes for systems including Lagrange multipliers [47]. Even though methods to ensure stability exist, the available time-integration schemes are at least limited (for example, a standard Newmark time-integration, assuming constant average accelerations, is in this case unconditionally unstable). If using the penalty method, a suitable penalty stiffness must be determined—if it is too low, the constraint equations might not be enforced properly and if it is too large, the system equations can be ill-conditioned with respect to inversion. Moreover, if using a conditionally stable time-integration scheme, such as the central difference method, a large penalty stiffness might result in a very small critical time increment (see Section 2.5.2).

5.2 COMPONENT MODE SYNTHESIS

On the substructure level, the system equations are expressed in terms of the substructure displacements $\mathbf{u}^{(s)}$, which can be approximated by a reduced set of generalized coordinates $\mathbf{q}^{(s)}$. The transformation can be expressed as

$$\mathbf{u}^{(s)} \approx \mathbf{T}^{(s)}\mathbf{q}^{(s)} \tag{5.14}$$

where superscript s is the substructure label and $\mathbf{T}^{(s)}$ is a $n^{(s)} \times m^{(s)}$ transformation (or reduction) matrix representing a reduction basis. Here, $n^{(s)}$ and $m^{(s)}$ are the number of variables in the unreduced and reduced subsystem, respectively. Typically, $m^{(s)} \ll n^{(s)}$.

An FE formulation of a linear substructure leads to an equation of motion of the following form:

$$\mathbf{M}^{(s)}\ddot{\mathbf{u}}^{(s)} + \mathbf{C}^{(s)}\dot{\mathbf{u}}^{(s)} + \mathbf{K}^{(s)}\mathbf{u}^{(s)} = \mathbf{p}^{(s)} + \mathbf{g}^{(s)} \tag{5.15}$$

where $\mathbf{M}^{(s)}, \mathbf{C}^{(s)}$ and $\mathbf{K}^{(s)}$ are the $n^{(s)} \times n^{(s)}$ substructure mass, damping and stiffness matrices, respectively, and $\mathbf{p}^{(s)}$ and $\mathbf{g}^{(s)}$ are the $n^{(s)} \times 1$ substructure external force and interface force vectors, respectively. By substituting Eq. 5.14 into Eq. 5.15 and pre-multiplying with $\mathbf{T}^{\mathrm{T}}$ the reduced system equations are given as:

$$\tilde{\mathbf{M}}^{(s)}\ddot{\mathbf{q}}^{(s)} + \tilde{\mathbf{C}}^{(s)}\dot{\mathbf{q}}^{(s)} + \tilde{\mathbf{K}}^{(s)}\mathbf{q}^{(s)} = \tilde{\mathbf{p}}^{(s)} + \tilde{\mathbf{g}}^{(s)} \tag{5.16}$$

where

$$\tilde{\mathbf{M}}^{(s)} = \mathbf{T}^{(s)\mathrm{T}}\mathbf{M}^{(s)}\mathbf{T}^{(s)}, \quad \tilde{\mathbf{C}}^{(s)} = \mathbf{T}^{(s)\mathrm{T}}\mathbf{C}^{(s)}\mathbf{T}^{(s)}, \quad \tilde{\mathbf{K}}^{(s)} = \mathbf{T}^{(s)\mathrm{T}}\mathbf{K}^{(s)}\mathbf{T}^{(s)}$$

$$\tilde{\mathbf{p}}^{(s)} = \mathbf{T}^{(s)\mathrm{T}}\mathbf{p}^{(s)}, \quad \tilde{\mathbf{g}}^{(s)} = \mathbf{T}^{(s)\mathrm{T}}\mathbf{g}^{(s)}.$$

Here, $\tilde{\mathbf{M}}^{(s)}, \tilde{\mathbf{C}}^{(s)}$ and $\tilde{\mathbf{K}}^{(z)}$ are the $m^{(s)} \times m^{(s)}$ reduced system matrices of the substructure, and $\tilde{\mathbf{p}}^{(s)}$ and $\tilde{\mathbf{g}}^{(s)}$ are the corresponding $m^{(s)} \times 1$ reduced external force and interface force vector.

In most CMS methods, a reduction basis is constructed using some form of pseudo-static and vibrational modes [21]. In particular, a set of pseudo-static modes may be constructed such that the generalized coordinates correspond to the physical displacements of the substructure boundary DOFs. This is convenient when enforcing intercomponent compatibility, i.e., the components can be assembled in a standard fashion as superelements. Accordingly, the reduced coordinate vector $\mathbf{q}^{(s)}$ may include both physical DOFs, often referred to as master, boundary, or interface DOFs, as well as other generalized coordinates representing the amplitudes of component modes. To simplify the notation, the substructure label s is left out in the remainder of this section, unless otherwise noted.

5.2.1 Condensation methods

Neglecting damping, the equation of motion in partitioned form for a substructure can be written as:

$$\begin{bmatrix} \mathbf{M}_{ii} & \mathbf{M}_{ib} \\ \mathbf{M}_{bi} & \mathbf{M}_{bb} \end{bmatrix} \begin{bmatrix} \ddot{\mathbf{u}}_i \\ \ddot{\mathbf{u}}_b \end{bmatrix} + \begin{bmatrix} \mathbf{K}_{ii} & \mathbf{K}_{ib} \\ \mathbf{K}_{bi} & \mathbf{K}_{bb} \end{bmatrix} \begin{bmatrix} \mathbf{u}_i \\ \mathbf{u}_b \end{bmatrix} = \begin{bmatrix} \mathbf{p}_i \\ \mathbf{p}_b \end{bmatrix} + \begin{bmatrix} \mathbf{0} \\ \mathbf{g}_b \end{bmatrix} \tag{5.17}$$

where the subscripts i and b denotes the internal and interface boundary DOFs, respectively. Here, the interface forces are by definition zero on the internal DOFs. Further, if assuming that the external forcing is zero on the internal DOFs, the internal displacements can be expressed as:

$$\mathbf{u}_i = -\mathbf{K}_{ii}^{-1} \left(\mathbf{M}_{ii}\ddot{\mathbf{u}}_i + \mathbf{M}_{ib}\ddot{\mathbf{u}}_b + \mathbf{K}_{ib}\mathbf{u}_b \right). \tag{5.18}$$

Using a CMS approach, the inertia effects related to the internal DOFs are considered by a component mode superposition according to Eq. 5.14. In particular, CMS methods where $\mathbf{q}$ only contains physical master DOFs are often referred to as *condensation methods*, which are arguably the most straightforward techniques.

A basic condensation method is the Guyan reduction [48], where the inertia terms in Eq. 5.18 are ignored. This leads to the following transformation:

$$\begin{bmatrix} \mathbf{u}_i \\ \mathbf{u}_b \end{bmatrix} = \begin{bmatrix} \mathbf{\Psi}_{ib} \\ \mathbf{I}_{bb} \end{bmatrix} \mathbf{u}_b = \mathbf{T}_G \mathbf{q} \tag{5.19}$$

where $\mathbf{I}_{bb}$ is a $m \times m$ identity matrix, $\mathbf{\Psi}_{ib} = -\mathbf{K}_{ii}^{-1}\mathbf{K}_{ib}$ is the internal part of the component modes, and $\mathbf{T}_G$ is the $n \times m$ Guyan reduction matrix. The columns of the transformation matrix are the so-called constraint modes, obtained by prescribing a unit displacement for a boundary DOF, while the internal DOFs are force-free and the other boundary DOFs are held fixed. Thus, for a beam element, the constraint modes correspond to the mode shapes shown in Figure 5.1. Further, note that if retaining only one boundary DOF, the reduced system represents a *generalized* SDOF system, as discussed in Section 2.1.

Using condensation methods, the displacements of the boundary nodes are related to a set of component modes. In the Guyan reduction technique, these modes are based on the static

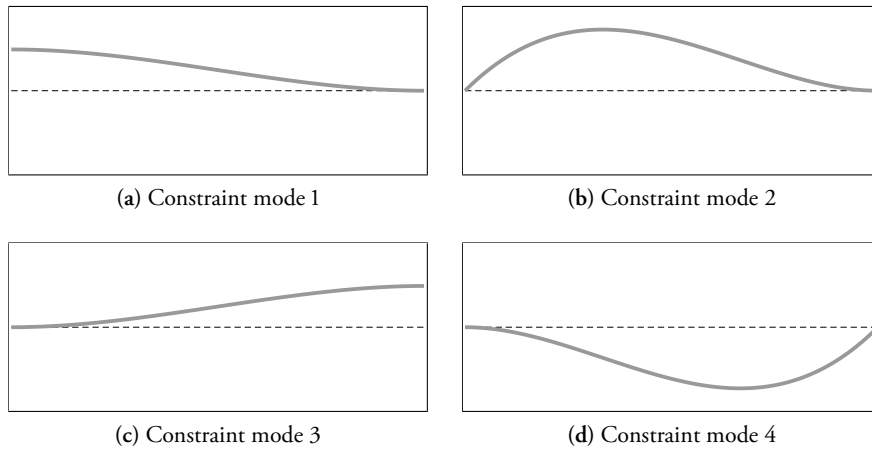

(a) Constraint mode 1 (b) Constraint mode 2

(c) Constraint mode 3 (d) Constraint mode 4

Figure 5.1: Constraint modes for beam with transversal (1 and 3) and rotational (2 and 4) boundary DOFs at beam ends.

displacement of the boundary, and accordingly "exact" results are achieved for static loading on the substructure boundary. For dynamic loading, however, the accuracy is highly dependent on the forcing frequency and the selected master DOFs.

Other condensation methods have been developed where the component modes are chosen differently. For example, the stiffness matrix can be replaced by the dynamic stiffness matrix, often referred to as dynamic reduction. Using this approach, "exact" results can be obtained in a steady state analysis for a certain forcing frequency. However, such a system is not "statically complete", i.e., the set of component modes does not span the possible displacements of the internal DOFs due to static loading on the boundary (note that the Guyan reduction can be interpreted as a dynamic reduction being evaluated at zero frequency). Other more sophisticated condensation methods have been developed, such as Improved Reduction System (IRS) and System Equivalent Reduction Expansion Process (SEREP) [24]. However, the number of exact resonances is always less or equal to the number of boundary nodes.

5.2.2 Fixed-interface methods

The component modes associated to the boundary DOFs, employed in the condensation methods, can be complemented by additional modes which enables reduced models that are both statically complete and that compensates for the neglected inertia terms related to the internal DOFs (cf. Eq. 5.18). These reduction methods, where the reduced coordinate vector includes both physical and/or generalized coordinates, may be divided into fixed- and free-interface methods [6]. The most common method is a fixed-interface method, namely the Craig–Bampton (C–B) method developed in the late 1960s [49], where the constraint modes are augmented by a set of fixed-interface normal modes (see Figure 5.2).

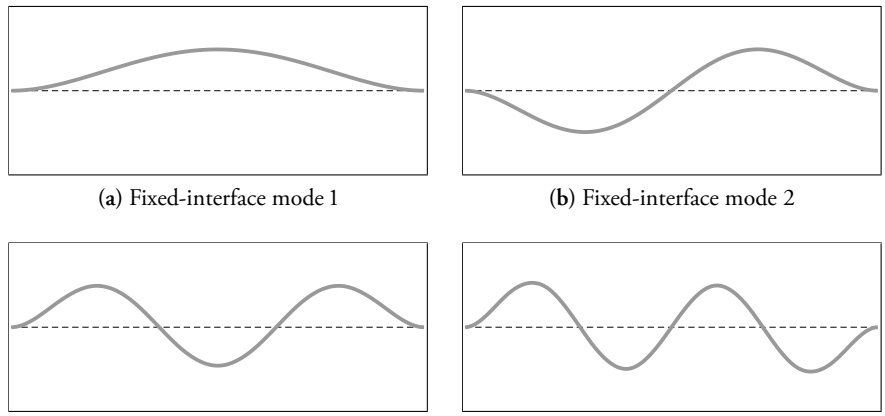

(**a**) Fixed-interface mode 1 (**b**) Fixed-interface mode 2

(**c**) Fixed-interface mode 3 (**d**) Fixed-interface mode 4

Figure 5.2: First four fixed-interface normal modes for beam element, with rotational and transversal DOFs at beam ends being boundary DOFs.

By setting the boundary displacements to zero in Eq. 5.17, the fixed-interface normal modes are obtained by the generalized eigenvalue problem:

$$\left(\mathbf{K}_{ii} - \omega_{i,j}^2 \mathbf{M}_{ii}\right) \boldsymbol{\phi}_{i,j} = 0 \tag{5.20}$$

where $\omega_{i,j}$ and $\boldsymbol{\phi}_{i,j}$ are the jth fixed-interface eigenfrequency and eigenmode, respectively. Further, $\mathbf{K}_{ii}$ and $\mathbf{M}_{ii}$ are the internal stiffness and mass matrices. The reduction matrix is then given by:

$$\begin{bmatrix} \mathbf{u}_i \\ \mathbf{u}_b \end{bmatrix} = \begin{bmatrix} \boldsymbol{\Phi}_{ik} & \boldsymbol{\Psi}_{ib} \\ \mathbf{0}_{bk} & \mathbf{I}_{bb} \end{bmatrix} \begin{bmatrix} \mathbf{q}_k \\ \mathbf{u}_b \end{bmatrix} = \mathbf{T}_{\mathrm{C-B}} \mathbf{q} \tag{5.21}$$

where the subscript k denotes the number of retained fixed-interface normal modes, $\mathbf{T}_{\mathrm{C-B}}$ is the Craig–Bampton transformation matrix, and $\boldsymbol{\Phi}_{ik}$ and $\boldsymbol{\Psi}_{ib}$ are the internal part of the set of fixed-interface normal modes and constraint modes, respectively. By setting $k \ll n_i$, a reduction is achieved in terms of a truncated fixed-interface modal basis. In contrast, if all fixed-interface modes are included in the basis, one obtains a pure transformation, without reducing the number of variables. Moreover, an important property of the C–B method is that the portion of the reduced system matrices related to the fixed-interface normal modes will by diagonal, thus, the reduced system matrices will in general be sparse (see further [6]).

A transformation according to Eq. 5.21 is employed in the standard C–B approach. In the early 2000s, an extension of the C–B method was proposed where the set of fixed-interface normal modes is augmented by higher order static correction modes [20]. The approach is similar to the generalized MTA method, discussed in Section 3.6. In particular, loading on the substructure boundary is considered in the derivation and, moreover, the static modes can be generated in a computationally efficient manner by means of matrix–vector multiplications.

If assuming that the external forces are only applied on boundary DOFs, the top row of Eq. 5.18 can be rewritten as:

$$\mathbf{M}_{ii}\ddot{\mathbf{u}}_i + \mathbf{K}_{ii}\mathbf{u}_i = -\mathbf{M}_{ib}\ddot{\mathbf{u}}_b - \mathbf{K}_{ib}\mathbf{u}_b. \tag{5.22}$$

Hence, the substructure internal DOFs can be considered excited by imposed displacement on its boundary. Similarly to the derivation in Section 3.5, the internal displacements can be split into a static and dynamic part:

$$\mathbf{u}_i = \mathbf{u}_{i,\text{stat}} + \mathbf{y}. \tag{5.23}$$

By setting the accelerations to zero in Eq. 5.22, the static part is given by $\mathbf{u}_{i,\text{stat}} = -\mathbf{K}_{ii}^{-1}\mathbf{K}_{ib}\mathbf{u}_b$. Then, by substituting Eq. 5.23 into Eq. 5.22 and rearranging the terms, the dynamic part $\mathbf{y}$ can be replaced by a quasi-static solution and a dynamic correction (cf. Eq. 3.24). Thus, a recursive procedure can be derived such that the displacement of the internal DOFs can be approximated as:

$$\mathbf{u}_i \approx -\mathbf{K}_{ii}^{-1}\mathbf{K}_{ib}\mathbf{u}_b + \sum_{j=1}^{k}\left(-\mathbf{K}_{ii}^{-1}\mathbf{M}_{ii}\right)^{j-1}\mathbf{K}_{ii}^{-1}\mathbf{Y}\frac{\mathrm{d}^{2j}\mathbf{u}_b}{\mathrm{d}t^{2j}} \tag{5.24}$$

where $\mathbf{Y} = \mathbf{M}_{ii}\mathbf{K}_{ii}^{-1}\mathbf{K}_{ib} - \mathbf{M}_{ib}$. As in the Krylov-subspace method and the generalized MTA method (cf. Sections 3.5 adn 3.6), the higher order derivatives may be replaced by generalized coordinates, i.e., which are treated as additional variables in the dynamic response analysis. Moreover, for numerical robustness, the static corrections may be computed using the residual flexibility, as discussed in Section 3.6. A set of jth-order correction modes are then given by:

$$\boldsymbol{\psi}_{i,\text{cor}.j} = \left(\mathbf{K}_{ii}^{-1} - \sum_{r=1}^{k}\frac{\boldsymbol{\phi}_r\boldsymbol{\phi}_r^{\mathrm{T}}}{\omega_r^2}\right)\left(\mathbf{M}_{ii}\mathbf{K}_{ii}^{-1}\right)^{j-1}\mathbf{Y}. \tag{5.25}$$

The resulting set of correction modes are mass- and stiffness-orthogonal to the fixed-interface normal modes. Similarly to the generalized MTA method, the correction modes can be made mutually orthogonal by solving a reduced eigenvalue problem (e.g., see Eq. 3.4). Then, a transformation of the following form is obtained:

$$\begin{bmatrix}\mathbf{u}_i\\ \mathbf{u}_b\end{bmatrix} = \begin{bmatrix}\boldsymbol{\Phi}_{ik} & \widetilde{\boldsymbol{\Psi}}_{il,\text{cor}.} & \boldsymbol{\Psi}_{ib}\\ \mathbf{0}_{bk} & \mathbf{0}_{bl} & \mathbf{I}_{bb}\end{bmatrix}\begin{bmatrix}\mathbf{q}_k\\ \mathbf{q}_l\\ \mathbf{u}_b\end{bmatrix} = \mathbf{T}_{\mathrm{C-B,cor}.}\mathbf{q} \tag{5.26}$$

where the columns of the matrix $\widetilde{\boldsymbol{\Psi}}_{il,\text{cor}.}$ are the total set of l (orthogonalized) pseudo-static modes and $\mathbf{T}_{\mathrm{C-B,cor}.}$ is the reduction matrix where the fixed-interface modal basis is augmented by higher order static modes.

The higher order static modes, as introduced above, are force-dependent in the sense that loading on the substructure boundary DOFs (i.e., expressed in terms of imposed displacements)

is considered. It should be noted, however, that the above procedure implies that the number of pseudo-static modes generated in each iteration correspond to the number of boundary DOFs. Hence, if the number of boundary DOFs is large, this methodology is best used in combination with an interface reduction technique, as further discussed in Section 5.2.4.

In both the standard C–B method and in an approach where the fixed-interface modal basis is augmented by higher order static modes, the physical boundary DOFs are retained in the reduction process. Hence, a global assembly can be formed using any of the assembly methods discussed in Section 5.1.

For instance, consider an assembly including two substructures reduced by means of the standard C–B method. Then, if assuming a conforming interface discretization, a unique set of coordinates can be obtained using the transformation:

$$\underbrace{\begin{bmatrix} \mathbf{q}_{k_1}^{(1)} \\ \mathbf{u}_b^{(1)} \\ \mathbf{q}_{k_2}^{(2)} \\ \mathbf{u}_b^{(2)} \end{bmatrix}}_{\hat{\mathbf{q}}} = \underbrace{\begin{bmatrix} \mathbf{I}_{k_1 k_1}^{(1)} & \mathbf{0} & \mathbf{0} \\ \mathbf{0} & \mathbf{0} & \mathbf{I}_{bb}^{(1)} \\ \mathbf{0} & \mathbf{I}_{k_2 k_2}^{(2)} & \mathbf{0} \\ \mathbf{0} & \mathbf{0} & \mathbf{I}_{bb}^{(2)} \end{bmatrix}}_{\mathbf{L}} \underbrace{\begin{bmatrix} \mathbf{q}_{k_1}^{(1)} \\ \mathbf{q}_{k_2}^{(2)} \\ \mathbf{u}_b \end{bmatrix}}_{\hat{\mathbf{q}}_P} \tag{5.27}$$

where $\mathbf{L}$ is a Boolean matrix localizing the boundary DOFs of the substructures, and $\hat{\mathbf{q}}_P$ is the unique set of coordinates in a primal formulation (cf. Section 5.1). Hence, a global assembly can be formed using Eq. 5.8, i.e., similar to a standard FE assembly procedure.

The assembly procedure, as described above, can be generalized to consider an arbitrary number of substructures, non-conforming meshes, etc. (e.g., see [21]). Furthermore, the global assembly may include nonlinear subsystems. Hence, the linear substructures can then be modeled using any of the fixed-interface CMS techniques discussed above, while the nonlinear subsystems may be formulated using full-order FE submodels.

5.2.3 Free-interface methods

In the 1970s, so-called free-interface methods were developed by MacNeal, Rubin, and Craig and Chang [50–52]. Instead of fixed-interface component modes, these methods use a reduction basis including free-interface normal modes and, possibly, rigid body modes.

The free-interface normal modes $\boldsymbol{\phi}_j$ (cf. Figure 5.3) are determined from the generalized eigenvalue problem:

$$\left(\mathbf{K} - \omega_j^2 \mathbf{M}\right) \boldsymbol{\phi}_j = 0 \tag{5.28}$$

where $\mathbf{K}$ and $\mathbf{M}$ are the component stiffness and mass matrices, respectively. Note that these matrices, in contrast to the system matrices in Eq. 5.20, include partitions related to both the internal and boundary DOFs (cf. Eq. 5.17).

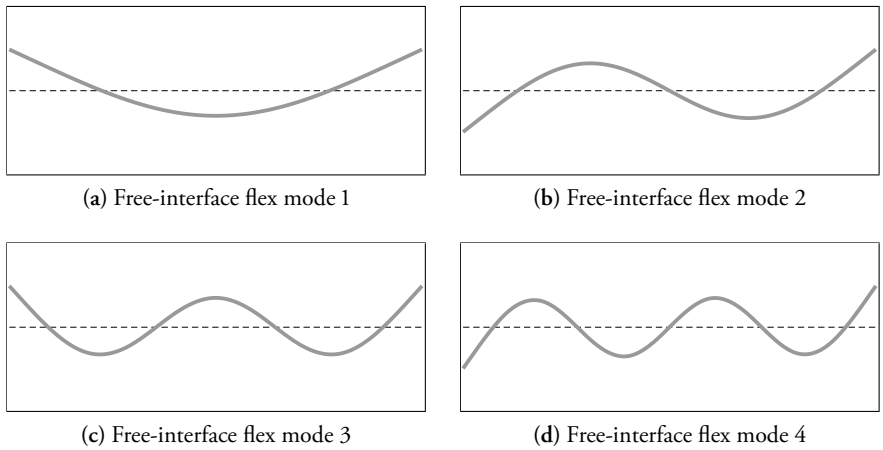

(a) Free-interface flex mode 1 (b) Free-interface flex mode 2

(c) Free-interface flex mode 3 (d) Free-interface flex mode 4

Figure 5.3: First four free-interface flex modes for beam element with free-free boundary conditions.

Further, using a free-interface approach, the constraint modes employed in the fixed interface methods are typically replaced by attachment modes, corresponding to unit loading on the boundary DOFs. More specifically, an attachment mode corresponds to a unit load applied on a boundary DOF while the other DOFs are force-free.

Moreover, the attachment modes can be computed based on the component residual flexibility, i.e. similar to what is done in the generalized MTA method as well as the fixed-interface CMS approach including higher-order static modes (see Sections 3.6 and 5.2.2, respectively). The *residual* attachment modes can be expressed as:

$$\boldsymbol{\Psi}_{nb} = \begin{bmatrix} \boldsymbol{\Psi}_{ib} \\ \boldsymbol{\Psi}_{bb} \end{bmatrix} = \mathbf{G}_{\text{res}} \begin{bmatrix} \mathbf{0}_{ib} \\ \mathbf{I}_{bb} \end{bmatrix} \tag{5.29}$$

where $\mathbf{G}_{\text{res}}$ is the components residual flexibility matrix, which can be expressed in terms of the spectral expansion of the inverse stiffness matrix (cf. Eq. 3.8):

$$\mathbf{G}_{\text{res}} = \sum_{j=k+1}^{n} \frac{\phi_j \phi_j^{\text{T}}}{\omega_j^2} = \left(\mathbf{K}^{+} - \sum_{j=1}^{k} \frac{\phi_j \phi_j^{\text{T}}}{\omega_j^2} \right). \tag{5.30}$$

Here, k is the number of retained free-interface eigenmodes (excluding rigid body modes), and $\mathbf{K}^{+}$ is a pseudo-inverse of the component stiffness matrix. Furthermore, as indicated by Eq. 5.29, the residual attachment modes correspond to columns of the residual flexibility matrix.

It should be noted that a computation of $\mathbf{G}_{\text{res}}$ based on the discarded modes, thus, by performing the summation from $k+1$ to n in Eq. 5.30, is in general not possible, i.e., since it necessitates a computation of all free-interface eigenmodes. Therefore, the second expression in Eq. 5.30 is used in practice. For components constrained such that there are no rigid body

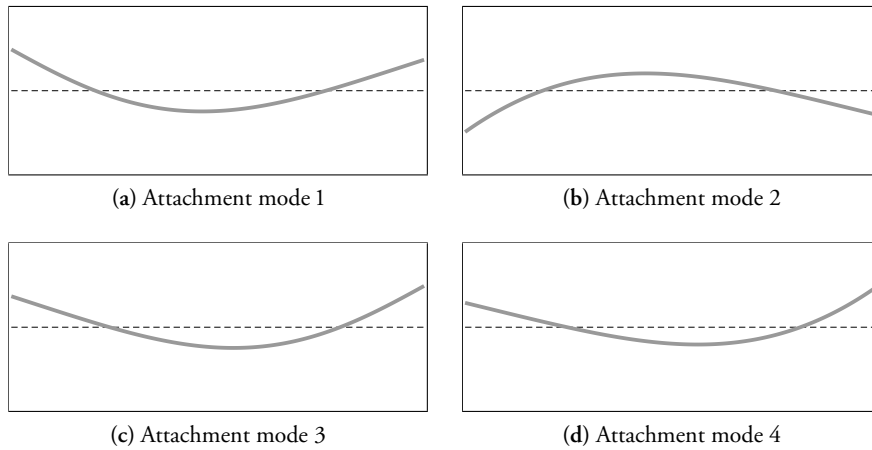

(**a**) Attachment mode 1 (**b**) Attachment mode 2

(**c**) Attachment mode 3 (**d**) Attachment mode 4

Figure 5.4: Inertia-relief attachment modes corresponding to loading at transversal (1 and 3) and rotational (2 and 4) DOFs at beam ends.

modes, the component stiffness matrix is invertible and the residual attachment modes can be computed in a straightforward manner, i.e., $\mathbf{K}^{+} = \mathbf{K}^{-1}$ (see also Paper E). However, if rigid body modes are present, which in general is the case, the stiffness matrix will be singular and a pseudo-inverse of the stiffness matrix is required.

Recall that the attachment modes correspond to unit loading on the boundary DOFs (cf. Eq 5.29). It follows that the problem of finding a pseudo-inverse can in principle be replaced by the problem of finding self-equilibrated force systems replacing the unit forces on the boundary DOFs (cf. Figure 5.4). A detailed description of how to compute a pseudo-inverse using this approach can e.g. be found in [6]. In summary, a pseudo-inverse, referred to as the *constrained flexibility matrix*, is first computed by constraining suitable DOFs. Then, a projection matrix termed *inertia-relief projection matrix* is constructed which converts a given force vector to a self-equilibrated force system. Further, by post-multiplying the constrained flexibility matrix with the inertia-relief projection matrix one obtains a matrix whose columns correspond to modes of self-equilibrated force systems. Finally, by pre-multiplying with the transpose of the inertia-relief projection matrix the corresponding modes are made orthogonal to the rigid body modes. The pseudo-inverse obtained using this procedure actually correspond to the elastic flexibility matrix, i.e. a spectral expansion of the inverse of the stiffness matrix where the rigid body modes are excluded (indeed, including rigid body modes in Eq. 5.30 would imply division by zero).

Now, a transformation matrix can be defined based on the rigid body modes, free-interface eigenmodes, and the residual-flexibility attachment modes, i.e.

$$\begin{bmatrix} \mathbf{u}_i \\ \mathbf{u}_b \end{bmatrix} = \begin{bmatrix} \boldsymbol{\Phi}_{ir} & \boldsymbol{\Phi}_{ik} & \boldsymbol{\Psi}_{ib} \\ \boldsymbol{\Phi}_{br} & \boldsymbol{\Phi}_{bk} & \boldsymbol{\Psi}_{bb} \end{bmatrix} \begin{bmatrix} \mathbf{q}_r \\ \mathbf{q}_k \\ \mathbf{g}_b \end{bmatrix} = \mathbf{T}_{\mathrm{RFA}} \mathbf{q}. \tag{5.31}$$

Here, r denotes the rigid body modes, $\mathbf{g}_b$ contain the generalized coordinates representing the amplitude of the residual attachment modes, and $\mathbf{T}_{\mathrm{RFA}}$ is the so-called *augmented free-interface transformation matrix* [6].

In a CMS technique where the boundary DOFs are kept as physical DOFs, an assembly can be formed in a straightforward manner using any of the assembly methods discussed in Section 5.1. However, this approach cannot be adopted if, e.g., using the transformation given by Eq. 5.31. Hence, because the constraint modes are replaced by attachment modes, the physical boundary DOFs are not available in the reduced coordinate vector. Instead, a global assembly has to be formed using alternative procedures, as further discussed below.

For a system including N substructures, the global displacement vector can be written in terms of the global coordinate vector $\mathbf{q}$, as:

$$\mathbf{u} \approx \mathbf{T}\mathbf{q} \tag{5.32}$$

where

$$\mathbf{T} = \mathrm{diag}\left(\mathbf{T}^{(1)}, \mathbf{T}^{(2)}, \ldots, \mathbf{T}^{(N)}\right), \quad \mathbf{q} = \begin{bmatrix} \mathbf{q}^{(1)\mathrm{T}} & \mathbf{q}^{(2)\mathrm{T}} & \ldots & \mathbf{q}^{(N)\mathrm{T}} \end{bmatrix}^{\mathrm{T}}. \tag{5.33}$$

Here, the component reduction matrices $\mathbf{T}^{(s)}$ $(s = 1, \ldots, N)$ can, e.g., be constructed in accordance with Eq. 5.31. By substituting Eq. 5.32 into Eq. 5.1b, it follows that the compatibility condition can be transformed to generalized coordinates, as (e.g., see [4]):

$$\mathbf{B}\mathbf{u} = \mathbf{B}\mathbf{T}\mathbf{q} = \mathbf{B}_q\mathbf{q} = \mathbf{0}. \tag{5.34}$$

Similar to the primal assembly approach for substructures with physical boundary DOFs, as described in Section 5.1, a unique set of global coordinates $\mathbf{q}_P$ satisfying the compatibility condition can be found from the expression $\mathbf{q} = \mathbf{L}_q\mathbf{q}_P$, where $\mathbf{L}_q = \mathrm{null}(\mathbf{B}_q)$. Here, $\mathbf{B}_q$ and $\mathbf{L}_q$ are in general non-Boolean.

Now, by applying $\mathbf{T}$ to Eq. 5.1a, the reduced substructures (cf. Eq. 5.16) can be written in block-diagonal form. It follows that, by adopting a primal formulation according to Eq. 5.8, a global assembly can be expressed in terms of the unique set of global coordinates $\mathbf{q}_P$. Alternatively, a global assembly may be established using a dual formulation. As described in [4], a dually formulated system can be expressed using Largange multipliers, similar to the approach used for substructures with physical boundary DOFs (cf. Eq. 5.11).

To further simplify the assembly process, it can be convenient to formulate the reduced components such that the boundary DOFs are available on the substructure level, i.e., such that each component can be treated as a superelement. This can be achieved using MacNeal's and Rubin's methods [50, 51], being free-interface methods that retains the physical boundary DOFs.

By rearranging the terms in the bottom row of Eq. 5.31, the generalized coordinates $\mathbf{g}_b$ can be expressed as:

$$\mathbf{g}_b = \boldsymbol{\Psi}_{bb}^{-1}\left(\mathbf{u}_b - \boldsymbol{\Phi}_{br}\mathbf{q}_r - \boldsymbol{\Phi}_{bk}\mathbf{q}_k\right). \tag{5.35}$$

It follows that an additional transformation may be defined, i.e.:

$$\begin{bmatrix} \mathbf{q}_r \\ \mathbf{q}_k \\ \mathbf{g}_b \end{bmatrix} = \begin{bmatrix} \mathbf{I}_{rr} & \mathbf{0} & \mathbf{0} \\ \mathbf{0} & \mathbf{I}_{kk} & \mathbf{0} \\ -\boldsymbol{\Psi}_{bb}^{-1}\boldsymbol{\Phi}_{br} & -\boldsymbol{\Psi}_{bb}^{-1}\boldsymbol{\Phi}_{bk} & \boldsymbol{\Psi}_{bb}^{-1} \end{bmatrix} \begin{bmatrix} \mathbf{q}_r \\ \mathbf{q}_k \\ \mathbf{u}_b \end{bmatrix}. \tag{5.36}$$

Hence, by applying both transformations, given by Eq. 5.31 and Eq. 5.36, respectivly, a reduced substructure can be constructed such that the physical boundary DOFs are kept in the coordinate vector. Accordingly, a global assembly can be formed in a standard manner using any of the assembly methods in Section 5.1. This procedure is employed in the Rubin method. The MacNeal approach is similar—an alternative approach is used for constructing a diagonal mass matrix, whereas the reduced stiffness matrix is identical in both methods (see e.g. [21] for further details).

In contrast to the fixed-interface methods, the sparsity of the system matrices is in general lost when using the free-interface approaches discussed above. However, another free-interface method was developed in the early 2000s, referred to as the dual C–B method [53] which, unlike the other free-interface methods, preserves the sparsity of the system matrices. It does not employ a true Rayleigh–Ritz transformation, however, and the compatibility condition is enforced in a weakened sense. In particular, it requires special techniques to ensure stability in direct time-integration schemes [54].

Finally, it should be mentioned that also the free-interface reduction bases discussed above can be augmented by higher order quasi-static modes, see e.g. [55]. This is, however, not further investigated herein.

5.2.4 Interface reduction

In practical applications, the number of physical interface DOFs can often be very large and, therefore, much can be gained if an interface reduction is performed. In both the free- and fixed-interface CMS approaches the sparsity is lost in the parts of the system matrices related to interface DOFs. Hence, models including a large number of boundary DOFs can become computationally expensive.

Various approaches can be used for reducing the number of interface DOFs (see e.g. [56, 57]). In general, the preferred interface reduction approach depends on the specific application. In particular, a reduction may be performed on the substructure level, before the substructures are assembled or, in contrast, on the global assembled structure.

The simplest interface reduction approach is obtained by assuming rigid interfaces, i.e., by constraining the interface DOFs to the motion of a virtual master node, having three translational and three rotational DOFs (in a three-dimensional domain). Using a similar approach, the displacements of a virtual node may be defined as the weighted mean value of the interface DOFs, a constraint often referred to as a *distributed coupling* (see e.g. [58, 59]). In particular, it turns out that the interface-forces on the interface DOFs are related to the weights (see

Papers C and E). Accordingly, the sum of the weights is related to the interface force acting on the virtual node (also referred to as condensation node or master node). Hence, a distributed coupling can be employed for establishing a coupling with an arbitrary interface-force distribution (see further Paper C and E).

Furthermore, a reduction may be performed using a secondary eigenvalue analysis on the *bb*-partitions of the assembled system [6]. Thus, the interface DOFs are replaced by a truncated set of interface eigenvectors. Using this approach, however, the physical interface DOFs are lost in the reduction process.

5.3 GEOMETRICALLY NONLINEAR SUBSTRUCTURES

Dynamic substructuring techniques for geometrically nonlinear structures have, e.g., been proposed in [60–68]. The linear CMS methods, as discussed in Section 5.2, are generally used as a starting point. Thus, on the substructure level, either the fixed-interface C–B or free-interface Rubin/MacNeal reduction basis is typically adopted.

More specifically, in [60], the fixed-interface C–B method was extended to consider geometric nonlinearity. Reduction bases including constraint modes and a truncated set of fixed-interface eigenmodes were considered. The nonlinear restoring forces were expressed as cubic mutivariate polynomials, i.e., using the concepts discussed in Section 4.1.1, and the NSCs were determined in a nonintrusive manner using the ICE method (cf. Section 4.2.4). Furthermore, an enriched basis was introduced in the post-processing stage using the expansion process described in Section 4.2.4. In [61], the nonlinear substructuring approach was extended to consider interface reduction.

A free-interface geometrically nonlinear substructuring approach was proposed in [62]. The Rubin/MacNeal reduction basis was adopted and the NSCs were determined using the ICE method. Similar to the procedure proposed in [60], the statically condensed response of (in-plane) modes were considered implicitly. Moreover, various interface reduction techniques were suggested.

Approaches using reduction bases enriched by modal derivatives were proposed in [63, 64], where the NSCs were precomputed using direct methods. Nonintrusive procedures for nonlinear reduced order modeling using C–B reduction bases enriched by modal derivatives were suggested in [65].

The reduced equations of motion for geometrically nonlinear substructures are briefly described in Section 5.3.1. Aspects regarding the coupling procedure for geometrically nonlinear substructures are discussed in Section 5.3.2.

5.3.1 Equations of motion for nonlinear substructures

Recall that the physical displacements of a substructure can be approximated such that $\mathbf{u}^{(s)} \approx \mathbf{T}^{(s)}\mathbf{q}^{(s)}$. Here, $\mathbf{T}^{(s)}$ is the substructure reduction basis and $\mathbf{q}^{(s)}$ is the associated reduced coordinate vector, which may include both physical boundary DOFs and additional generalized coordinates associated to fixed- or free-interface component modes (cf. Section 5.2).

The reduced equation of motion of a geometrically nonlinear substructure can then be expressed as:

$$\tilde{\mathbf{M}}^{(s)}\ddot{\mathbf{q}}^{(s)} + \tilde{\mathbf{C}}^{(s)}\dot{\mathbf{q}}^{(s)} + \tilde{\mathbf{f}}^{(s)}(\mathbf{q}^{(s)}) = \tilde{\mathbf{p}}^{(s)} + \tilde{\mathbf{g}}^{(s)} \tag{5.37}$$

where the reduced mass and damping matrices $\tilde{\mathbf{M}}^{(s)}$ and $\tilde{\mathbf{C}}^{(s)}$, and the external and interface force vectors $\tilde{\mathbf{p}}^{(s)}$ and $\tilde{\mathbf{g}}^{(s)}$ were defined in Eq. 5.16 (linear damping is considered here to simplify the notation). Moreover, the reduced nonlinear restoring forces are given by $\tilde{\mathbf{f}}^{(s)} = \mathbf{T}^{(s)\mathrm{T}}\mathbf{f}^{(s)}(\mathbf{T}^{(s)}\mathbf{q}^{(s)})$, where $\mathbf{f}^{(s)}$ is the full-order nonlinear restoring force vector.

If assuming large displacements and small strains, the reduced nonlinear restoring forces for a substructure can be expressed as cubic polynomials, i.e., as described in Section 4.1.1. Hence, using the compact tensor notation, the restoring forces can be expressed as:

$$\tilde{\mathbf{f}}^{(s)}(\mathbf{q}^{(s)}) = \mathbf{K}^{(1)(s)}\mathbf{q}^{(s)} + \mathbf{K}^{(2)(s)}\mathbf{q}^{(s)}\mathbf{q}^{(s)} + \mathbf{K}^{(3)(s)}\mathbf{q}^{(s)}\mathbf{q}^{(s)}\mathbf{q}^{(s)}. \tag{5.38}$$

The coefficients of the stiffness tensors $\mathbf{K}^{(2)(s)}$ and $\mathbf{K}^{(3)(s)}$ can, e.g., be determined in a non-intrusive manner using the ICE or ED method, as described in detail in [60, 65] (see also Section 4.2 and Paper E).

5.3.2 Substructure coupling procedure

An assembly can be formed using, e.g., a primal assembly approach, as described in Section 5.1. To this end, the global system including reduced substructures can be written in block-diagonal form, as:

$$\tilde{\mathbf{M}}\ddot{\mathbf{q}} + \tilde{\mathbf{C}}\dot{\mathbf{q}} + \tilde{\mathbf{f}}(\mathbf{q}) = \tilde{\mathbf{p}} + \tilde{\mathbf{g}} \tag{5.39}$$

where

$$\tilde{\mathbf{M}} = \mathbf{T}^{\mathrm{T}}\mathbf{M}\mathbf{T}, \quad \tilde{\mathbf{C}} = \mathbf{T}^{\mathrm{T}}\mathbf{C}\mathbf{T}, \quad \tilde{\mathbf{p}} = \mathbf{T}^{\mathrm{T}}\mathbf{p}, \quad \tilde{\mathbf{g}} = \mathbf{T}^{\mathrm{T}}\mathbf{g}.$$

Here, the full-order matrices and vectors $\mathbf{M}$, $\mathbf{C}$, $\mathbf{p}$, and $\mathbf{g}$ were defined in Eq. 5.1, and $\mathbf{T}$ and $\mathbf{q}$ are given by Eq. 5.33. Further, the reduced restoring force vector of the global system is given by:

$$\tilde{\mathbf{f}}(\mathbf{q}) = \begin{bmatrix} \tilde{\mathbf{f}}^{(1)}(\mathbf{q}^{(1)}) \\ \vdots \\ \tilde{\mathbf{f}}^{(N)}(\mathbf{q}^{(N)}) \end{bmatrix}. \tag{5.40}$$

As described in Section 5.2, the compatibility condition can be written as $\mathbf{B}\mathbf{u} = \mathbf{B}\mathbf{T}\mathbf{q} = \mathbf{B}_q\mathbf{q} = \mathbf{0}$. Furthermore, the equilibrium condition is expressed by $\mathbf{L}_q^{\mathrm{T}}\tilde{\mathbf{g}}$, where $\mathbf{L}_q$ is the

null-space of $\mathbf{B}_q$. Using a primal formulation, a unique set of assembled coordinates $\mathbf{q}_P$ are then given by $\mathbf{q} = \mathbf{L}_q \mathbf{q}_P$. It follows that the constrained equations of motion can be written as:

$$\mathbf{L}_q^{\mathrm{T}} \tilde{\mathbf{M}} \mathbf{L}_q \ddot{\mathbf{q}}_P + \mathbf{L}_q^{\mathrm{T}} \tilde{\mathbf{C}} \mathbf{L}_q \dot{\mathbf{q}}_P + \mathbf{L}_q^{\mathrm{T}} \tilde{\mathbf{f}}(\mathbf{L}_q \hat{\mathbf{q}}_P) = \mathbf{L}_q^{\mathrm{T}} \tilde{\mathbf{p}}. \tag{5.41}$$

If the nonlinear reduced model is solved using Newmark implicit time-integration, the equilibrium iterations necessitates evaluations of the tangent stiffness matrix (cf. Section 2.5.2). In a primal formulation, the assembled tangent stiffness matrix can be expressed as:

$$\tilde{\mathbf{K}}_P = \mathbf{L}_q^{\mathrm{T}} \tilde{\mathbf{K}}(\mathbf{q}) \mathbf{L}_q \tag{5.42}$$

where

$$\tilde{\mathbf{K}}(\mathbf{q}) = \mathrm{diag}\left(\tilde{\mathbf{K}}^{(1)}(\mathbf{q}^{(1)}), \ldots, \tilde{\mathbf{K}}^{(N)}(\mathbf{q}^{(N)}) \right)$$

and where the tangent stiffness matrices of the substructures, $\tilde{\mathbf{K}}^{(s)}$ ($s = 1, \ldots, N$), are given by Eq. 4.26.

The physical boundary DOFs are retained in both the fixed-interface C–B method and the free-interface Rubin/MacNeal method. Accordingly, if assuming a conforming discretization on interfaces, the matrix $\mathbf{L}_q$ will be a Boolean localization matrix, as exemplified in Eq. 5.27.

6 Applications: structures subjected to blast and impact loading

This chapter presents an overview of applications concerning blast and impact loading. Focus is on the development of time-efficient modeling strategies which are suitable for a structural verification or design process. More specifically, the aim is to establish reduced models which are computationally efficient, while maintaining sufficient accuracy of important output quantities. In particular, this allows for an interactive design process where parameters and design concepts may be evaluated in a time-efficient manner. The proposed models are primarily intended to be implemented in user-friendly FE tools, such as ClearSight [5], being specialized for specific engineering applications. Details regarding the developed modeling strategies are provided in the appended papers.

Structural engineering applications within two different areas have been investigated; namely, concerning concrete structures subjected to blast loading (Papers A and B) and glass panels subjected to impact loading (Papers C and E). Some of the challenges with regard to computational aspects are similar. In particular, the structural dynamics problems involve transient loading and various types of nonlinear behaviors, e.g., localized nonlinearities in the form of contact conditions or nonlinear materials, as well as geometric nonlinearities which, in contrast, is a distributed nonlinearity where degrees of freedoms throughout the structure are nonlinearly coupled.

Due to the presence of nonlinear behaviors, the efficient modal techniques commonly used in linear dynamics cannot be utilized (cf. Chapters 2 and 3). However, locally nonlinear reduced models may be formulated using DS, as described in Chapter 5. Hence, the parts of the structures that remain linear elastic can be modeled using a reduced set of generalized coordinates, while the nonlinear parts are expressed in terms of physical displacements. Further, by assuming small strains and large displacements, geometrically nonlinear effects can be effectively modeled using the techniques discussed in Chapter 4.

Section 6.1 presents an overview of modeling techniques for analysis of concrete structures subjected to blast loading. Simplified models commonly used in the industry as well as alternative procedures using reduced models are briefly discussed. In Section 6.2, modeling strategies for predicting the response of glass panels subjected to impact loading are discussed, which is an

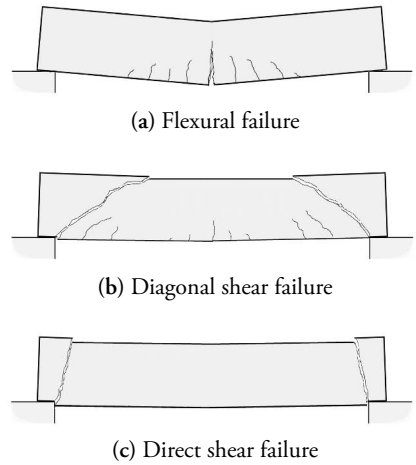

(**a**) Flexural failure

(**b**) Diagonal shear failure

(**c**) Direct shear failure

Figure 6.1: Example of failure modes for reinforced concrete beam subjected to uniform impulse pressure.

important load case in design of glazed barriers.

6.1 CONCRETE STRUCTURES SUBJECTED TO BLAST LOADING

Several aspects in the structural design of concrete structures subjected to blast loading are fundamentally different compared to a verification of static loads. Not only the load-bearing capacity, but also the ductility of the structure is of considerable importance. To ensure that the structure can withstand the external pulse, it must be designed such that the induced kinetic energy can be absorbed. For example, the kinetic energy may be converted into elastic and plastic strain energy. Thus, the ductility of the structure, i.e. the capability to deform plastically without failure, is of importance. In particular, concrete members, such as beams and plates, must be designed to resist brittle failure modes.

With regard to the semi-global response (i.e. the global response of an individual member, such as beams and slabs) at least three failure modes must be considered to ensure an adequate design; namely, flexural failure, diagonal shear failure, and direct shear failure, as illustrated in Figure 6.1 [8]. If the concrete member is designed using bending reinforcement with sufficient ductility and an appropriate reinforcement arrangement, a flexural failure mode is typically desirable, while brittle failure modes, such as shear failure, should be avoided. Further, if a flexural failure mode can be ensured, the elastic strain energy upon failure is often significantly smaller than the plastic dissipation. Consequently, a model that considers the nonlinear structural behavior is required to avoid a too conservative design.

Generalized SDOF systems (cf. Section 2.1) are commonly used for evaluating concrete mem-

bers, such as beams and slabs, subjected to blast loading. More specifically, a so-called equivalent SDOF system is formulated by means of an assumed shape function and a reference point, e.g., located at midspan. Then, an equivalent stiffness, mass, and load are determined such that the internal energy, kinetic energy, and external work for the SDOF system and the continuous structure are equivalent (e.g., see [69]). In particular, this approach allows for estimating the nonlinear elasto-plastic response of beams or slabs where plastic hinges/yield lines may develop, at least in an approximate manner. However, the locations of the plastic hinges are predefined, e.g., for a simply supported beam, a plastic hinge may be introduced at midspan. Further, the assumed mode shape is no longer continuous. Instead, a shape function is typically obtained by neglecting the elastic deformations and only consider the plastic rotation at the plastic joints (cf. Figure 2.2). Hence, the shape function corresponds to a rigid body mode of the system, assuming free-rotations at the predefined joints (however, as suggested in [8], a combined elastic and plastic shape function can be considered in an approximate manner using weight factors). This methodology, which was proposed already in the mid 1960s [70], can be very useful, particularly in the conceptual design phase. In fact, if assuming that the pulse time is negligible, which is reasonable in many practical applications, a peak response can be estimated without conducting a response analysis, namely, by simply equating the internal work and the kinetic energy induced in the system due to the external impulse.

Despite its utility, the approach using an equivalent SDOF system has several limitations. In particular, the response of higher order modes is neglected. For a concrete member subjected to blast loading, resulting in a very large pressure with short duration, the influence of higher order modes can, however, have a significant influence on the response. For example, the shear force close to supports might not be accurately represented by an SDOF model (see e.g. [71]). Particularly for concrete members without shear reinforcement, brittle failure modes, such as shear failure, are often critical.

In Paper A, the influence of higher order modes on the shear force close to supports is further investigated. More specifically, reduced models of beams with predefined plastic joints were developed by use of DS. The rotational DOFs at the plastic joints were selected as boundary DOFs, while the remaining structure was represented by a few fixed-interface eigenmodes. The model thus considers the response of higher order modes as well as the ductility of a flexural failure mode.

If using an SDOF model, a proper representation of the interaction between structural members and the global load-bearing structure is in general not possible. Instead, the global structure is often considered rigid in the response analysis of an individual member. In many applications, this simplified approach can be sufficiently accurate, since the mass of the global structure is often large compared to the mass of the individual member. However, some applications necessitate a more detailed modeling of the supporting structure. For instance, consider a concrete frame structure, as illustrated in Figure 6.2, subjected to a uniformly distributed horizontal impulse pressure. Indeed, a verification considering the two failure modes shown in the figure—related to lateral stability and progressive collapse, respectively—cannot be properly captured by an SDOF model. Thus, to consider mixed failure modes, an integ-

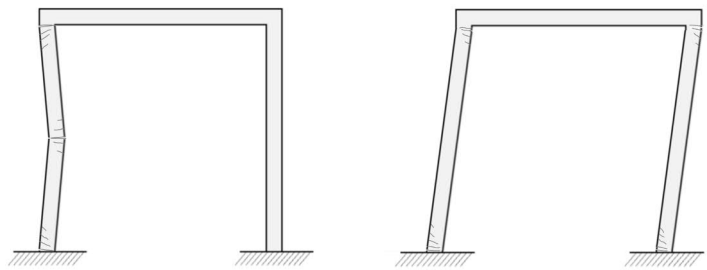

(**a**) Progressive collapse (**b**) Lateral stability

Figure 6.2: Example of failure modes for concrete frame structure subjected to blast loading.

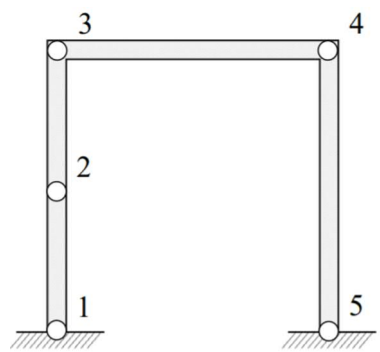

Figure 6.3: Example of predefined plastic hinges for a concrete frame structure.

rated analysis is required where the response of the frame columns as well as the horizontal beam are computed simultaneously.

In Paper B, strategies are presented for modeling concrete-frame structures with an arbitrary number of predefined plastic joints. Furthermore, to obtain computationally efficient models, parts remaining linear elastic were reduced by means of DS. For the concrete frame in Figure 6.2, an approximate model, being suitable at least in a conceptual design phase, can be established by allowing plastic hinges to be developed at five positions, as illustrated in Figure 6.3. Furthermore, a more accurate model can be obtained by including additional joints, e.g., by adding multiple joints at the frame corners, such that the mass of the frame corners is considered.

6.2 GLASS STRUCTURES SUBJECTED TO IMPACT LOADING

Building regulations in many countries prescribe that glazed barriers, such as full-height facades and parapets for balconies or interior level changes, which may constitute a safety risk for

building occupants, must be designed to withstand accidental impact of humans. To ensure an adequate design, the glass structure load-bearing capacity is often verified using experimental tests, based on the standardized soft-body pendulum described in the European Standard EN 12600 [72]. A typical test arrangement is shown in Figure 6.4.

Alternatively, the structural dynamic response can be evaluated using numerical methods. To this end, a simplified approach is commonly adopted, where the response of higher order modes is neglected. Similarly to the methodology for design of concrete members, the glass structure is then modeled by means of a generalized SDOF system. Here, however, an integrated analysis of the glass structure and the impacting body is generally required. Thus, the glass panel is represented by an SDOF model which interacts with the soft impact body, being modeled by a (linear or nonlinear) SDOF lumped mass model. The interacting glass-impactor system is thus represented by a two-DOF system (e.g., see [73, 74]). Because the external forcing is zero, the dynamic problem constitutes an initial value problem. Specifically, the analysis is initiated just before impact and an initial impactor velocity is prescribed based on the pendulum drop height.

The simplified modeling approach for verifying glass panels is similar to the SDOF modeling approach for analysis of concrete members in two ways; firstly, higher order modes of the glass panel/concrete member is neglected and, secondly, the supporting structure is considered rigid. However, glass is a brittle material, being essentially linear elastic before failure [75], while the reinforcement in a concrete structure can be arranged to obtain a ductile behavior. Hence, an approach considering nonlinear materials is necessary in an analysis of concrete members, while a glass panel can be assumed linear elastic before failure. However, the load–

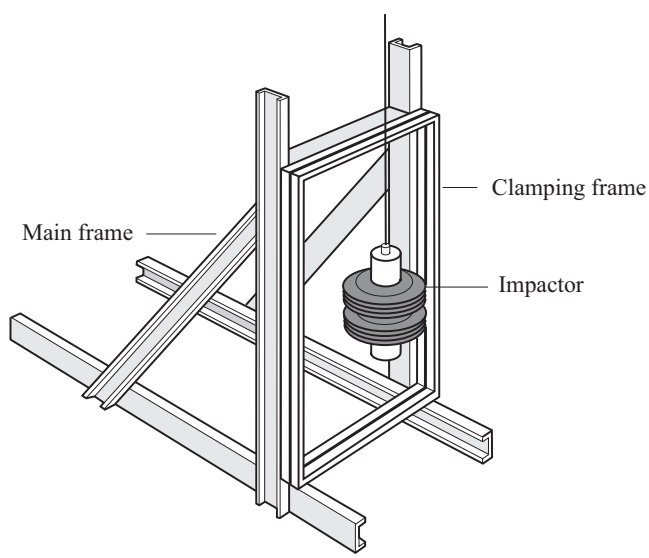

Figure 6.4: Standardized soft-body pendulum for glass classification according to the European Standard EN 12600 [72].

displacement response of the standardized impactor, consisting of two pneumatic rubber tires and steel weights, is nonlinear. Moreover, the contact interaction between the glass panel and the impactor introduces a nonlinear behavior. Thus, localized nonlinearities are present in both structural dynamics problems; namely, in the form of plastic hinges, local contact interactions, and nonlinear subsystems. In addition, the response of glass panels, having a small thickness compared to the span width, are typically characterized by bending–stretching coupling effects, resulting in a geometrically nonlinear behavior, as illustrated in Figure 6.5.

In Paper C, experimental as well as numerical studies of simply-supported glass panels subjec-

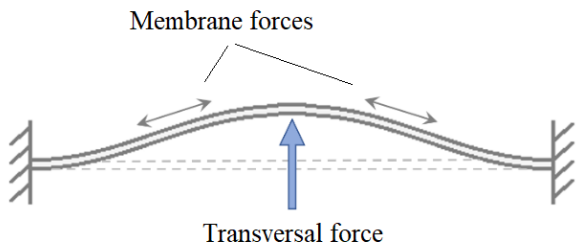

Figure 6.5: Principle sketch of bending–stretching coupling behavior for fixed–fixed glass panel.

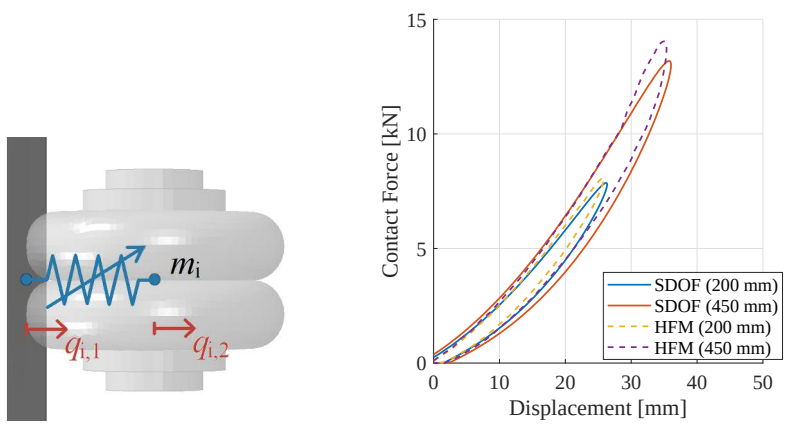

Figure 6.6: Schematic representation of nonlinear SDOF model representing the standardized impactor (a) and impactor response for impact with a rigid surface (b), as provided by a high-fidelity FE model (HFM) (dashed lines) and the SDOF model (solid lines), respectively. The load–displacement curves represent the total contact force and the displacement of the impactor center of mass. results are presented for a pendulum drop height of 200 mm and 450 mm, respectively.

ted to soft-body impacts are presented. In particular, the glass strain was measured on simply supported monolithic glass panels subjected to impact loading. The glass panels were mounted in a steel frame and impact loads were generated by releasing the standardized EN 12600 impactor from various drop heights. Furthermore, impact tests were performed to determine the dynamic characteristics of the impactor. Moreover, a nonlinear viscous SDOF model representing the impactor was developed, see Figure 6.6. The linearized pre-failure elastic response of the glass panel was represented by a modal basis including a set of force-dependent Krylov-vectors (see Sections 3.5 and 5.2.2). A coupled system, including the impactor SDOF model as well as the reduced model representing the glass panel, was formulated using DS. For the load cases studied, it was shown that an accurate prediction of the pre-failure glass strain can be obtained by considering only a few generalized coordinates. However, the influence of higher order modes can be expected to be more pronounced for larger glass panels or glass panels with other fixing methods.

The reduced order model of the glass–impactor system, as proposed in Paper C, does not consider the geometrically nonlinear response of the glass panel, nor the time dependency of the contact pressure distribution. However, in Paper E, an enhanced nonlinear reduced order model for simulating the soft-body impact is suggested, which considers both these effects. More specifically, a geometrically nonlinear model for the glass panel was established using the condensed system equations, discussed in Section 4.1.3. An out-of-plane reduction basis for the glass structure was generated using a Krylov-subspace approach, which considers the position, as well as the spatial distribution, of the impact loading. The quasi-static in-plane response was then generated using static modal derivatives (cf. Section 4.3.1). Hence, coordinates representing the in-plane motion need not be considered explicitly in the dynamic response analysis. Further, the reduced order models were implemented using the modeling strategies presented in Paper D.

Moreover, a procedure for modeling an approximate (and time-dependent) contact pressure distribution was introduced. Specifically, the physical DOFs involved in the contact are replaced by a significantly reduced set of generalized variables, representing scaling coefficients of time-invariant pressure distributions. The approximate contact model was established by means of a POD analysis (cf. Section 4.3.2) of contact pressure time-histories, generated based on a reference load case. The methodology is described in detail in Paper E.

The numerical studies presented in Paper E suggests that the proposed nonlinear glass–impactor model can be used for an accurate prediction of important output quantities, e.g., the glass panel principal stresses. Furthermore, the calculated principal tensile stresses are in good agreement with the reference curves provided in the German standard DIN 18008-4 [76], as manifested by the results presented in Figure 6.7.

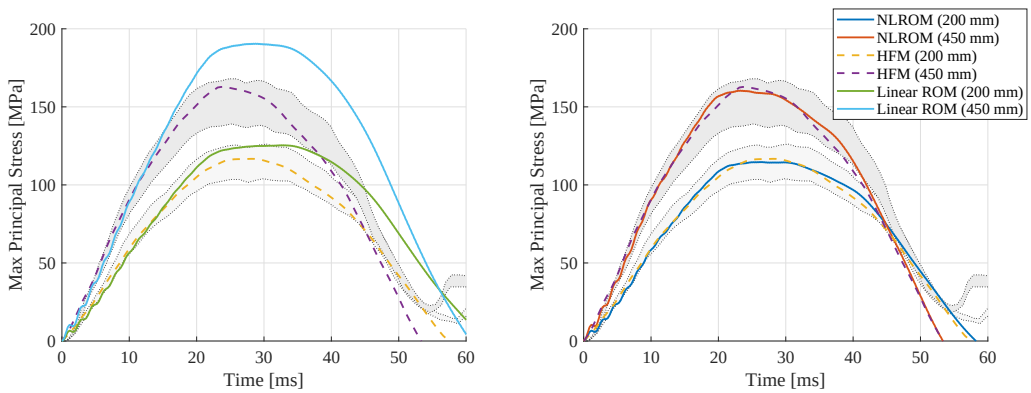

Figure 6.7: Example of principal tensile stresses on the backside of a glass panel, having dimensions according to the reference plate given in the German standard DIN 18008-4 [76]. The principal stresses due to a centric impact is shown, as provided by a linear (a) and geometrically nonlinear (b) reduced order model. The dashed lines show the corresponding result provided by a detailed high-fidelity FE model (cf. Paper C). The gray areas indicate the reference stresses given in DIN 18008-4 [76]. The stresses are presented for a pendulum drop height of 200 mm and 450 mm, respectively. The results were calculated in the numerical investigations presented in Paper E.

7 Summary of appended papers

PAPER A

Reduced order modeling for the dynamic analysis of structures with nonlinear interfaces.
Linus Andersson, Peter Persson, Per-Erik Austrell, Kent Persson
In proceedings of COMPDYN 2019, 7:th International Conference on Computational Methods in Structural Dynamics and Earthquake Engineering, pp. 2395–2406, Crete, Greece, 2019.

Abstract

In the present paper, linear substructures with nonlinearities localized at their interfaces, such as the joints in a beam structure, are studied. By subdivision of the total structure into substructures, reduced subsystems are obtained by component mode synthesis. Nonlinear elements are introduced at supports or between substructures. A numerical example is presented where a beam subjected to blast loading is studied. The influence of the nonlinear behavior as well as the number of retained fixed-interface normal modes in the reduced subsystems are evaluated. The response is also compared to the response of equivalent single-degree-of-freedom systems, which are frequently employed in blast load design calculations. For the load cases studied, the displacement computed from an equivalent single-degree-of-freedom system correspond fairly well to the displacement given by a refined two-dimensional beam model, reduced by substructuring. In contrast, the shear force differs significantly due to that higher order modes are neglected in the single-degree-of-freedom system.

Contributions by Linus Andersson

Main author of the paper and wrote the manuscript. He formulated research aims, developed the modeling strategies, implemented the models, and performed the simulations as well as synthesized the results and drew conclusions.

PAPER B

Model reduction for structures subjected to blast loading by use of dynamic substructuring.
Linus Andersson, Peter Persson, Kent Persson
In proceedings of EURODYN 2020, XI International Conference on Structural dynamics, pp. 2544–2564, Streamed from Athens, Greece, 2020.

Abstract

In the present study, strategies are developed to enable time-efficient models for structures subjected to blast loading, appropriate for use in a structural design process. Dynamic substructuring is employed to obtain reduced models with localized nonlinearities, such as predefined plastic hinges in a beam–column structure. The parts of the substructures that remains linear elastic are modeled by Ritz-vectors whereas parts with a nonlinear response are retained as physical degrees-of-freedom. Furthermore, a time-stepping method is presented that is shown to be suitable for reduced models including local and predefined rigid–plastic behavior. The proposed methodology is applied and demonstrated in a numerical example of a concrete frame structure. Both the well-established Craig-Bampton method and reduction bases enriched by so-called correction modes are evaluated. For the load case studied, it is shown that the standard Craig-Bampton technique is suitable for reducing the substructures. Furthermore, it is shown that only a few Ritz-vectors are needed to sufficiently describe the deformation of the structure. However, additional modes are needed to ensure an accurate representation of the interface forces between the substructures.

Contributions by Linus Andersson

Main author of the paper and wrote the manuscript. He formulated research aims, developed the modeling strategies, implemented the numerical models and performed the simulations. He synthesized the results and contributed to the conclusions drawn.

PAPER C

Reduced order modeling of soft-body impact on glass panels.
Linus Andersson, Marcin Kozłowski, Peter Persson, Per-Erik Austrell, Kent Persson
Engineering Structures, Volume 256, 1 April 2022, 113988.

Abstract

In the paper, strategies for reduced order modeling of glass panels subjected to soft-body impact are developed by means of dynamic substructuring. The aim is to obtain accurate and computationally efficient models for prediction of the pre-failure elastic response. More specifically, a reduction basis for the subsystem representing the glass panel is established using correction modes, being fixed-interface component modes that considers loading on the substructure boundary. The soft-body impactor is effectively modeled by a nonlinear single-degree-of-freedom system, calibrated by experimental data. Furthermore, a simplified and computationally efficient modeling approach is proposed for the contact interaction between the glass panel and the impact body. An experimental campaign was carried out to validate the developed models. In particular, the glass strain was measured on simply supported monolithic glass panels subjected to soft-body impact. Additional impact tests were performed to determine the dynamic characteristics of the impactor. Moreover, a detailed numerical reference model was developed to evaluate the discrepancy between the experimental tests and the results provided by the reduced order models. The developed models show good agreement with the experimental results. For the studied load cases, it is shown that an accurate prediction of the pre-failure glass strain can be obtained by systems including only a few generalized degrees-of-freedom.

Contributions by Linus Andersson

Main author of the paper and wrote the manuscript. He contributed to the conceptualization of ideas and the experimental methodologies. He conducted the experiments for determining the dynamic properties of the impactor. He developed the numerical modeling strategies, implemented the numerical models, and performed the simulations. He synthesized the results and contributed to the conclusions drawn.

PAPER D

Efficient nonlinear reduced order modeling for dynamic analysis of flat structures.
Linus Andersson, Peter Persson, Kent Persson
Mechanical Systems and Signal Processing, Volume 191, 15 May 2023, 110143.

Abstract

In the present paper, strategies for reduced order modeling of geometrically nonlinear finite element models are investigated. Simulation-free, non-intrusive approaches are considered, which do not require access to the source code of a finite element program (e.g., proprietary knowledge). Our study focus on but is not restricted to flat structures. Reduction bases are generated using bending modes and the associated modal derivatives, which span the additional subspace needed for an adequate approximation of the geometrically nonlinear response. Moreover, the reduced nonlinear restoring forces are expressed as third order polynomials in modal coordinates. Consequently, the reduced systems can be effectively solved using time-integration schemes involving only the reduced coordinates. A bottleneck in the non-intrusive methods is typically the computational effort for precomputing the polynomial coefficients and generating the reduction basis. In this regard, we demonstrate that modal derivatives have several useful properties. In particular, the modal derivatives essentially provide all the information needed for generating the polynomial coefficients for the in-plane coordinates. For condensed systems, which ignores the inertia of the in-plane modes, we show that the modal derivatives can be used effectively for recovering the in-plane displacements. Based on these findings, we propose a methodology for generating reduced order models of geometrically nonlinear flat structures in a computationally efficient manner. Moreover, we demonstrate that the concepts extend also to curved structures. The modeling techniques are validated by means of numerical examples of solid beam models and continuously supported shell models. The computational efficiency of the proposed methodology is evaluated based on the number of static evaluations needed for identifying the polynomial coefficients, as compared to the state-of-the-art methods. Furthermore, strategies for efficient time integration are discussed and evaluated.

Contributions by Linus Andersson

Main author of the paper and wrote the manuscript. He formulated research aims, developed the modeling strategies, implemented the numerical models, and performed the simulations. He synthesized the results and drew conclusions.

PAPER E

Nonlinear reduced order modeling of glass panels subjected to soft-body impact.
Linus Andersson, Peter Persson, Kent Persson
Submitted for publication.

Abstract

In the paper, we propose a nonlinear reduced order model for dynamic analysis of glass panels subjected to soft-body impact. The aim is to determine the pre-failure elastic response of the glass panel in a computationally efficient manner, while maintaining sufficient accuracy of important output quantities. The response of glass panels, having a small thickness compared to the span width, are typically characterized by bending–stretching coupling effects, which result in a geometrically nonlinear behavior. To consider these effects, a reduction basis for the glass panel was established using out-of-plane bending modes and the associated modal derivatives, which span the additional subspace needed to adequately predict the geometrically nonlinear response. The reduced nonlinear restoring forces for the glass structure were expressed as cubic polynomials in modal coordinates. Consequently, the transient dynamic response can be effectively solved using direct time integration. The impacting body was modeled using a nonlinear, viscous single-degree-of-freedom system. Furthermore, a contact model was developed, allowing for approximating the contact pressure distribution using only a few time-dependent variables. For the studied load cases, the glass panel displacements as well as the principal tensile stresses predicted by the proposed model are in good agreement with the corresponding results provided by a detailed, full order finite element model.

Contributions by Linus Andersson

Main author of the paper and wrote the manuscript. He developed the numerical modeling strategies, implemented the numerical models, and performed the simulations. He synthesized the results and drew conclusions.

8 Concluding remarks

8.1 CONCLUSIONS

Reduced order models were developed for use in structural engineering applications within two different areas, namely, concerning concrete structures subjected to blast loading and glass structures subjected to impact loading. In particular, modeling strategies were developed that are sufficiently accurate, computationally efficient, and suitable for use in a structural design process. Moreover, the models consider the response of higher order modes as well as nonlinear effects, e.g., localized nonlinearities of various forms and geometric nonlinearities. The main contributions to the research field are:

- Modeling strategies for time-efficient analysis of concrete structures subjected to blast loading (see Papers A and B).
- Time-stepping scheme for systems with localized rigid–plastic behavior (see Paper B).
- Modeling strategies for analysis of glass panels subjected to soft-body impact (see Paper C).
- Experimental methodology for estimating damping of standardized impactor (see Paper C).
- Novel nonlinear viscous SDOF model for reduced modeling of standardized impactor, and methodology for calibrating the SDOF model based on detailed FE models (see Paper C).
- Strategies for efficient nonintrusive computation of nonlinear stiffness coefficients for geometrically nonlinear reduced order models using static modal derivatives (see Paper D).
- Strategies for efficient analysis of geometrically nonlinear flat or slightly curved structures using static modal derivatives (see Paper D).
- Nonlinear reduced order model for analysis of glass panels subjected to soft-body impact, considering contact conditions as well as geometrically nonlinear effects (see Paper E).

- Modeling procedure for considering varying contact pressure distribution in reduced order model (see Paper E).

Furthermore, a review of various reduced order modeling techniques is presented which, in a broader perspective, provides a basis for developing reduced order models in various structural engineering applications.

8.2 FURTHER RESEARCH

The modeling strategies proposed for analyzing concrete structures subjected to blast loading can possibly be further developed to consider geometric nonlinearity. Thus, by means of dynamic substructuring, reduced models including predefined plastic joints as well as geometrically nonlinear substructures could be investigated. However, the bending moment capacity of concrete structures is strongly influenced by the normal force, which can be expected to be fairly large in applications influenced by geometrically nonlinear effects. Consequently, it might be necessary to replace the simplified rigid–perfectly plastic joints with more sophisticated submodels.

The glass–impactor model proposed in Paper E for simulating soft-body impact could be further developed. For instance, the accuracy could be evaluated for various load cases, fixing methods, and glass panel sizes. Also, an implementation of loss-of-contact could be considered, and the influence of in-plane inertia could be studied for cantilevered glass structures. Moreover, modeling strategies for considering the dynamic response of the supporting structure could be studied; e.g., guidelines for when the supporting structure can be considered rigid could possibly be established, and modeling strategies for taking into account the flexibility could be investigated.

The approach using static modal derivatives for efficient analysis of flat and slightly curved structures, as suggested in Paper D, could be further evaluated. In particular, it is of interest to investigate for which strain levels this simplified approach provide satisfactory results. Moreover, the suggested generalization, where the modal derivatives are computed using the residual flexibility, could be applied and evaluated for thin-walled structures with arbitrary geometries.

References

[1] Bathe, K.J. (2006), *Finite element procedures*, Prentice Hall.

[2] Rutzmoser, J. (2018), *Model order reduction for nonlinear structural dynamics*, Ph.D. thesis, Technische Universität München.

[3] Tiso, P., Karamooz Mahdiabadi, M., Marconi, J. (2021), *Modal methods for reduced order modeling*, in: *Model Order Reduction: Volume 1: System-and Data-Driven Methods and Algorithms*, 97–138, De Gruyter.

[4] de Klerk, D., Rixen, D., Voormeeren, S. (2008), *General Framework for Dynamic Substructuring: History, Review, and Classification of Techniques*, AIAA Journal **46**(5), 1169–1181.

[5] ClearSight (2017), *Computer Software*, Department of Construction Sciences, Lund University.

[6] Craig, R.J., Kurdila, A. (2006), *Fundamentals of Structural Dynamics, 2nd Edition*, John Wiley & Sons.

[7] Pilkey, W. (2005), *Formulas for Stress, Strain and Structural Matrices, Second Edition*, Wiley.

[8] Unified Facilities Criteria (UFC) (2008), *Structures to Resist the Effects of Accidental Explosions*, UFC 3-340-02, U. S. Army Corps of Engineers, Naval Facilities Engineering Command, Air Force Civil Engineer Support Agency.

[9] Ottosen, N., Petersson, H. (1992), *Introduction to the finite element method*, Prentice Hall.

[10] De Borst, R., Crisfield, M.A., Remmers, J.J., Verhoosel, C.V. (2012), *Nonlinear finite element analysis of solids and structures*, John Wiley & Sons.

[11] Holzapfel, G.A. (2000), *Nonlinear solid mechanics: a continuum approach for engineering science*, Wiley.

[12] Chopra, A. (2016), *Dynamics of structures. Theory and Applications to Earthquake Engineering, 5th Edition.*, Prentice Hall.

[13] Hoen, C. (2005), *An Engineering Interpretation of the Complex Eigensolution of Linear Dynamic Systems*, in: *Proceedings of International Modal Analysis Conference XXIII, Orlando, USA*.

[14] Johnson, C.D., Kienholz, D.A. (1982), *Finite element prediction of damping in structures with constrained viscoelastic layers*, AIAA journal **20**(9), 1284–1290.

[15] Geradin, M., Rixen, D. (2015), *Mechanical Vibrations: Theory and Applications to Structural Dynamics, Third Edition*, Wiley.

[16] Hilber, H.M., Hughes, T.J., Taylor, R.L. (1977), *Improved numerical dissipation for time integration algorithms in structural dynamics*, Earthquake Engineering & Structural Dynamics **5**(3), 283–292.

[17] Chung, J., Hulbert, G. (1993), *A time integration algorithm for structural dynamics with improved numerical dissipation: the generalized-α method*, Journal of applied mechanics **60**(2), 371–375.

[18] Dickens, J., Pool, K. (1992), *Modal truncation vectors and periodic time domain analysis applied to a cyclic symmetry structure*, Computers & structures **45**(4), 685–696.

[19] Dickens, J., Nakagawa, J., Wittbrodt, M. (1997), *A critique of mode acceleration and modal truncation augmentation methods for modal response analysis*, Computers & structures **62**(6), 985–998.

[20] Rixen, D. (2002), *High Order Static Correction Modes for Component Mode Synthesis*, in: *Proceedings of the fifth World Congress on Computational Mechanics, Vienna, Austria*.

[21] Voormeeren, S.N. (2012), *Dynamic Substructuring Methodologies for Integrated Dynamic Analysis of Wind Turbines*, Ph.D. thesis, Delft University of Technology.

[22] Trefethen, L., Bau, D. (1997), *Numerical Linear Algebra*, SIAM.

[23] Besselink, B., Tabak, U., Lutowska, A., van de Wouw, N., Nijmeijer, H., Rixen, D., Hochstenbach, M., Schilders, W. (2013), *A comparison of model reduction techniques from structural dynamics, numerical mathematics and systems and control*, Journal of Sound and Vibration **332**, 4403–4422.

[24] Flodén, O., Persson, K., Sandberg, G. (2014), *Reduction methods for the dynamic analysis of substructure models of lightweight building structures*, Computers & Structures **138**, 49–61.

[25] Vizzaccaro, A., Givois, A., Longobardi, P., Shen, Y., Deü, J.F., Salles, L., Touzé, C., Thomas, O. (2020), *Non-intrusive reduced order modelling for the dynamics of geometrically nonlinear flat structures using three-dimensional finite elements*, Computational Mechanics **66**, 1293–1319.

[26] Perez, R.A. (2012), *Multiscale reduced order models for the geometrically nonlinear response of complex structures*, Ph.D. thesis, Arizona State University.

[27] Touzé, C., Vizzaccaro, A., Thomas, O. (2021), *Model order reduction methods for geometrically nonlinear structures: a review of nonlinear techniques*, Nonlinear Dynamics **105**(2), 1141–1190.

[28] Kim, K., Khanna, V., Wang, X., Mignolet, M.P. (May 2009), *Nonlinear reduced order modeling of flat cantilevered structures*, in: *Proceedings of the 50th Structures, Structural Dynamics, and Materials Conference, Palm Springs, California*, AIAA–2009–2492.

[29] Wang, X., Khanna, V., Kim, K., Mignolet, M.P. (2021), *Nonlinear reduced-order modeling of flat cantilevered structures: Identification challenges and remedies*, Journal of Aerospace Engineering **34**(6), 04021085.

[30] Barbič, J., James, D.L. (2005), *Real-time subspace integration for St. Venant-Kirchhoff deformable models*, ACM transactions on graphics (TOG) **24**(3), 982–990.

[31] Mahdiabadi, M.K., Tiso, P., Brandt, A., Rixen, D.J. (2021), *A non-intrusive model-order reduction of geometrically nonlinear structural dynamics using modal derivatives*, Mechanical Systems and Signal Processing **147**, 107126.

[32] Mignolet, M., Przekop, A., Rizzi, S., Spottswood, S. (2013), *A review of indirect/non-intrusive reduced order modeling of nonlinear geometric structures*, Journal of Sound and Vibration **332**, 2437–2460.

[33] Muravyov, A., Rizzi, S. (2003), *Determination of nonlinear stiffness with application to random vibration of geometrically nonlinear structures*, Computers & Structures **81**, 1513–1523.

[34] Perez, R., Wang, X., Mignolet, M.P. (2014), *Nonintrusive structural dynamic reduced order modeling for large deformations: enhancements for complex structures*, Journal of Computational and Nonlinear Dynamics **9**(3), 031008.

[35] McEwan, M., Wright, J.R., Cooper, J.E., Leung, A.Y.T. (2001), *A combined modal/finite element analysis technique for the dynamic response of a non-linear beam to harmonic excitation*, Journal of Sound and Vibration **243**(4), 601–624.

[36] Hollkamp, J.J., Gordon, R.W. (2008), *Reduced-order models for nonlinear response prediction: Implicit condensation and expansion*, Journal of Sound and Vibration **318**(4-5), 1139–1153.

[37] Givois, A., Grolet, A., Thomas, O., Deü, J.F. (2019), *On the frequency response computation of geometrically nonlinear flat structures using reduced-order finite element models*, Nonlinear Dynamics **97**(2), 1747–1781.

[38] Gordon, R., Hollkamp, J. (2011), *Reduced-order models for acoustic response prediction. Air Force Research Laboratory*, Tech. rep., AFRL-RB-WP-TR-2011-3040, Dayton, OH.

[39] Kerschen, G., Golinval, J.c., Vakakis, A.F., Bergman, L.A. (2005), *The method of proper orthogonal decomposition for dynamical characterization and order reduction of mechanical systems: an overview*, Nonlinear dynamics **41**, 147–169.

[40] Idelsohn, S.R., Cardona, A. (1985), *A reduction method for nonlinear structural dynamic analysis*, Computer Methods in Applied Mechanics and Engineering **49**(3), 253–279.

[41] Idelsohn, S.R., Cardona, A. (1985), *A load-dependent basis for reduced nonlinear structural dynamics*, Computers & Structures **20**(1-3), 203–210.

[42] Jain, S., Tiso, P., Rutzmoser, J.B., Rixen, D.J. (2017), *A quadratic manifold for model order reduction of nonlinear structural dynamics*, Computers & Structures **188**, 80–94.

[43] Wu, L., Tiso, P., Van Keulen, F. (2016), *A modal derivatives enhanced Craig-Bampton method for geometrically nonlinear structural dynamics*, in: *27th International Conference on Noise and Vibration Engineering and International Conference on Uncertainty in Structural Dynamics*, 3615–3624, KU Leuven.

[44] Tiso, P. (2011), *Optimal second order reduction basis selection for nonlinear transient analysis*, in: *Modal Analysis Topics, Volume 3: Proceedings of the 29th IMAC, A Conference on Structural Dynamics*, 27–39, Springer.

[45] Liang, Y., Lee, H., Lim, S., Lin, W., Lee, K., Wu, C. (2002), *Proper orthogonal decomposition and its applications—Part I: Theory*, Journal of Sound and vibration **252**(3), 527–544.

[46] Allen, M.S., Rixen, D., Van der Seijs, M., Tiso, P., Abrahamsson, T., Mayes, R.L. (2020), *Substructuring in engineering dynamics*, Springer.

[47] Farhat, C., Crivelli, L., Géradin, M. (1995), *Implicit time integration of a class of constrained hybrid formulations—Part I: Spectral stability theory*, Computer Methods in Applied Mechanics and Engineering **125**(1–4), 71–107.

[48] Guyan, R. (1965), *Reduction of Stiffness and Mass Matrices*, AIAA Journal **3**(2), 380.

[49] Craig, R., Bampton, M. (1968), *Coupling of Substructures for Dynamic Analysis*, AIAA Journal **6**(7), 1313–1319.

[50] MacNeal, R. (1971), *A Hybrid Method of Component Mode Synthesis*, Computers & Structures **1**(4), 581–601.

[51] Rubin, S. (1975), *Improved Component-Mode Representation for Structural Dynamic Analysis*, AIAA Journal **13**(8), 995–1006.

[52] Craig, R., Chang, C. (1977), *On the Use of Attachment Modes in Substructure Coupling for Dynamic Analysis*, in: *Proceedings of the 18th Structures, Structural Dynamics and Material Conference, San Diego, California*.

[53] Rixen, D. (2004), *A dual Craig–Bampton method for dynamic substructuring*, Journal of Computational and Applied Mathematics **168**(1–2), 383–391.

[54] Gruber, F., Gille, M., Rixen, D. (2017), *Time integration of dual Craig-Bampton reduced systems*, in: *Proceedings of the 6th ECCOMAS Thematic Conference on Computational Methods in Structural Dynamics and Earthquake Engineering (COMPDYN 2017), Rhodes Island, Greece*.

[55] Rixen, D. (2009), *Dual Craig-Bampton with enrichment to avoid spurious modes*, in: *Proceedings of the IMAC-XXVII, Orlando, USA*.

[56] Krattiger, D., Wu, L., Zacharczuk, M., Buck, M., Kuether, R., Allen, M., Tiso, P., Brake, M. (2019), *Interface reduction for Hurty/Craig-Bampton substructured models: Review and improvements*, Mechanical Systems and Signal Processing **114**, 579–603.

[57] Gibanica, M., Abrahamsson, T., Rixen, D. (2019), *Multifidelity component interface reduction and modal truncation augmentation*, International Journal for Numerical Methods in Engineering **120**(1), 105–124.

[58] Persson, P., Persson, K., Sandberg, G. (2016), *Reduced order modelling of liquid-filled pipe systems*, Journal of Fluids and Structures **61**, 205–217.

[59] Floden, O., Sandberg, G., Persson, K. (2018), *Reduced order modelling of elastomeric vibration isolators in dynamic substructuring*, Engineering Structures **155**, 102–114.

[60] Kuether, R.J., Allen, M.S., Hollkamp, J.J. (2016), *Modal substructuring of geometrically nonlinear finite-element models*, AIAA Journal **54**(2), 691–702.

[61] Kuether, R.J., Allen, M.S., Hollkamp, J.J. (2017), *Modal substructuring of geometrically nonlinear finite element models with interface reduction*, AIAA Journal **55**(5), 1695–1706.

[62] Mahdiabadi, M.K., Bartl, A., Xu, D., Tiso, P., Rixen, D.J. (2019), *An augmented free-interface-based modal substructuring for nonlinear structural dynamics including interface reduction*, Journal of Sound and Vibration **462**, 114915.

[63] Wenneker, F., Tiso, P. (2014), *A substructuring method for geometrically nonlinear structures*, in: *Dynamics of Coupled Structures, Volume 1: Proceedings of the 32nd IMAC, A Conference and Exposition on Structural Dynamics*, 157–165, Springer.

[64] Wu, L. (2018), *Model order reduction and substructuring methods for nonlinear structural dynamics*, Ph.D. thesis, Delft University of Technology.

[65] Karamooz Mahdiabadi, M. (2019), *Nonlinear Model Order Reduction and Substructuring for Structural Dynamics Analysis*, Ph.D. thesis, Technische Universität München.

[66] Wu, L., Tiso, P., Van Keulen, F. (2016), *A modal derivatives enhanced Craig-Bampton method for geometrically nonlinear structural dynamics*, in: *27th International Conference on Noise and Vibration Engineering and International Conference on Uncertainty in Structural Dynamics*, 3615–3624, KU Leuven.

[67] Wu, L., Tiso, P. (2016), *Nonlinear model order reduction for flexible multibody dynamics: a modal derivatives approach*, Multibody System Dynamics **36**, 405–425.

[68] Wu, L., Tiso, P., Tatsis, K., Chatzi, E., van Keulen, F. (2019), *A modal derivatives enhanced Rubin substructuring method for geometrically nonlinear multibody systems*, Multibody system dynamics **45**, 57–85.

[69] Johansson, M., Laine, L. (2012), *Bebyggelsens motståndsförmåga mot extrem dynamisk belastning (in Swedish)*, Tech. Rep. MSB142, Swedish Civil Contingencies Agency (MSB).

[70] Biggs, J. (1964), *Introduction to Structural Dynamics*, McGraw-Hill, New York.

[71] Johansson, M. (2015), *Beräkningsstöd, Moment och tvärkraft (in Swedish)*, Tech. Rep. B06-201, Swedish Civil Contingencies Agency (MSB).

[72] SS-EN-12600 (2003), *Glass in building-pendulum test-impact test method and classification for flat glass*, Swedish Standards Institute.

[73] Schneider, J. (2001), *Festigkeit und Bemessung punktgelagerter Gläser und stoßbeanspruchter Gläser (in German)*, Ph.D. thesis, Technische Universität Darmstadt.

[74] Schneider, J., Schula, S. (2016), *Simulating soft body impact on glass structures*, Proceedings of the Institution of Civil Engineers: Structures and Buildings **169**(6), 416–31.

[75] M., F., Kaspar, R., Abeln, B., Gessler, A., Langosch, K., Beyer, J.e.a. (2014), *Guidance for European structural design of glass components*, Publications Office of the European Union.

[76] DIN (2013), *18008-4: Glass in building – design and construction rules – part 4: additional requirements for barrier glazing*, DIN, Berlin, Germany.

Part II

Appended Publications

Paper A

Available online at www.eccomasproceedia.org
Eccomas Proceedia COMPDYN (2019) 2395-2406

ECCOMAS
Proceedia

COMPDYN 2019
7th ECCOMAS Thematic Conference on
Computational Methods in Structural Dynamics and Earthquake Engineering
M. Papadrakakis, M. Fragiadakis (eds.)
Crete, Greece, 24–26 June 2019

REDUCED ORDER MODELING FOR THE DYNAMIC ANALYSIS OF STRUCTURES WITH NONLINEAR INTERFACES

Linus Andersson [1], **Peter Persson** [1], **Per-Erik Austrell** [1], **Kent Persson** [1]

[1] Department of Construction Sciences, Lund University
P.O. Box 118, SE-221 00 Lund, Sweden
e-mail: {linus.andersson,peter.persson,per_erik.austrell,kent.persson}@construction.lth.se

Abstract

In the present paper, linear substructures with nonlinearities localized at their interfaces, such as the joints in a beam structure, are studied. By subdivision of the total structure into substructures, reduced subsystems are obtained by component mode synthesis. Nonlinear elements are introduced at supports or between substructures. A numerical example is presented where a beam subjected to blast loading is studied. The influence of the nonlinear behavior as well as the number of retained fixed-interface normal modes in the reduced subsystems are evaluated. The response is also compared to the response of equivalent single-degree-of-freedom systems, which are frequently employed in blast load design calculations. For the load cases studied, the displacement computed from an equivalent single-degree-of-freedom system correspond fairly well to the displacement given by a refined two-dimensional beam model, reduced by substructuring. In contrast, the shear force differs significantly due to that higher order modes are neglected in the single-degree-of-freedom system.

Keywords: Substructuring, Component Mode Synthesis, Blast Loading, Structural Dynamics

ISSN:2623-3347
Peer-review under responsibility of the organizing committee of COMPDYN 2019.
doi: 10.7712/120119.7082.19746

1 INTRODUCTION

Design of structures subjected to accidental loading, such as impact and blast loading, can be challenging compared to the design of static loading. As for dynamic loading in general, the structure mass, stiffness and strength affect the response and must be considered to determine whether a certain design fulfill the design code requirements. Consequently, it is often necessary to consider accidental loads in both the conceptual and detailed design phase and, therefore, it is important to employ simplified, conservative and computationally efficient models to estimate the structure response in a time-efficient manner. Moreover, the response computed from a large complex nonlinear model can be difficult to interpret and verify, hence, a smaller and less complex model simplifies the result evaluation.

In the present paper, linear substructures with nonlinearities localized at their interfaces, such as the joints in a beam structure, are studied. By subdivision of the total structure into substructures, reduced subsystems are obtained by dynamic substructuring [1]. Nonlinear elements are introduced at supports or between substructures [3]. The concept is presented in a numerical example in which a simply supported beam subjected to blast loading is studied. The influence of the nonlinear behavior as well as the number of retained fixed-interface normal modes in the reduced subsystem are evaluated. The response is also compared to the response of equivalent single-degree-of-freedom (SDOF) systems which are frequently employed in blast load design calculations.

2 REDUCED ORDER MODELING OF BEAMS SUBJECTED TO BLAST LOADING

The response of a linear structural dynamic system can be analyzed in a computationally efficient manner by considering an approximate reduced order model. For example, the response of a few important eigenmodes can form a reduced model. However, in analyses related to blast loading it is important to include the nonlinear behavior to ensure a model that predicts a realistic structural response. The material nonlinearities are often localized to certain areas such as plastic hinges in heavily loaded beams and plates. Hence, the structure can be subdivided into substructures with a linear response, connecting the nonlinear elements introduced at the supports or between substructures. Since each subsystem is linear, dynamic substructuring can be employed to form a reduced model.

2.1 Impulse pressure due to unconfined explosion

An unconfined explosion results in a shock wave that moves radially away from the center of the explosion [6]. Upon impact, the initial wave is reinforced and reflected. The reflected impulse acting on the structure is characterized by a very large pressure and short duration. For design purposes, the reflected impulse can, in general, be replaced by an equivalent triangular pulse where the actual duration is replaced by a fictitious duration, calculated based on the peak reflected pressure and reflected impulse. Moreover, if the explosion is unconfined and the explosion center is reasonable far from the structure considered, the pressure acting on a structure member can, in general, be approximated by a uniform pressure.

2.2 Single-degree-of-freedom systems

Equivalent SDOF systems are frequently employed for the design of the semi-global response of structural members subjected to blast loading, e.g. as proposed in [4]. This is a well-established approach compatible with the requirements in several design codes, e.g. UFC [6].

Equivalent SDOF systems can be derived for structures idealized as either beams or plates. In the study presented here only beams are considered.

The main assumption when developing an equivalent SDOF system is that the member deforms according to an assumed shape, $\varphi(x)$, which is constant through time. Hence, the member deflection $u(x,t)$ can be expressed as $\varphi(x)u_s(t)$, where u_s is the displacement of a reference point, e.g. the point of maximum displacement, see Figure 1. The shape function $\varphi(x)$ is often chosen as a Ritz vector corresponding to the static deflection of the external pressure. Note that, as for the deformed shape, the load distribution is assumed constant through time. The beam model is then transformed into a SDOF system by calculating an equivalent mass, stiffness and load in terms of the reference point displacement.

The equation of motion for an equivalent SDOF system can be expressed as:

$$\kappa_m m\ddot{u} + \kappa_k R(u) = \kappa_F p(t) \tag{1}$$

where κ_m, κ_k and κ_F are dimensionless transformation factors for the mass (m), resistance (R) and load (p), respectively. The mass factor, by which the total distributed mass of an element is multiplied to obtain an equivalent lumped mass, is derived by assuming conservation of kinetic energy [4]. If the mass is uniformly distributed, the mass factor for a beam with length L is given by:

$$\kappa_m = \frac{1}{L}\int_0^L \frac{\varphi(x)^2}{u_s{}^2}\,\mathrm{d}x \tag{2}$$

The load factor, by which the total pressure on the element is multiplied to obtain an equivalent concentrated force, is derived by assuming conservation of external work [4]. If the external pressure is uniformly distributed, the load factor for a beam with length L is given by:

$$\kappa_F = \frac{1}{L}\int_0^L \frac{\varphi(x)}{u_s}\,\mathrm{d}x \tag{3}$$

The resistance factor, by which the resistance of the structural element is multiplied to obtain the equivalent resistance of the SDOF system, is derived by assuming conservation of strain energy for the structural member, computed based on the assumed deformed shape. According to [4], it can be shown that the resistance-factor must always be equal to the load-factor, i.e.:

$$\kappa_k = \kappa_F \tag{4}$$

Hence, the equation of motion (1) for the SDOF system can be rewritten as

$$\frac{\kappa_m}{\kappa_F} m\ddot{u} + R(u) = p(t) \tag{5}$$

Consequently, the beam can be transformed into an equivalent SDOF system by scaling the mass only and, therefore, it is convenient to define a load-mass factor $\kappa_{mF} = \kappa_m/\kappa_F$.

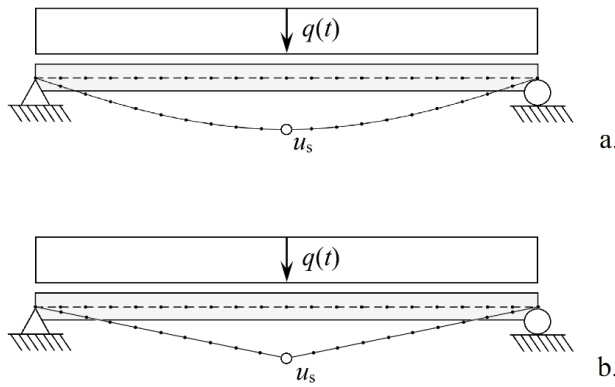

Figure 1: Assumed shape for elastic (a) and plastic (b) response.

When the ultimate moment capacity of a beam member is reached, in general, a plastic hinge is developed, which indeed affect the shape of the deflection. Hence, the assumed deflection shape considered for an elastic response, reasonable in the initial stage, differ significantly from the assumed plastic deflection shape which is reasonable in the second stage where a plastic hinge has been developed, cf. Figure 1. Moreover, the transformation factors given by Eqs. (2) and (3), which are constant through time, depend on the assumed shape $\varphi(x)$. Consequently, the equivalent SDOF system must be derived based on either an elastic or plastic deflection shape. For example, the κ_{mF} factors corresponding to a simply supported beam subjected to a uniform pressure are 0.787 and 0.667 for an elastic and plastic deflection shape respectively.

For a simply supported beam subjected to a uniform pressure the ultimate resistance can be calculated as:

$$R_{\mathrm{u}} = \frac{8M_{\mathrm{u}}}{L} \tag{6}$$

where M_{u} is the ultimate moment capacity, which implies that the maximum shear force at the supports can be calculated as $V = R_{\mathrm{u}}/2$. Hence, the ultimate moment capacity has, in general, a large impact on the shear force magnitude and clearly a larger moment capacity is not beneficial (however, the moment capacity must be sufficiently large to ensure that the plastic rotation is smaller than the rotation capacity). For example, if the amount of bending reinforcement in a concrete member is increased the amount of shear reinforcement due to blast loading must be increased accordingly. Since both the mass, stiffness and ultimate capacity affect the response, the design often requires iterative design calculations where simplified models, as the equivalent SDOF system, are important.

However, it should be noted that the shear force given by an equivalent SDOF system is computed with the assumption that the beam deflection shape is constant through time and, consequently, higher order modes are neglected. Furthermore, the shear forces are in general large at the initial stage, due to that higher order modes are excited. As e.g. observed in [7], the neglection of higher order modes indeed affect the precision of the shear force computed from an equivalent SDOF analysis.

For concrete members, a shear failure at the initial stage is referred to as a *direct shear* failure and is characterized by a rapid propagation of a vertical crack, located at the supports. Unlike *diagonal shear* failure, shear reinforcement perpendicular to the beam axis does not prevent this type of failure, instead inclined bars may be needed to ensure an adequate design. However,

it is in general not possible to determine the actual magnitude of the maximum shear force based on the response computed from an equivalent SDOF system.

2.3 Substructuring of beam model with plastic hinges

The response of a beam subjected to blast loading is, in general, elastic in a first stage and a mixture of both elastic and plastic in a second stage. Furthermore, in contrast to the response computed from an equivalent SDOF system, the fundamental mode as well as higher order modes are excited. To fully capture the structural behavior, it is therefore necessary to employ a nonlinear multi-degree-of-freedom (MDOF) model. Nonlinear analyses of large systems are, however, time consuming and might not be suitable in a design calculation. Nevertheless, a more refined model, compared to an equivalent SDOF system, might be necessary to enable accurate predictions of both the maximum displacement and shear force.

If the material nonlinearities are localized to certain areas, such as plastic hinges in heavily loaded beams, the total structure can be subdivided into substructures. Each substructure then consists of a subsystem with a linear response, connecting the nonlinear elements introduced at interfaces, i.e. at the supports or between substructures. Since each subsystem is linear, it is straight-forward to employ component mode synthesis (CMS) to form a reduced model [3]. Hence, a reduced model that captures a combined elastic and plastic response as well as including higher order modes can be derived. This procedure can be extended further to include both material and geometrically nonlinearities, i.e. to allow for large translations and rotations of the substructures. However, in the study presented here only material nonlinearities are considered.

The substructures can for example be reduced by condensation methods, such as Guyan reduction [2], where only physical DOFs are involved or by hybrid methods, such as component mode synthesis by Craig-Bampton or Krylov subspace component mode synthesis, where both physical and generalized DOFs are considered [8].

A finite element formulation of a subsystem leads to a linear equation of motion of the following form:

$$\mathbf{M}\ddot{\mathbf{u}} + \mathbf{C}\dot{\mathbf{u}} + \mathbf{K}\mathbf{u} = \mathbf{p} \tag{7}$$

Neglecting damping the partitioned mass and stiffness matrices can be written as:

$$\begin{bmatrix} \mathbf{M}_{ii} & \mathbf{M}_{ib} \\ \mathbf{M}_{bi} & \mathbf{M}_{bb} \end{bmatrix} \begin{bmatrix} \ddot{\mathbf{u}}_i \\ \ddot{\mathbf{u}}_b \end{bmatrix} + \begin{bmatrix} \mathbf{K}_{ii} & \mathbf{K}_{ib} \\ \mathbf{K}_{bi} & \mathbf{K}_{bb} \end{bmatrix} \begin{bmatrix} \mathbf{u}_i \\ \mathbf{u}_b \end{bmatrix} = \begin{bmatrix} \mathbf{p}_i \\ \mathbf{p}_b \end{bmatrix} \tag{8}$$

where the subscripts *i* and *b* denotes the *interior* and interface *boundary* DOFs, respectively. If assumed force-free, the interior DOFs can be expressed as:

$$\mathbf{u}_i = -\mathbf{K}_{ii}^{-1}(\mathbf{M}_{ii}\ddot{\mathbf{u}}_i + \mathbf{M}_{ib}\ddot{\mathbf{u}}_b + \mathbf{K}_{ib}\mathbf{u}_b) \tag{9}$$

By neglecting the inertia terms this leads to the following transformation matrix:

$$\begin{bmatrix} \mathbf{u}_i \\ \mathbf{u}_b \end{bmatrix} = \begin{bmatrix} -\mathbf{K}_{ii}^{-1}\mathbf{K}_{ib} \\ \mathbf{I}_{bb} \end{bmatrix} \mathbf{u}_b = \begin{bmatrix} \mathbf{\Psi}_{ib} \\ \mathbf{I}_{bb} \end{bmatrix} \mathbf{u}_b = \mathbf{T}_G \mathbf{u}_b \tag{10}$$

where $\mathbf{T}_G$ is the Guyan transformation matrix. By applying the transformation matrix to Eq. (7) a reduced system is given by:

$$\mathbf{M}_G\ddot{\mathbf{u}}_b + \mathbf{C}_G\dot{\mathbf{u}}_b + \mathbf{K}_G\mathbf{u}_b = \mathbf{p}_G \tag{11}$$

where,

$$\begin{aligned} \mathbf{M}_{\mathrm{G}} &= \mathbf{T}_{\mathrm{G}}{}^{\mathrm{T}}\mathbf{M}\mathbf{T}_{\mathrm{G}} \\ \mathbf{C}_{\mathrm{G}} &= \mathbf{T}_{\mathrm{G}}{}^{\mathrm{T}}\mathbf{C}\mathbf{T}_{\mathrm{G}} \\ \mathbf{K}_{\mathrm{G}} &= \mathbf{T}_{\mathrm{G}}{}^{\mathrm{T}}\mathbf{K}\mathbf{T}_{\mathrm{G}} \\ \mathbf{p}_{\mathrm{G}} &= \mathbf{T}_{\mathrm{G}}{}^{\mathrm{T}}\mathbf{p} \end{aligned} \tag{12}$$

The Craig-Bampton method combines the retained physical DOFs with fixed-interface normal modes, obtained by the generalized eigenvalue problem:

$$\left(\mathbf{K}_{ii} - \omega_j^2 \mathbf{M}_{ii}\right)\left\{\boldsymbol{\phi}_i\right\}_j = 0 \tag{13}$$

The eigenvectors are then normalized in order that

$$\boldsymbol{\Phi}_{ii}{}^{\mathrm{T}}\mathbf{M}_{ii}\boldsymbol{\Phi}_{ii} = \mathbf{I}_{ii} \tag{14}$$

where $\boldsymbol{\Phi}_{ii}$ is the complete set of fixed-interface normal modes. The physical coordinates can be represented as:

$$\begin{bmatrix}\mathbf{u}_i \\ \mathbf{u}_b\end{bmatrix} = \begin{bmatrix}\boldsymbol{\Phi}_{ik} & \boldsymbol{\Psi}_{ib} \\ \mathbf{0}_{bi} & \mathbf{I}_{bb}\end{bmatrix}\begin{bmatrix}\mathbf{q}_k \\ \mathbf{u}_b\end{bmatrix} = \mathbf{T}_{\mathrm{C\text{-}B}}\begin{bmatrix}\mathbf{q}_k \\ \mathbf{u}_b\end{bmatrix} \tag{15}$$

where the subscript k denotes the retained (*kept*) fixed-interface normal modes, $\mathbf{T}_{\mathrm{C\text{-}B}}$ is the Craig-Bampton transformation matrix, $\mathbf{q}_k$ is the generalized DOFs and $[\boldsymbol{\Psi}_{ib} \quad \mathbf{I}_{bb}]^{\mathrm{T}}$ is the interface constraint mode matrix, equal to the Guyan transformation matrix. Hence, the Craig-Bampton method can be interpreted as an extension of the Guyan reduction where the neglected inertia terms are compensated by including a set of fixed-interface normal modes.

By applying the transformation matrix to Eq. (7) a reduced system is given by:

$$\mathbf{M}_{\mathrm{C\text{-}B}}\begin{bmatrix}\ddot{\mathbf{q}}_k \\ \ddot{\mathbf{u}}_b\end{bmatrix} + \mathbf{C}_{\mathrm{C\text{-}B}}\begin{bmatrix}\dot{\mathbf{q}}_k \\ \dot{\mathbf{u}}_b\end{bmatrix} + \mathbf{K}_{\mathrm{C\text{-}B}}\begin{bmatrix}\mathbf{q}_k \\ \mathbf{u}_b\end{bmatrix} = \mathbf{p}_{\mathrm{C\text{-}B}} \tag{16}$$

where,

$$\begin{aligned} \mathbf{M}_{\mathrm{C\text{-}B}} &= \mathbf{T}_{\mathrm{C\text{-}B}}{}^{\mathrm{T}}\mathbf{M}\mathbf{T}_{\mathrm{C\text{-}B}} \\ \mathbf{C}_{\mathrm{C\text{-}B}} &= \mathbf{T}_{\mathrm{C\text{-}B}}{}^{\mathrm{T}}\mathbf{C}\mathbf{T}_{\mathrm{C\text{-}B}} \\ \mathbf{K}_{\mathrm{C\text{-}B}} &= \mathbf{T}_{\mathrm{C\text{-}B}}{}^{\mathrm{T}}\mathbf{K}\mathbf{T}_{\mathrm{C\text{-}B}} \\ \mathbf{p}_{\mathrm{C\text{-}B}} &= \mathbf{T}_{\mathrm{C\text{-}B}}{}^{\mathrm{T}}\mathbf{p} \end{aligned} \tag{17}$$

Note that each constraint mode is the deflection shape due to a unit displacement of a boundary DOF, while the interior DOFs are force-free and the other boundary DOFs are held fixed, i.e.

$$\begin{bmatrix}\mathbf{K}_{ii} & \mathbf{K}_{ib} \\ \mathbf{K}_{bi} & \mathbf{K}_{bb}\end{bmatrix}\begin{bmatrix}\boldsymbol{\Psi}_{ib} \\ \mathbf{I}_{bb}\end{bmatrix} = \begin{bmatrix}\mathbf{0}_{ib} \\ \mathbf{R}_{bb}\end{bmatrix} \tag{18}$$

where $\mathbf{R}_{bb}$ is the reaction forces acting on the substructure.

By using a similar procedure as presented above, the fixed-interface normal modes employed in the Craig-Bampton method can be replaced by other Ritz vectors, e.g. Krylov subspace vectors derived from a suitable load distribution, see for example [5].

3 NUMERICAL EXAMPLE: SIMPLY SUPPORTED CONCRETE BEAM SUBJECTED TO BLAST LOADING

3.1 Reduced two-dimensional beam model

The effect of higher order modes on the displacement and shear force is studied by evaluating the response for a simply supported concrete beam subjected to a uniform distributed impulse pressure. The beam length is L = 3 m and the cross-section width and height is 1000 mm and 200 mm respectively. The load consists of a uniform reflected impulse pressure of 1500 Pa·s. Two load cases are studied with a peak reflected pressure of 1000 kPa in Load Case 1 and 300 kPa in Load Case 2, respectively. The pulse is approximated by an equivalent triangular pulse, hence, a fictitious duration can be calculated to 3 ms and 10 ms for Load Cases 1 and 2 respectively.

The beam is assumed to consist of concrete C30/37 with reinforcement Ø16s200 K500C-T. The modulus of elasticity for concrete and reinforcement steel is 32 GPa and 200 GPa respectively and the density for reinforced concrete is set to 2500 kg/m^3. The ultimate moment capacity is set to M_p = 80 kNm. The response is calculated with a two-dimensional beam model with a total of 20 Euler-Bernoulli two-node beam elements, as shown in Figure 2. Due to symmetry, only half of the beam is included in the FE model. Furthermore, small deformations are considered and the axial DOFs of the beam elements are neglected. It is assumed that a plastic hinge can appear at the beam midspan only. The plastic hinge is modelled by adding a rigid-perfectly plastic rotational spring to the rotational DOF at the symmetry line, as shown in Figure 2. Several effects are neglected in the model, e.g. catenary effects, reduced stiffness due to concrete cracking, concrete spalling etc. Nevertheless, the beam model is appropriate for evaluating the influence of higher order modes on the shear force and midspan displacement.

The beam model consists of a linear elastic subsystem, namely the beam element assemblage, which is connected to a nonlinear element. As discussed in Section 2, a reduced model can therefore be obtained by substructuring, e.g. by Guyan reduction or CMS by Craig-Bampton. Only one boundary DOF is kept, i.e. the rotational DOF at the beam symmetry line, denoted with superscript *b* in Figure 2. All other DOFs are internal DOFs and denoted with superscript *i* in Figure 2. Accordingly, the fixed-interface normal modes are calculated with fixed boundaries, i.e. with fixed rotation at the symmetry line. Hence, the substructure normal modes correspond to the symmetric eigenmodes for a simply supported beam, which are also the only modes that are excited by a uniform load. Thus, for an elastic response the system response is equivalent to the response of a linear elastic simply supported beam analyzed with modal truncation.

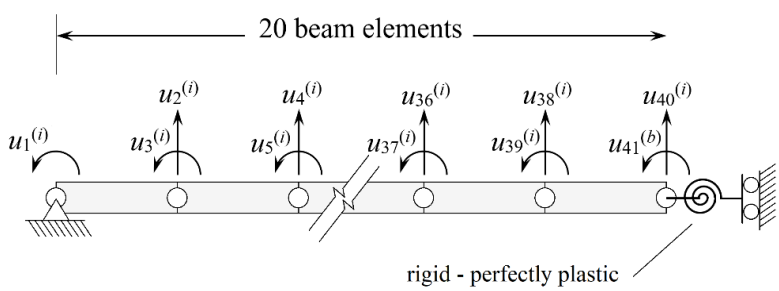

Figure 2: Two-dimensional beam model with nonlinear rotational spring at the symmetry line.

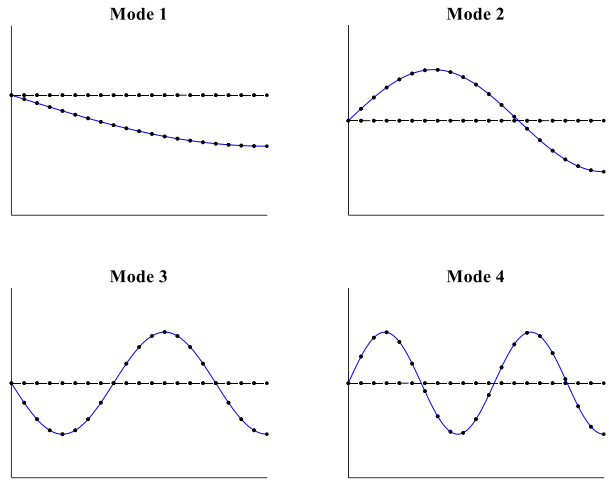

Figure 3: First four fixed-interface normal modes.

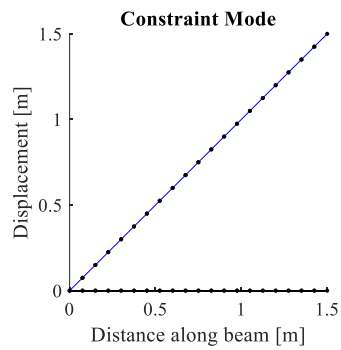

Figure 4: Constraint mode.

3.2 Structural analysis and results

In Figure 3 the first four fixed-interface normal modes are shown, which correspond to the first, third, fifth and seventh eigenmodes for a simply supported beam. Hence, by employing a symmetry model instead of a full model both the number of physical DOFs and modal coordinates are halved.

The constraint mode is shown in Figure 4 and correspond to a unit rotation of the boundary DOF, i.e. a unit rotation of the rotational DOF at the symmetry line. Hence, the constraint mode corresponds to a rigid body mode of the beam element assemblage which in turn correspond to the plastic deflection shape considered for an equivalent SDOF system, cf. Figure 1b.

The nonlinear dynamic response is calculated using the Newmark β-method with $\gamma = ½$ and $\beta = ¼$ (constant average acceleration) combined with the modified Newton-Raphson method. The total analysis time is 50 ms and the time-stepping is performed with very fine time increment < 0.01 ms to ensure sufficient resolution of the shear force.

The midspan displacement and shear force at the supports are evaluated for the beam model reduced by both Guyan reduction and the Craig-Bampton method for Load Cases 1 and 2 respectively. The response is compared to the response computed from an equivalent SDOF system. The stiffness of the SDOF system is calculated based on an uncracked cross section and the ultimate resistance is computed from the ultimate moment capacity, according to Eq. (6). A plastic deflection shape in accordance with Figure 1b is considered when determining the load-mass factor.

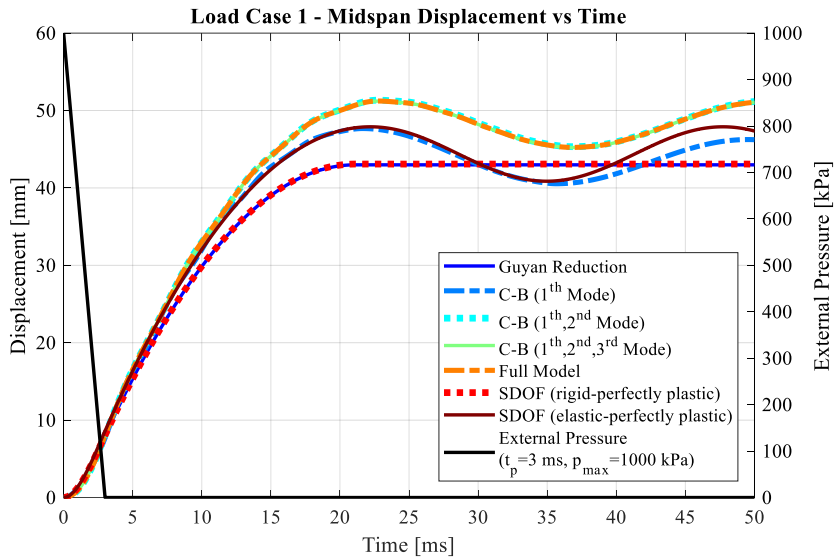

Figure 5: Midspan displacement vs. time for Load Case 1.

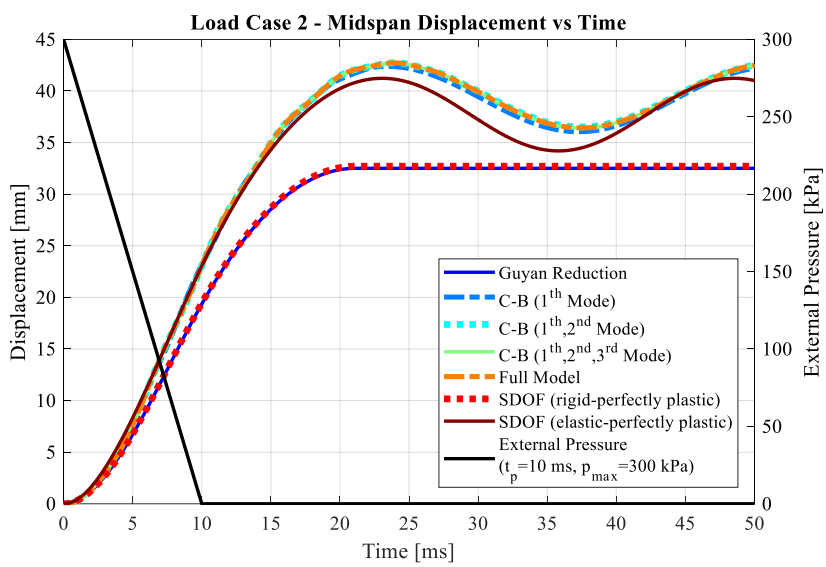

Figure 6: Midspan displacement vs. time for Load Case 2.

As shown in Figure 6, the midspan displacement for Load Case 2 calculated by the two-dimensional beam model is close to the displacement computed from an equivalent SDOF system. However, for Load Case 1 the response somewhat differs due to a larger influence of higher order modes, see Figure 5. Furthermore, as shown in Figures 5 and 6, only two fixed-interface normal modes need to be retained to obtain a response very close to the response for the full unreduced model.

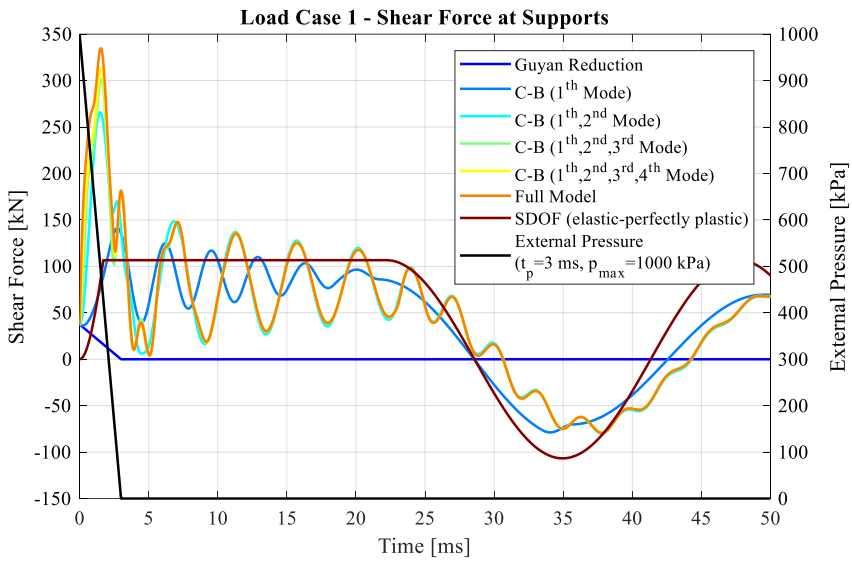

Figure 7: Shear force at supports for Load Case 1.

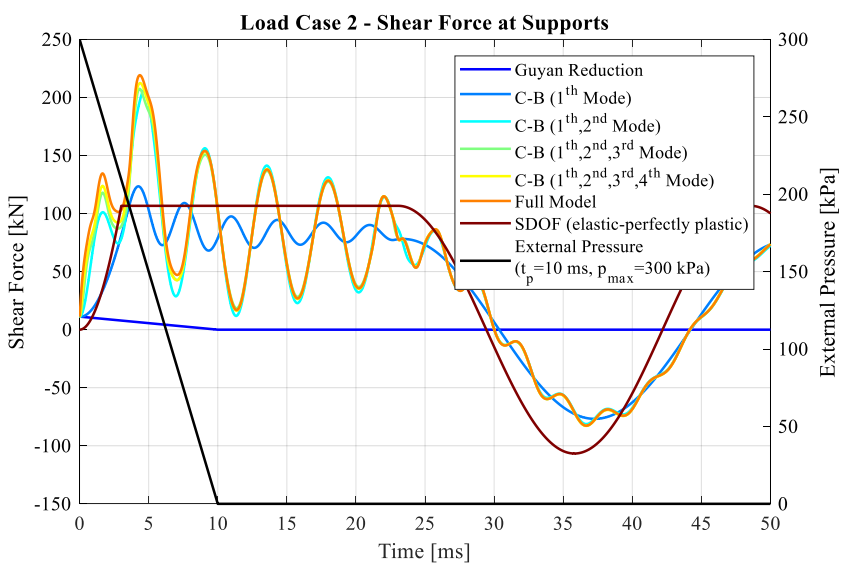

Figure 8: Shear force at the supports for Load Case 2.

The response obtained with Guyan reduction is included for comparison only. Additional boundary (or master) DOFs must be added to increase the precision of the Guyan reduction. As shown in Figures 5 and 6, a Guyan reduction where only the rotational DOF at the symmetry line is kept correspond to an equivalent rigid-plastic SDOF system, i.e. only the rigid mode of the beam assemblage is activated and the external work is dissipated by plastic deformation of the rigid-perfectly plastic rotational spring alone.

The shear force at the supports for Load Cases 1 and 2, computed from both an equivalent SDOF system and the two-dimensional beam model, are shown in Figures 7 and 8, respectively. As shown in the figures, the shear force computed from the two-dimensional model is, as expected, much larger due to that higher order modes are considered. The difference is greater for Load Case 1, where the impulse duration is shorter. As shown in Figure 7, at least four fixed-interface normal modes need to be included to capture the peak shear force. For Load Case 2, however, the shear force computed from a reduced model with two to three fixed-interface normal modes is fairly close to the peak shear force given by the full model.

Note that the shear force is $V \neq 0$ at $t = 0$. This is due to the discretization of the beam substructure. Half of the pressure on the beam element connected to the vertical support is instantaneously transferred to the support. Hence, the shear force/reaction force at $t = 0$ due to discretization can be calculated as $V(0) = p(0) \cdot L/(2 \cdot 2 \cdot \mathrm{n})$, where n is the number of beam elements in the symmetry model. Since a Guyan reduction only includes a rigid body mode of the beam elements the shear force should clearly be equal to zero, thus, the shear force shown in the diagrams is only due to the discretization of the beam assemblage. For Load Cases 1 and 2 the shear force due to discretization is calculated to 38 kN and 11 kN, respectively, i.e. in accordance with the response shown in Figures 7 and 8.

4 CONCLUSIONS

In the present paper, linear substructures with nonlinearities localized at their interfaces, such as plastic hinges in a beam member, are studied. By subdivision of the structure into substructures, reduced subsystems are obtained by use of the Craig-Bampton method. A numerical example is presented where a simply supported beam subjected to blast loading is studied.

For the Load Cases studied, the midspan displacement computed from an equivalent SDOF system, which are frequently employed in blast load design calculations, correspond fairly well to the displacement computed from a refined two-dimensional beam model, reduced by substructuring. In contrast, the shear force computed from an equivalent SDOF systems differ significantly from the peak shear force given by a refined two-dimensional beam model. This is due to that higher order modes are neglected in the equivalent SDOF system. As expected, the difference is greater for Load Case 1, where the beam is subjected to a pulse with higher peak pressure and shorter duration. To capture the peak shear force at least the first three to four fixed-interface normal modes need to be included in the reduced model. However, one boundary DOF and three to four generalized DOFs result in a MDOF system with five DOFs, which is still a very small system appropriate for time efficient iterative design calculations in both the conceptual and detailed design phase.

For a simply supported beam with a plastic hinge at the midspan the boundary DOFs in the Craig-Bampton method can be selected so that the linear response is equivalent to a linear elastic beam analyzed by modal truncation. Furthermore, the fixed-interface normal modes employed in the Craig-Bampton method can be replaced by other Ritz vectors, such as Krylov subspace vectors, which are derived from the current load configuration. Krylov subspace component mode synthesis can be expected to be efficient if the load configuration does not match the first normal modes.

ACKNOWLEDGMENTS

The research was carried out in the framework of the project "Urban Tranquility" under the Interreg V program funded by the European Regional Development Fund, as well as within the research project titled "Wooden Buildings in Silent Sustainable Cities", funded by the Swedish Governmental Agency for Innovation Systems (Vinnova), grant ref. no. 2018-04159.

REFERENCES

[1] D. de Klerk, D.J. Rixen, S.N. Voormeeren, General Framework for Dynamic Substructuring: History, Review, and Classification of Techniques, *AIAA Journal*, **46 (5)**, 1169-1181, 2008.

[2] R.J. Guyan, Reduction of Stiffness and Mass Matrices, *AIAA Journal*, **3 (2)**, 380, 1965.

[3] Bathe K.-J., Gracewski S., On nonlinear dynamic analysis using substructuring and mode superposition, *Computers and Structures*, **13**, 699-707, 1981.

[4] Biggs J.M., *Introduction to Structural Dynamics*, McGraw-Hill, New York, 1964.

[5] O. Flodén, K. Persson, G. Sandberg, Reduction methods for the dynamic analysis of substructure models of lightweight building structures, *Computers and Structures*, **138**, 49-61, 2014.

[6] Unified Facilities Criteria (UFC), *Structures to Resist the Effects of Accidental Explosions*, U. S. Army Corps of Engineers, Naval Facilities Engineering Command, Air Force Civil Engineer Support Agency, UFC 3-340-02, 5 December 2008.

[7] M. Johansson, B06-201, *Beräkningsstöd, Moment och tvärkraft* (in Swedish), Swedish Civil Contingencies Agency (MSB), 2015.

[8] R.R. Jr. Craig, A.J. Kurdila, *Fundamentals of Structural Dynamics, 2nd Edition*, John Wiley & Sons, New Jersey, 2006.

Paper B

Available online at www.easdprocedia.org
EASD Procedia EURODYN (2020) 2544-2564

EURODYN 2020
XI International Conference on Structural Dynamics
M. Papadrakakis, M. Fragiadakis, C. Papadimitriou (eds.)
Athens, Greece, 23–26 November 2020

MODEL REDUCTION FOR STRUCTURES SUBJECTED TO BLAST LOADING BY USE OF DYNAMIC SUBSTRUCTURING

Linus Andersson, Peter Persson, Kent Persson

Department of Construction Sciences, Lund University
P.O. Box 118, SE-221 00 Lund, Sweden
e-mail: {linus.andersson, peter.persson, kent.persson}@construction.lth.se

Keywords: Dynamic substructuring, Blast loading, Direct time-integration, Beam frame structure

Abstract. *In the present study, strategies are developed to enable time-efficient models for structures subjected to blast loading, appropriate for use in a structural design process. Dynamic substructuring is employed to obtain reduced models with localized nonlinearities, such as predefined plastic hinges in a beam–column structure. The parts of the substructures that remains linear elastic are modeled by Ritz-vectors whereas parts with a nonlinear response are retained as physical degrees-of-freedom. Furthermore, a time-stepping method is presented that is shown to be suitable for reduced models including local and predefined rigid–plastic behavior. The proposed methodology is applied and demonstrated in a numerical example of a concrete frame structure. Both the well-established Craig-Bampton method and reduction bases enriched by so-called correction modes are evaluated. For the load case studied, it is shown that the standard Craig-Bampton technique is suitable for reducing the substructures. Furthermore, it is shown that only a few Ritz-vectors are needed to sufficiently describe the deformation of the structure. However, additional modes are needed to ensure an accurate representation of the interface forces between the substructures.*

ISSN:2311-9020
Peer-review under responsibility of the Organizing Committee of EURODYN 2020.
doi: 10.47964/1120.9207.19160

1 INTRODUCTION

Simplified models, such as equivalent single-degree-of-freedom (SDOF) systems, are often used for design of concrete members subjected to blast loading, an approach proposed already in the mid-1960s [1]. When this simplified approach is used for studying individual structural members, the supporting global structure is often considered as rigid and thus represented by prescribed displacement boundary conditions in the local response analyses. Hence, if a global response analysis is required it is in general performed in a subsequent stage, where the reaction forces computed in the local analyses are applied on the global structure. Such a procedure can be suitable if the stiffness and/or mass of the global structure are relatively large. However, in cases where the structural member is stiff and heavy, or even integrated as a part of the global lateral load-bearing structure, it can be necessary to employ a model of the coupled system. Furthermore, it can be necessary to include higher order modes to accurately capture the force transmitted between individual members and the global structure, in particular if the structure is subjected to a pulse with short duration and large peak pressure, as e.g. discussed in [2].

The dynamic response of a structure can e.g. be computed by use of a nonlinear finite element (FE) model, including the members subjected to external loading and the supporting global structure. However, the design of concrete structures subjected to blast loading is often an iterative process, where the cross-section dimensions and the amount and arrangement of bending reinforcement affect the dynamic response. Therefore, simplified and computationally efficient models are key in the conceptual design phase.

In the present study, strategies are developed to enable time-efficient models for structures subjected to blast loading, appropriate for use in a structural design process. More specifically, reduced models with localized nonlinearities, such as predefined plastic hinges in a beam–column structure, are obtained by use of dynamic substructuring (DS) (for an overview of DS techniques see e.g. [3,4]). Hence, parts that remains linear elastic are reduced and modeled by Ritz-vectors whereas the degrees-of-freedom (DOFs) included in parts with a nonlinear response are retained as physical DOFs. Furthermore, a time-stepping scheme is presented that is shown to be suitable for reduced models including local and predefined rigid–plastic behavior, such as frame structures with plastic hinges.

2 SIMPLIFIED MODELING OF CONCRETE STRUCTURES SUBJECTED TO BLAST LOADING

As for dynamic loading in general, the design of concrete structures subjected to blast loading can be challenging due to that the response is affected by the structure's mass, stiffness and strength. Hence, a modification of the dimensions, the amount and/or arrangement of reinforcement must, in general, be verified by an updated dynamic response analyses. Furthermore, a nonlinear response analysis is often required. The kinetic energy induced by the external pressure is converted into elastic and plastic strain energy, and if the plastic dissipation is omitted in the analysis the response can be inaccurate, e.g. resulting in a very conservative design. Therefore, simplified nonlinear SDOF models are often employed to evaluate the response of individual structural members.

In addition to the design of individual members, the global structure must be designed to resist progressive collapse and to ensure lateral stability. If a nonlinear response analysis is required for studying the global response, it is in general not straight-forward to construct a simplified model. Hence, a more refined nonlinear FE model of the whole structure can be necessary.

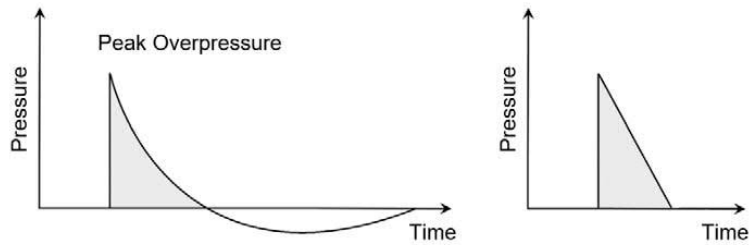

Figure 1: Typical (left) and idealized (right) blast pressure–time history.

2.1 Impulse pressure due to unconfined explosion

An unconfined explosion located on the ground surface results in a ground reflected shock wave that moves radially away from the center of the explosion [5]. If the explosion center is reasonable far from a structure, the pressure acting on the structure can be approximated by a uniform pressure. Upon impact, the initial wave is reinforced and reflected. The reflected impulse pressure acting on the structure is characterized by a very short duration and large peak pressure. For design purposes, the reflected impulse can, in general, be replaced by an equivalent triangular pulse, as shown in Figure 1. The actual duration is then replaced by a fictitious duration, computed from the peak reflected pressure and the reflected impulse.

2.2 Reduced models for design of concrete members

To ensure an adequate design of concrete members, such as beams and plates, subjected to blast loading, both the local response and the semi-global response (i.e. the global response of an individual member) must be considered. Hence, concrete members must be designed to resist local failure modes, such as punching shear failure, scabbing, spalling and penetration. Further, the shear force capacity and rotation capacity must be sufficiently large. Thus, it is crucial to ensure sufficient ductility and to avoid brittle failure modes.

A common procedure when evaluating the semi-global response of beams and plates is to set up an equivalent elasto-plastic SDOF system, where the yield force is derived from the ultimate moment capacity [1]. In fact, the yield force corresponds to the ultimate load, which implies that the maximum shear force in the dynamic response analysis is equal to the shear force given by a static yield line analysis. As e.g. shown in [2], the shear force computed using this simplified approach might be underestimated due to the neglection of higher order modes. Nonetheless, the approach can be reasonably accurate and in accordance with several design codes, such as UFC [5].

Using a simplified equivalent SDOF system implies that the position of the yield lines and/or plastic hinges can by assumed in accordance with a static yield line analysis, where the spatial load distribution correspond to the spatial distribution of the impulse pressure. This assumption is also the basis in the modeling strategies developed in Sections 3 and 4. However, it should be noted that this approach is primarily intended to be used in a conceptual design phase, i.e. a full nonlinear analysis can be necessary to verify the final design.

3 DYNAMIC SUBSTRUCTURING OF STRUCTURES WITH PLASTIC HINGES

By use of dynamic substructuring (DS) the aim is to efficiently compute the dynamic response of a structure by subdivision of the structure into substructures. Solving several substructures can be computationally less expensive than solving one large system. Moreover, DS can be employed to reduce systems with localized nonlinearities, such as predefined plastic

hinges in a beam–column structure. The parts of the structure that remains linear elastic is then reduced and modeled by Ritz-vectors whereas the DOFs included in parts with a nonlinear response are retained as physical DOFs.

In most DS techniques reduction is performed on the substructure level. Hence, the substructure displacements $\mathbf{u}^{(s)}$ are represented by a reduced set of coordinates $\mathbf{q}^{(s)}$, given by

$$\mathbf{u}^{(s)} = \mathbf{T}\mathbf{q}^{(s)} \tag{1}$$

where superscript s is the substructure label and $\mathbf{T}$ is a $n^{(s)} \times m^{(s)}$ transformation matrix, whose columns are Ritz-vectors, or so-called component modes. Depending on the DS technique, the reduced vector $\mathbf{q}^{(s)}$ can include physical master (or boundary) DOFs and/or generalized coordinates. Typically, $m^{(s)} << n^{(s)}$.

A FE formulation of a substructure leads to a linear equation of motion of the following form:

$$\mathbf{M}^{(s)}\ddot{\mathbf{u}}^{(s)} + \mathbf{C}^{(s)}\dot{\mathbf{u}}^{(s)} + \mathbf{K}^{(s)}\mathbf{u}^{(s)} = \mathbf{p}^{(s)} \tag{2}$$

where $\mathbf{p}^{(s)}$ is a $n^{(s)} \times 1$ substructure load vector and $\mathbf{M}^{(s)}$, $\mathbf{C}^{(s)}$ and $\mathbf{K}^{(s)}$ are the $n^{(s)} \times n^{(s)}$ substructure mass, damping and stiffness matrices, respectively. By inserting Equation (1) in (2) and pre-multiplying with $\mathbf{T}^{\mathrm{T}}$ the reduced subsystem is given by:

$$\widetilde{\mathbf{M}}^{(s)}\ddot{\mathbf{q}}^{(s)} + \widetilde{\mathbf{C}}^{(s)}\dot{\mathbf{q}}^{(s)} + \widetilde{\mathbf{K}}^{(s)}\mathbf{q}^{(s)} = \tilde{\mathbf{p}}^{(s)} \tag{3}$$

where

$$\widetilde{\mathbf{M}}^{(s)} = \mathbf{T}^{\mathrm{T}}\mathbf{M}^{(s)}\mathbf{T}, \qquad \widetilde{\mathbf{C}}^{(s)} = \mathbf{T}^{\mathrm{T}}\mathbf{C}^{(s)}\mathbf{T}, \qquad \widetilde{\mathbf{K}}^{(s)} = \mathbf{T}^{\mathrm{T}}\mathbf{K}^{(s)}\mathbf{T}, \qquad \tilde{\mathbf{p}}^{(s)} = \mathbf{T}^{\mathrm{T}}\mathbf{p}^{(s)} \tag{4}$$

The size of the reduced system matrices $\widetilde{\mathbf{M}}^{(s)}$, $\widetilde{\mathbf{C}}^{(s)}$ and $\widetilde{\mathbf{K}}^{(s)}$ is thus $m^{(s)} \times m^{(s)}$ and the reduced load vector $\tilde{\mathbf{p}}^{(s)}$ is $m^{(s)} \times 1$ (to simplify the notation the superscript s will be left out until Section 3.3, on substructure coupling procedures). The substructures are then reassembled to form a reduced model of the full coupled system, why DS is sometimes referred to as Component Mode Synthesis (CMS).

Arguably the most straight-forward methods within DS are the so-called condensation methods, where only physical master DOFs are included in $\mathbf{q}$. The most common condensation method is Guyan reduction, also referred to as static condensation due to that inertia effects are ignored [6]. The Guyan transformation matrix is given by

$$\begin{bmatrix}\mathbf{u}_i \\ \mathbf{u}_b\end{bmatrix} = \begin{bmatrix}-\mathbf{K}_{ii}^{-1}\mathbf{K}_{ib} \\ \mathbf{I}_{bb}\end{bmatrix}\mathbf{u}_b = \begin{bmatrix}\boldsymbol{\Psi}_{ib} \\ \mathbf{I}_{bb}\end{bmatrix}\mathbf{u}_b = \mathbf{T}_{\mathrm{G}}\mathbf{q} \tag{5}$$

where the subscripts i and b denotes the *interior* and interface *boundary* DOFs, $\mathbf{T}_{\mathrm{G}}$ is the Guyan transformation matrix and $\mathbf{q}$ contains the physical boundary DOFs. The columns of the transformation matrix are the so-called constraint modes, obtained by prescribing a unit displacement for a boundary DOF, while the interior DOFs are force-free and the other boundary DOFs are held fixed. Using this approach, "exact" results are achieved for static loading. However, due to neglected inertia effects the accuracy can be expected to decrease with an increasing forcing frequency.

Using a similar procedure but replacing the stiffness matrix with the dynamic stiffness matrix, exact result can instead be achieved for a certain forcing frequency, often referred to as dynamic reduction. There are also other more sophisticated condensation methods, such as Improved Reduction System (IRS) and System Equivalent Reduction Expansion Process (SEREP),

where the number of exact resonances is less or equal to the number of boundary DOFs [7]. However, using condensation methods, it is not possible to both obtain a reduced model that is "statically complete" (i.e. a basis for all possible deformations that result from loading at the substructure boundary nodes) and at the same time keeping exact resonances. To achieve this, a CMS approach is required that uses generalized coordinates representing the amplitudes of additional Ritz-vectors.

Several CMS techniques have been developed since the 1960s, which can be divided into *fixed-interface* and *free-interface* methods. The most popular approach, a fixed-interface method, is CMS by Craig-Bampton (C-B), developed in the late 1960s [8]. The C-B method combines fixed-interface normal modes with so-called constraint modes, see further Section 3.1. Free-interface methods, using so-called free-interface component modes, were developed by MacNeal, Rubin and Craig and Chang in the 1970s [9,10,11]. In addition, another free-interface method, the dual Craig-Bampton method, was proposed in the early 2000s which, in contrast to the other free-interface methods, preserves the sparsity of the system matrices [12].

Reducing a structure with plastic hinges, it is important to employ a DS technique where the physical boundary DOFs, namely the rotational DOFs at the plastic hinges, are retained. Therefore, the CMS method proposed by Craig and Chang is excluded due to an assembling procedure that removes the physical boundary DOFs. The dual C-B method is an interesting approach since the interface forces are kept as DOFs in the assembled system. However, this method produces negative eigenvalues which make a stable time integration impossible [13] (an approach to overcome this issue is e.g. proposed in [13], unfortunately this approach includes removing all physical DOFs).

Apart from retaining the physical boundary DOFs at the plastic hinges, the plastic deformations of the assembled system must be resolved. Hence, the reduced subsystems should be "statically complete" and rigid body modes of the subsystems should be included in the reduction basis. Using the C-B method, the rigid body modes are not explicitly included in the reduction basis. However, the rigid body modes are spanned by the constraint modes. In fact, the set of constraint modes is a basis for all possible deformations that result from loading at the substructure boundary nodes [14]. In addition to the C-B method, the free-interface methods by MacNeal and Rubin retains the physical boundary DOFs in the assembled system and explicitly includes the rigid body modes in the reduction basis.

In summary, either the fixed-interface C-B method or the free-interface methods by MacNeal and Rubin are judged to be the most suitable methods for reducing a beam–column structure including predefined plastic joints. A free-interface approach can be expected to be more accurate upon yielding, i.e. when the joint stiffness is zero, whereas a fixed-interface approach can be expected to be more accurate when the joints are fixed, i.e. when yielding does not occur. Based on this observation it is assumed that the classic C-B approach, which preserves the sparsity of the system matrices, is the preferred choice.

3.1 Craig-Bampton method

The Craig-Bampton method combines the retained physical DOFs with generalized coordinates corresponding to the amplitudes of so-called fixed-interface normal modes. Neglecting damping the partitioned mass and stiffness matrices can be written as:

$$\begin{bmatrix} \mathbf{M}_{ii} & \mathbf{M}_{ib} \\ \mathbf{M}_{bi} & \mathbf{M}_{bb} \end{bmatrix} \begin{bmatrix} \ddot{\mathbf{u}}_i \\ \ddot{\mathbf{u}}_b \end{bmatrix} + \begin{bmatrix} \mathbf{K}_{ii} & \mathbf{K}_{ib} \\ \mathbf{K}_{bi} & \mathbf{K}_{bb} \end{bmatrix} \begin{bmatrix} \mathbf{u}_i \\ \mathbf{u}_b \end{bmatrix} = \begin{bmatrix} \mathbf{p}_i \\ \mathbf{p}_b \end{bmatrix} \tag{6}$$

By setting the boundary displacements to zero in Equation (6), the fixed-interface normal modes are obtained by the generalized eigenvalue problem:

$$\left(\mathbf{K}_{ii} - \omega_j^2 \mathbf{M}_{ii}\right)\left\{\boldsymbol{\phi}_i\right\}_j = 0 \tag{7}$$

where $\mathbf{K}_{ii}$ and $\mathbf{M}_{ii}$ are the interior stiffness and mass matrices. The eigenvectors are normalized so that $\boldsymbol{\Phi}_{ii}{}^{\mathrm{T}}\mathbf{M}_{ii}\boldsymbol{\Phi}_{ii} = \mathbf{I}_{ii}$, where $\boldsymbol{\Phi}_{ii}$ is the complete set of fixed-interface normal modes. The physical coordinates can then be represented as:

$$\begin{bmatrix}\mathbf{u}_i \\ \mathbf{u}_b\end{bmatrix} = \begin{bmatrix}\boldsymbol{\Phi}_{ik} & \boldsymbol{\Psi}_{ib} \\ \mathbf{0}_{bk} & \mathbf{I}_{bb}\end{bmatrix}\begin{bmatrix}\mathbf{q}_k \\ \mathbf{u}_b\end{bmatrix} = \mathbf{T}_{\text{C-B}}\mathbf{q} \tag{8}$$

where the subscript k denotes the kept fixed-interface normal modes, $\mathbf{T}_{\text{C-B}}$ is the Craig-Bampton transformation matrix, $\mathbf{q}_k$ is the generalized coordinates and $[\boldsymbol{\Psi}_{ib} \quad \mathbf{I}_{bb}]^{\mathrm{T}}$is the constraint mode matrix, equivalent to the Guyan reduction basis. Hence, the Craig-Bampton method can be interpreted as an extension of the Guyan reduction where the neglected inertia terms are compensated by including a set of fixed-interface normal modes.

3.2 Craig-Bampton with Modal Truncation Augmentation

The fixed-interface normal modes included in the C-B reduction basis can be augmented by so-called high order static correction modes, which can be interpreted as a form of generalization of the Guyan static modes. The C-B method with so-called Modal Truncation Augmentation (MTA) is presented in [15].

If the internal forces are zero, the top row of Equation (6) can be rewritten as:

$$\mathbf{M}_{ii}\ddot{\mathbf{u}}_i + \mathbf{K}_{ii}\mathbf{u}_i = -\mathbf{M}_{ib}\ddot{\mathbf{u}}_b - \mathbf{K}_{ib}\mathbf{u}_b \tag{9}$$

Hence, the substructure can be considered excited by imposed displacements on its boundary. Further, the internal displacements can be approximated as

$$\mathbf{u}_i = \mathbf{u}_{i,\text{stat}} + \mathbf{y} \tag{10}$$

where $\mathbf{u}_{i,\text{stat}} = -\mathbf{K}_{ii}{}^{-1}\mathbf{K}_{ib}\mathbf{u}_b$ is the quasi-static solution modified by the second term $\mathbf{y}$ to obtain the dynamic response, i.e. similarly to the well-established mode acceleration method, e.g. described in [16]. By inserting Equation (10) into Equation (9) the dynamic response of the relative solution is given by

$$\mathbf{M}_{ii}\ddot{\mathbf{y}} + \mathbf{K}_{ii}\mathbf{y} = -\mathbf{M}_{ii}\ddot{\mathbf{u}}_{i,\text{stat}} - \mathbf{M}_{ib}\ddot{\mathbf{u}}_b = \mathbf{Y}\ddot{\mathbf{u}}_b \tag{11}$$

where $\mathbf{Y} = \mathbf{M}_{ii}\mathbf{K}_{ii}{}^{-1}\mathbf{K}_{ib} - \mathbf{M}_{ib}$, which can be interpreted as inertia forces associated to static modes [15]. This procedure can be continued by replacing $\mathbf{y}$ with a quasi-static solution and a dynamic correction. Hence, a recursive procedure is obtained, indicating that the dynamic response can be approximated as

$$\mathbf{u}_i \approx -\mathbf{K}_{ii}{}^{-1}\mathbf{K}_{ib}\mathbf{u}_b + \sum_{j=1}^{n}\left(-\mathbf{K}_{ii}{}^{-1}\mathbf{M}_{ii}\right)^{j-1}\mathbf{K}_{ii}{}^{-1}\mathbf{Y}\frac{\mathrm{d}^{2j}\mathbf{u}_b}{\mathrm{d}t^{2j}} \tag{12}$$

where n is the number of static corrections.

According to Equation (12) a dynamic response analysis is not included in the approximation. However, if a dynamic analysis including k eigenmodes has been performed, part of the corrections is already considered. The expression for the higher order corrections can then be rewritten as:

$$\mathbf{u}_{i,cor.j} \approx \left(\mathbf{K}_{ii}^{-1} - \sum_{r=1}^{k} \frac{\boldsymbol{\phi}_r \boldsymbol{\phi}_r^{\mathrm{T}}}{\omega_r^2} \right) \left(-\mathbf{M}_{ii} \mathbf{K}_{ii}^{-1} \right)^{j-1} \mathbf{Y} \frac{\mathrm{d}^{2j} \mathbf{u}_b}{\mathrm{d}t^{2j}} \tag{13}$$

where we use that the inverse of the stiffness matrix can be expressed as

$$\mathbf{K}_{ii}^{-1} = \sum_{r=1}^{N} \frac{\boldsymbol{\phi}_r \boldsymbol{\phi}_r^{\mathrm{T}}}{\omega_r^2} = \sum_{r=1}^{k} \frac{\boldsymbol{\phi}_r \boldsymbol{\phi}_r^{\mathrm{T}}}{\omega_r^2} + \sum_{r=k+1}^{N} \frac{\boldsymbol{\phi}_r \boldsymbol{\phi}_r^{\mathrm{T}}}{\omega_r^2} \tag{14}$$

where N is the total number of eigenmodes, and $\boldsymbol{\phi}_r$ and ω_r is the eigenmode and eigenfrequency for mode r. Hence, the space already spanned by the fixed-interface normal modes is removed from the corrections. The total response is then given by

$$\mathbf{u}_i \approx \sum_{r=1}^{k} \boldsymbol{\phi}_r q_r + \sum_{j=0}^{n} \mathbf{u}_{i,cor.j} \tag{15}$$

where $\mathbf{u}_{i,cor.0} = -\mathbf{K}_{ii}^{-1} \mathbf{K}_{ib} \mathbf{u}_b$. Furthermore, the amplitudes $\frac{\mathrm{d}^{2j} \mathbf{u}_b}{\mathrm{d}t^{2j}}$ can be treated as separate DOFs, i.e. instead of high order corrections the modal basis is augmented by high order correction *modes*, also referred to as force-dependent Ritz-vectors or Krylov vectors. Hence, the j-th order correction modes is given by:

$$\mathbf{x}_{i,cor.j} = \left(\mathbf{K}_{ii}^{-1} - \sum_{r=1}^{k} \frac{\boldsymbol{\phi}_r \boldsymbol{\phi}_r^{\mathrm{T}}}{\omega_r^2} \right) \left(\mathbf{M}_{ii} \mathbf{K}_{ii}^{-1} \right)^{j-1} \mathbf{Y} \tag{16}$$

Note that the number of vectors generated in each iteration equals the number of boundary DOFs, why the subspace spanned by the generated vectors is sometimes referred to as a block-Krylov subspace [14]. The static correction modes are both mass- and stiffness-orthogonal to the fixed-interface normal modes. However, they are not mutually orthogonal. This can e.g. be achieved by solving a small eigenvalue problem:

$$(\mathbf{X}_{cor}^{\mathrm{T}} \mathbf{K} \mathbf{X}_{cor}) \mathbf{Z} = (\mathbf{X}_{cor}^{\mathrm{T}} \mathbf{M} \mathbf{X}_{cor}) \mathbf{Z} \boldsymbol{\Lambda} \tag{17}$$

where $\mathbf{X}_{\mathrm{cor}}$ is the correction mode matrix. The eigenvectors are normalized so that $\mathbf{Z}^{\mathrm{T}} \left(\mathbf{X}_{\mathrm{cor}}^{\mathrm{T}} \mathbf{M} \mathbf{X}_{\mathrm{cor}} \right) \mathbf{Z} = \mathbf{I}$ and the orthonormal basis of the correction vectors is then given by $\widetilde{\mathbf{X}}_{\mathrm{cor}} = \mathbf{X}_{\mathrm{cor}} \mathbf{Z}$. The relation between the substructure physical DOFs and the reduced coordinate is then given by

$$\begin{bmatrix} \mathbf{u}_i \\ \mathbf{u}_b \end{bmatrix} = \begin{bmatrix} \boldsymbol{\Phi}_{ik} & \widetilde{\mathbf{X}}_{cor} & \boldsymbol{\Psi}_{ib} \\ \mathbf{0}_{bk} & \mathbf{0}_{bn} & \mathbf{I}_{bb} \end{bmatrix} \begin{bmatrix} \mathbf{q}_k \\ \mathbf{q}_n \\ \mathbf{u}_b \end{bmatrix} = \mathbf{T}_{\mathrm{C\text{-}B,cor}} \mathbf{q} \tag{18}$$

where $\mathbf{q}_n$ is the amplitudes of the correction modes and $\mathbf{T}_{\mathrm{C\text{-}B,cor}}$ is the C-B transformation matrix augmented by correction modes.

Using the above procedure, correction modes are generated based on interface excitation. Using a similar procedure, the correction modes, or so-called force dependent Ritz-vectors, can also be generated based on external loads applied to the substructure interior DOFs.

3.3 Substructure coupling procedures

Since the physical boundary DOFs are preserved in the C-B reduction process the assembly method is straight-forward, hence each substructure can be treated as a super-element. However, the substructures can either be assembled by eliminating one set of interface DOFs, a so-called *primal* assembled system, or so that all interface DOFs are preserved, a so-called *dual* assembled system.

The block diagonal system matrices for a structure consisting of N_s substructures are given by

$$\mathbf{M} = \mathrm{diag}(\mathbf{M}^{(s)}), \qquad \mathbf{C} = \mathrm{diag}(\mathbf{C}^{(s)}), \qquad \mathbf{K} = \mathrm{diag}(\mathbf{K}^{(s)}) \tag{19}$$

where **M**, **C** and **K** have size $n \times n$ and the superscript s is the substructure label. The equation of motion can then be written as

$$\mathbf{M}\ddot{\mathbf{u}} + \mathbf{C}\dot{\mathbf{u}} + \mathbf{K}\mathbf{u} = \mathbf{p} \tag{20}$$

where **u** is the $n \times 1$ global displacement vector, including all DOFs at the interfaces between substructures. Assuming compatible meshes, constraints enforced between substructures for individual DOF pairs, e.g. $u_i^{(s_1)} = u_j^{(s_2)}$, can be written in matrix form:

$$\mathbf{B}\mathbf{u} = \mathbf{0} \tag{21}$$

where the constraint matrix **B** is a signed Boolean matrix with size $m \times n$, where m is the number of constraints and n is the total number of DOFs.

As e.g. shown in [3], a primal assembly can be enforced by using the so-called Boolean localization matrix **L**, found by computing the null-space for **B**, i.e.

$$\mathbf{L} = \mathrm{Null}(\mathbf{B}) \tag{22}$$

The relation between the global displacement vector and a displacement vector with a unique set of interface DOFs, $\mathbf{u}_P$, is then given by

$$\mathbf{u} = \mathbf{L}\,\mathbf{u}_P \tag{23}$$

By inserting Equation (23) in Equation (20) and pre-multiplying with $\mathbf{L}^T$ the equation of motion for the primal assembled system is given by

$$\mathbf{M}_P\ddot{\mathbf{u}}_P + \mathbf{C}_P\dot{\mathbf{u}}_P + \mathbf{K}_P\mathbf{u}_P = \mathbf{p}_P \tag{24}$$

where

$$\mathbf{M}_P = \mathbf{L}^T\mathbf{M}\mathbf{L}, \qquad \mathbf{C}_P = \mathbf{L}^T\mathbf{C}\mathbf{L}, \qquad \mathbf{K}_P = \mathbf{L}^T\mathbf{K}\mathbf{L}, \qquad \mathbf{p}_P(t) = \mathbf{L}^T\mathbf{p} \tag{25}$$

The number of DOFs in the primal assembled system is thus $n_P = n - m$ and, accordingly, the size of $\mathbf{M}_P$, $\mathbf{C}_P$, $\mathbf{K}_P$ is $[n_P \times n_P]$ and $\mathbf{p}_P$ is $[n_P \times 1]$.

Instead of eliminating one set of DOFs, a dual assembled system can be achieved by enforcing the interface constraints using Lagrange multipliers $\boldsymbol{\lambda}$. The system of equations can then be written as

$$\begin{bmatrix} \mathbf{M} & \mathbf{0} \\ \mathbf{0} & \mathbf{0} \end{bmatrix} \begin{bmatrix} \ddot{\mathbf{u}} \\ \boldsymbol{\lambda} \end{bmatrix} + \begin{bmatrix} \mathbf{C} & \mathbf{0} \\ \mathbf{0} & \mathbf{0} \end{bmatrix} \begin{bmatrix} \dot{\mathbf{u}} \\ \boldsymbol{\lambda} \end{bmatrix} + \begin{bmatrix} \mathbf{K} & \mathbf{B}^{\mathrm{T}} \\ \mathbf{B} & \mathbf{0} \end{bmatrix} \begin{bmatrix} \mathbf{u} \\ \boldsymbol{\lambda} \end{bmatrix} = \begin{bmatrix} \mathbf{p} \\ \mathbf{0} \end{bmatrix} \tag{26}$$

thus, preserving all interface DOFs [17]. Note that $\boldsymbol{\lambda}$ can be interpreted as an interface force vector, i.e. the forces required to enforce equal displacements for interface DOF pairs.

A dual assembled system can also be enforced using the penalty method, e.g. expressed as

$$\mathbf{M}\ddot{\mathbf{u}} + \mathbf{C}\dot{\mathbf{u}} + (\mathbf{K} + \alpha \mathbf{B}^{\mathrm{T}}\mathbf{B})\mathbf{u} = \mathbf{p} \tag{27}$$

where α is the penalty stiffness, chosen sufficiently large so that $\mathbf{Bu} \approx \mathbf{0}$ [17]. Note that this approach corresponds to adding stiff springs between the constrained DOFs.

The preferred assembly method, or constraint enforcement method, depend on several factors such as the analysis type, the output data of interested, etc.

4 TIME-STEPPING METHOD FOR STRUCTURES WITH RIGID–PERFECTLY PLASTIC JOINTS

Simplified models are often used for design of concrete structures where linear elastic beam elements are combined with predefined discrete plastic hinges, approximated as rigid–perfectly plastic. To enforce a rigid–perfectly plastic coupling between two DOFs, namely the rotational DOFs at the plastic hinges, one alternative is to utilize the penalty method, i.e. by introducing a stiff elastic–perfectly plastic rotational spring. However, one obvious problem when using the penalty method is to choose a suitable penalty stiffness—if it is too low, the results will be inaccurate and if it is too large, the system equations will be ill-conditioned with respect to inversion. Furthermore, the highest eigenfrequency of the system can be expected to increase significantly, which can result in a very small critical time increment size in conditionally stable time integration schemes.

Another alternative is to set up a dual assembled system according to Equation (26) and setting a maximum value, corresponding to the plastic moment, for the Lagrange multipliers. The Lagrange multipliers will then be either known, i.e. treated as external forces equal to the plastic moments, or unknown. However, ensuring stability for a system including Lagrange multipliers, for so-called Differential-Algebraic Equations (DAEs), is often found to be problematic in direct time integration of dual assembled systems. For example, a standard Newmark time integration scheme, assuming constant average accelerations, is in this case unconditionally unstable. However, methods to ensure stability exist, see e.g. [18]. Nonetheless the available time integration schemes are somewhat limited.

Instead of using a pure dual or primal formulation, a methodology is proposed where the system is reassembled when yielding of the rigid–perfectly plastic hinges starts or stops. Such a procedure implies that the nonlinear analysis is performed as a series of linear analyses. Hence, the plastic hinges are either modeled as fixed by eliminating one of the rotational DOFs or as external moments applied on both rotational DOFs at the plastic hinges. This approach can be expected to be particularly suitable for systems consisting of reduced substructures, with a limited number of plastic hinges. The critical time increment is then related to the highest eigenfrequency of the assembled substructures, which in turn have already been reduced by a modal truncation on the substructure level, removing the high frequency content. Furthermore, high frequency noise induced by penalty elements is avoided.

4.1 Time-stepping algorithm

Starting with the system in Equation (20), a $m \times n$ signed Boolean matrix $\mathbf{B}$ can be constructed to define all the interface couplings between the substructures. The couplings can either be fixed constraints or rigid–perfectly plastic couplings. The matrix is then partitioned as:

$$\mathbf{B} = \begin{bmatrix} \mathbf{B}_r \\ \mathbf{B}_c \\ \mathbf{B}_y \end{bmatrix} \tag{28}$$

where $\mathbf{B}_r$ defines m_r constraints (or boundary conditions) that are not limited by a yield force, e.g. the translational DOFs at a plastic hinge, $\mathbf{B}_c$ defines the m_c rigid–plastic couplings not yielding and $\mathbf{B}_y$ defines the m_y rigid–plastic couplings currently yielding. Hence, the Boolean matrices $\mathbf{B}_c$ and $\mathbf{B}_y$ must be updated in a time-stepping scheme. The constraints defined by $\mathbf{B}_r$ are enforced using a primal formulation before the time-stepping is initialized, hence by eliminating m_r interface DOFs. The equation of motion for the assembled system can then be written as

$$\widehat{\mathbf{M}}\ddot{\mathbf{u}}_r + \widehat{\mathbf{C}}\dot{\mathbf{u}}_r + \widehat{\mathbf{K}}\mathbf{u}_r = \hat{\mathbf{p}} \tag{29}$$

where

$$\widehat{\mathbf{M}} = \mathbf{L}_r^{\mathrm{T}}\mathbf{M}\mathbf{L}_r, \qquad \widehat{\mathbf{C}} = \mathbf{L}_r^{\mathrm{T}}\mathbf{C}\mathbf{L}_r, \qquad \widehat{\mathbf{K}} = \mathbf{L}_r^{\mathrm{T}}\mathbf{K}\mathbf{L}_r, \qquad \hat{\mathbf{p}} = \mathbf{L}_r^{\mathrm{T}}\mathbf{p} \tag{30}$$

and where the Boolean localization matrix $\mathbf{L}_r = \mathrm{Null}(\mathbf{B}_r)$. To simplify the implementation the eliminated DOFs are then removed from the matrices $\mathbf{B}_c$ and $\mathbf{B}_y$, i.e. by removing the corresponding m_r columns containing zeros. The size of the updated matrices $\widehat{\mathbf{B}}_c$ and $\widehat{\mathbf{B}}_y$ is then $m_c \times (n - m_r)$ and $m_y \times (n - m_r)$, respectively. At the initial stage, the couplings defined by $\widehat{\mathbf{B}}_c$ is enforced in the same manner by computing $\mathbf{L}_c = \mathrm{Null}(\widehat{\mathbf{B}}_c)$. At each time increment $t^{(i)}$, the interface forces $\boldsymbol{\lambda}^{(i)}$ is computed from the expression

$$\widehat{\mathbf{B}}_c^{\mathrm{T}}\boldsymbol{\lambda}^{(i)} = \hat{\mathbf{p}}^{(i)} - \widehat{\mathbf{M}}\mathbf{L}_c\ddot{\mathbf{u}}_c{}^{(i)} - \widehat{\mathbf{C}}\mathbf{L}_c\dot{\mathbf{u}}_c{}^{(i)} - \widehat{\mathbf{K}}\mathbf{L}_c\mathbf{u}_c{}^{(i)} \tag{31}$$

where the relation $\mathbf{u}_r = \mathbf{L}_c\mathbf{u}_c$ has been applied. If the interface force for a coupling is larger than the specified yield force, the Boolean matrices $\widehat{\mathbf{B}}_c$ and $\widehat{\mathbf{B}}_y$ are updated, i.e. the row in $\widehat{\mathbf{B}}_c$ defining the coupling is moved to $\widehat{\mathbf{B}}_y$. Thereafter, the system is reassembled by computing the localization matrix $\mathbf{L}_c = \mathrm{Null}(\widehat{\mathbf{B}}_c)$ and applying it to Equation (29). The couplings currently yielding are then considered by adding the yield forces as external loads, hence

$$\mathbf{L}_c^{\mathrm{T}}\widehat{\mathbf{M}}\mathbf{L}_c\ddot{\mathbf{u}}_c{}^{(i)} + \mathbf{L}_c^{\mathrm{T}}\widehat{\mathbf{C}}\mathbf{L}_c\dot{\mathbf{u}}_c{}^{(i)} + \mathbf{L}_c^{\mathrm{T}}\widehat{\mathbf{K}}\mathbf{L}_c\mathbf{u}_c{}^{(i)} = \mathbf{L}_c^{\mathrm{T}}\left(\hat{\mathbf{p}}^{(i)} - \widehat{\mathbf{B}}_y^{\mathrm{T}}\mathbf{f}_y\right) \tag{32}$$

where $\mathbf{f}_y$ is a $m_y \times 1$ vector containing the specified yield forces. Unloading of the m_y couplings currently yielding is detected by checking the relative velocity sign, i.e. if

$$\mathrm{sign}\left(\left\{\widehat{\mathbf{B}}_y\dot{\mathbf{u}}_r{}^{(i)}\right\}_j\right) \neq \mathrm{sign}\left(\left\{\widehat{\mathbf{B}}_y\dot{\mathbf{u}}_r{}^{(i+1)}\right\}_j\right) \tag{33}$$

where subscript j denotes an element of the column vector $\widehat{\mathbf{B}}_y\dot{\mathbf{u}}_r$. If unloading occurs, the system is updated by moving rows from $\widehat{\mathbf{B}}_y$ to $\widehat{\mathbf{B}}_c$, computing the localization matrix $\mathbf{L}_c = \mathrm{Null}(\widehat{\mathbf{B}}_c)$ and applying it to Equation (29).

The time integration between the system updates can be performed in a standard manner by the Newmark-β method, as e.g. described in [19]. However, for a nonlinear system including both elastic and plastic deformations it is convenient to use incremental quantities,

$$\Delta\mathbf{u}^{(i)} = \mathbf{u}^{(i+1)} - \mathbf{u}^{(i)}, \quad \Delta\mathbf{u}^{(i)} = \mathbf{u}^{(i+1)} - \mathbf{u}^{(i)}, \quad \Delta\ddot{\mathbf{u}}^{(i)} = \ddot{\mathbf{u}}^{(i+1)} - \ddot{\mathbf{u}}^{(i)}, \quad \Delta\mathbf{p}^{(i)} = \mathbf{p}^{(i+1)} - \mathbf{p}^{(i)} \tag{34}$$

In fact, the time-stepping algorithm is constructed so that the computed incremental displacements are always transformed and appended to $\mathbf{u}_r$, thus

$$\mathbf{u}_r{}^{(i+1)} = \mathbf{u}_r{}^{(i)} + \mathbf{L}_c \Delta\mathbf{u}_c{}^{(i)} \tag{35}$$

Consequently, the displacement vector need not to be transformed at the system updates. Merging DOF pairs in couplings where yielding is stopped would certainly be an ambiguous operation, since the displacement in each DOF in general will differ.

Upon yielding, the system is updated so that couplings where yielding is initiated are released. The interpretation of this update is straight-forward since the initial state of the physical quantities (i.e. displacements, velocities, accelerations) in the new configuration is well defined by the previous state. If yielding is stopped, rigid couplings are enforced by eliminating one set of interface DOFs. The velocities for the constrained DOFs are by definition equal when unloading is detected and it is thus straight-forward to eliminate one set of DOFs. The initial acceleration in the updated system is computed as

$$\ddot{\mathbf{u}}_c{}^{(i)} = \left(\mathbf{L}_c^{\mathrm{T}}\widehat{\mathbf{M}}\mathbf{L}_c\right)^{-1}\mathbf{L}_c^{\mathrm{T}}\left(\hat{\mathbf{p}}^{(i)} - \widehat{\mathbf{B}}_y^{\mathrm{T}}\mathbf{f}_y - \widehat{\mathbf{C}}\dot{\mathbf{u}}_r{}^{(i)} - \widehat{\mathbf{K}}\mathbf{u}_r{}^{(i)}\right) \tag{36}$$

Note that the time increment between system updates, $\Delta t^{(i)} = t^{(i)} - t^{(i-1)}$, is zero. Hence, the velocities and deformations are equal in increment i and $i - 1$. However, the accelerations are changed at the system updates in accordance with Equation (36). Even though an instantaneous change of the accelerations might seem unreasonable, this is a consequence of the unphysical assumption of a perfectly rigid connection, which however can be a very useful approximation; in particular when modeling plastic hinges in beam–column structures. Furthermore, it should be noted that both the strain and kinetic energy is preserved.

4.2 Remarks on performance and accuracy

In contrast to a conventional implicit direct time integration, the proposed time-stepping scheme, as presented above, is a non-iterative procedure. However, in general an adjustment of the last increment size before a system update is needed to ensure that the system is updated just before yielding start or stop. This adjustment can be set up in an iterative fashion.

If the system consists of reduced substructures the critical time increment, in a conditionally stable time integration scheme, can be expected to be reasonably large since the high frequency content has been removed in the reduction process on the substructure level. The time increment size prescribed in the analysis is then instead governed by the precision of the requested time-histories. Consequently, the Newmark parameters can be optimized to increase the analysis accuracy (or performance) rather than to ensure stability. For example, setting the parameters to $\beta = 1/12$ and $\gamma = 1/2$ ensures forth-order accuracy and $\beta = 0$ and $\gamma = 1/2$ enables the explicit central difference scheme [19]. Furthermore, if the system at hand is relatively small and if the number of system updates can be assumed rather limited, the critical time increment can be updated based on an eigenvalue analysis of the updated system. However, an alternative is to prescribe a conservative time increment and thereby skip this check.

5 NUMERICAL EXAMPLE: CONCRETE FRAME SUBJECTED TO BLAST LOADING

A concrete frame structure subjected to blast loading is studied to demonstrate the discussed substructuring and time-stepping method. The dynamic response is computed using a simplified two-dimensional model, suitable in a conceptual design phase. Various strategies to reduce the model by use of DS are investigated, both in terms of accuracy and computationally efficiency (i.e. number of DOFs). Focus is primarily on evaluating DS techniques applied to the lateral load-bearing structure that is not subjected to external loading, i.e. the supporting structure consisting of the horizontal beam and the right column, as shown in Figure 2a. The dynamic response is computed using the time-stepping scheme proposed in Section 4. Furthermore, the highest eigenfrequency, which is related to the critical increment size in conditionally stable time-integration schemes, is evaluated for the reduced models.

The concrete frame is subjected to a uniformly distributed reflected impulse pressure of 1500 Pa·s, as shown in Figure 2a. The pulse is approximated by an equivalent triangular pulse with a fictitious duration of 10 ms and a peak reflected pressure of 300 kPa at $t = 0$ s. The length of the frame members is 3 m and the cross-section width and height, for the columns as well as the horizontal beam, are 1000 mm and 200 mm, respectively. Young's modulus for concrete is set to 32 GPa and the density for reinforced concrete is set to 2500 kg/m^3. The ultimate moment capacity for the columns and the horizontal beam is set to 60 kNm.

5.1 Frame structure model reduced by dynamic substructuring

The frame structure is analyzed with a two-dimensional beam model. The positions of possible plastic hinges are predefined and approximated as five discrete rigid–perfectly plastic joints, as shown in Figure 2b. Yielding of the frame corners are approximated by one distinct plastic hinge, i.e. Joints 3 and 4, respectively. However, it should be noted that a more accurate approximation can be achieved by modeling the corners as separate substructures. Moreover, several effects are neglected in the analysis, e.g. catenary effects, reduced stiffness due to concrete cracking etc. Nevertheless, the model is suitable for studying different DS techniques and to evaluate the efficiency of the proposed time-stepping method.

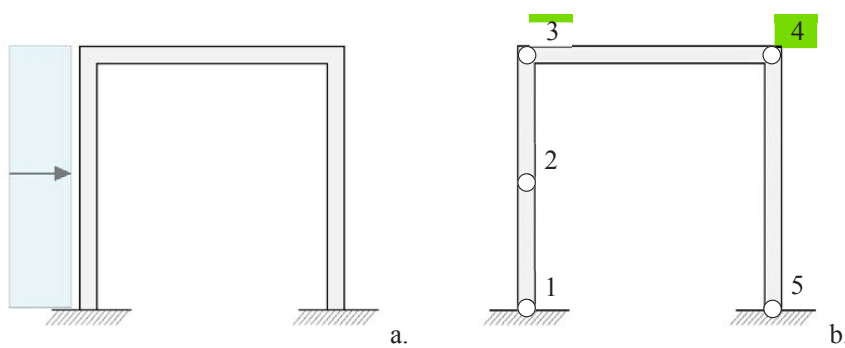

Figure 2: Concrete frame structure subjected to blast loading (a) and locations and labeling of plastic hinges (b).

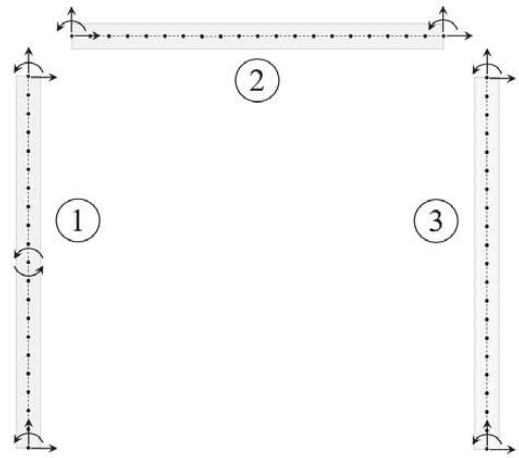

Figure 3: Boundary DOFs and numbering of substructures.

The structure is divided into three substructures, as shown in Figure 3. Each substructure is modeled by 20 Euler–Bernoulli two-node beam elements. Six interface DOFs are retained for Substructures 2 and 3, namely the translational and rotational DOFs at the beam ends. By selecting these boundary DOFs, the fixed-interface normal modes will be the exact mode-shapes of a fixed–fixed beam. Further, eight boundary DOFs are retained for Substructure 1, namely the translational and rotational DOFs at the top and bottom and the rotational DOFs at the joint positioned at midspan. By selecting these boundary DOFs the fixed-interface normal modes will include the exact symmetric modes for a fixed–fixed beam, whereas the antisymmetric modes will be affected by the constrained rotational DOFs at midspan. The fixed-interface normal modes and the constraint modes included in the reduction basis for Substructure 1 is shown in Figures 4 and 5. Note that the antisymmetric modes for a fixed–fixed beam are not excited by a uniformly distributed load. However, since Substructure 1 is not fully supported at the top, some antisymmetric normal modes (modes 2, 5 and 8) are included in the reduction basis.

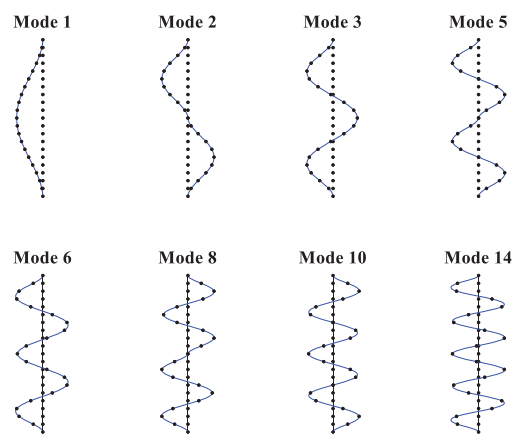

Figure 4: Substructure 1 – fixed-interface normal modes.

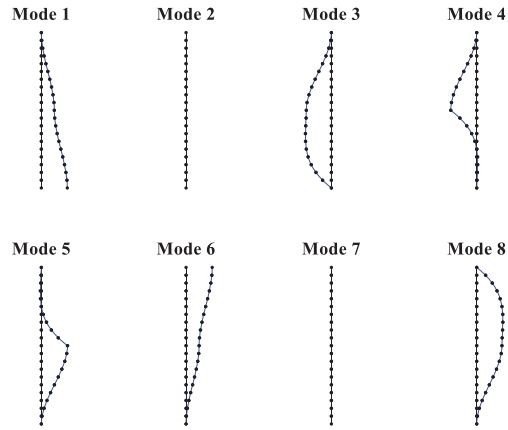

Figure 5: Substructure 1 – constraint modes.

During a dynamic response analysis, the predefined plastic hinges can be either fixed or free, i.e. non-yielding or yielding. A total of five predefined plastic hinges are included in the model, which implies that a response analysis can include up to ten different system configurations. However, to get a rough estimate of the reduced model accuracy two configurations are evaluated—where all joints are either fixed or free, respectively.

The eigenfrequencies for the assembled reduced systems are evaluated by computing the so-called normalized relative frequency difference (NRFD), given by $\text{NRFD} = \left|f_i^{red} - f_i^{full}\right| / f_i^{full}$, that relate the eigenfrequencies of the reduced system to those of the full system. As previously described, the reduction basis for Substructure 1 includes the fixed-interface normal modes and constraint modes shown in Figures 4 and 5, respectively. Five different reduction bases for Substructures 2 and 3 are evaluated. Using a standard C-B approach, reduction is performed including two or four fixed-interface normal modes. Furthermore, reduction bases including two or four correction modes, as described in Section 3.2, are evaluated. The correction modes are generated based on the constraint modes associated to the rotational boundary DOFs at the beam ends. Hence, two modes are generated by computing a set of first-order correction modes and two additional modes are generated by computing a set of second-order correction modes. In addition, the accuracy of a reduction basis including both four fixed-interface normal modes and two first-order correction modes is evaluated. The analyzed models are summarized in Table 1.

Model name	Normal modes	Correction modes[1]	No of DOFs[2]
Mode 1-2	1, 2	-	19
Cor. 1st	-	2 × 1st	19
Mode 1-4	1, 2, 3, 4	-	23
Cor. 1st, 2nd	-	2 × 1st + 2 × 2nd	23
Mode 1-4, Cor.1st	1, 2, 3, 4	2 × 1st	27
Full model	-	-	177

[1] Correction modes associated to rotational boundary DOFs.
[2] Total number of DOFs for model with fixed joints.

Table 1: Normal modes and correction modes for Substructures 2 and 3.

The computed NRFD values are shown in Figures 6 and 7. As shown in the figures, at least, the first seven free and fixed global modes, respectively, are well-described by all the evaluated reduced models; measured as NRFD < 1 %. However, to increase the precision for higher order modes, the constraint modes in Substructures 2 and 3 need to be complemented by at least four modes. However, increasing the number of fixed-interface normal modes and/or correction modes in the reduction basis result in additional generalized DOFs in the reduced system, hence, increasing the computational cost. Moreover, the accuracy when using correction modes and normal modes are comparably, as long as the same number of modes are included in the reduction basis.

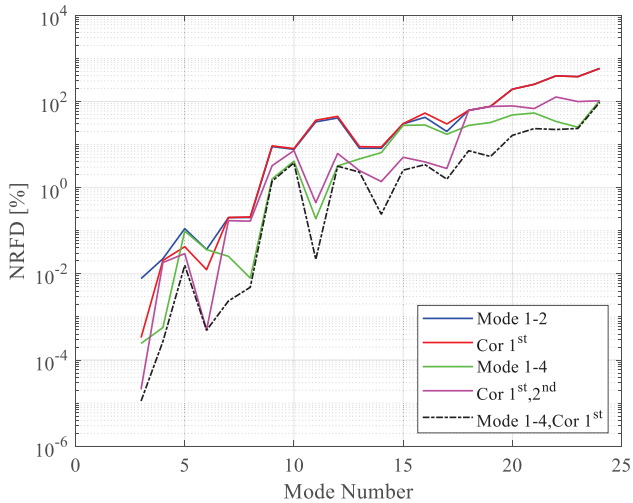

Figure 6: NRFD values for systems with unconstrained rotations at joints.

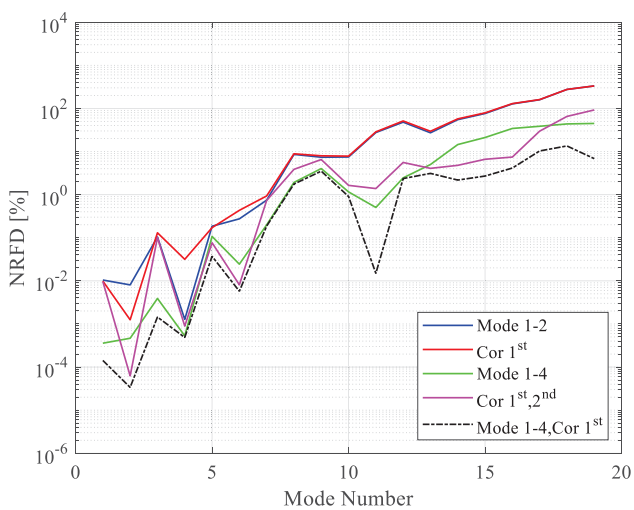

Figure 7: NRFD values for systems with constrained rotations at joints.

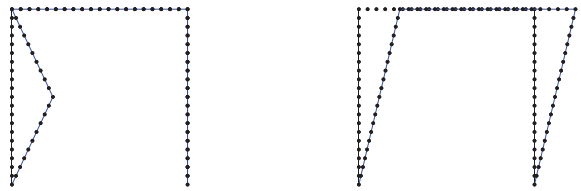

Figure 8: Failure modes spanned by rigid body modes.

Note that the NRFD value is not computed for the first two eigenmodes for the systems with free rotations at the joints. This is due to that the first two modes are rigid body modes with zero frequency. By properly scaling of the rigid body modes, the failure modes, shown in Figure 8, are obtained.

5.2 Dynamic response analysis and results

The dynamic response is computed for the reduced system where the reduction basis for Substructures 2 and 3 includes four normal modes and two first order correction modes. Again, the reduction basis for Substructure 1 includes the normal modes and constraint modes shown in Figures 4 and 5, respectively. The reduced model has a total of 27 DOFs in the initial stage, i.e. when the plastic hinges are fixed, whereas the full model has a total of 177 DOFs. The response is computed using the time-stepping scheme presented in Section 4. Direct time-integration is performed using the Newmark method, with parameters $\beta = 1/12$ and $\gamma = 1/2$ that result in a conditionally stable integration scheme with forth order accuracy [19]. The critical time increment is computed as $dt_{crit} = 2.45/\omega_{max}$. The analysis is performed with a time increment $dt = dt_{crit}/10$ and the analysis time is set to 150 ms.

Snapshots of the deformed shape during the first 50 ms is shown in Figure 9. As shown in the figure, the response of the left column during the first, approximately, 10 ms is similar to that of a fully supported fixed–fixed column due to the inertia of the supporting horizontal beam.

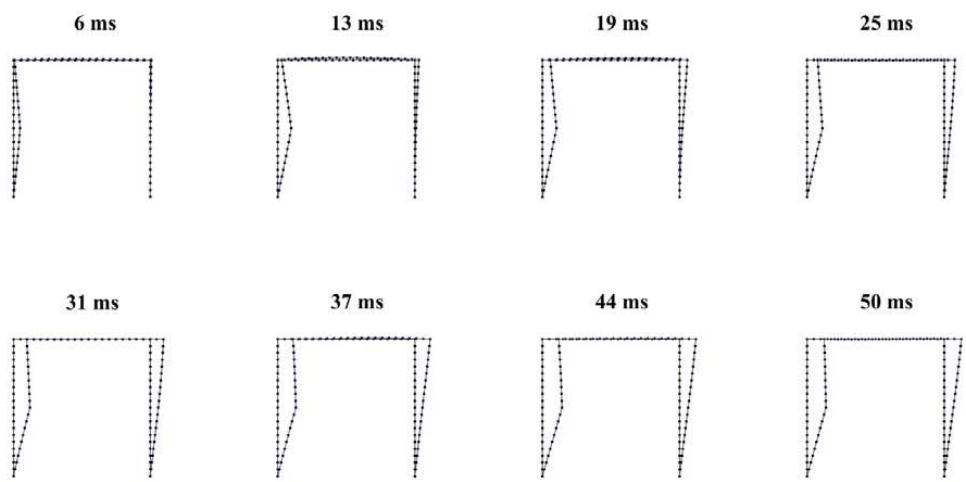

Figure 9: Snapshots of the deformed shape during the first 50 ms. The deformation is scaled by a factor of 15.

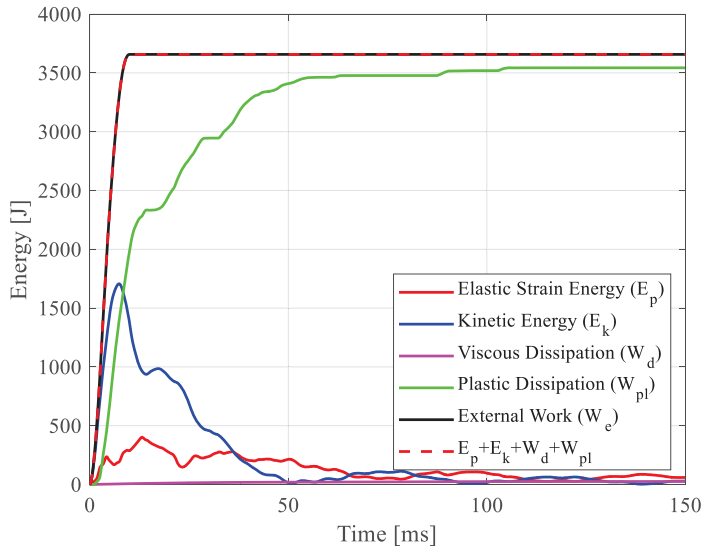

Figure 10: Elastic strain and kinetic energy, plastic and viscous dissipation and external work for the reduced system.

As shown in Figure 10, the energy induced by the external impulse pressure is mainly dissipated by plastic deformations, i.e. by rotation of the predefined plastic hinges. A low Rayleigh beta damping is included in the analysis by setting $\mathbf{C} = 10^{-5} \cdot \mathbf{K}$. As shown in the figure, the viscous dissipation is almost zero.

The relative rotation of the plastic hinges is shown in Figure 11. As shown, most of the plastic dissipation is due to plastic rotation in Joints 1 and 2. The rotation computed with the full model is shown in light gray color. As shown in the figure, the response is almost identical to that of the reduced model. Note that the relative rotation of the plastic hinges is an important parameter in a design calculation, which should not exceed the rotation capacity of the cross-section.

The horizontal displacement at Joints 2 and 4 is shown in Figure 12. The displacement is very close to the displacement computed with the full model. The fundamental eigenfrequency for the non-yielding frame structure is 11.7 Hz, corresponding to a period of 1/11.7 = 85 ms. Clearly, the displacement after approximately 50 ms can essentially be described by the fundamental mode and a plastic displacement.

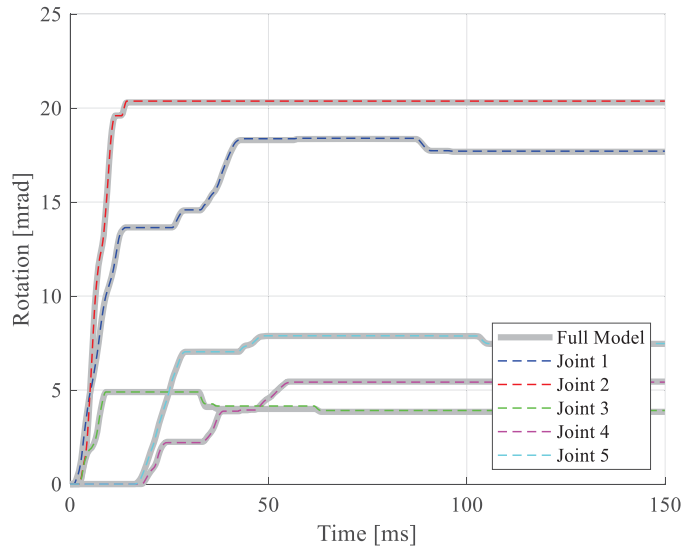

Figure 11: Relative rotations at Joints 1–5, positioned according to Figure 2b.

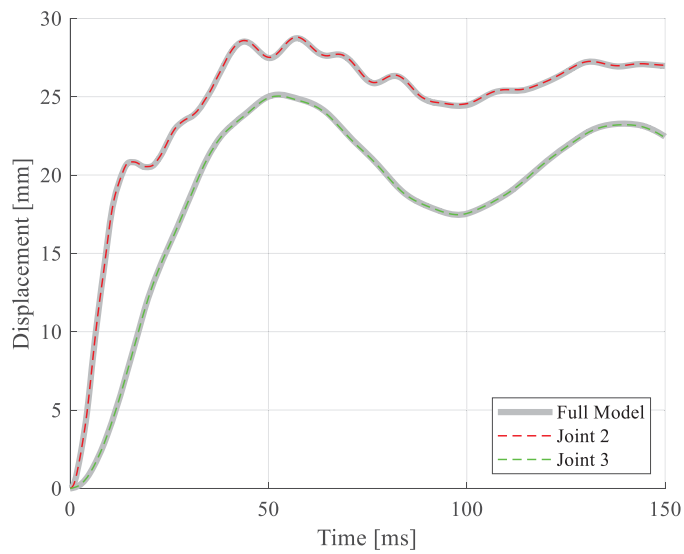

Figure 12: Horizontal displacements at Joints 2 and 3, positioned according to Figure 2b.

If a suitable reduction basis is applied to Substructure 1, to properly describe the application of the external pressure, the global displacements can be well-described by only including two fixed-interface normal modes (or correction modes) for Substructures 2 and 3, as indicated by Figures 11 and 12. However, a more refined reduction basis is needed to properly describe the reaction and interface forces between the substructures. The influence of the reduction basis on the horizontal interface force in Joint 4 is shown in Figure 13. As shown, the constraint modes need to be complemented by at least four modes to obtain a reasonable accurate response. The

accuracy for the models reduced by using fixed-interface normal modes and correction modes, respectively, are comparable. Hence, the correction modes are then the preferred choice since the generation of these modes are less computationally expensive (in this simple example, however, the computational cost of generating either normal modes or corrections modes is negligible).

The critical time increment in a conditionally stable direct time integration method is inversely proportional to the highest eigenfrequency. Consequently, a reduction of a system that removes the high frequency content can result in a more computationally efficient analysis. To get an estimation of how much the eigenfrequency is affected by the reduction bases studied herein, the highest eigenfrequency is computed for the initial state of the reduced systems, i.e. when all joints are fixed.

The highest eigenfrequency of the reduced models including two and four fixed-interface normal modes in the reduction bases for Substructure 2 and 3 is 4.2 kHz and 4.3 kHz, respectively. The highest eigenfrequency when using two and four correction modes is 4.2 kHz and 4.4 kHz, i.e. almost equal to the eigenfrequencies obtained when using normal modes. However, the highest eigenfrequency in the reduced models is in this case most likely governed by Substructure 1, reduced by a more refined reduction basis.

For the reduced model including four fixed-interface normal modes and two first-order correction modes the highest eigenfrequency is 4.7 kHz. In comparison, the highest eigenfrequency of the full model is 74.5 kHz, i.e. a factor of 74.5/4.7 ≈ 16. Furthermore, the highest eigenfrequency for a reduced system where the rigid–perfectly plastic joints are modeled using penalty elements, with a stiffness 10 times the mean stiffness of the corresponding entries in the unreduced stiffness matrix, is 64.4 kHz. Hence, for the model studied herein, the number of time increments can be decreased by a factor 64.4/4.7 ≈ 14 by avoiding penalty elements.

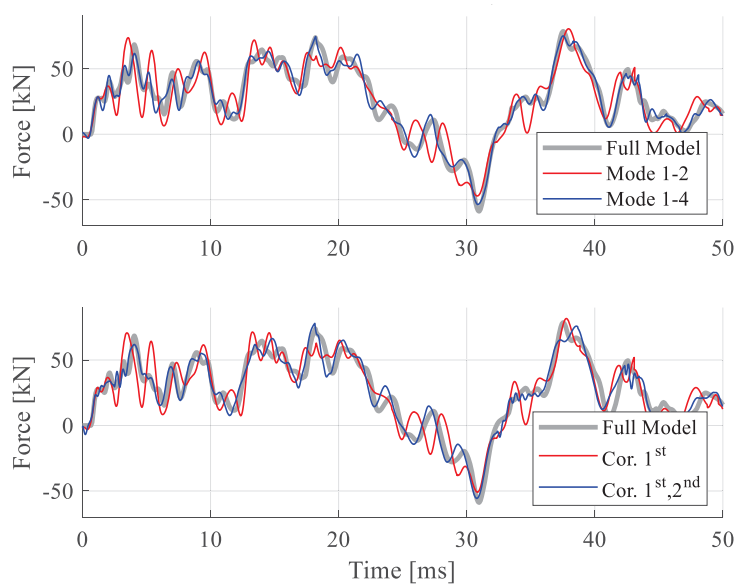

Figure 13: Horizontal interface force at Joint 4.

6 CONCLUSIONS

In the study, strategies are developed to enable time-efficient models for concrete frame structures subjected to blast loading, appropriate for use in a structural design process. Dynamic substructuring is employed to obtain reduced models with localized nonlinearities, such as predefined plastic hinges in a beam–column structure. The parts of the substructures that remains linear elastic are modeled by Ritz-vectors whereas parts with a nonlinear response are retained as physical degrees-of-freedom. Furthermore, a time-stepping scheme is presented that is shown to be suitable for reduced models including local and predefined rigid-plastic behavior.

The proposed methodology is applied and demonstrated in a numerical example of a concrete frame structure. The standard Craig-Bampton method that uses fixed-interface normal modes and constraint modes is evaluated. Furthermore, reduction bases augmented by so-called correction modes are investigated. Various reduction bases are evaluated for the substructures included in the supporting structure, i.e. the substructures that are not subjected to external loading. Two correction modes or two standard fixed-interface normal modes are sufficient to describe the displacement and relative rotations at the plastic hinges. However, to obtain an acceptable accuracy of the interface forces between the substructures, at least four correction modes or four standard fixed-interface modes are needed. For the studied load case, the accuracy when using correction modes and fixed-interface normal modes are comparable.

Moreover, the highest eigenfrequency for the reduced systems, which is related to the critical increment size in conditionally stable direct time integration methods, is evaluated. It is shown that a reduction of the studied model by use of dynamic substructuring can increase the critical time increment by a factor of approximately 16. Furthermore, it is shown that by enforcing a rigid–plastic behavior using the proposed time-stepping scheme, the critical increment size can increase by a factor of approximately 14 compared to a modeling approach where the rigid–plastic behavior is enforced using penalty elements.

The present methodology can be extended further to, for example, consider large deformations and failure, e.g. by considering the rotation capacity of the cross-sections. Furthermore, the methods can be applied and evaluated for larger and more complex structures, e.g. three-dimensional beam–column structures. Also, a more refined modeling approach for frame corners can be investigated, where the corner itself is treated as a separate substructure.

REFERENCES

[1] J.M. Biggs, *Introduction to Structural Dynamics*. McGraw-Hill, New York, 1964.

[2] L. Andersson, P. Persson, P. Austrell, K. Persson, Reduced order modeling for the dynamic analysis of structures with nonlinear interfaces. *Proceedings of the 7th ECCOMAS Thematic Conference on Computational Methods in Structural Dynamics and Earthquake Engineering (COMPDYN 2019)*, Crete, Greece, 24–26 June, 2019.

[3] D. de Klerk, D.J. Rixen, S.N. Voormeeren, General Framework for Dynamic Substructuring: History, Review, and Classification of Techniques, *AIAA Journal*, **46 (5)**, 1169–1181, 2008.

[4] O. Flodén, K. Persson, G. Sandberg, Reduction methods for the dynamic analysis of substructure models of lightweight building structures, *Computers and Structures*, **138**, 49–61, 2014.

[5] Unified Facilities Criteria (UFC), *Structures to Resist the Effects of Accidental Explosions*, U. S. Army Corps of Engineers, Naval Facilities Engineering Command, Air Force Civil Engineer Support Agency, UFC 3-340-02, December 5 2008.

[6] R.J. Guyan, Reduction of Stiffness and Mass Matrices, *AIAA Journal*, **3 (2)**, 380, 1965.

[7] J. O'Callahan, P. Avitabile, R. Riemer, System Equivalent Reduction Expansion Process (SEREP), *Proceedings of the 7th International Modal Analysis Conference*, Las Vegas, Nevada, 1989.

[8] R.R. Craig, M.C.C. Bampton, Coupling of Substructures for Dynamic Analysis, *AIAA Journal*, **6 (7)**, 1313–1319, 1968.

[9] R.H. MacNeal, A Hybrid Method of Component Mode Synthesis, *Computers and Structures*, **1 (4)**, 581–601, 1971.

[10] S. Rubin, Improved Component-Mode Representation for Structural Dynamic Analysis, *AIAA Journal*, **13 (8)**, 995–1006, 1975.

[11] R.R. Craig, C.J. Chang, On the Use of Attachment Modes in Substructure Coupling for Dynamic Analysis. *Proceedings of the 18th Structures, Structural Dynamics and Material Conference*, San Diego, CA, 1977.

[12] D.J. Rixen, A dual Craig–Bampton method for dynamic substructuring, *Journal of Computational and Applied Mathematics*, **168(1–2)**, 383–391, 2004.

[13] F.M. Gruber, M. Gille, D.J. Rixen, Time integration of dual Craig-Bampton reduced systems. *Proceedings of the 6th ECCOMAS Thematic Conference on Computational Methods in Structural Dynamics and Earthquake Engineering (COMPDYN 2017)*, Rhodes Island, Greece, 15–17 June, 2017.

[14] R. Craig, A. Hale, Block-Krylov Component Synthesis Method for Structural Model Reduction. *Journal of Guidance, Control and dynamics, American Institute of Aeronautics and Astronautics*, **11(6)**, 562–570, 1988.

[15] D.J. Rixen, High Order Static Correction Modes for Component Mode Synthesis. *Proceedings of the fifth World Congress on Computational Mechanics*, Vienna, Austria, 7–12 July, 2002.

[16] R.R. Jr. Craig, A.J. Kurdila, *Fundamentals of Structural Dynamics, 2nd Edition*, John Wiley & Sons, New Jersey, 2006.

[17] K. J. Bathe, *Finite element procedures*. Prentice-Hall, 1996.

[18] C. Farhat, L. Crivelli, M. Géradin, Implicit time integration of a class of constrained hybrid formulations—Part I: Spectral stability theory, *Computer Methods in Applied Mechanics and Engineering*, **125 (1–4)**, 71–107, 1995.

[19] M. Geradin, D.J. Rixen, *Mechanical Vibrations: Theory and Applications to Structural Dynamics, Third Edition*. Wiley, New York, 2014.

Paper C

Engineering Structures 256 (2022) 113988

Contents lists available at ScienceDirect

Engineering Structures

journal homepage: www.elsevier.com/locate/engstruct

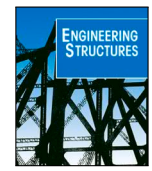

Reduced order modeling of soft-body impact on glass panels

Linus Andersson [a,*], Marcin Kozłowski [b], Peter Persson [a], Per-Erik Austrell [a], Kent Persson [a]

[a] Department of Construction Sciences, Lund University, Sweden
[b] Department of Structural Engineering, Silesian University of Technology, Poland

ARTICLE INFO

Keywords:
Reduced order model
Dynamic substructuring
Soft-body impact
Structural glass
Impact testing
Damping
Finite element analysis

ABSTRACT

In the paper, strategies for reduced order modeling of glass panels subjected to soft-body impact are developed by means of dynamic substructuring. The aim is to obtain accurate and computationally efficient models for prediction of the pre-failure elastic response. More specifically, a reduction basis for the subsystem representing the glass panel is established using correction modes, being fixed-interface component modes that considers loading on the substructure boundary. The soft-body impactor is effectively modeled by a nonlinear single-degree-of-freedom system, calibrated by experimental data. Furthermore, a simplified and computationally efficient modeling approach is proposed for the contact interaction between the glass panel and the impact body. An experimental campaign was carried out to validate the developed models. In particular, the glass strain was measured on simply supported monolithic glass panels subjected to soft-body impact. Additional impact tests were performed to determine the dynamic characteristics of the impactor. Moreover, a detailed numerical reference model was developed to evaluate the discrepancy between the experimental tests and the results provided by the reduced order models. The developed models show good agreement with the experimental results. For the studied load cases, it is shown that an accurate prediction of the pre-failure glass strain can be obtained by systems including only a few generalized degrees-of-freedom.

1. Introduction

During the last few decades, glass has become an increasingly common building material in modern architecture. Glass is not only used for building enclosures and translucent facades allowing sunlight into the building, but also in load-bearing structures and glazed barriers, such as full-height façades and parapets for balconies or interior level changes.

If the glass barrier constitutes a safety risk for building occupants, building regulations in most countries prescribes that the glazing must be designed to withstand accidental impact of humans. A dynamic verification is then required, usually performed by experimental testing using the standardized soft-body pendulum for glass classification according to the European Standard EN 12600 [1]. The test arrangement used for glass classification, shown in Fig. 1, consists of a glass panel fixed in a steel frame and a soft impact body on a pendulum, representing a human body falling towards the glass panel. Hence, a soft-body impact is considered, where the impact body is deformed under impact and thus redistribute the impact load.

Impact tests can be very costly, especially for large and complex glass structures. Furthermore, it can be difficult to set-up a test arrangement that accurately capture the structural behavior of the underlying load-bearing structure. Moreover, a structural verification using tests applied to the real structure can be both costly and requires a redesign of the existing structure if the load-bearing capacity turns out to be inadequate. Therefore, it can be preferable to instead perform the verification by means of dynamic calculation methods. Beside a reduced cost and the possibility to easily evaluate different design concepts, numerical analyzes enable an increased insight into the structural behavior and additional control of e.g. structural and material parameters. In a physical impact test, however, the material parameters can vary depending on the specific glass specimen, why several tests are needed to adequately account for statistical variations. The validity of using numerical simulations for strength evaluation of glass structures have been shown by several researchers, see e.g. [2–5].

Static load cases are often verified by means of a commercial finite element (FE) software. For this purpose, a specialized FE tool *ClearSight* [6] has been developed at the Department of Construction Science, Lund University, being streamlined for an interactive and efficient verification of glass panels subjected to static load cases. However, using an FE analysis to calculate the dynamic response due to impact can be time-consuming and computationally expensive. In general, a nonlinear transient response analysis is required, and the FE model should include the glass panel and its fixings, the impactor, and

* Corresponding author.
E-mail address: linus.andersson@construction.lth.se (L. Andersson).

https://doi.org/10.1016/j.engstruct.2022.113988
Received 16 April 2021; Received in revised form 30 January 2022; Accepted 4 February 2022
Available online 24 February 2022

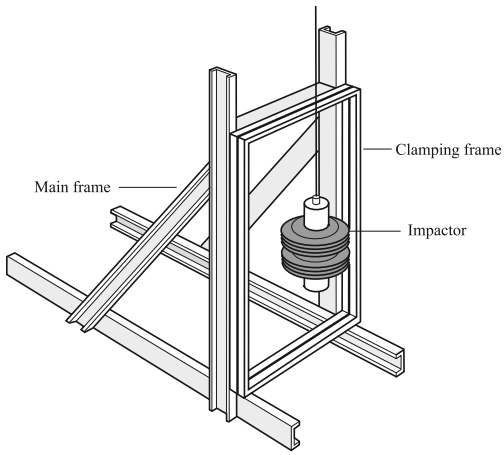

Fig. 1. Test frame with impactor according to the European Standard EN 12600 [1].

a suitable description of the contact interaction between the impactor and the glass structure. To set up and perform such an analysis can be time-consuming and often requires a relatively advanced FE software and extensive user knowledge.

To enable a more time-efficient and straightforward approach for evaluating dynamic load cases, reduced modeling techniques specialized for glass panels subjected to impact loading have been proposed by several researchers, see e.g. [7–14]. For instance, in [7], reduction bases were successfully constructed using predefined load patterns, employed for reduced modeling of glass panels in a Rayleigh–Ritz fashion. In [8], various reduced models of unsupported glass panels subjected to low-velocity impact were investigated. For example, a three degree-of-freedom (DOF) spring–mass model was proposed, constructed by calibrating the system matrices to the strain energies and eigenfrequencies of the fundamental flexural modes of a glass panel in free–free conditions. Thus, the mode shapes are used implicitly for identifying eigenfrequencies and energies, which are then employed in a second stage for calibrating the lumped-mass systems. Furthermore, a lumped mass model based on Hertz contact law (see e.g. [15]) was proposed for modeling the impactor. However, the low-velocity impacts studied in [8] were generated using a specialized spherical impactor, particularly suitable for approximation using Hertz law. Further, the reduced models were successfully validated by experimental studies, suggesting that the importance of higher order modes increases for larger glass panels and a stiffer impactor. In [10], a nonlinear SDOF model was proposed for modeling the impactor with a spring force expressed in terms of a quadratic polynomial. Further, the contact between the impactor tires and the glass panel was modeled by assuming a uniform contact stress applied on a contact area having a predefined elliptical shape, with a variable size governed by the impactor spring displacement. This impactor model has also been implemented in the commercial finite element package SJ Mepla [16], where it is typically assembled with a glass structure represented by shell elements considering large deflection theory. A reduction on the glass substructure level is, however, not possible. In [11], a simplified engineering model based on equivalent static loads is presented, which enables a very quick and straightforward verification of impact loading. However, because the response of higher order modes is neglected, it is only applicable for two- and four-sided rectangular, continuously supported glass panels within a limited range of dimensions.

In the present paper, strategies for reduced order modeling of soft-body impact on glass panels are developed by means of dynamic substructuring (DS). The aim is to achieve an accurate prediction of the pre-failure elastic response while significantly reducing the computational cost. More specifically, a reduction basis for the subsystem representing the glass panel is established using correction modes, being fixed-interface component modes that considers loading on the substructure boundary [17,18]. Because information related to the loading pattern is considered in the derivation, all the generated correction modes will, by definition, be excited by the applied load. In contrast, a reduced basis established using eigenmodes may include redundant modes, e.g. anti-symmetric modes that cannot be excited by a centric impact. The soft impact body is effectively modeled by a nonlinear viscous single-degree-of-freedom (SDOF) system, calibrated by experimental data. Furthermore, a simplified and computationally efficient modeling approach, assuming a constant contact area, is employed for modeling the contact interaction between the glass panel and the impact body. The developed reduced order models are intended for analyzing glass panels with various support configurations. However, because a linear response is assumed for the glass substructure, second order effects (e.g. due to membrane action) is not considered. Thus, the proposed models are suitable for analyzing glass panels where the response is mildly influenced by second order effects or where an assumed linear response of the glass structure yields a reasonably conservative design.

An experimental campaign was carried out to validate the developed models. In particular, the glass strain was measured on simply supported monolithic glass panels subjected to impact loading. The test arrangement was similar to the standardized impact test for glass classification described in EN 12600 [1]—the glass panels were mounted in a steel frame and impact loads were generated by releasing the standardized EN 12600 impactor from various drop heights. Additional impact tests on a very stiff steel column (which was considered rigid) were also performed to determine the dynamic characteristics of the impactor. The test arrangement and the standardized impactor employed in the experimental campaign are shown in Fig. 2.

To evaluate the differences between the measured glass strain and the strain provided by the reduced models, a detailed FE model, herein referred to as the reference model, was established using the commercial FE software Abaqus [19]. The reference model includes a penalty contact formulation to consider the interaction between the impactor and the glass panel, geometric nonlinearity, hyperelastic constitutive models for rubber, and a sophisticated modeling of the tire air pressure, aiming to mimic the impact tests. Evaluating the deviation between the response computed with the reduced models, the reference model and the experimental tests makes it possible to distinguish between errors related to modeling abstractions and simplifications employed in the reduced models and other, unknown error-sources.

To summarize, the aim of the paper is to:

- develop accurate reduced order models for computation of the pre-failure glass strain, suitable for implementation in user-friendly design tools,
- validate the developed models by experimental data,
- set up a detailed numerical reference model to get further insight into the structural behavior and to evaluate the discrepancy between measurements and the response computed with the reduced order models.

The paper is structured as follows. In Section 2, reduced modeling concepts for simulating soft-body impact are presented, including techniques for reduced modeling of the impactor, the glass panel, and the contact interaction. In Section 3, a detailed FE model of the standardized impactor is presented, herein referred to as the reference model, being used for calibration as well as validation of the reduced models. Experimental tests are presented and discussed in Section 4—both experiments involving testing of glass panels subjected to soft-body impact as well as tests to characterize the dynamic properties of the impactor. In Section 5, calibrations of the impactor models as well as

(a) (b)

Fig. 2. Experimental set-up for glass impact tests (a) and impactor (b).

a validation of the assembled reduced models are presented, both by comparison to experimental results and the response computed with the numerical reference model. Finally, the results are discussed in Section 6 and conclusions are presented in Section 7.

2. Reduced order models for analysis of soft-body impact on glass panels

Upon impact, contact is established between the glass panel and the impactor. Hence, a coupled system is formed consisting of the glass structure and the impacting body. Glass is a brittle material that is essentially linear elastic before failure [20]. Hence, if neglecting geometric nonlinearity, the pre-failure structural response of monolithic glass panels can be accurately represented by a linear model. It should be noted, however, that in some applications the influence of second order effects can be of considerable importance. For such cases, a nonlinear model representing the glass substructure is required for an accurate prediction of the glass strain. For example, the investigation presented in [7] shows that the influence of second order effects (i.e. membrane action) are significant for four-sided, continuously supported glass panels. Moreover, the investigations suggest that the glass strain is overestimated if second order effects are neglected. A linear representation of the glass panel can thus be suitable if the response is only mildly influenced by second order effects or, arguably, in applications where an assumed linear response yields a reasonably conservative design. However, a nonlinear model may still be required to properly describe the contact interaction between the soft impact body and the glass panel, as well as the nonlinear behavior of the pneumatic tires. For such models, the coupled system can be reduced by means of DS, allowing for a reduction of the linear glass substructure while retaining the physical DOFs interacting with the soft impact body.

Several DS methods have been developed since the late 1960s, extensive reviews can be found in [21–23]. We base our approach on the Craig–Bampton (C-B) method [24], which preserves the physical boundary DOFs of the substructures. However, instead of using the fixed-interface normal modes, employed in the standard C-B method, a reduction basis for the glass substructure is established using correction modes that considers loading on the substructure boundary, see further Section 2.1. Furthermore, the impactor is effectively modeled as a nonlinear single-degree-of-freedom (SDOF) system, see Section 2.2.

The subdivision of the coupled glass–impactor system into substructures is illustrated in Fig. 3. Interface reduction is applied, as further discussed in Section 2.3, such that only one virtual boundary DOF is retained for the glass substructure, corresponding to a weighted

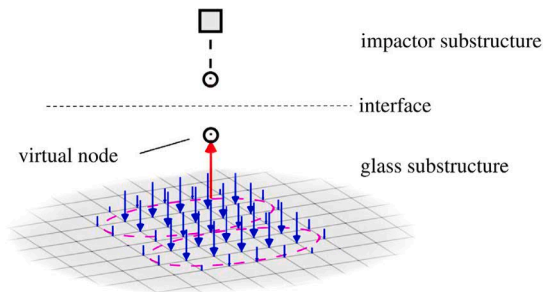

Fig. 3. Subdivision of the coupled glass–impactor system into substructures. As further described in Section 2.3, the blue arrows represent the contact forces acting on the glass panel top surface, corresponding to a uniform contact pressure applied on the regions with elliptical shapes, marked with purple dashed lines. The red arrow represent the total contact force acting on a virtual node. (For interpretation of the references to color in this figure legend, the reader is referred to the web version of this article.)

mean vertical displacement of a group of nodes considered to be in contact with the impactor tires (see Fig. 3). The reduced substructures are assembled in a standard manner to form a reduced model of the coupled system. Strategies for computing the dynamic response of the assembled system is further discussed in Section 2.4.

2.1. Reduced order modeling of glass panels

A reduction of a system including local nonlinearities, such as the coupled glass–impactor system, necessitates a DS technique that preserves the physical boundary DOFs. For example, the standard C-B method [24] or the MacNeal/Rubin approaches [25,26], which uses the fixed- and free-interface normal modes, respectively, are suitable methods. The preferred method can be due to both accuracy and computational efficiency, which in turn considers both the computational cost of establishing the reduction basis and the number of variables required in the final system.

In the present study, a DS method that uses fixed-interface correction modes is employed for reducing the glass panel, an approach first proposed in [17] and later extended in [18] to enable a mixed usage of normal modes and correction modes (this method was also employed in [27] for establishing reduced models of concrete frame structures, where plastic joints were treated as local nonlinearities). For

the glass–impactor system, this type of reduction basis turns out to be favorable both regarding the system size and the computational cost related to the computation of the reduction basis vectors. As shown in the derivation below, the correction modes are generated by a sequence of matrix–vector multiplications, whereas the fixed- or free-interface normal modes are computed by solving an eigenvalue problem. Furthermore, information related to loading on the substructure boundary DOFs is considered in the derivation of the correction modes and, consequently, redundant modes that cannot be excited by loads applied on the substructure boundary are automatically excluded. Reduction bases including correction modes, also referred to as block-Krylov subspaces, can be derived in several ways. Following Rixen in [18], but excluding the fixed-interface normal modes in the reduction basis, the derivation is as follows.

Neglecting damping, the equation of motion for the glass substructure in partitioned form can be written as:

$$\begin{bmatrix}\mathbf{M}_{ii} & \mathbf{M}_{ib}\\ \mathbf{M}_{bi} & \mathbf{M}_{bb}\end{bmatrix}\begin{bmatrix}\ddot{\mathbf{u}}_i\\ \ddot{\mathbf{u}}_b\end{bmatrix}+\begin{bmatrix}\mathbf{K}_{ii} & \mathbf{K}_{ib}\\ \mathbf{K}_{bi} & \mathbf{K}_{bb}\end{bmatrix}\begin{bmatrix}\mathbf{u}_i\\ \mathbf{u}_b\end{bmatrix}=\begin{bmatrix}\mathbf{p}_i\\ \mathbf{p}_b\end{bmatrix} \tag{1}$$

where the subscripts i and b denotes the interior and interface boundary DOFs, respectively (the number of interior and boundary DOFs is henceforth denoted n_i and n_b, respectively, and the total number of DOFs is thus $n = n_i + n_b$). Notice that, in this case, the virtual DOF interacting with the impactor model is selected as the interface DOF (cf. Fig. 3). Furthermore, if the external forces on the interior DOFs are zero, the top row of Eq. (1) can be rewritten as:

$$\mathbf{M}_{ii}\ddot{\mathbf{u}}_i+\mathbf{K}_{ii}\mathbf{u}_i=-\mathbf{M}_{ib}\ddot{\mathbf{u}}_b-\mathbf{K}_{ib}\mathbf{u}_b. \tag{2}$$

Hence, the substructure can be considered excited by imposed displacements on its boundary. Further, the internal displacements can be split into a static part and a dynamic correction

$$\mathbf{u}_i=\mathbf{u}_{i,\,\mathrm{stat}}+\mathbf{y} \tag{3}$$

where $\mathbf{u}_{i,\,\mathrm{stat}}=-\mathbf{K}_{ii}^{-1}\mathbf{K}_{ib}\mathbf{u}_b$ is the quasi-static solution, obtained from Eq. (2) assuming $\ddot{\mathbf{u}}_i$ and $\ddot{\mathbf{u}}_b$ are zero. The dynamic part, $\mathbf{y}$, is added to the quasi-static solution to provide the dynamic response. Further, by inserting Eq. (3) into Eq. (2) and rearranging the terms, the dynamic response of $\mathbf{y}$ can be expressed as

$$\mathbf{M}_{ii}\ddot{\mathbf{y}}+\mathbf{K}_{ii}\mathbf{y}=-\mathbf{M}_{ii}\ddot{\mathbf{u}}_{i,\mathrm{stat}}-\mathbf{M}_{ib}\ddot{\mathbf{u}}_b=\mathbf{Y}\ddot{\mathbf{u}}_b \tag{4}$$

where $\mathbf{Y}=\mathbf{M}_{ii}\mathbf{K}_{ii}^{-1}\mathbf{K}_{ib}-\mathbf{M}_{ib}$ can be interpreted as inertia forces associated to static modes [18]. Thus, the acceleration of the boundary DOFs, the mode shapes and the mass distribution determines the forces applied in Eq. (4). This procedure can be continued by replacing $\mathbf{y}$ with a quasi-static solution and a dynamic correction $\mathbf{z}$:

$$\mathbf{y}=\mathbf{y}_{\mathrm{stat}}+\mathbf{z} \tag{5}$$

where $\mathbf{y}_{\mathrm{stat}}=\mathbf{K}_{ii}^{-1}\mathbf{Y}\ddot{\mathbf{u}}_b$ is the static solution obtained from Eq. (4), assuming $\ddot{\mathbf{y}}$ is zero. By inserting Eq. (5) into Eq. (4), and rearranging the terms, the dynamic response of $\mathbf{z}$ can be expressed as

$$\mathbf{M}_{ii}\ddot{\mathbf{z}}+\mathbf{K}_{ii}\mathbf{z}=-\mathbf{M}_{ii}\mathbf{K}_{ii}^{-1}\mathbf{Y}\frac{\mathrm{d}^4\mathbf{u}_b}{\mathrm{d}t^4}. \tag{6}$$

Thus, the response of the interior displacements is given by a sequence of quasi-static solutions:

$$\mathbf{u}_i=\mathbf{u}_{i,\,\mathrm{stat}}+\mathbf{y}_{\mathrm{stat}}+\mathbf{z}_{\mathrm{stat}}+\cdots \tag{7}$$

where, in a similar manner, $\mathbf{z}_{\mathrm{stat}}=-\mathbf{K}_{ii}^{-1}\mathbf{M}_{ii}\mathbf{K}_{ii}^{-1}\mathbf{Y}\frac{\mathrm{d}^4\mathbf{u}_b}{\mathrm{d}t^4}$ is the quasi-static solution of Eq. (6). Hence, a recursive procedure is obtained, indicating that the dynamic response can be approximated as

$$\mathbf{u}_i\approx-\mathbf{K}_{ii}^{-1}\mathbf{K}_{ib}\mathbf{u}_b+\sum_{j=1}^{l}\left(-\mathbf{K}_{ii}^{-1}\mathbf{M}_{ii}\right)^{j-1}\mathbf{K}_{ii}^{-1}\mathbf{Y}\frac{\mathrm{d}^{2j}\mathbf{u}_b}{\mathrm{d}t^{2j}} \tag{8}$$

where l is the number of static corrections. Furthermore, the higher order derivatives $\frac{d^{2j}u_b}{dt^{2j}}$ can be treated as separate DOFs. Hence, instead of computing a sequence of static corrections, a dynamic response analysis is conducted by means of generalized coordinates representing the amplitudes of the correction modes. The set of jth order correction modes are then given by:

$$\mathbf{x}_{\mathrm{cor},j}=\left(\mathbf{K}_{ii}^{-1}\mathbf{M}_{ii}\right)^{j-1}\mathbf{K}_{ii}^{-1}\mathbf{Y} \tag{9}$$

where $\mathbf{x}_{\mathrm{cor},j}$ is a $n_i \times n_b$ matrix, containing the correction modes generated in iteration j. Notice that each correction mode is associated to a boundary DOF. Consequently, a large number of boundary DOFs result in a large number of correction modes being generated in each iteration, why this method is best used in combination with an interface reduction technique (see further Section 2.3).

To avoid numerical round-off errors, the correction modes are generated using the modified Gram–Schmidt orthogonalization procedure [28,29]. Furthermore, the static correction modes are not mutually mass- and stiffness orthogonal. This can e.g. be achieved by solving a small eigenvalue problem:

$$\left(\mathbf{X}_{ik,\mathrm{cor}}^{\top}\mathbf{K}_{ii}\mathbf{X}_{ik,\mathrm{cor}}\right)\mathbf{Z}=\left(\mathbf{X}_{ik,\mathrm{cor}}^{\top}\mathbf{M}_{ii}\mathbf{X}_{ik,\mathrm{cor}}\right)\mathbf{Z}\boldsymbol{\Lambda} \tag{10}$$

where $\mathbf{X}_{ik,\mathrm{cor}}=\begin{bmatrix}\mathbf{x}_{\mathrm{cor},1} & \mathbf{x}_{\mathrm{cor},2} & \cdots & \mathbf{x}_{\mathrm{cor},l}\end{bmatrix}$ is the $n_i \times k$ correction mode matrix, $\boldsymbol{\Lambda}$ is a diagonal matrix containing pseudo-frequencies and $\mathbf{Z}$ contains the corresponding eigenvectors, which are normalized such that $\mathbf{Z}^{\top}\left(\mathbf{X}_{ik,\mathrm{cor}}^{\top}\mathbf{M}\mathbf{X}_{ik,\mathrm{cor}}\right)\mathbf{Z}=\mathbf{I}$. An orthonormal basis of the correction modes is then provided by $\tilde{\mathbf{X}}_{ik,\mathrm{cor}}=\mathbf{X}_{ik,\mathrm{cor}}\mathbf{Z}$, and the relation between the substructure physical DOFs and the generalized coordinates $\mathbf{q}$ is given by

$$\begin{bmatrix}\mathbf{u}_i\\ \mathbf{u}_b\end{bmatrix}=\begin{bmatrix}\tilde{\mathbf{X}}_{ik,\mathrm{cor}} & \boldsymbol{\Psi}_{ib}\\ \mathbf{0}_{bk} & \mathbf{I}_{bb}\end{bmatrix}\begin{bmatrix}\mathbf{q}_k\\ \mathbf{u}_b\end{bmatrix}=\mathbf{T}\mathbf{q} \tag{11}$$

where $\mathbf{q}_k$ is the amplitudes of the (orthonormal) correction modes and $\boldsymbol{\Psi}_{ib}=-\mathbf{K}_{ii}^{-1}\mathbf{K}_{ib}$ is the internal part of the constraint modes, corresponding to the static displacement of a unit displacement on a boundary node while the other boundary nodes are held fixed. Using the transformation given by Eq. (11), the reduced system equations for the glass substructure is obtained by means of subspace projection in a standard fashion (see e.g. [23]), i.e.

$$\tilde{\mathbf{M}}\ddot{\mathbf{q}}+\tilde{\mathbf{C}}\dot{\mathbf{q}}+\tilde{\mathbf{K}}\mathbf{q}=\tilde{\mathbf{f}} \tag{12}$$

where

$$\tilde{\mathbf{M}}=\mathbf{T}^{\top}\mathbf{M}\mathbf{T},\quad \tilde{\mathbf{C}}=\mathbf{T}^{\top}\mathbf{C}\mathbf{T},\quad \tilde{\mathbf{K}}=\mathbf{T}^{\top}\mathbf{K}\mathbf{T},\quad \tilde{\mathbf{f}}=\mathbf{T}^{\top}\mathbf{f}.$$

Here, $\mathbf{M}$, $\mathbf{C}$ and $\mathbf{K}$ are the un-reduced $n\times n$ system matrices and $\mathbf{f}$ is a $n\times 1$ external force vector. Further, for this procedure to be meaningful, the reduction basis should be established using a reduced set of generalized coordinates, i.e. $k \ll n$.

Notice that the generated correction modes are in fact forming a Krylov sequence [28], why these are also referred to as Krylov modes. As indicated by Eq. (9), the modes can be generated by matrix–vector multiplications. Furthermore, the generated modes, as derived above, are force dependent in the sense that the substructure is considered loaded by imposed displacements on its boundary.

An example is presented in Fig. 4 showing the constraint mode and the first three fixed-interface normal modes for a simply supported 1000 mm × 800 mm glass panel. Further, Fig. 5 shows the constraint mode and the first three correction modes. One boundary DOF is considered, corresponding to the out-of-plane direction for the virtual node shown in Fig. 3. As shown in Fig. 4, two of the fixed-interface normal modes are anti-symmetric and cannot be excited by a vertical force applied at the center of the panel. On the contrary, all the correction modes will, by definition, be excited.

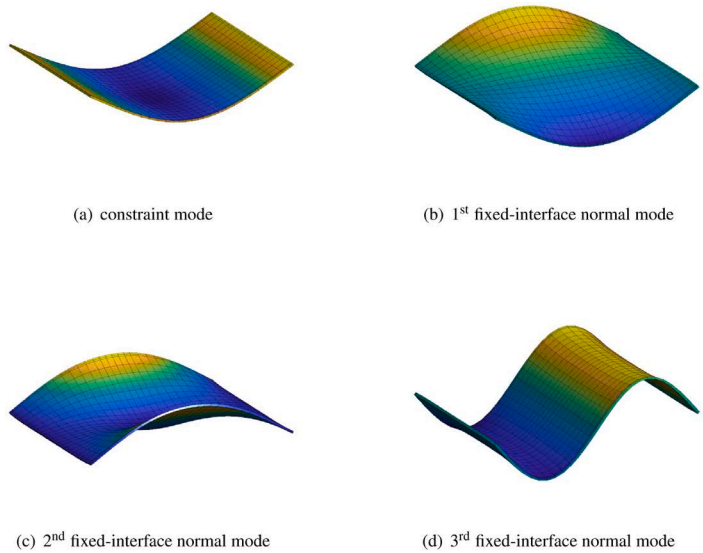

(a) constraint mode (b) 1st fixed-interface normal mode

(c) 2nd fixed-interface normal mode (d) 3rd fixed-interface normal mode

Fig. 4. Constraint mode and first three fixed-interface normal modes.

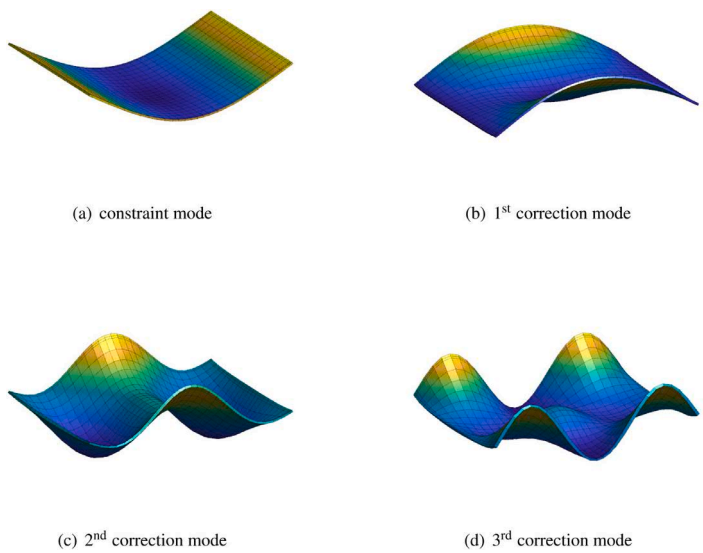

(a) constraint mode (b) 1st correction mode

(c) 2nd correction mode (d) 3rd correction mode

Fig. 5. Constraint mode and first three correction modes.

2.2. Reduced order modeling of the impactor

The standardized impactor, described in EN 12600 [1], consist of two pneumatic rubber tires and steel weights, as shown in Fig. 2b. The impactor mass is almost entirely concentrated to two rigid solids (i.e. the steel weights), positioned symmetrically around the impactor centroid. Consequently, the impactor can, when in contact with the glass panel, be well-represented by a generalized SDOF system. Hence, the impactor mass is lumped to a single DOF. However, due to the contact interaction between the tire and the glass panel, and the behavior of the pneumatic tires, the SDOF model can be expected to be nonlinear.

With inspiration from Hertz contact law [15], a nonlinear load–displacement relation of the following form was assumed:

$$f_s(u) = k_0 u + k_1 u^{\alpha} \tag{13}$$

Hence, an SDOF model consisting of a linear spring in parallel with a nonlinear spring. Furthermore, a stiffness-proportional viscous damping model was adopted, such that the damping force f_d is proportional to the secant stiffness, i.e.

$$f_d(u,\dot{u}) = \left(\beta_0 k_0 + \beta_1 k_1 u^{\alpha-1}\right)\dot{u} \tag{14}$$

where β_0 and β_1 are factors that determines the amount of damping (i.e. a nonlinear Rayleigh β-damping). The damping factors and the

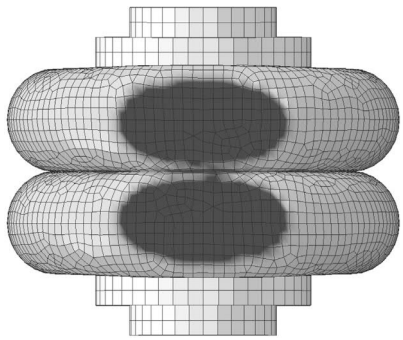

Fig. 6. Example of contact area, shown in dark-gray color, provided by the reference model.

unknown factors k_0, k_1, and α were calibrated using experimental data as well as results provided by the numerical reference model, see further Sections 4 and 5. A similar nonlinear SDOF model was proposed in [10] which, however, is undamped and calibrated based on a polynomial expression (further, in [10], a reduction of the glass substructure was not considered).

Note that a linear dashpot model, independent of the displacement, result in an unrealistic damping force having its peak value just upon impact, when the impactor mass velocity has its peak value. Nonetheless, it is of interest to investigate the accuracy of a linear approximate model for the impactor, which enables the use of computationally efficient analysis techniques. Approximate linear models representing the impactor are further discussed in Section 5.1.

2.3. Coupling procedures and interface reduction

The impactor is modeled by an SDOF system, thus, only one DOF is to be connected to the glass panel substructure. Furthermore, the nonlinearity introduced due to contact between the impactor and the glass panel is partly integrated in the nonlinear impactor model, as described in Section 2.2. However, the distribution of the contact stresses determines which DOFs on the glass panel that should be included in the coupling.

Upon impact, contact is established and a small contact area is formed which gradually increases when the impactor kinetic energy is transformed into strain energy (and damping energy dissipation). Consequently, the contact area varies significantly during impact. Nonetheless, an approximate modeling approach assuming a constant contact area can be reasonably accurate, as e.g. demonstrated by the investigations presented in [7,11]. Hence, instead of including a full description of the contact interaction the contact stress distribution $\theta(x, y)$ is assumed constant while the total contact force $F_c(t)$ varies through time, i.e.

$$F_c(t) = \int \sigma_c(t, x, y) dA = F_c(t) \int \theta(x, y) dA \tag{15}$$

where σ_c is the contact stress and $\int \theta(x, y) dA = 1$.

Furthermore, it is reasonable to assume that an approximation that underestimates the contact area in general overestimates the peak-strain in the glass panel, since the contact pressure can then be expected to be larger. Accordingly, a more realistic peak-strain can be obtained if a somewhat larger "best-estimate" contact area is chosen, assuming that the peak-strain occur at a point in time when the contact area is relatively large.

An example of the shape and size of the contact area computed with the numerical reference model (see further Section 3.1) is shown as dark-gray colored elliptical area in Fig. 6. Based on the results provided by the reference model, the contact area in the reduced models is assumed to have the shape of two ellipses, shown with purple dashed lines in Fig. 7. The major and minor radius of the ellipses are set to 90 mm and 50 mm, respectively. These values are assumed to correspond to the contact area developed when the glass strain reaches a peak value. However, the contact area varies both in time and for different load cases, thus, the specified values should only be regarded as rough estimations. Furthermore, a uniform contact stress is assumed within the predefined contact area. In [10], the contact interaction is modeled using a similar approach. In particular, a uniform contact stress and elliptical contact surfaces are assumed. However, in [10], the glass panel physical DOFs are retained in the final system, while such an approach is more computationally expensive it allows for an update of the contact area size in a direct time-stepping scheme.

The simplified modeling approach described above was implemented by means of a multi-point constraint (MPC) where the interface forces between a master DOF and a group of slave DOFs are controlled using weight factors. This type of constraint can e.g. be found in Abaqus [19], where it is referred to as a *distributed coupling*. However, because no detailed information describing the implementation have been found, a proposal of how to enforce such a MPC constraint is presented herein. For simplicity, and the fact that only one master DOF is present, a one-dimensional MPC is considered (i.e. only interface forces perpendicular to the glass panel are considered). The MPC constraint, as described below, was implemented in Matlab.

The basis in the MPC method is the requirement that the sum of the interface forces acting on the slave DOFs is equal to the interface force acting on the master DOF, cf. Fig. 7. This requirement is not that restrictive and can in principle be fulfilled by any interface force distribution, as long as equilibrium is maintained. As shown further below, this is also why this method allows for customized interface force distributions.

Assume that a set of weight factors w_i, related to the MPC slave DOFs, are normalized such that

$$\hat{w}_i = \frac{w_i}{\Sigma_{j=1}^{p} w_j} \tag{16}$$

where p is the number of slave DOFs. Further, the constraint is enforced so that the displacement of the master DOF is the weighted mean value of the slave DOFs [19], i.e.

$$u^{(m)} = \sum_{j=1}^{p} \hat{w}_j u_j^{(s)} \tag{17}$$

which implies that the displacement associated to slave DOF i can be expressed as:

$$u_i^{(s)} = \frac{1}{\hat{w}_i} \left(u^{(m)} - \sum_{j=1, j\neq i}^{p} \hat{w}_j u_j^{(s)} \right). \tag{18}$$

Hence, one DOF is redundant and can be calculated based on the displacements of the other DOFs included in the MPC. Further, Eq. (18) can be expressed in matrix form

$$\mathbf{B}\mathbf{u} = 0 \tag{19}$$

where $\mathbf{B}$ is a vector containing the normalized weight factors $\hat{w}_i$ at entries corresponding to slave DOFs, a negative one at the entry corresponding to the master DOF and zeros in the remaining entries. The size of $\mathbf{B}$ is $1 \times \tilde{n}$, where $\tilde{n} = n + 1$ (thus, one master DOF is added to the glass panel substructure having n DOFs).

The displacement can be partitioned in a set of unique $\mathbf{u}_u$ and redundant $\mathbf{u}_r$ DOFs [21]. If slave DOF p is chosen as the redundant DOF, then $\mathbf{u}_r = u_p^{(s)}$ and $\mathbf{u}_u = \begin{bmatrix} \mathbf{0} & u^{(m)} & u_1^{(s)} & \dots & u_{p-1}^{(s)} \end{bmatrix}$. Hence,

$$\mathbf{B} = \begin{bmatrix} \mathbf{B}_u & \mathbf{B}_r \end{bmatrix} \begin{bmatrix} \mathbf{u}_u \\ \mathbf{u}_r \end{bmatrix} = 0 \tag{20}$$

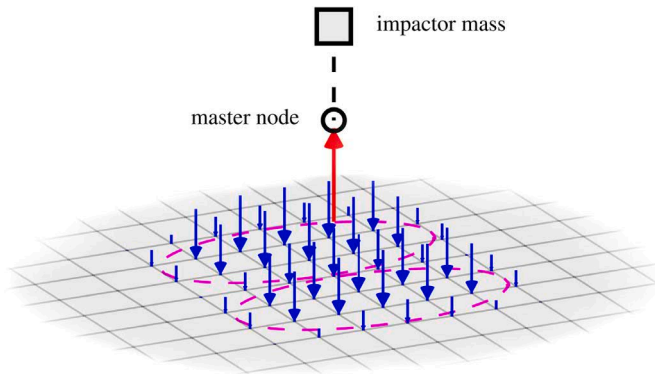

Fig. 7. Distributed coupling between a master node and the glass panel slave nodes. The interface forces acting on the slave nodes and the master node are shown in blue and red color, respectively. The SDOF system representing the impactor is shown by the black dashed line. Note that the arrow length is not to scale. (For interpretation of the references to color in this figure legend, the reader is referred to the web version of this article.)

where $\mathbf{B}_u = \begin{bmatrix}\mathbf{0} & -1 & \widehat{w}_1 & \dots & \widehat{w}_{p-1}\end{bmatrix}$ and $\mathbf{B}_r = \widehat{w}_p$. By rewriting Eq. (20), the redundant displacement can be expressed as

$$\mathbf{u}_r = -\mathbf{B}_r^{-1}\mathbf{B}_u\mathbf{u}_u. \tag{21}$$

Thus, the displacement vector can be expressed in terms of the unique displacements,

$$\begin{bmatrix}\mathbf{u}_u \\ \mathbf{u}_r\end{bmatrix} = \begin{bmatrix}\mathbf{I}_{uu} \\ -\mathbf{B}_r^{-1}\mathbf{B}_u\end{bmatrix}\mathbf{u}_u = \mathbf{L}\mathbf{u}_u \tag{22}$$

where $\mathbf{L}$ is a $\tilde{n}\times n$ transformation matrix.

The equation of motion for a linear system, including the redundant DOFs, can be written as:

$$\mathbf{M}\ddot{\mathbf{u}} + \mathbf{C}\dot{\mathbf{u}} + \mathbf{K}\mathbf{u} = \mathbf{f} + \mathbf{g} \tag{23}$$

where $\mathbf{M}$, $\mathbf{C}$ and $\mathbf{K}$ are the $\tilde{n}\times\tilde{n}$ mass, damping and stiffness matrix, $\mathbf{u}$ is the $\tilde{n}\times 1$ displacement vector, $\mathbf{f}$ is the $\tilde{n}\times 1$ external force vector and $\mathbf{g}$ is a $\tilde{n}\times 1$ interface force vector, which is included due to the presence of MPCs. Now, inserting the transformation according to Eq. (22) in Eq. (23) and pre-multiplying with $\mathbf{L}^\top$ yields:

$$\mathbf{L}^\top\mathbf{M}\mathbf{L}\ddot{\mathbf{u}}_u + \mathbf{L}^\top\mathbf{C}\mathbf{L}\dot{\mathbf{u}}_u + \mathbf{L}^\top\mathbf{K}\mathbf{L}\mathbf{u}_u = \mathbf{L}^\top\mathbf{f} \tag{24}$$

thus,

$$\mathbf{L}^\top\mathbf{g} = \begin{bmatrix}\mathbf{I} & \mathbf{0} & \mathbf{0} & \cdots & \mathbf{0} & \mathbf{0} \\ \mathbf{0} & 1 & 0 & \cdots & 0 & \frac{1}{\widehat{w}_p} \\ \mathbf{0} & 0 & 1 & \cdots & 0 & -\frac{\widehat{w}_1}{\widehat{w}_p} \\ \vdots & \vdots & \vdots & \ddots & \vdots & \vdots \\ \mathbf{0} & 0 & 0 & \cdots & 1 & -\frac{\widehat{w}_{p-1}}{\widehat{w}_p}\end{bmatrix}\begin{bmatrix}\mathbf{0} \\ g^{(m)} \\ g_1^{(s)} \\ \vdots \\ g_{p-1}^{(s)} \\ g_p^{(s)}\end{bmatrix} = \mathbf{0} \tag{25}$$

where we use that $-\mathbf{B}_r^{-1}\mathbf{B}_u = -\frac{1}{\widehat{w}_p}\begin{bmatrix}\mathbf{0} & -1 & \widehat{w}_1 & \dots & \widehat{w}_{p-1}\end{bmatrix}$.

As indicated by Eq. (25), the weight factors control the distribution of the interface forces acting on the slave DOFs. For example, Eq. (25) implies that $g_p^{(s)} = -\widehat{w}_p g^{(m)}, g_1^{(s)} = \frac{\widehat{w}_1}{\widehat{w}_p}g_p^{(s)} = -\widehat{w}_1 g^{(m)}$ and, in general, $g_i^{(s)} = \frac{\widehat{w}_i}{\widehat{w}_p}g_p^{(s)} = -\widehat{w}_i g^{(m)}$. Further, according to Eq. (16), the weight factors are normalized, which implies that

$$\sum_{j=1}^{p} g_j^{(s)} = \sum_{j=1}^{p} -g^{(m)}\widehat{w}_j = -g^{(m)}\sum_{j=1}^{p}\widehat{w}_j = -g^{(m)}. \tag{26}$$

Hence, equilibrium is maintained. Moreover, it should be noted that the above formulation allows for arbitrary weight factors, e.g. to consider a non-uniform interface force distribution or a non-uniform element mesh.

2.4. Dynamic response analysis

In the experimental tests, the pendulum impactor is released from a specific drop height and starts a swing motion until, at its lowest point, impact with the glass panel. The numerical analyzes are initiated just upon impact. Thus, the dynamic response of the glass–impactor system is obtained by solving an initial value problem—the external forces are zero and an initial velocity is prescribed to the impactor. The initial velocity $v_{0,\text{imp}}$ is computed based on the pendulum drop height:

$$v_{0,\text{imp}} = \sqrt{2gh} \tag{27}$$

where g is the gravitational acceleration and h is the drop height. Using this approach, the impactor angular velocity is assumed negligible which is reasonable considering that the length of the pendulum employed in the experimental campaign was approximately 2 m. (If assuming rigid body motion it follows that the ratio between the linear and rotational kinetic energy upon impact is given by $E_{\omega_0}/E_{v_0} = I/(mL^2) < 1\%$, where m and I are the impactor mass and moment of inertia, respectively, and L is the distance between the impactor center of mass and the pendulum fixed point.)

Solution methods for both linear and nonlinear systems are investigated. Furthermore, only the first phase, when there is contact between the impactor and the glass panel, is considered.

2.4.1. Linear systems with nonclassical damping

If the coupled impactor–glass structure is approximated using a linear model with classical damping, a closed-form solution is straightforward to obtain by means of modal expansion techniques applied to the assembled system [29]. However, this approach is in general not feasible for systems with non-classical (also referred to as non-proportional) damping since a projection of the system equations onto a modal basis would then not result in a diagonal damping matrix. According to Section 5.1, the damping ratio of a linear impactor model can be estimated to be about 5%, whereas the damping ratio of the simply supported glass panels is approximately 1.7%, as discussed further in Section 4. Thus, the damping of the assembled system is indeed non-proportional and, consequently, a traditional modal analysis cannot be utilized. Nonetheless, a closed-form solution can be achieved. For example, by means of the complex damped eigenmodes using a state-space formulation (see e.g. [30]) or by use of the so-called modal strain energy (MSE) method, which is an approximate method to account for non-proportional damping [31,32]. An advantage using the MSE method compared to a state-space formulation is that the number of system variables are halved and that imaginary variables can be avoided. Furthermore, the numerical investigations presented in [32]

suggests that the MSE method is accurate for systems with damping less than approximately 20%, thus, it can be assumed sufficiently accurate for the studied glass–impactor system.

The damping ratio of an SDOF system representing a modal coordinate can be expressed as:

$$\zeta = \frac{E_D}{4\pi E_S} \tag{28}$$

where E_D is the one-cycle modal energy loss due to viscous damping and E_S is the modal strain energy amplitude, given by:

$$E_S = \frac{1}{2}\boldsymbol{\phi}_j^\top \hat{\mathbf{K}} \boldsymbol{\phi}_j \tag{29}$$

where $\hat{\mathbf{K}}$ is the $\hat{m} \times \hat{m}$ global stiffness matrix, representing the coupled impactor–glass system, and $\boldsymbol{\phi}_j$ is the eigenvector for mode j, obtained by solving the generalized eigenvalue problem:

$$\left(\hat{\mathbf{K}} - \omega_j^2 \hat{\mathbf{M}}\right)\phi_j = 0 \tag{30}$$

where ω_j is the corresponding eigenfrequency. Notice that the elements of the eigenvectors includes physical as well as generalized DOFs.

In accordance with the MSE method, the modal energy loss is computed as:

$$E_D = \pi \omega_j \boldsymbol{\phi}_j^\top \hat{\mathbf{C}} \boldsymbol{\phi}_j \tag{31}$$

where ω_j is the eigenfrequency for mode j and $\hat{\mathbf{C}}$ is the $\hat{m} \times \hat{m}$ global damping matrix, containing the damping submatrices related to the glass and impactor, respectively. It follows that the modal damping ratio for mode j can be computed as:

$$\zeta_j = \frac{\boldsymbol{\phi}_j^\top \hat{\mathbf{C}} \boldsymbol{\phi}_j}{2\omega_j \boldsymbol{\phi}_j^\top \hat{\mathbf{M}} \boldsymbol{\phi}_j} \tag{32}$$

where $\hat{\mathbf{M}}$ is the $\hat{m} \times \hat{m}$ global mass matrix.

As in a traditional modal decomposition applied to systems expressed in terms of physical DOFs, a linear system reduced by means of DS can be expressed in modal coordinates:

$$\mathbf{q} = \sum_j \boldsymbol{\phi}_j \eta_j \tag{33}$$

where η_j is the modal coordinate for mode j.

If neglecting damping, the system equations can be diagonalized by projecting the system onto the modal basis:

$$\boldsymbol{\Phi}^\top \hat{\mathbf{M}} \boldsymbol{\Phi} \ddot{\eta} + \boldsymbol{\Phi}^\top \hat{\mathbf{K}} \boldsymbol{\Phi} \eta = \boldsymbol{\Phi}^\top \tilde{\mathbf{p}} \tag{34}$$

where $\boldsymbol{\Phi} = \begin{bmatrix} \boldsymbol{\phi}_1 & \boldsymbol{\phi}_2 & \dots & \boldsymbol{\phi}_{\hat{m}} \end{bmatrix}$ is the modal matrix and $\eta = \begin{bmatrix} \eta_1 & \eta_2 & \dots & \eta_{\hat{m}} \end{bmatrix}^\top$ is the modal amplitudes. Hence, a set of $\hat{m}$ uncoupled differential equations, which can be solved independently, is obtained.

Now, by introducing the modal damping ratios determined by means of the MSE method, and assuming that the external force is zero, each modal response is given by:

$$\eta_j(t) = e^{-\zeta_j \omega_j t}\left(\eta_j(0)\cos(\omega_{jD}t) + \frac{\dot{\eta}_j(0) + \zeta_j \omega_j \eta_j(0)}{\omega_{jD}}\sin(\omega_{jD}t)\right) \tag{35}$$

where ζ_j is the damping ratio for mode j and $\omega_{jD} = \omega_j\sqrt{1-\zeta_j^2}$ is the jth natural frequency with damping [29]. In contrast to a traditional modal response analysis, which commonly uses a truncated modal basis, it is in this case reasonable to include all $\hat{m}$ modes in the modal basis because a reduction has already been performed on the substructure level. Hence, the modal analysis is primarily employed for diagonalizing the system matrices, not for reducing the system size.

In a standard modal analysis, the modal damping matrix is in general constructed directly in the modal domain by means of modal damping ratios, e.g. provided by experimental tests. However, using the MSE method, the global damping matrix $\hat{\mathbf{C}}$, containing the damping submatrices, is required. The SDOF model representing the impactor uses stiffness-proportional damping, as discussed in Section 2.2. Hence, if considering a linear impactor model, viscous damping is modeled by a ordinary dashpot. The damping matrix related to the glass panel is constructed by means of Rayleigh-damping, i.e.

$$\mathbf{C} = \alpha\mathbf{M} + \beta\mathbf{K} \tag{36}$$

where α and β are the Rayleigh damping parameters [29]. The glass panel damping is further investigated in Section 4 and the calibration of the Rayleigh parameters is discussed in Section 5.

By using the above methodology, a closed-form solution is obtained for initial value problems of linear systems even though non-proportional damping is present. Notice, however, that the above procedure is indeed an approximation due to that possible off-diagonal terms is not considered in the modal damping matrix given by $\boldsymbol{\Phi}^\top \hat{\mathbf{C}} \boldsymbol{\Phi}$.

2.4.2. Direct time-integration of nonlinear systems

The dynamic response of the nonlinear systems is solved using implicit direct time-integration. For the reduced models, direct time-integration is performed using Newmark's method [29]. The Newmark parameters are set to $\beta = \frac{1}{4}$ and $\gamma = \frac{1}{2}$ resulting in a unconditionally stable system, which is convenient when solving a nonlinear system. Further, force equilibrium in each time increment is established by means of Newton–Raphson iterations [29].

3. Numerical reference model

A detailed FE model of the impactor was established using the commercial FE analysis software Abaqus [19]. The response computed with the reference model complements the experimental results in a validation of the reduced models (see further Section 5.3). Furthermore, the FE model provides insight into the impactor structural behavior and its interaction with the glass panel, which is vital knowledge in the process of deriving and evaluating a reduced model.

Furthermore, a FE model of the glass panel was developed, employed both in the Abaqus analyzes including the impactor reference model and for generating system matrices, being necessary in the process of establishing reduced models representing the glass panel. The FE model of the glass panel was modeled in Abaqus. However, to get full access to the FE procedures a separate, but in practice equivalent, FE model was made using Matlab.

3.1. Impactor

The impactor rubber tires are pneumatic bias-ply tires which consist of rubber reinforced by nylon ply-cords, usually in an angle ± 30°–40° from the direction of travel, with each additional ply positioned in opposite direction [4].

In Abaqus, the nearly incompressible rubber material was modeled using a hyperelastic model. The strains in the rubber turns out to be relatively small (< 20%), why a Neo-Hookean model, with parameters according to Table 1, is judged to be sufficiently accurate. The rubber tires were modeled by four-node shell elements and the nylon cords were modeled using so-called rebar layers, a feature in Abaqus that allows for specifying orthogonal or skew reinforcement embedded in shell or membrane elements. Hence, the nylon cords are not modeled by separate elements, but is rather modeled as a smeared rebar layer positioned at the shell element reference surface. The cords diameter was set to 0.45 mm with spacing 1.6 mm, in accordance with [3]. By an optical investigation of a cut of a tire, the thickness of the rubber was estimated to 5 mm.

An accurate model of the stiffness distribution of the nylon ply-cords is important for a realistic behavior of the tire model. The pressure exerted by the contained air is mainly balanced by tensile stresses in the nylon cords having a stiffness several order of magnitude larger than the rubber (even when considering the difference in cross-section area). Therefore, the stiffness of the inflated tires is primarily due to

Table 1
Material models employed in the reference model.

Material	Material model	Material parameters
Rubber	Hyperelastic, Neo-Hookean	$G = 1.2$ MPa, $K = 2$ GPa, $\rho = 1100$ kg/m^3 [3,4]
Nylon	Linear elastic	$E = 3$ GPa, $\nu = 0.3$, $\rho = 1100$ kg/m^3 [3,33]
Steel	Linear elastic	$E = 210$ GPa, $\nu = 0.3$, $\rho = 7830$ kg/m^3 [3]
Glass	Linear elastic	$E = 72$ GPa, $\nu = 0.23$, $\rho = 2500$ kg/m^3 [34]

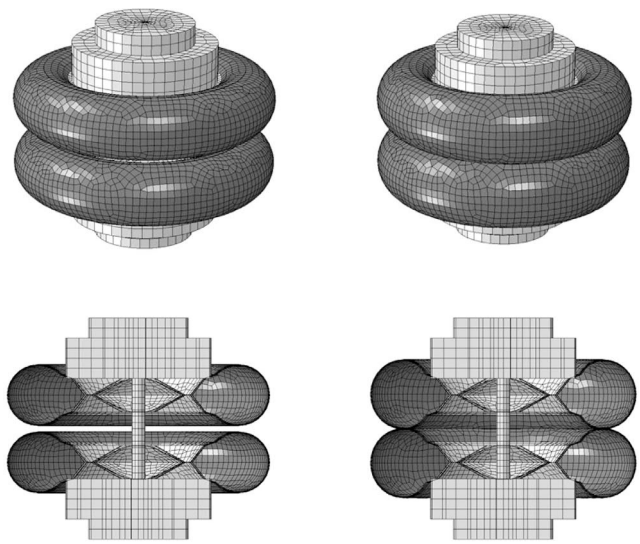

Fig. 8. Undeformed (left) and inflated (right) configuration. The rubber/nylon and steel are shown in dark-gray and gray color, respectively.

prestressing of the nylon ply-cords and, consequently, the angle of the nylon cords have a relatively large effect on the structural behavior. However, data for the nylon cord angle for the specific tires used in this study were not available. Instead, the angle was determined by comparison of the deformed shape of the actual tire, when inflated and non-inflated, with the deformed shape given by a quasi-static analysis of the tire inflation. Based on this comparison, the angle was estimated to be 40°.

The tire air pressure was modeled using a feature in Abaqus denoted *fluid cavity*, which considers the coupling between the deformation of the tire structure and the pressure exerted by the contained air. Using this modeling approach, only the quasi-static air pressure is considered, whereas the dynamic pressure is ignored. An overpressure of 4.07 bar was prescribed in the undeformed configuration to obtain an air pressure of 3.5 bar in the deformed configuration.

The steel weights, rims, and the screw spindle (the axis connecting the two weights) were modeled using linear elastic material properties according to Table 1. In principle, the weights can be modeled as rigid bodies since these are much stiffer than the tires. However, the deformation of the rim and the screw spindle might not be negligible. Also, the off-center location of the weights causes the screw spindle to bend, which in turn effects the deformation of the tires. To consider a possible influence of these effects the steel weights and the screw spindle were modeled by eight-node solid elements, whereas the rim was modeled with four-node shell elements. The impactor model mesh, for both the undeformed and inflated configuration, is shown in Fig. 8.

A viscous stiffness-proportional damping was calibrated to the energy loss measured in the impact tests, as discussed in Sections 4 and 5.1. Moreover, a contact interaction was prescribed between the tires, with a friction coefficient of $\mu = 0.7$ in accordance with [4].

3.2. Glass panel

The glass panel was modeled with solid shell elements, which uses an assumed strain distribution for an enhanced modeling of bending [35]. An advantage using these elements compared to conventional shell elements is that no special treatment is needed to consider offsets of loads or prescribed boundary conditions. An evaluation of using solid shells for modeling glass panels is e.g. presented in [36].

The supporting steel frame was assumed rigid and the EPDM rubber strips positioned between the glass and the steel were modeled by linear elastic spring beds. In the experimental set-up, the rubber along the supports were prestressed due to bolting of the glass panels, which affect the rubber stiffness. Therefore, the stiffness of the spring beds were calibrated based on the fundamental frequencies as measured for the 8, 10 and 12 mm, respectively, simply supported glass panels. Using this approach, the stiffness of the rubber strips, modeled with a thickness of 10 mm and a width of 15 mm, was estimated to 10 MPa (the glass geometry, density, and stiffness, which also affect the fundamental periods, are thus regarded as relatively well-known parameters). The in-plane stiffness of the rubber strips was modeled in a similar manner using elastic springs.

In accordance with the measurements discussed in Section 4, a damping ratio of 1.7% was assumed for the glass panels being modeled by means of Rayleigh α- and β-damping. The derivation of the Rayleigh parameters is further discussed in Section 5.

4. Experimental testing

Experimental tests were performed to validate the reduced models. In particular, the strain was measured on simply supported monolithic glass panels with dimensions 1000 mm×800 mm, made of regular soda-lime silicate toughened glass. The glass panel impact tests were part

(a) (b)

Fig. 9. Soft-body impact test set-up (a) and strain gauge on the rear side of the glass panel (b).

Table 2
Impactor rigid impact energy loss.

Test No	Drop height (h_0) [mm]	Height diff. ($\Delta h = h_0 - h_1$) [mm]	Energy loss ($\frac{\Delta h}{h_0}$) [%]	Mean [%]
1	100	20	20	20
2	100	20	20	
3	200	55	27.5	28
4	200	55	27.5	
5	300	80	26.7	27
6	300	80	26.7	
7	450	140	31.1	30
8	450	130	28.8	
9	700	230	32.9	32
10	700	220	31.4	

of an experimental campaign summarized in [37,38], which includes additional tests of glass panels mounted with various fixing methods, such as linear clamps, local clamp fixings and point fixings. Moreover, glass with different heat treatment as well as glass laminated with different materials were also tested.

Additional measurements were performed to identify the dynamic characteristics of the impactor. The dynamic properties of the impactor, such as the dynamic stiffness and damping turn out to have a large impact on the dynamic behavior of the coupled impactor–glass system. Also, an increased insight into the structural behavior is essential in the process of developing reduced models, to ensure that no significant characteristics of the system are lost in the reduction process.

4.1. Dynamic characteristics of impactor

The impactor design is described in [1], where the impactor parts are specified in detail. The tires should be of the type 3.50-R8 4PR (by Vredestein) or tires that are demonstrated equivalent. In the present study, two Michelin 3.50-S83 tires were used (see Fig. 9b), which were also used in the experimental tests presented in [3]. The inflation pressure is 3.5 bar and the total weight of the impactor is 50 kg.

The impactor damping and stiffness were evaluated based on impact with a very stiff steel column, which can be considered rigid. The impactor acceleration was measured at several locations on the impactor weights, as shown in Fig. 2b. Similar tests were also performed in [3]. However, the tests performed in the present study also included an estimation of the impactor damping. More specifically, the difference between the maximum height of the impactor after impact h_1 and the initial drop height h_0 was measured. Hence, the energy loss during impact (ΔE) was estimated as

$$\Delta E = mg\left(h_0 - h_1\right). \tag{37}$$

The measurement of the impactor position was performed by recording the impact sequence on video at a frame rate of 240 frames per second, sufficiently high to enable a smooth slow-motion video. Before the impact tests were performed, a physical measurement-grid was positioned in the plane of the pendulum, filmed at the same angle and position as the impact tests. This measurement grid was then used to calibrate the measurements performed directly in the slow-motion videos. Tests were preformed with an impactor drop height of 100, 200, 300, 450 and 700 mm, respectively.

The experimental results and the estimated energy loss, which in turn determines the damping, is presented in Table 2. Note that the experimental methodology implies that the mass of the impactor weights can be assumed sufficiently large such that the system can be well-represented by an SDOF system when in contact with the rigid wall and a rigid mass floating in space when contact is not established. Furthermore, the kinetic energy related to the impactor angular velocity is assumed negligible being reasonable given that the pendulum length is approximately 2 m.

4.2. Soft-body impact on glass panels

Experimental results from impact tests of two-sided simply supported glass panels, as shown in Fig. 9a, was used for validation of the reduced order models. The glass panels consist of toughened monolithic glass with nominal thickness 8, 10 and 12 mm, respectively. As described in [38], the horizontal strain was measured by a strain gauge bonded at the rear side (tensile side) of the glass panels at the point of impact, see Fig. 9b. Impact tests were conducted with a drop height of 100, 200, 300, 400 and 500 mm, respectively.

The signal from the strain gauge was logged at a frequency of 600 Hz for a few seconds. However, the impactor contact time is typically less than 80 ms. Hence, the logged strain data includes the decay of motion after impact, which was utilized for estimating the damping of the glass panels and its fixings. An example of the logged strain data is shown in Fig. 10a. Further, the logarithmic decrement is given by:

$$\delta = \frac{1}{n}\ln\left(\frac{u_i}{u_{i+n}}\right) = \frac{2\pi\zeta}{\sqrt{1-\zeta^2}} \tag{38}$$

where u_i is the amplitude measured at cycle i, n is the number of cycles between the measured amplitudes and ζ is the damping ratio. If assuming linear elasticity, the displacement amplitudes in Eq. (38) can be replaced by the measured strain amplitude. The estimated damping for some of the tests is presented in Fig. 10b. The horizontal axis denotes the strain amplitude measured at cycle i, corresponding to u_i in Eq. (38). As shown in the figure, the damping ratio does not vary much with neither the glass thickness nor the amplitude. However, it should be noted that the strain amplitude is fairly low in all the measurements, i.e. less than 0.25 mm/m. Based on the data from the impact tests, the damping ratio of the glass and its fixings was estimated to 1.7%. This is slightly larger than the damping ratios reported in e.g. [39,40] where, however, different test arrangements were used.

In addition to the estimation of the glass panel damping ratio, the measured strain due to free vibration after impact was used for estimation of the fundamental periods of the simply supported glass panels. Note that the glass strain, which is measured in the center of the glass panel, is mainly due to vibration of the fundamental mode. For glass panels with thickness 8, 10 and 12 mm, respectively, the fundamental period was estimated to 46, 37 and 31 ms, respectively.

Finally, the strain was measured in a double impact test, as shown in Fig. 11. More specifically, the soft-body pendulum was released and the glass strain was measured during the first as well as the second impact, by letting the pendulum move freely after the first impact until a second impact was initiated. Using this procedure, the impact energy in the second impact approximately corresponds to the impactor kinetic energy after the first impact. This test was done for one impact test:

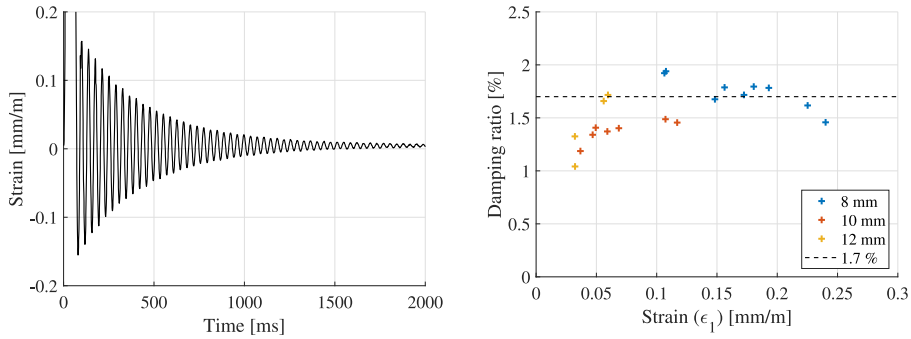

(a) Horizontal strain measured on rear side of glass (b) Damping ratios estimated for various glass thicknesses

Fig. 10. Decay of motion in terms of glass strain for test with a drop height of 500 mm and a glass thickness of 10 mm (a) and estimated damping ratios (b). The strain ϵ_1 is the strain measured at cycle i, corresponding to u_i in Eq. (38). The mean damping ratio for measurements with $\epsilon_1 > 0.1$ mm/m is equal to 1.7% and is shown by the black dashed line.

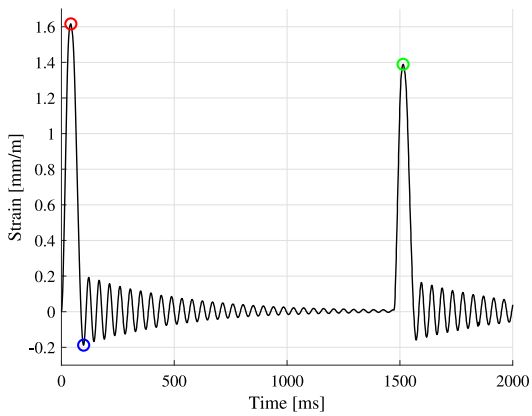

Fig. 11. Horizontal strain measured on the rear side of the glass panel with thickness 8 mm for the double impact test. The initial drop height was 200 mm. The red and green circle indicate the peak strain during the first and second impact, respectively. The blue circle indicates the peak strain after the first impact. (For interpretation of the references to color in this figure legend, the reader is referred to the web version of this article.)

the 8 mm glass panel subjected to an impact corresponding to a drop height of 200 mm. The measured strain was exploited to implicitly estimate the energy loss during impact for the whole system. This includes energy dissipation due to deformation of the impactor (e.g. frictional or viscous damping), through frictional effects due to contact, and deformation of the glass panel and its fixings.

If assuming linear elastic behavior, the response can be obtained by solving an initial value problem of a linear system. As implied by Eqs. (33) and (35), the displacements of such a system is linearly dependent on the initial velocity. Accordingly, the displacements are quadratically dependent on the initial kinetic energy of the impact body $E_{K,0}$, given by

$$E_{K,0} = \frac{m_{\text{imp}} \dot{u}_{0,\text{imp}}^2}{2}. \tag{39}$$

It follows that the square of the ratio between the peak strain in the first and second impact is proportional to the ratio between the kinetic energies induced in the system upon the first and second impact, respectively. Hence,

$$\left(\frac{\epsilon^{(2)}}{\epsilon^{(1)}}\right)^2 = \frac{E_{K,0}{}^{(2)}}{E_{K,0}{}^{(1)}} \tag{40}$$

where $\epsilon^{(1)}$ and $\epsilon^{(2)}$ are the strains measured for the first and second impact, and $E_{K,0}{}^{(1)}$ and $E_{K,0}{}^{(2)}$ are the kinetic energy just before the first and second impact, respectively. From the measured peak strains according to Fig. 11 (red and green circle), the ratio between the kinetic energy in the first and second impact can be estimated to $(1.386/1.616)^2 = 0.74$. Thus, the energy induced in the system upon the second impact is 74% of the impact energy in the first impact and, accordingly, the energy loss is approximately 26%. This is fairly close to the energy loss measured in the rigid impact tests, shown in Table 3, which may indicate that the energy dissipation related to the deformation of the glass panel is fairly small. However, it should be noted that the energy loss computed from a double impact test using the above procedure is in principle only valid for linear systems, why it should only be regarded as a rough estimate. Moreover, some of the induced energy is not dissipated during the impact but instead causes the glass panel to oscillate after impact. The glass panel strain energy is related to the square of the glass strain. Accordingly, a strain energy ratio can be estimated based on the peak strain during impact and the peak strain after impact. Using the measured strains according to Fig. 11 for the first impact (red and blue circle), the strain energy ratio is $(0.1925/1.616)^2 = 1\%$, which principally is negligible.

5. Model validation

In order to validate the reduced models, the computed response is compared to both experimental results and the response provided by the reference model. Two load cases are evaluated where the point of impact is centric (load case A) and eccentric (load case B), respectively. In both load cases impact loading of a two-sided continuously supported monolithic glass panel, with width 1000 mm and height 800 mm, is studied. The position of the impactor for load cases A and B, respectively, is shown in Fig. 12.

Calibrations of the impactor reference model and the developed SDOF models, representing the impactor, are presented in Section 5.1. In Section 5.2, the response computed with the reference model and the reduced models are compared and evaluated based on load cases A and B. Furthermore, in Section 5.3, a validation based on experimental results is presented for load case A.

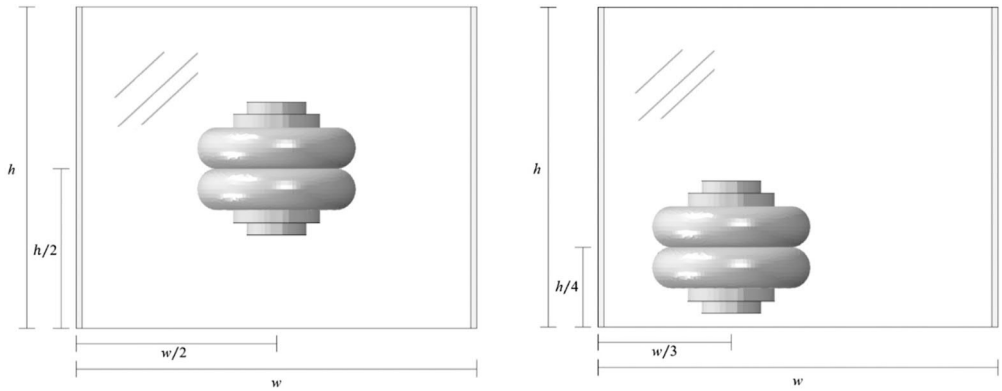

(a) Load case A (b) Load case B

Fig. 12. Position of impactor in load case A and B. The glass panel dimensions are h = 800 mm and w = 1000 mm. Spring beds are applied on the parts of the glass panels marked with light gray color.

Table 3
Impactor energy loss due to impact with rigid beam.

Drop height [mm]	Experiment [%]	FE model[a] [%]	SDOF model [%]
100	20	24	22
200	28	26	25
300	27	28	27
450	30	30	30
700	32	32	32

[a]Viscous dissipation and frictional damping due to contact interaction.

5.1. Calibration of impactor models

A calibration of the numerical reference Abaqus model of the impactor was conducted based on the rigid impact tests discussed in Section 4. Numerical analyzes of impact with a rigid surface was performed to simulate the experimental tests. The analyzes were initiated just upon impact by prescribing an initial velocity to the impactor. The model was calibrated in the sense that a stiffness-proportional viscous damping was prescribed to match the energy loss obtained in the experimental tests, see Table 3. Based on this calibration, a damping parameter of $\beta = 0.022$ was prescribed to the rubber, proportional to the strain-free elastic stiffness. The other material parameters were set according to Table 1.

The impactor acceleration is shown in Fig. 13 for a drop height of 100, 200, 300, 450 and 700 mm, respectively. The dashed lines are the accelerations measured in the impact tests and the solid lines are the accelerations provided by the numerical simulations, extracted from a node close to the position of the accelerometer in the experimental tests. As shown in the figure, the computed accelerations show good agreement with the experimental results for drop heights 450 and 700 mm. However, the measured peak acceleration is higher, and the measured pulse time is shorter for drop heights 100, 200 and 300 mm. It may be that some of the discrepancy is due to that the damping of the impactor is in fact frictional rather than viscous for lower amplitudes; a Coulomb type damping would result in an unsymmetrical and shorter acceleration pulse with a larger peak acceleration. Notice that even though friction is considered in the contact interactions in the reference model, this has a small impact on the total energy dissipation, which is mainly due to viscous damping. Moreover, the rotational motion of the impactor upon impact is not considered in the analysis, which may be another reason for the discrepancy between the calculated and measured accelerations.

The nonlinear SDOF model, presented in Section 2.2, was calibrated to the impactor reference model. More specifically, a hysteresis loop, representing the behavior of a generalized SDOF system, was obtained from the reference model by plotting the movement of the impactor mass centroid and the total contact force between the impactor and the rigid surface. The total contact force is equal (but with opposite sign) to the sum of the impactor damping force and elastic force. To distinguish the total elastic force from the total internal force, the elastic force was approximated as the derivative of the total strain energy with respect to the displacement of the impactor mass centroid, as shown by the green curve in Fig. 14. In a similar manner, the damping force was estimated as the derivative of the viscous dissipation. Hence, the sum of the derivatives, shown by the yellow curve in Fig. 14, represent the total internal force, which is very close to the total contact force shown by the dashed red curve. The unknown stiffness factors in the generalized SDOF model (i.e. k_0, k_1 and α in Eq. (13)) were then computed from the load–displacement curve in a least-square sense. More specifically, the factors k_0, k_1 were determined by a least-squares problem for a given α value. By traversing a sequence of α values, a best estimate was obtained. For instance, the blue dashed curve in Fig. 14 correspond to the nonlinear SDOF model calibrated to the data pairs marked by blue circles. Note that the derivatives are ill-conditioned close to the peak displacement, why these are only computed for displacements less than approximately 35 mm.

The acceleration given by the nonlinear SDOF model, with factors calibrated to $k_0 = 1.59 \cdot 10^5$, $k_1 = 1.25 \cdot 10^7$, and $\alpha = 2.242$, respectively, is shown for various drop heights in Fig. 15a. The damping parameters in Eq. (14) were calibrated to $\beta_0 = 8 \cdot 10^{-4}$ and $\beta_1 = 4 \cdot 10^{-3}$, respectively, based on the shape of the hysteresis loop provided by the reference model and the measured energy loss, presented in Table 3. The hysteresis loop for various drop heights are shown in Fig. 16, computed with the reference model and the nonlinear SDOF system, respectively.

As discussed in Section 2.4, a linear system can be solved using modal expansion techniques and, in particular, a closed-form solution can be achieved for initial value problems. A linear model of the assemble system implies the use of a linear impactor model. However, as shown in Fig. 13, the pulse time vary with the impact energy, which is expected for a nonlinear system. The system appears stiffer, i.e. the pulse time is shorter, for an increasing drop height, which is also consistent with the nonlinear system discussed above. Nonetheless, a simplified approximate model can be derived using the measured pulse time.

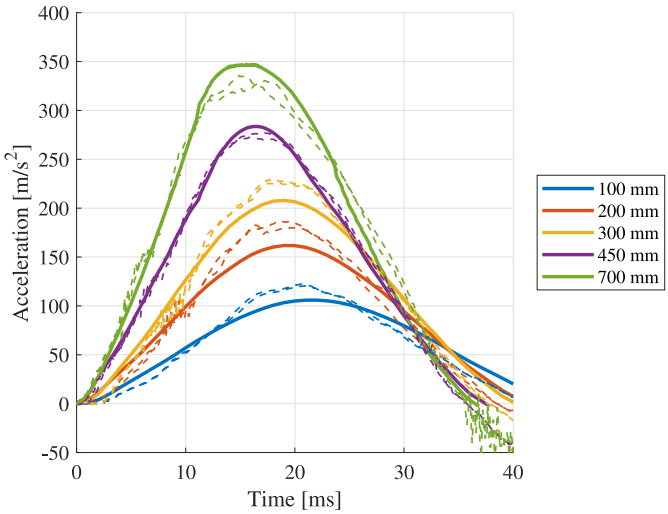

Fig. 13. Comparison of impactor acceleration according to reference model (solid line) and experiments (dashed line).

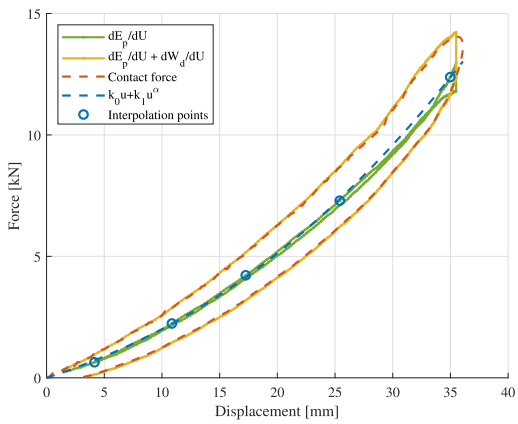

Fig. 14. Example of calibration of nonlinear SDOF model from the hysteresis loop provided by the reference model.

When contact is established, the movement of the impactor mass centroid can be represented by an SDOF system subjected to free vibration. It then follows that the pulse time, which corresponds to half the natural period of the system, can be employed for estimating a linear stiffness. Using this approach, a pulse time of 38 ms was considered for estimating an approximate stiffness, which is close to the pulse time measured for a drop height of 450 mm. Hence, the natural period of the system can be approximated as $T = 2 \cdot 38 = 76$ ms, corresponding to an angular frequency of $\omega = 82.7$ rad/s. Accordingly, the stiffness is given by $k = m\omega^2 = 342$ kN/m. Similar to the nonlinear system, a stiffness-proportional damping was considered (i.e. a ordinary dashpot) with a damping coefficient calibrated to $c = 445$ N s/m (corresponding to a damping ratio of $\zeta = 5.4\%$). The acceleration computed with the linear SDOF model is shown in Fig. 15b. Notice that there is an instantaneous acceleration in the acceleration curves, which is a consequence of the initial damping force being linearly proportional to the prescribed initial velocity. Also, the computed pulse time is, as expected for a linear system, not dependent on the impact energy.

Table 4
Rayleigh parameters for the glass panel substructure and natural periods and damping ratios for the assembled system.

Glass thickness	α	β	T_1 [ms]	T_2 [ms]	ζ_1[a] [%]	ζ_2[a] [%]
8 mm	1.25	$1.21 \cdot 10^{-4}$	144.8	26.6	1	9.4
10 mm	1.49	$1.14 \cdot 10^{-4}$	117.6	25.7	1.6	9.1
12 mm	1.67	$1.07 \cdot 10^{-4}$	103.1	24.5	2.3	8.1

[a]Damping ratio computed by means of the MSE method, as described in Section 2.4.

5.2. Evaluation of reduced order models

One of the benefits of the reduced linear model is the possibility to perform a modal decomposition of the coupled system. Beside the possibility to perform computationally efficient modal analyzes, the eigenfrequencies, eigenmodes, and modal responses can be investigating to get further insight into the structural behavior. Moreover, the eigenfrequencies of the global system can be used for calibrating the Rayleigh damping model employed for constructing a damping matrix for the glass panel substructure. The Rayleigh damping parameters can then be utilized in the linear as well as the nonlinear analyzes.

Fig. 17 shows the glass panel mid-point displacement provided by the linear reduced order model, including six component modes in the glass panel reduction basis. Furthermore, the mid-point displacement has been decomposed into the contributions from the first three global modes, shown by separate curves in the figure. As shown, the response can be almost entirely represented by the first two modes, this is true for all the thicknesses studied. In the fundamental global mode, the displacement of the impactor DOF and the glass panel have the same sign, i.e. they are oscillating in-phase as shown in Fig. 19. The second mode, however, is an "out-of-phase"-mode, where the displacement of the impactor and the glass panel have opposite signs. For higher order modes, it turns out that the impactor deformation is very small. This is due to that the impactor mass is large compared to the effective mass in the out-of-plane direction for higher order modes—for anti-symmetric modes the effective mass is zero, and for symmetric modes the effective mass decreases rapidly with the mode order.

The Rayleigh damping parameters for the glass panel were calibrated to match a "best-estimate" damping of 1.7% (c.f. Section 4) for the eigenfrequency of the first and second global mode, respectively [29]. The damping parameters, the corresponding natural periods, and the modal damping ratios are presented in Table 4. Notice

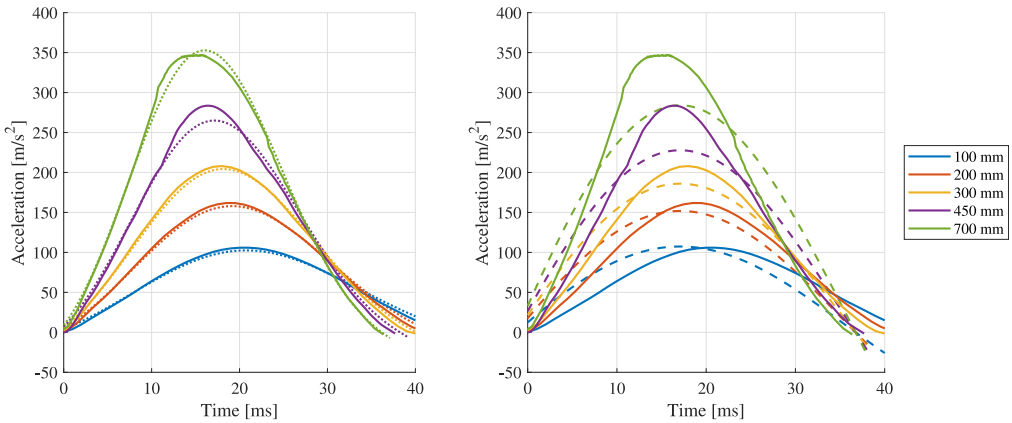

(a) Reference model / Nonlinear SDOF (b) Reference model / Linear SDOF

Fig. 15. Comparison of impactor acceleration according to reference model (solid), nonlinear (dotted) and linear (dashed) SDOF model.

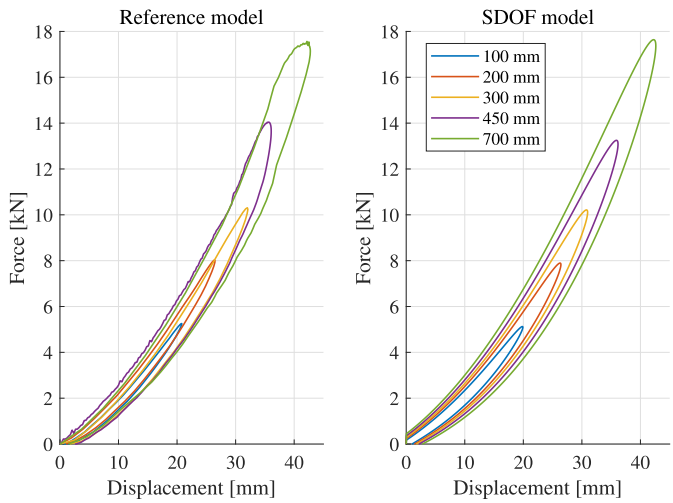

Fig. 16. Comparison of total contact force and centroid displacement computed using the reference model and SDOF system, respectively.

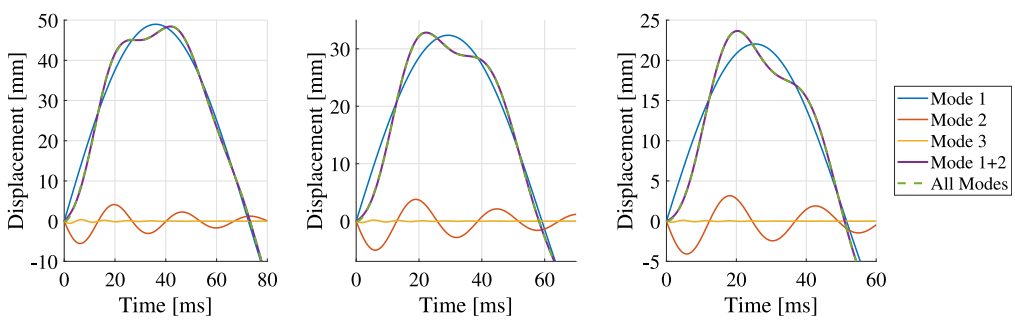

(a) h = 500 mm, t = 8 mm (b) h = 500 mm, t = 10 mm (c) h = 500 mm, t = 12 mm

Fig. 17. Displacement of glass panel mid-point computed with the linear model. The modal contributions for the first three global modes are plotted separately.

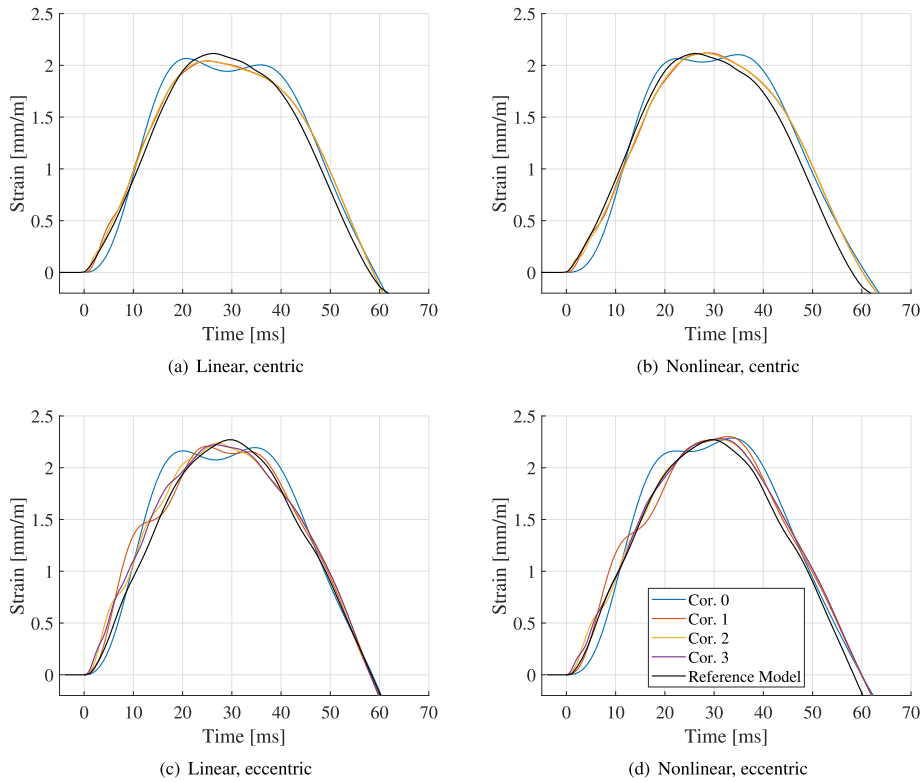

(a) Linear, centric (b) Nonlinear, centric

(c) Linear, eccentric (d) Nonlinear, eccentric

Fig. 18. Horizontal strain provided by the linear and nonlinear reduced order models using various reduction bases. The glass thickness is 10 mm and the drop height is 500 mm. The label "Cor. i" denotes the order of the correction modes, where $i = 0$ implies that only constraint modes are considered.

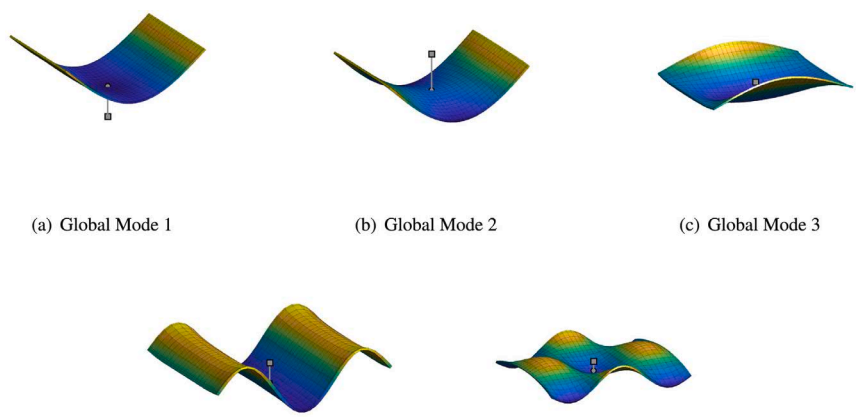

(a) Global Mode 1 (b) Global Mode 2 (c) Global Mode 3

(d) Global Mode 4 (e) Global Mode 5

Fig. 19. First five global modes for assembled reduced system consisting of a linear impactor SDOF model and a reduction basis for the glass panel including a total of six component modes. The impactor mass is shown by the black square.

that the modal damping ratios for the assembled system, computed by means of the MSE method, considers both the Rayleigh-damping prescribed to the glass panel substructure as well as the viscous damping model employed in the impactor SDOF model, which is linearly proportional to the frequency. Consequently, the computed global damping ratios will be frequency dependent, as shown in Table 4.

As discussed in Section 4, the energy loss of the glass–impactor system was estimated to be around 26% for a glass panel thickness of 8 mm and a drop height of 200 mm. The corresponding energy loss provided by the linear model is approximately 18%, indicating that the damping prescribed to the assembled system is somewhat low. However, as discussed in Section 4, the energy loss estimated based on a double impact test should be regarded as a rough estimation due to limitations in the experimental methodology; for example, energy loss related to the motion of the pendulum is not considered, and a linear elastic behavior is assumed.

Fig. 18 shows the horizontal strain on the rear side of the glass panel at the point of impact for various reduction bases applied to the glass substructure. As shown in the figure, the peak-strain is similar for all the models. However, a refined reduction basis is required for the glass substructure to capture the shape of the strain curve, in particular for the eccentric load case. Notice that the reduction basis employed for reducing the glass substructure should be sufficiently large so that the deformed shape of the glass panel for the important global modes can be resolved. Hence, the number of component modes required may be larger than the number of global modes needed for an accurate representation of the global response.

5.3. Validation of numerical models using experimental data

The measured horizontal strain on the rear side of the glass panels are shown for various drop heights and glass thicknesses in Fig. 20, together with the corresponding strain given by the reference model and the reduced linear and nonlinear model, respectively. In the reduced models, the glass panel was reduced using six component modes (i.e. five fixed-interface correction modes and a constraint mode). As shown in the figure, the strain computed with the reference model and the reduced nonlinear model corresponds well to the measured strains for impact tests with a drop height 100 mm. However, the differences are amplified for impact tests with an increasing drop height. The deviation is especially pronounced for the glass panels with thickness 12 mm. Furthermore, it is of interest to evaluate not only the peak strain (even though this, in general, is the governing parameter in a design calculation) but also the shape of the strain curves indicating how well the models capture the structural behavior. As shown in the figure, the shape of the strain curves is relatively close for glass panels with thickness 8 mm, whereas the shape of the computed strain curves somewhat differ for glass panels with larger thickness.

The strain provided by the linear model is very close to the response computed with the nonlinear reduced model for the cases with a drop height of 500 mm. This is due to that the stiffness prescribed to the linear model fits better for larger amplitudes, as manifested by the acceleration curves in Fig. 15. Accordingly, the pulse time is slightly underestimated by the linear model for lower drop heights .

To further corroborate the results, the calculated and measured data can be evaluated based on the reference diagrams presented in [11], which are also included in DIN 18008-4 [41]. The reference diagrams result from experimental data and numerical simulations and provide the pendulum acceleration as well as the peak principal stress for a reference plate, having width 1000 mm and height 700 mm. Both results for all-sided and two-sided (supported at the short ends), continuously supported plates are presented, the latter being comparable to the glass plates studied herein. Further, the reference diagrams consider a pendulum drop height of 200 mm and 450 mm, respectively. In particular, the principal peak stress for impact with drop height 200 mm against the center of the two-sided reference plate is approximately 140 MPa. The corresponding stress given by the Abaqus reference analysis is 131 MPa (the peak strain shown in Fig. 20 is thus given by $\epsilon_{xx} = (\sigma_{xx} - \nu\sigma_{yy})/E$, where the vertical stress according to the analysis is $\sigma_{yy} = 59$ MPa). It should be noted, however, that the height of the glass plate studied herein is 800 mm. Thus, a slightly lower stress is expected.

According to the reference diagrams, the pendulum peak acceleration during impact with a rigid body is approximately 170 m/s^2 and 265 m/s^2 for drop heights 200 mm and 450 mm, respectively. As shown in Fig. 13, this is in good agreement with the computed and measured accelerations.

6. Discussion

When verifying the load-bearing capacity of glass structures subjected to impact loading, time efficient and user-friendly design tools can be of great utility, allowing for an interactive design process where alternative designs may be tested. In the present study, an approach using DS have been employed for developing reduced order models that are computationally efficient while providing an accurate prediction of the pre-failure elastic response. For the studied load cases, the coupled glass–impactor system can be well-represented by only two global modes. However, it should be noted that the influence of higher order modes might not be negligible for larger glass panels or panels with other boundary conditions. Moreover, it was shown that up to four component modes may be required to resolve the displacement of the glass panel in the global modes.

A reduction basis for the glass panel was constructed using correction modes, as further discussed in Section 2.1. An alternative could be to construct a reduction basis by means of the traditional C-B or Rubin approaches, that uses the fixed- and free-interface normal modes, respectively. However, not much would be gained if these methods were applied to linear systems, i.e. where linear subsystems are used for modeling the glass panel as well as the impactor. The assembled system includes $m + 1$ DOFs, i.e. the glass panel has a total of m DOFs and an additional DOF is added representing the displacement of the lumped impactor mass. Clearly, the computational cost for generating a set of component normal modes or global eigenmodes is in practice identical. On the contrary, an approach using correction modes replaces the eigenvalue problem by a number of matrix–vector multiplications. Furthermore, the set of correction modes, by definition, excludes redundant modes, which cannot be excited by loading on the substructure boundary. Accordingly, there are no anti-symmetric mode shapes in the global modal basis, as shown in Fig. 19.

As discussed in Section 2.4, linear systems can be solved by means of modal dynamics, which in turn enables a closed-form solution for initial value problems. However, a time discretization is required for identifying the peak glass strain during impact. Moreover, the generalized coordinates must be transformed to physical displacements in each time increment, which in turn can be used for computing the glass strain. Consequently, the post-processing of the dynamic response can become computationally expensive. An approach using modal summation techniques can be employed to overcome this problem. For example, a conservative evaluation can be made by means of an absolute summation of the modal responses. Since only one set of data needs to be evaluated in the physical domain the computational effort in the post-processing stage is reduced significantly. However, it should be noted that the modal phase information is lost in a modal summation, why an absolute summation may be too conservative in some applications.

In general, the developed models show good agreement with the experimental results. However, there are some discrepancies, which are especially pronounced for glass panels with a nominal thickness of 12 mm (see Fig. 20). The deviation can be due to errors/imperfections in the experimental set-up and/or inadequate modeling abstractions, such as the assumption of a constant contact area, neglection of geometric nonlinearity (i.e. membrane action), and an assumed viscous

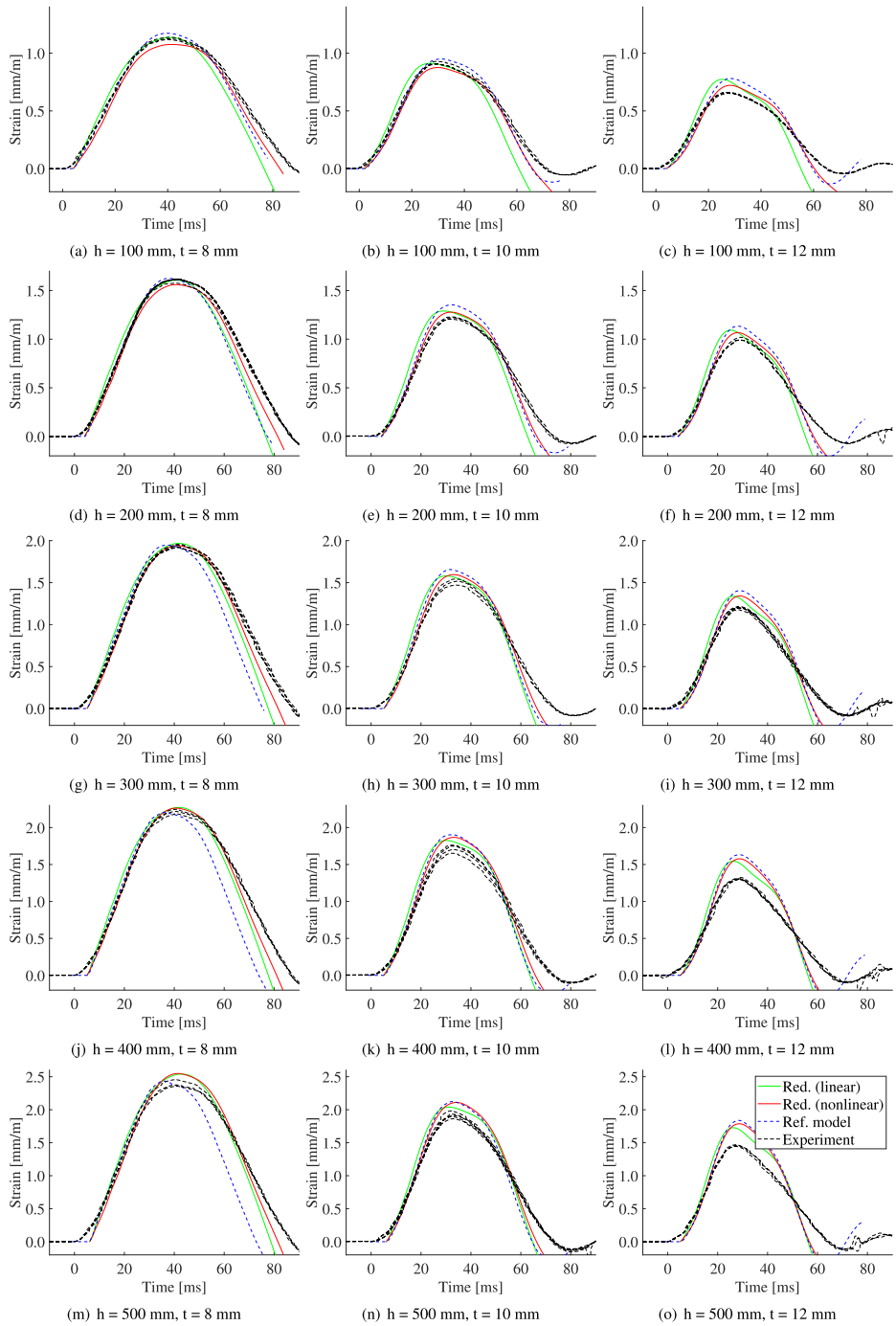

Fig. 20. Comparison between the measured and computed glass strain on the rear side of the glass panel at the center of impact. The impactor drop height, h, is 100 to 500 mm and the glass panel thickness is 8, 10 and 12 mm, respectively.

damping model. Notice, however, that the glass strain curves provided by the reduced models and the numerical reference model are very similar, suggesting that the deviations are due to simplifications made in both models. Recall that both the reduced models and the numerical reference model uses a viscous damping model (in contrast to e.g. a frictional modal) and, furthermore, ignores the dynamic air pressure in the impactor tires. One can thereby assume that these simplifications, or other unknown errors, are the reason for the deviations.

The damping matrix of the glass substructure was constructed by means of Rayleigh-damping, using both mass- and stiffness-proportional damping. This damping model is convenient since it can be utilized in the physical as well as the modal domain. It should be noted, however, that a damping model being proportional to the structure mass is clearly unphysical (see e.g. [29]). A more refined damping model may be developed. Moreover, by means of further experimental studies, the frequency dependency of the glass panel as well as the impactor damping can be investigated.

For the glass panel with thickness 8 mm, the shape of the strain curve given by the numerical reference model deviates from the curves obtained with the other models. The pulse is shorter whereas the peak strain is fairly close to the peak strain of the other curves. Because the deviation is pronounced for the 8 mm glass panel, having a bending stiffness considerably lower than the thicker panels, it is reasonable to claim that this discrepancy is due to membrane action being manifested by a stiffer response (i.e. shorter pulse). Recall that geometric nonlinearity is considered in the numerical reference model, while these effects are ignored in the reduced order models. However, one would then expect the measured strains to be closer to the strain provided by the reference model, which is not what the experimental data suggests. Nonetheless, the influence of membrane action can still be one of the reasons for the discrepancy. The stiffness of the rubber strips along the supports, modeled by means of elastic spring beds, affects the influence of membrane action. The stiffness of the rubber strips (and the in-plane stiffness, in particular) can be regarded as a particularly uncertain parameter, which is influenced by the prestressing force due to bolting of the glass panels. Hence, the influence of membrane action might not be accurately captured by the reference model, even though geometric nonlinearity is considered. Furthermore, it is plausible that the stiffness of the rubber strips are in fact nonlinear, e.g. due to friction between the rubber and the glass/steel surface.

Finally, it should be noted that the presented reduced order models may also be employed for analyzing laminated glass, as long as the glass panel response can be approximated as linear.

7. Conclusions

The paper presents strategies for reduced order modeling of glass panels subjected to soft-body impact. The aim was to develop accurate reduced order models for computation of the pre-failure elastic response, suitable for implementation in user-friendly interactive design tools. Concepts for reduced modeling of the glass panel, the impactor and the contact interaction between the glass panel and the impact body were investigated. In particular, a methodology is proposed for calibrating a nonlinear SDOF model representing the impactor. Furthermore, a model validation was performed based on experimental tests and a detailed numerical reference model. Moreover, a fixed-interface DS method that uses correction modes was successfully employed for developing computationally efficient models of the coupled impactor–glass system. The following conclusions can be drawn:

- The measured glass strains and the strains provided by the numerical models are fairly close. The discrepancy is similar for the reduced models and the reference model, suggesting that the deviations are due to inadequate modeling abstractions applied in both models.
- The impactor acceleration measured during impact with a very stiff steel column (which can be considered rigid) is close the acceleration provided by the numerical reference model.
- A nonlinear SDOF model representing the impactor was successfully calibrated to the reference model. In particular, the acceleration computed for impact with a rigid surface with the nonlinear SDOF model showed very good agreement with the acceleration provided by the numerical reference model.
- The evaluation of the reduced order models suggests that a simplified modeling approach assuming a constant contact area is fairly accurate.
- Reduction bases including correction modes turn out to be particularly suitable for implementation in design tools, such as *ClearSight*, where a manual selection of component modes should be avoided. The set of correction modes automatically excludes redundant modes that cannot be excited by loading on the substructure boundary.
- If the impactor is approximated by a linear model, a closed-form solution can be obtained by means of the modal strain energy method, which enables the use of modal expansion techniques for lightly damped systems with non-proportional damping. For the studied load cases, the coupled glass–impactor system can be well-represented by only two global modes.
- A very computationally efficient approximate evaluation of the glass strain can be obtained if a closed-form modal solution is combined with a modal summation technique, e.g. an absolute summation of the peak modal responses. Using this approach, a time discretization in the physical domain is avoided.

CRediT authorship contribution statement

Linus Andersson: Conceptualization, Methodology, Investigation, Validation, Software, Formal analysis, Writing – original draft, Writing – review & editing. **Marcin Kozłowski:** Conceptualization, Investigation, Validation, Writing – review & editing, Funding acquisition. **Peter Persson:** Conceptualization, Investigation, Validation, Writing – review & editing. **Per-Erik Austrell:** Conceptualization, Validation, Writing – review & editing. **Kent Persson:** Conceptualization, Investigation, Validation, Software, Writing – review & editing, Funding acquisition.

Declaration of competing interest

The authors declare that they have no known competing financial interests or personal relationships that could have appeared to influence the work reported in this paper.

Acknowledgments

Financial support from the Reconcile project, a part of the EU program Interreg IVA, and the Swedish glass associations; Glasbranschföreningen, Svensk Planglasförening and Balkongföreningen i Norden is gratefully acknowledged. ÅForsk Foundation is acknowledged for financing the part with the experimental campaign, grant ref. no. 18-510.

References

[1] SS-EN-12600. Glass in building-pendulum test-impact test method and classification for flat glass. Swedish Standards Institute; 2003.
[2] Persson K, Doepker B. Glass panes subjected to dynamic impact loads. In: Proceedings of the xxiv a.t.i.v. conference. 2009.
[3] Kozłowski M. Experimental and numerical assessment of structural behaviour of glass balustrade subjected to soft body impact. Compos Struct 2019;229:111380.
[4] Pelfrene J, Dam SV, Kuntsche J, Paepegem WV. Numerical simulation of the EN 12600 pendulum test for structural glass. In: Challenging glass, Vol. 5. Ghent: Ghent University; 2016.
[5] Timmel M, Kolling S, Osterrieder P, Du Bois P. A finite element model for impact simulation with laminated glass. Int J Impact Eng 2007;34(8):1465–78.

[6] ClearSight. Computer software. Department of Construction Sciences, Lund University.
[7] Fröling M, Persson K, Austrell P-E. A reduced model for the design of glass structures subjected to dynamic impulse load. Eng Struct 2014;80:53–60.
[8] Janda T, Schmidt J, Hála P, Konrád P, Zemanová A, Sovják R, Zeman J, Šejnoha M. Reduced order models of elastic glass plate under low velocity impact. Comput Struct 2020;244:106430.
[9] Viviani L, Consolaro A, Maffeis M, Royer-Carfagni G. Engineered modelling of the soft-body impact test on glazed surfaces. Eng Struct 2021;226:111315.
[10] Schneider J, Bohmann D. Glasscheiben unter stoß belastung - experimentelle und theoretische untersuchungen für absturzsichernde verglasungen bei weichem stoß. Bauingenieur 2002;77(12):581–92.
[11] Schneider J, Schula S. Simulating soft body impact on glass structures. Proc Inst Civ Eng: Struct Build 2016;169(6):416–31.
[12] Alonso J, Parra J, Pacios A, Huerta M. Similarity index: A procedure for comparing impact time histories validated with soft impact test. Eng Struct 2019;198:109513.
[13] Parra J, Alonso J, Pacios A, Huerta M. Effective energy applied to a glass plate during an impact test. Int J Impact Eng 2019;130:11–8.
[14] Bez A, Bedon C, Manara G, Amadio C, Lori G. Calibrated numerical approach for the dynamic analysis of glass curtain walls under spheroconical bag impact. Buildings 2021;11(4):154.
[15] Popov VL, Heß M, Willert E. Handbook of contact mechanics. Berlin Heidelberg: Springer; 2019.
[16] Bohmann D, Mepla SJ. Software for structural glass design. 2000, www.mepla.net.
[17] Craig R, Hale A. Block-krylov component synthesis method for structural model reduction. J Guid Control Dyn Amer Inst Aeronaut Astronaut 1988;11(6):562–70.
[18] Rixen DJ. High order static correction modes for component mode synthesis. In *Proceedings of the fifth world congress on computational mechanics*, Vienna, Austria, 7–12 July, 2002.
[19] Simulia. Abaqus v. 6.14. Computer software and online documentation, Providence, RI, USA: Dassault Systems.
[20] Feldman M, Kaspar R, Abeln B, Gessler A, Langosch K, Beyer J, et al. Guidance for european structural design of glass components. Publications Office of the European Union; 2014.
[21] de Klerk D, Rixen DJ, Voormeeren SN. General framework for dynamic substructuring: History, review, and classification of techniques. AIAA J 2008;46(5):1169–81.
[22] Flodén O, Persson K, Sandberg G. Reduction methods for the dynamic analysis of substructure models of lightweight building structures. Comput Struct 2014;138:49–61.
[23] Craig Jr RR, Kurdila AJ. Fundamentals of structural dynamics. 2nd ed.. New Jersey: John Wiley & Sons; 2006.
[24] Craig RR, Bampton MCC. Coupling of substructures for dynamic analysis. AIAA J 1968;6(7):1313–9.
[25] MacNeal RH. A hybrid method of component mode synthesis. Comput Struct 1971;1(4):581–601.
[26] Rubin S. Improved component-mode representation for structural dynamic analysis. AIAA J 1975;13(8):995–1006.
[27] Andersson L, Persson P, Persson K. Model reduction for structures subjected to blast loading by use of dynamic substructuring. In: Proceedings of eurodyn 2020, xi international conference on structural dynamics. Greece: Streamed from Athens; 2020, p. 2544–64.
[28] Trefethen LN, Bau D. Numerical linear algebra. Philadelphia: SIAM; 1997.
[29] Chopra AK. Dynamics of structures. In: Theory and applications to earthquake engineering. 5th ed.. NJ: Prentice Hall; 2016.
[30] Hoen C. An engineering interpretation of the complex eigensolution of linear dynamic systems. In: Imac xxiii. Orlando, USA; 2005.
[31] Jiang Q, Zhou Z, Huang W. Investigation on the modal strain energy for dynamic analysis of steel-concrete vertically mixed structures. J Asian Archit Build Eng 2015;14(3):671–8.
[32] Tsai M-H, Chang K-C. A study of the modal strain energy method for viscoelastically damped structures. J Chin Inst Eng 2001;24(3):311–20.
[33] Bolarinwa EO, Olatunbosun OA. Finite element simulation of the tire burst test. In *Proceedings of the institution of mechanical engineers*, Birmingham, England, 2004.
[34] Björklund E, Christoffersson A. Computational modeling and experimental verification of soft-body impact on glass structures Report TVSM-5246, (Master's thesis), Lund: Lund University; 2020.
[35] Cardoso RPR, Yoon JW, Mahardika M, Choudhry S, Alves de Sousa RJ, Fontes Valente RA. Enhanced assumed strain (EAS) and assumed natural strain (ANS) methods for one-point quadrature solid-shell elements. Internat J Numer Methods Engrg 2008;75(2):156–87.
[36] Fröling M, Persson K. Computational methods for laminated glass. J Eng Mech 2013;139(7):780–90.
[37] Kozłowski M, Persson K, Honfi D, Portal NW. Structural behaviour of glass panels under soft-body impact. In: Challenging glass 7. Ghent: Ghent University; 2020.
[38] Kozłowski M. Structural safty of glass components. Report tvsm-7169, Sweden: Lund University; 2020.
[39] Ramos A, Pelayo F, Lamela MJ, Fernández Canteli A. Evaluation of damping properties of structural glass panes under impact loading. In *Proceedings of cost action tu0905, mid-term conference on structural glass*, Poreč, Croatia, 2013.
[40] Bedon C, Fasan M, Amadio C. Vibration analysis and dynamic characterization of structural glass elements with different restraints based on operational modal analysis. Buildings 2019;9(13).
[41] DIN 18008-4: glass in building – design and construction rules – part 4: additional requirements for barrier glazing. Berlin, Germany: DIN; 2013.

Paper D

Mechanical Systems and Signal Processing 191 (2023) 110143

Contents lists available at ScienceDirect

Mechanical Systems and Signal Processing

journal homepage: www.elsevier.com/locate/ymssp

Efficient nonlinear reduced order modeling for dynamic analysis of flat structures

Linus Andersson *, Peter Persson, Kent Persson

Department of Construction Sciences, Lund University, Sweden

ARTICLE INFO

Communicated by J. Noël

Keywords:
Geometrically nonlinear
Dynamic analysis
Non-intrusive model order reduction
Flat structures
Nonlinear finite element model
Modal derivatives

ABSTRACT

In the present paper, strategies for reduced order modeling of geometrically nonlinear finite element models are investigated. Simulation-free, non-intrusive approaches are considered, which do not require access to the source code of a finite element program (e.g., proprietary knowledge). Our study focus on but is not restricted to flat structures. Reduction bases are generated using bending modes and the associated modal derivatives, which span the additional subspace needed for an adequate approximation of the geometrically nonlinear response. Moreover, the reduced nonlinear restoring forces are expressed as third order polynomials in modal coordinates. Consequently, the reduced systems can be effectively solved using time-integration schemes involving only the reduced coordinates. A bottleneck in the non-intrusive methods is typically the computational effort for precomputing the polynomial coefficients and generating the reduction basis. In this regard, we demonstrate that modal derivatives have several useful properties. In particular, the modal derivatives essentially provide all the information needed for generating the polynomial coefficients for the in-plane coordinates. For condensed systems, which ignores the inertia of the in-plane modes, we show that the modal derivatives can be used effectively for recovering the in-plane displacements. Based on these findings, we propose a methodology for generating reduced order models of geometrically nonlinear flat structures in a computationally efficient manner. Moreover, we demonstrate that the concepts extend also to curved structures. The modeling techniques are validated by means of numerical examples of solid beam models and continuously supported shell models. The computational efficiency of the proposed methodology is evaluated based on the number of static evaluations needed for identifying the polynomial coefficients, as compared to the state-of-the-art methods. Furthermore, strategies for efficient time integration are discussed and evaluated.

1. Introduction

In many engineering applications, numerical models are vital tools for investigating structures subjected to dynamic loading. The most popular method for developing numerical models is the finite element (FE) method, which allows for a discretization of continuous structural dynamic problems [1]. Particularly for thin, lightweight structures, it can be important to use an FE formulation considering large deformation theory. This implies solving a geometrically nonlinear system, requiring a time-stepping procedure where the nonlinear restoring forces are updated, in general using iterative techniques (e.g. the Newton–Raphson method) [2]. Because the FE models typically include a large number of degrees-of-freedoms (DOFs), such analyses can be time-consuming and, consequently, there is a need for efficient modeling strategies. To this end, several reduced order modeling

* Corresponding author.
E-mail address: linus.andersson@construction.lth.se (L. Andersson).

https://doi.org/10.1016/j.ymssp.2023.110143
Received 11 July 2022; Received in revised form 25 November 2022; Accepted 19 January 2023
Available online 7 February 2023

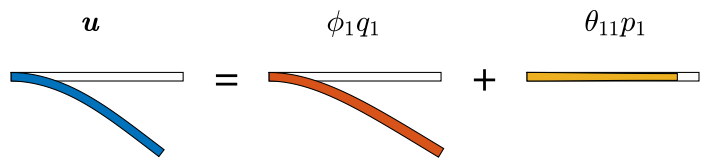

Fig. 1. Example of approximate displacements **u** for a transversely loaded cantilever beam, decomposed into the first eigenmode ϕ_1 and an in-plane mode, namely the associated modal derivative θ_{11}. Note that the physical displacement fields are unscaled whereas the modal amplitudes are governed by the modal coordinates q_1 and p_1, respectively.

techniques have been proposed during the last few decades, aiming to decrease the system size while providing accurate results [3–13].

Analogous to the modal techniques commonly used for linear FE models (see e.g. [14,15]), nonlinear reduced order models (NLROMs) can be obtained by projecting the system equations onto a reduction basis. Thus, instead of solving a system expressed in terms of physical DOFs, the structural response is approximated using a substantially reduced set of modal coordinates. Furthermore, by using a Taylor series expansion around the point of equilibrium, the reduced nonlinear restoring forces can be expressed in terms of the reduced coordinates [6,16]. Consequently, the NLROM approach, sometimes referred to as polynomial tensor hyper-reduction [16], avoids computationally expensive evaluations of the nonlinear restoring forces based on the full system. Hence, the NLROM can be solved using standard time-stepping procedures (e.g. Newmark's family of methods) involving a substantially reduced set of variables and, accordingly, a significantly reduced computational cost.

The non-intrusive NLROM approaches, which uses the polynomial tensor technique, have turned out to be particularly useful because it enables the use of numerical routines already implemented in most FE analysis software packages (e.g. Abaqus, Nastran). Furthermore, proprietary knowledge of the FE implementation, such as element formulations, is not required. In principle, establishing a non-intrusive NLROM involves two fundamental problems: generating a suitable reduction basis, and computing the entries of the higher order stiffness tensors, often referred to as nonlinear stiffness coefficients (NSCs) [13].

The accuracy of an NLROM is highly dependent on the properties of the reduction basis. More specifically, the reduction basis should span a subspace where a good approximation of the full solution can be established. For a linear system, the dynamic response can typically be well-represented by a small set of low-frequency eigenmodes. However, this is generally not true for geometrically nonlinear systems. For instance, the bending normal modes of a linearized, cantilever beam model only involve out-of-plane displacements. However, the geometrically nonlinear response of a transversely loaded cantilever beam result in out-of-plane as well as in-plane displacements. Hence, to obtain an accurate model, a reduction basis enriched by high frequency in-plane modes is required (cf. Fig. 1). The same issue arises for a general structure; thus, a sufficient subspace is not spanned by a few low-frequency modes, and, accordingly, additional basis vectors are required.

Various techniques have been proposed to approach the problem. Kim et al. [17] introduced so-called dual (or companion) modes. McEwan et al. [4] proposed a regression analysis, referred to as implicit condensation (IC), to account for high frequency modes. Hollkamp et al. [7] further developed this approach by introducing an additional post-processing step, referred to as the implicit condensation and expansion (ICE) method. Specifically for flat structures, Kim et al. [9], Wang et al. [18], and Vizzaccaro et al. [19] proposed condensation methods using similar concepts, where only the quasi-static response of the high frequency (in-plane) modes are considered. Barbič and Doug [6], Rutzmoser [16], Wu et al. [20,21], Weeger et al. [22] and Mahdiabadi et al. [13] introduced reduction bases enriched by modal derivatives. Furthermore, a somewhat different technique was proposed in [10,11,16], referred to as the quadratic manifold (QM) approach, which uses a nonlinear (quadratic) mapping instead of an invariant linear subspace. The preferred approach depend on the specific application and, in particular, if it allows for static condensation of certain coordinates, e.g. related to high-frequency (in-plane) modes. For the sake of completeness, it should be mentioned that reduction bases can also be generated using data-driven methods, such as the Proper Orthogonal Decomposition (POD) (see e.g. [16]). In this context, the QM approach has also been proposed for cost-effective generation of training sets [23]. Furthermore, machine learning based simulation frameworks using neural networks have been introduced for general ROM approaches, see e.g. [24]. However, in this study, focus is on simulation-free methods, meaning that training simulations of the full-order dynamic problem are avoided. While the data-driven methods allow for arbitrary NLROMs, the simulation-free approaches can be particularly useful for structures where the nonlinear restoring forces can be well-represented by cubic polynomials, since the generation of training sets is avoided.

Regarding the second problem of non-intrusive NLROMs—determining the NSCs—two procedures are commonly used, sometimes referred to as the applied force (AF) and the enforced displacement (ED) method, respectively [12]. The AF approach, first proposed by McEwan et al. [4], requires that several nonlinear static problems are solved for the full-order system. However, it is the basis in the ICE method, which in turn enables a particularly efficient approach for recovering the displacements of the full model. The ED method, also referred to as STEP (STiffness Evaluation Procedure), was first introduced by Muravyov and Rizzi [3], and is the basis in several techniques [3,9,13,17–19,25–27]. Similar to the AF method, this procedure requires that several static problems are solved. However, the static problems are defined using enforced displacement fields instead of external forces. Consequently, iterative solution techniques can be avoided if using hyperelastic ("memoryless") constitutive models; thus, static solutions are simply obtained by evaluating the internal forces for prescribed displacement fields. Moreover, the number of required load cases can be further decreased by using the enhanced enforced displacement (EED) method [27]. A review of non-intrusive NLROM techniques can be found in [28].

With respect to computational efficiency, a bottleneck in the non-intrusive methods is typically the *offline* cost, referring to the computational cost required for establishing the system matrices before the dynamic response analysis is initiated. This includes both the computational effort related to the generation of basis vectors as well as calculating the NSCs. In contrast, the computational *online* cost concerns the time-stepping procedure. For cases where the dynamic response is to be evaluated during a short time frame, such as impact analyses, the online cost is typically significantly smaller than the offline cost. However, if the analysis necessitates long time records, e.g. in random response analyses, the online cost can be significant. Furthermore, as discussed in e.g. [13,18], issues related to numerical round-off errors can be a significant problem, both with regard to convergence and accuracy. Thus, to enable efficient and accurate NLROMs using non-intrusive methods, there is a need to develop methods for reducing the offline and online cost, and ensuring sufficient accuracy of the NSCs.

In the present paper, the aim is to develop cost-effective strategies for non-intrusive reduced order modeling of geometrically nonlinear structures. Our study is focused on flat and slightly curved, shallow structures. These types of structures are often characterized by a geometrically nonlinear behavior and appear in several engineering applications, such as design of glass barriers (see e.g. [29,30]), or applications within the aerospace industry [8,27]. The NLROMs are generated using reduction bases including out-of-plane bending modes and the associated modal derivatives. Moreover, the generation of the out-of-plane modes is accelerated by means of a Krylov-subspace approach that considers the spatial distribution of the external load [31]. Using this approach, redundant eigenmodes, that cannot be (explicitly) excited by the external load is automatically excluded.

For the specific case of flat structures, it turns out that the modal derivatives associated to out-of-plane bending modes have several useful properties. In particular, we show that the modal derivatives essentially provide all the information needed for generating the NSCs for the in-plane basis. Furthermore, the modal derivatives can be used effectively for recovering the in-plane displacements for condensed systems, which ignores the dynamics of the in-plane coordinates (see e.g. [9,18,19]).

Based on these findings, we propose a procedure for developing NLROMs in a computationally efficient manner. The modeling strategies can, in addition to beam and shell models, be applied to structures modeled using solid elements. Moreover, we show that the concepts can be extended also to slightly curved structures. Finally, a decondensation approach for mitigating the influence of numerical round-off errors, which was proposed in [9,18], is investigated for NLROMs established using modal derivatives.

The paper is structured as follows. In Section 2, the governing equations for NLROMs and techniques for precomputing the NSCs are presented. Section 3 presents methods for generating reduction bases. In Section 4, we introduce methodologies for developing NLROMs in a computationally efficient manner. In particular, concepts with/without in-plane dynamics are considered. In Section 5, the NLROM techniques are evaluated by means of numerical examples, based on FE models developed using both MATLAB and the commercial software Abaqus. Various approaches for considering the in-plane response are evaluated as well as strategies for mitigating the influence of numerical round-off errors. Finally, the results are discussed in Section 6 and conclusion are presented in Section 7.

2. Equations of motion for nonlinear reduced order models

An FE formulation of a structural dynamics problem result in a multi-degree-of-freedom (MDOF) system, for which the equations of motion can be expressed in matrix form:

$$\mathbf{M}\ddot{\mathbf{u}}(t) + \mathbf{C}\dot{\mathbf{u}}(t) + \mathbf{f}(\mathbf{u}(t)) = \mathbf{g}(t) \tag{1}$$

where $\mathbf{M}$ and $\mathbf{C}$ are the $n \times n$ mass and (viscous) damping matrix, respectively, n being the number of physical DOFs. Further, $\mathbf{u}$ is the $n \times 1$ displacement vector (dot notation is used for differentiation with respect to time), and $\mathbf{f}$ and $\mathbf{g}$ are the $n \times 1$ restoring force and external force vector, respectively (henceforth, the time-dependence of variables is left out for compactness).

In this work, lightly damped, geometrically nonlinear systems are considered and, accordingly, the restoring force vector in Eq. (1) is amplitude-dependent. Further, it is assumed that the viscous damping matrix is stiffness-proportional (i.e. Rayleigh β-damping [15]), which implies that the damping matrix in general depend on the displacement magnitude. However, to simplify the notation, the amplitude-dependence of the damping is omitted in the derivations (for further details on the specific damping applied in the numerical investigations, see Section 5).

The FE model typically involves a large number of DOFs which can lead to a significant computational cost. To decrease the system size, a ROM can be obtained by applying a $n \times N$ reduction basis, $\mathbf{V}$, where N is the number of basis vectors, also referred to as mode shapes (in the following, the terms *mode* and *basis vector* are used interchangeably). Further, it is assumed that the number of modes is significantly smaller than the number of physical DOFs, i.e. $N \ll n$. It follows that the FE model physical displacements can be expressed in terms of a reduced set of generalized coordinates $\boldsymbol{\eta}$:

$$\mathbf{u} = \mathbf{V}\boldsymbol{\eta} \tag{2}$$

where the size of $\boldsymbol{\eta}$ is $N \times 1$. Hence, the physical displacements are expressed in terms of a linear transformation, such that the generalized coordinates determines the amplitude of the mode shapes, corresponding to the columns of $\mathbf{V}$. A reduction of the system size is thus achieved by assuming that the solution lives in a subspace, spanned by $\mathbf{V}$. This projective reduced order modeling approach are frequently used in linear dynamics, where the reduction basis typically consist of a few low-freqency eigenmodes of the linearized system (see e.g. [14,15]). However, it should be noted that any type of basis vectors can be used, and the subspace projection technique is not restricted to linear systems. Specifically, the equations of motion for a NLROM can be expressed as:

$$\mathbf{M}_r\ddot{\boldsymbol{\eta}} + \mathbf{C}_r\dot{\boldsymbol{\eta}} + \mathbf{f}_r(\boldsymbol{\eta}) = \mathbf{g}_r \tag{3}$$

where

$$\mathbf{M}_r = \mathbf{V}^{\mathrm{T}}\mathbf{M}\mathbf{V}, \quad \mathbf{C}_r = \mathbf{V}^{\mathrm{T}}\mathbf{C}\mathbf{V}, \quad \mathbf{f}_r = \mathbf{V}^{\mathrm{T}}\mathbf{f}(\mathbf{V}\boldsymbol{\eta}), \quad \mathbf{g}_r = \mathbf{V}^{\mathrm{T}}\mathbf{g}.$$

Here, $\mathbf{M}_r$ and $\mathbf{C}_r$ are the $N \times N$ reduced mass and damping matrix, respectively, and $\mathbf{f}_r$ and $\mathbf{g}_r$ are the $N \times 1$ reduced nonlinear restoring force and external force vector, respectively.

The NLROM can be solved using standard time-stepping schemes (e.g. Newmark's family of methods), where the nonlinear restoring forces, in general, needs to be updated in each time increment using iterative techniques (e.g. the Newton–Raphson method). However, as indicated by Eq. (3), this would require an evaluation of the full nonlinear restoring force vector in each iteration, which can be computationally expensive. To enable a time-stepping procedure involving only the reduced set of generalized coordinates, the reduced nonlinear restoring forces can be expressed as multivariate cubic polynomials [3–9,11,12]. More specifically, an expression can be derived using a Taylor series expansion of the reduced nonlinear restoring forces around the point of equilibrium, namely:

$$\mathbf{f}_r(\boldsymbol{\eta}) \approx \frac{\partial \mathbf{f}_r}{\partial \boldsymbol{\eta}}\boldsymbol{\eta} + \frac{1}{2}\frac{\partial^2 \mathbf{f}_r}{\partial \boldsymbol{\eta}^2}\boldsymbol{\eta}\boldsymbol{\eta} + \frac{1}{6}\frac{\partial^3 \mathbf{f}_r}{\partial \boldsymbol{\eta}^3}\boldsymbol{\eta}\boldsymbol{\eta}\boldsymbol{\eta} = \mathbf{K}^{(1)}\boldsymbol{\eta} + \mathbf{K}^{(2)}\boldsymbol{\eta}\boldsymbol{\eta} + \mathbf{K}^{(3)}\boldsymbol{\eta}\boldsymbol{\eta}\boldsymbol{\eta} \tag{4}$$

where we used the compact tensor notation e.g. employed in [16,19]. Further, $\mathbf{K}^{(1)} = \mathbf{V}^{\mathrm{T}}\mathbf{K}_0\mathbf{V}$ is the $N \times N$ reduced linear stiffness matrix, which can be obtained in a standard manner by projection of the $n \times n$ linearized stiffness matrix $\mathbf{K}_0 = \left.\frac{\partial \mathbf{f}}{\partial \mathbf{u}}\right|_{\mathbf{0}}$. In addition, $\mathbf{K}^{(2)}$ and $\mathbf{K}^{(3)}$, having sizes $N \times N \times N$ and $N \times N \times N \times N$, respectively, are higher order stiffness arrays introduced to consider the nonlinear part of the restoring forces. Methods for precomputing the elements of these higher order stiffness arrays (i.e. the NSCs) are further discussed in Section 2.3. Then, it follows that the reduced nonlinear equation of motion can be expressed, using index notation, as:

$$M_{r,ij}\ddot{\eta}_j + C_{r,ij}\dot{\eta}_j + K^{(1)}_{ij}\eta_j + K^{(2)}_{ijk}\eta_j\eta_k + K^{(3)}_{ijkl}\eta_j\eta_k\eta_l = g_{r,i}. \tag{5}$$

Hence, a NLROM is obtained that only involves the reduced set of generalized coordinates, and thus avoids evaluations of the nonlinear restoring forces in the physical domain.

It can be shown that a Taylor series expansion up to 3rd order (i.e. by considering the higher order stiffness arrays $\mathbf{K}^{(2)}$ and $\mathbf{K}^{(3)}$) provide an exact solution for models that uses a hyperelastic, St-Venant Kirchhoff constitutive model (see e.g. [16]). In general, however, Eq. (4) is an approximation. It should be noted that a fast convergence of the Taylor series expansion is crucial, because the number of NSCs grows exponentially. However, the tensors are fully symmetric, i.e. the indices i, j, k, l, are fully interchangeable; thus, in a numerical implementation, only the unique values need to be considered. Furthermore, the accuracy of the NLROM is highly dependent on the reduction basis, which ideally should span a subspace where the nonlinear solution can be fully resolved. In particular, to obtain an adequate approximation of the response, geometrically nonlinear systems typically require additional high-frequency modes, as further discussed in Section 3.

2.1. Simplified form for flat structures

For flat structures, modeled using beam or shell elements, a linearized FE model can be formulated such that the physical in-plane and out-of-plane displacements are uncoupled (see e.g. [32]). It follows that the in-plane displacements for bending eigenmodes, or any static displacement field due to external forcing in the out-of-plane direction, are zero. Similarly, the out-of-plane displacements for membrane eigenmodes, or any static displacement field due to external forcing in the in-plane direction, are zero. Thus, it is possible to separate the modal basis generated from a flat, linearized structure into in-plane and out-of-plane modes, respectively.

Now, let $\mathbf{q}$ and $\mathbf{p}$ denote the generalized coordinate vectors for the N_b bending modes, and N_m membrane modes, respectively. Then, the physical displacements can be expressed in partitioned form:

$$\underbrace{\begin{bmatrix} \mathbf{u}_b \\ \mathbf{u}_m \end{bmatrix}}_{\mathbf{u}} = \underbrace{\begin{bmatrix} \hat{\mathbf{V}}_b & \mathbf{0} \\ \mathbf{0} & \hat{\mathbf{V}}_m \end{bmatrix}}_{\mathbf{V}} \underbrace{\begin{bmatrix} \mathbf{q} \\ \mathbf{p} \end{bmatrix}}_{\boldsymbol{\eta}} \tag{6}$$

where subscripts b and m refers to bending and membrane coordinates/DOFs, respectively. Further, $\hat{\mathbf{V}}_b$ and $\hat{\mathbf{V}}_m$ have sizes $n_b \times N_b$ and $n_m \times N_m$, respectively, and include the basis vectors for the bending and membrane modes. Here, $\hat{\bullet}$ is introduced to distinguish these matrices from the corresponding bases including the full set of $n = n_b + n_m$ DOFs, henceforth denoted $\mathbf{V}_b$ and $\mathbf{V}_m$, respectively.

By exploiting the partitioned form of the generalized coordinates, Eq. (5), which describe the equation of motion for a general NLROM, can be further simplified. In particular, as e.g. shown in [18], all quadratic coefficients involving three bending coordinates are zero due to the symmetry of the restoring forces, i.e. for flat structures $K^{(2)}_{ijk} = 0$ for all $i, j, k = 1, \ldots, N_b$. Moreover, as demonstrated in [9,18,19], it can be reasonable to assume a linear response of the membrane-modes, which typically have resonance frequencies well-above the frequency content of the forcing. Then, as e.g. shown in [16,18,19], the nonlinear equation of motion can be written in simplified, partitioned form. Specifically, the system equations for the generalized coordinates associated to bending modes can be expressed using index notation, as (where subscript r of the reduced mass and damping matrix, and the reduced external force vector has been omitted to simplify the notation):

$$M_{b,ij}\ddot{q}_j + C_{b,ij}\dot{q}_j + K^{(1)}_{b,ij}q_j + K^{(2)}_{bm,ijk}q_j p_k + K^{(3)}_{b,ijkl}q_j q_k q_l = g_{b,i} \tag{7}$$

and for the in-plane coordinates:

$$M_{m,ij}\ddot{p}_j + C_{m,ij}\dot{p}_j + K^{(1)}_{m,ij}p_j + K^{(2)}_{mb,ijk}q_jq_k = g_{m,i} \tag{8}$$

where a linear response is assumed for the in-plane coordinates.

Similarly, if using compact tensor notation, the system equations can be expressed schematically as follows (where the viscous damping has been excluded for compactness):

$$\begin{bmatrix} \mathbf{M}_b & \mathbf{0} \\ \mathbf{0} & \mathbf{M}_m \end{bmatrix}\begin{bmatrix} \ddot{\mathbf{q}} \\ \ddot{\mathbf{p}} \end{bmatrix} + \begin{bmatrix} \mathbf{K}^{(1)}_b & \mathbf{0} \\ \mathbf{0} & \mathbf{K}^{(1)}_m \end{bmatrix}\begin{bmatrix} \mathbf{q} \\ \mathbf{p} \end{bmatrix} + \begin{bmatrix} \mathbf{K}^{(2)}_{bm}\mathbf{qp} + \mathbf{K}^{(3)}_b\mathbf{qqq} \\ \mathbf{K}^{(2)}_{mb}\mathbf{qq} \end{bmatrix} = \begin{bmatrix} \mathbf{g}_b \\ \mathbf{g}_m \end{bmatrix}. \tag{9}$$

As evident by Eq. (9), the simplified system equations consider the linearized stiffness as well as quadratic coupling coefficients and cubic stiffness coefficients involving three bending coordinates. Further, notice that multiple subscripts of b and m are omitted to simplify the notation (for instance, $\mathbf{K}^{(1)}_{bb}$, $\mathbf{K}^{(2)}_{mbb}$, and $\mathbf{K}^{(3)}_{bbbb}$ are replaced by $\mathbf{K}^{(1)}_b$, $\mathbf{K}^{(2)}_{mb}$ and $\mathbf{K}^{(3)}_b$, respectively).

In addition to flat structures modeled using beam or shell elements, the simplified form can be used to approximate the response of flat structures modeled using solid elements, as e.g. demonstrated in [19]. Then, the in-plane modes are replaced by *non-bending* modes involving longitudinal and/or thickness displacements.

2.2. Static condensation of in-plane modes

As mentioned previously, the eigenfrequencies of the in-plane (or non-bending) modes are typically significantly higher than the frequency of the forcing. Therefore, it can be reasonable to neglect the dynamics of the in-plane coordinates, and thus only consider the quasi-static response (see e.g. [9,18,19]).

By neglecting the inertia terms in Eq. (8), and assuming that the external forcing on the in-plane DOFs is zero, the in-plane coordinates can be expressed in terms of the out-of-plane coordinates:

$$p_j = -\left[K^{(1)}_m\right]^{-1}_{jr} K^{(2)}_{mb,rkl}q_kq_l \tag{10}$$

Furthermore, by substituting Eq. (10) into Eq. (7), the *condensed* system equations can be expressed as:

$$M_{b,ij}\ddot{q}_j + C_{b,ij}\dot{q}_j + K^{(1)}_{b,ij}q_j + \tilde{K}^{(3)}_{b,ijkl}q_jq_kq_l = g_{b,i} \tag{11}$$

where

$$\tilde{K}^{(3)}_{b,ijkl} = K^{(3)}_{b,ijkl} - K^{(2)}_{bm,ijr}\left[K^{(1)}_m\right]^{-1}_{rs} K^{(2)}_{mb,skl} \tag{12}$$

are the condensed stiffness coefficients, meaning that they are adjusted with respect to the quasi-static response of the in-plane coordinates. Hence, even though only the out-of-plane modal coordinates are kept as system variables, the structure is in fact not fully constrained in the in-plane direction. For example, prescribing an out-of-plane modal coordinate q_i, in general, result in out-of-plane as well as in-plane displacements (cf. Fig. 1).

2.3. Precomputation of nonlinear stiffness coefficients

In this work, we utilize the ED and EED method for precomputing the NSCs, which are briefly described in Sections 2.3.1 and 2.3.2 (for further details, see [3] and [27], respectively). Techniques for identifying the condensed stiffness coefficients are discussed in Section 2.3.3, and a brief description of a decondensation method [18] for mitigating the influence of numerical round-off errors is presented in Section 2.3.4.

2.3.1. Enforced displacement method

Because the polynomial structure of the nonlinear forces are known, the NSCs can be determined based on prescribed displacement fields for which the nonlinear internal force vector is known. This is the basic idea of the ED method. Specifically, the reduced nonlinear restoring forces can be calculated as:

$$\mathbf{f}_r(\boldsymbol{\eta}) = \mathbf{V}^{\mathrm{T}}\mathbf{f}(\mathbf{u}) \tag{13}$$

where, as stated previously, $\mathbf{f}$ is the full-order restoring force vector due to the prescribed displacement field $\mathbf{u}$. Furthermore, recall that the reduced nonlinear restoring force vector can be expressed as (cf. Eq. (4)):

$$f_{r,i}(\boldsymbol{\eta}) = K^{(1)}_{ij}\eta_j + K^{(2)}_{ijk}\eta_j\eta_k + K^{(3)}_{ijkl}\eta_j\eta_k\eta_l. \tag{14}$$

Now, assume that the static solution is available for an enforced displacement field given by $\mathbf{u} = \mathbf{v}_j\alpha_1$, where α_1 is an arbitrary scalar. Further, in a similar manner, a static solution can be calculated using a different scalar, α_2. Then, by using Eqs. (13) and (14), and assuming that $\mathbf{V}$ is orthogonal, the NSCs of the form $K^{(2)}_{ijj}$ and $K^{(3)}_{ijjj}$ can be solved by means of algebraic systems of equations (no summation over repeated indices):

$$\begin{cases} f_{r,i}(\boldsymbol{\eta} = \mathbf{e}_j\alpha_1) = K^{(1)}_{ij}\alpha_1 + K^{(2)}_{ijj}\alpha_1^2 + K^{(3)}_{ijjj}\alpha_1^3 \\ f_{r,i}(\boldsymbol{\eta} = \mathbf{e}_j\alpha_2) = K^{(1)}_{ij}\alpha_2 + K^{(2)}_{ijj}\alpha_2^2 + K^{(3)}_{ijjj}\alpha_2^3 \end{cases} \tag{15}$$

where it is assumed that the linear stiffness coefficients $K_{ij}^{(1)}$ are known. Then, as demonstrated in [3], stiffness coefficients having three different indices (i.e. $K_{ijk}^{(2)}$, $K_{ijjk}^{(3)}$, and $K_{ijkk}^{(3)}$) can be determined in a second step, by prescribing displacement fields composed of two different basis vectors. Finally, stiffness coefficients having four different indices ($K_{ijkl}^{(3)}$) can be determined by prescribing displacement fields composed of three different basis vectors. In total, $2N+3N(N-1)+N(N-1)(N-2)/6$ static solutions is needed to determine all the NSCs [27].

For models using St-Venant Kirchhoff materials, an arbitrary magnitude of the prescribed displacement fields can be selected [16]. However, the magnitude may still affect the influence of numerical round-off errors. In the general case, the magnitude should be sufficiently small to ensure convergence, but large enough such that the nonlinear regime is entered.

2.3.2. Enhanced enforced displacement method

The ED method only require a FE program capable of solving nonlinear static problems. Nonetheless, for reduction bases of large or moderate sizes, the number of load cases can become immense and, consequently, the computational offline cost can be unmanageable. However, if the tangent stiffness matrix is available (which, for example, is the case in the commercial software Abaqus), the number of static load cases can be significantly decreased by means of the EED method [27], which is briefly described as follows:

The reduced tangent stiffness matrix can be expressed in terms of the full tangent stiffness matrix, as:

$$\mathbf{K}_r(\boldsymbol{\eta}) = \mathbf{V}^{\mathrm{T}}\mathbf{K}(\mathbf{V}\boldsymbol{\eta})\mathbf{V}. \tag{16}$$

Moreover, the reduced tangent stiffness matrix is the Jacobian of the reduced nonlinear restoring forces with respect to the generalized coordinates $\boldsymbol{\eta}$. Thus, by using Eq. (14), the reduced tangent stiffness can be expressed as follows (see e.g. [13,27]):

$$K_{r,iu} = \frac{\partial}{\partial \eta_u}\left[K_{ij}^{(1)}\eta_j + K_{ijl}^{(2)}\eta_j\eta_l + K_{ijlp}^{(3)}\eta_j\eta_l\eta_p\right] = K_{iu}^{(1)} + \left[K_{iju}^{(2)} + K_{iuj}^{(2)}\right]\eta_j + \left[K_{ijlu}^{(3)} + K_{ijul}^{(3)} + K_{iujl}^{(3)}\right]\eta_j\eta_l \tag{17}$$

Then, similarly to the ED method, sets of two static solutions are generated based on the full-order FE model for enforced displacement fields corresponding to a reduction basis vector, scaled by α_1 and α_2, respectively. Thus, by using Eqs. (16) and (17), one obtains (no summation over repeated indices):

$$\begin{cases} K_{r,iu}(\boldsymbol{\eta} = \mathbf{e}_j\alpha_1) = K_{iu}^{(1)} + \left[K_{iju}^{(2)} + K_{iuj}^{(2)}\right]\alpha_1 + \left[K_{ijju}^{(3)} + K_{ijuj}^{(3)} + K_{iujj}^{(3)}\right]\alpha_1^2 \\ K_{r,iu}(\boldsymbol{\eta} = \mathbf{e}_j\alpha_2) = K_{iu}^{(1)} + \left[K_{iju}^{(2)} + K_{iuj}^{(2)}\right]\alpha_2 + \left[K_{ijju}^{(3)} + K_{ijuj}^{(3)} + K_{iujj}^{(3)}\right]\alpha_2^2 \end{cases} \tag{18}$$

Thereafter, by utilizing that the higher order stiffness arrays are fully symmetric (i.e. the indices are fully interchangeable), all NSCs of the form $K_{iuj}^{(2)}$, $K_{ijj}^{(2)}$, $K_{iujj}^{(3)}$, $K_{ijju}^{(3)}$, and $K_{ijjj}^{(3)}$ can be determined by means of algebraic systems of equations, assuming that the linear stiffness matrix is known. Finally, in a second step, coefficients of the form $K_{ijlu}^{(3)}$ can be determined by enforcing displacement fields composed of two different basis vectors. Further details on the EED method can be found in [27].

It should be noted that, in contrast to the ED method, static displacement fields composed of three different basis vectors is not needed in the identification process. Accordingly, the total number of static cases to be solved for determining all the NSCs is of order $\mathcal{O}(N^2)$, namely $2N + N(N-1)/2$. Hence, significantly smaller than for the ED method.

2.3.3. Condensed stiffness coefficients

For flat structures modeled using beams or shells, the condensed stiffness coefficients $\tilde{K}_{b,ijkl}^{(3)}$ (cf. Eq. (12)) can be computed explicitly by applying the ED method on the out-of-plane DOFs. Hence, the modal displacements are enforced on the $\mathbf{u}_b$ DOFs, while the $\mathbf{u}_m$ DOFs are allowed to move freely, as e.g. demonstrated in [9,18]. This implies that several full nonlinear static problems must be solved using iterative procedures, such as the Newton–Raphson method. In contrast, if all DOFs are prescribed, iterative solution techniques can be avoided; thus, the internal forces can be determined by a single evaluation based on the prescribed displacement field (i.e., as in the original version of the ED method). Nonetheless, because the number of in-plane modes scales quadratically with the number of out-of-plane modes (see Section 3), the condensed approach can still be beneficial. It should be emphasized, however, that this approach implies that the dynamics of the in-plane coordinates is ignored.

A similar approach, referred to as the Modified-STEP (M-STEP) method, was recently proposed by Vizzaccaro et al. [19] for estimating the condensed stiffness coefficients for flat structures (or straight beams) modeled using solid elements. More specifically, the M-STEP method can be applied to flat, solid models where the geometrical and material distribution as well as boundary conditions are symmetric with respect to the middle line/plane of the structure. The resulting NLROM is given by Eq. (11) and, thus, uses the out-of-plane coordinates q as system variables. Further, the M-STEP method assumes that the external forcing is applied solely on the out-of-plane DOFs located in the middle line/plane. Results obtained using the M-STEP method is further investigated in Section 5.1.

2.3.4. Decondensation for mitigating the influence of numerical round-off errors

As discussed in [18], the influence of numerical round-off errors can be a significant issue when using the non-intrusive methods, both with respect to convergence and accuracy. Numerical errors can arise due to the finite precision of computations, but can also be attributed the discrepancies between the total Lagrangian formulation used for defining the NLROMs and the updated Lagrangian formulation commonly employed in commercial FE codes.

To mitigate the influence of such numerical round-off errors, Wang et al. [18] proposed a decondensation technique, specialized for flat structures. In summary, they suggest that the condensed stiffness coefficients $\tilde{K}^{(3)}_{b,ijkl}$ are calculated in a first step, i.e., by enforcing the ED procedure on the out-of-plane DOFs while the in-plane DOFs are allowed to move freely (cf. Section 2.3.3). Further, the coefficients $K^{(2)}_{mb,ijk}$ and $K^{(2)}_{bm,ijk}$ are determined by applying the ED method on all the DOFs in a standard manner. Then, by rearranging the terms in Eq. (12), the decondensed NSCs are calculated as

$$K^{(3)}_{b,ijkl} = \tilde{K}^{(3)}_{b,ijkl} + K^{(2)}_{bm,ijr}\left[K^{(1)}_{m}\right]^{-1}_{rs} K^{(2)}_{mb,slp}. \tag{19}$$

In [18], the in-plane basis was constructed using dual modes. However, the decondensation technique can also be used for reduction bases constructed using modal derivatives, as demonstrated in Section 5.2.

3. Reduction basis for geometrically nonlinear models

There are several ways to generate mode shapes that can be used for constructing a reduction basis. In structural dynamic applications, the most common approach is to generate a set of modes based on the linearized system. This type of modes are herein referred to as *linear modes*, and are further discussed in Section 3.1. Furthermore, modal derivatives, which are derived using modal perturbations, are investigated as means for generating enriched reduction bases appropriate for nonlinear models, see further Section 3.2.

3.1. Linear modes

As described in Section 2.1, the reduction basis for a flat structure can be separated into in-plane and out-of-plane modes. In the following, it is assumed that the set of linear modes only include out-of-plane bending modes. Further, two different types of linear modes are investigated: normal modes (see Section 3.1.1) and force-dependent modes, generated using a Krylov-subspace approach (see Section 3.1.2).

3.1.1. Normal modes

In linear dynamics applications, the eigenmodes of the undamped linearized system, often referred to as *normal modes*, are arguable the most common type of reduction basis vectors. Typically, a reduction basis is constructed based on a set of low frequency eigenmodes, computed based on the generalized eigenvalue problem:

$$\left(\mathbf{K}_0 - \omega_j^2\mathbf{M}\right)\boldsymbol{\phi}_j = \mathbf{0} \tag{20}$$

where the eigenmodes are commonly scaled such that $\boldsymbol{\phi}_i^{\mathrm{T}}\mathbf{M}\boldsymbol{\phi}_i = 1$ for all $i = 1, \dots, N_b$. Further, it should be noted that the eigenmodes are both stiffness- and mass-orthogonal [2].

The frequency content of the loading in structural dynamics applications are generally in the range of the low-frequency eigenmodes of a structure. Furthermore, the eigenmodes are not affected by the spatial distribution of the external load. Thus, the reduction basis can be applicable for several types of loading (see e.g. [13]).

3.1.2. Krylov-subspace

In some applications it can be beneficial to instead generate a set of basis vectors using a Krylov sequence, which consider the spatial distribution of the external load [31]. For this technique to be meaningful, the spatial variation of the load must be time-independent in some manner. For example, the external load may be decomposed into a set of p spatial load vectors such that

$$\mathbf{g} = \sum_{j=1}^{p} \mathbf{g}_j \boldsymbol{\alpha}_j(t) = \mathbf{G}\boldsymbol{\alpha}(t) \tag{21}$$

where $\mathbf{G}$ is a $n \times p$ matrix containing the spatial load vectors and $\boldsymbol{\alpha}(t)$ contains the corresponding time functions. Then, a block Krylov-subspace is given by

$$\mathcal{K}_r(\mathbf{K}_0^{-1}\mathbf{M}; \mathbf{K}_0^{-1}\mathbf{G}) = \mathrm{span}\left(\mathbf{K}_0^{-1}\mathbf{G}, (\mathbf{K}_0^{-1}\mathbf{M})\mathbf{K}_0^{-1}\mathbf{G}, \dots, (\mathbf{K}_0^{-1}\mathbf{M})^{r-1}\mathbf{K}_0^{-1}\mathbf{G}\right). \tag{22}$$

Hence, a set of basis vectors can be generated using repeated matrix–vector multiplications and, consequently, a reduction basis can be generated with a small computational effort, in contrast to the computational cost required for solving an eigenvalue problem. To avoid numerical round-off errors, the Krylov-subspace should be generated using e.g. the modified Gram–Schmidt orthogonalization procedure (see e.g. [15,33]). Furthermore, the basis vectors are not mutually mass- and stiffness orthogonal. This can be achieved by solving a small eigenvalue problem:

$$\left(\tilde{\mathbf{V}}^{\mathrm{T}}\mathbf{K}_0\tilde{\mathbf{V}}\right)\mathbf{Z} = \left(\tilde{\mathbf{V}}^{\mathrm{T}}\mathbf{M}\tilde{\mathbf{V}}\right)\mathbf{Z}\boldsymbol{\Lambda} \tag{23}$$

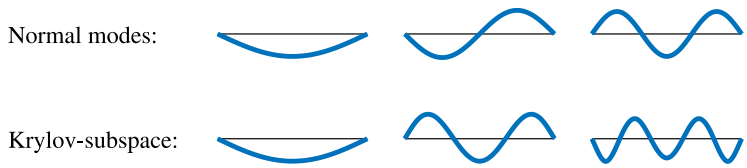

Fig. 2. Comparison of normal modes and reduction basis vectors generated using the Krylov-subspace approach for a simply supported beam subjected to a uniform pressure. Note that the anti-symmetric modes, not being excited by a uniform pressure, are automatically excluded when using the Krylov-subspace approach.

where $\tilde{\mathbf{V}}$ is the original basis, $\mathbf{\Lambda}$ is a diagonal matrix containing pseudo-frequencies, and $\mathbf{Z}$ contains the corresponding eigenvectors, which are normalized such that $\mathbf{Z}^{\mathrm{T}}\left(\mathbf{V}^{\mathrm{T}}\mathbf{M}\mathbf{V}\right)\mathbf{Z}=\mathbf{I}$. An orthonormal basis can then be calculated as $\mathbf{V}=\tilde{\mathbf{V}}\mathbf{Z}$.

Because the spatial distribution of the load is used as input in the derivation, the generated modes will, by definition, be excited by the applied load. On the contrary, a reduction basis established using normal modes may include redundant modes, which are not excited by the external load (see Fig. 2). Limiting the size of the linear basis is particularly important for cost-effective generation of NLROMs, as demonstrated in Section 5.

If the external load is applied on the out-of-plane DOFs of flat structures modeled using beam or shell elements, the Krylov-subspace will not involve the in-plane DOFs. As further discussed in Section 3.2.2, this result extend also to shallow solid models being symmetric with respect to the middle plane. Furthermore, the Krylov-subspace technique considers the quasi-static response of the external load. Accordingly, specialized techniques for considering the quasi-static response of eigenmodes excluded from the basis, such as the mode acceleration method [14], are not needed. It should be noted, however, that modes orthogonal to the applied load can be excited in the nonlinear regime due to internal resonances between pair of modes. The Krylov subspace approach is thus most suitable if such internal resonances have negligible impact. Nonetheless, the Krylov basis can be enriched by additional normal modes which are not explicitly excited by the external forcing. For further details on the Krylov-subspace technique, and examples of linear dynamics applications, see e.g. [31,34,35].

3.2. Modal derivatives

As demonstrated in [19], reduction bases suitable for analyzing geometrically nonlinear systems must typically span a significant number of eigenmodes, having eigenfrequencies considerably higher than the forcing frequency. Thus, an approach using a truncated modal basis, which is standard procedure in linear dynamics, is not feasible. This can be realized by evaluating the static response of an FE model. Clearly, the static displacements of a linearized model can be fully represented by a single mode, i.e. corresponding to an arbitrary scaling of the static displacement field ($\mathbf{u}=\mathbf{K}_0^{-1}\mathbf{g}$). However, for a geometrically nonlinear model, additional modes would be required to resolve the displacement field, because the tangent stiffness of the system is amplitude-dependent. This is apparent for cantilever structures, where bending modes as well as in-plane modes are required for an accurate representation of the static deformation, as exemplified in Fig. 1. In the general case, the reduction basis should span the eigenmodes needed for analyzing the corresponding linearized system, as well as high-frequency modes that may neither be explicitly excited nor have eigenfrequencies in the range of the forcing frequency. Hence, constructing a reduction basis using linear modes, suitable for NLROMs, is not a trivial task.

To approach the problem, reduction bases enriched by *modal derivatives* were proposed in [6,13,16,22,36,37]. In the following, the modal derivatives are derived using an approach similar to the one presented in [36]. However, by using the generalization first proposed in [37], the below derivation allows for applying the concept of modal derivatives to any type of linear modes.

By neglecting the inertia terms in Eq. (1), the static response for a FE model can be expressed as:

$$\mathbf{f}(\mathbf{u})=\mathbf{g} \tag{24}$$

where $\mathbf{f}$ and $\mathbf{g}$ are the $n\times 1$ nonlinear restoring force and external force vector, respectively. Further, let the external load be defined by

$$\mathbf{g}=\mathbf{K}_0\sum_{i=1}^{N_b}\mathbf{v}_{b,i}q_i \tag{25}$$

where $\mathbf{v}_{b,i}$ are linear modes scaled by the associated coordinates q_i (cf. Section 3.1). Hence, the external load correspond to the internal forces of a linearized system, obtained by prescribing the displacement fields $\mathbf{v}_{b,i}q_i$. Now, assume that $\mathbf{u}$ is C^2-differentiable with respect to the modal coordinates $\mathbf{q}$. Then, differentiate Eq. (24) with respect to q_i:

$$\frac{\partial\mathbf{f}}{\partial\mathbf{u}}\frac{\partial\mathbf{u}}{\partial q_i}=\mathbf{K}\frac{\partial\mathbf{u}}{\partial q_i}=\frac{\partial\mathbf{g}}{\partial q_i}=\frac{\partial}{\partial q_i}\left(\mathbf{K}_0\sum_{i=1}^{N_b}\mathbf{v}_{b,i}q_i\right)=\mathbf{K}_0\mathbf{v}_{b,i}. \tag{26}$$

Evaluating Eq. (26) around $\mathbf{u}=\mathbf{0}$ yields:

$$\left.\frac{\partial\mathbf{u}}{\partial q_i}\right|_{\mathbf{0}}=\mathbf{v}_{b,i}. \tag{27}$$

Thus, the modes $\mathbf{v}_{b,i}$ used for generating the external force vector (cf. Eq. (25)) are obtained. Here, it should be emphasized that these modes can be either normal modes or the load-dependent modes discussed in Section 3.1.2. Then, differentiate Eq. (26) with respect to q_j, as:

$$\frac{\partial}{\partial q_j}\left(\mathbf{K}\frac{\partial \mathbf{u}}{\partial q_i}\right) = \frac{\partial \mathbf{K}}{\partial q_j}\frac{\partial \mathbf{u}}{\partial q_i} + \mathbf{K}\frac{\partial^2 \mathbf{u}}{\partial q_j \partial q_i} = \mathbf{0}. \tag{28}$$

Evaluating around $\mathbf{u} = \mathbf{0}$ yields:

$$\left.\frac{\partial \mathbf{K}}{\partial q_j}\right|_{\mathbf{0}} \mathbf{v}_{b,i} + \mathbf{K}_0 \left.\frac{\partial^2 \mathbf{u}}{\partial q_i \partial q_j}\right|_{\mathbf{0}} = \mathbf{0}. \tag{29}$$

Thus, the *modal derivative* is given by

$$\boldsymbol{\theta}_{ij} = \left.\frac{\partial^2 \mathbf{u}}{\partial q_i \partial q_j}\right|_{\mathbf{0}} = -\mathbf{K}_0^{-1} \left.\frac{\partial \mathbf{K}}{\partial q_j}\right|_{\mathbf{0}} \mathbf{v}_{b,i}. \tag{30}$$

Furthermore, a Taylor series expansion of $\mathbf{u}(\mathbf{q})$ around $\mathbf{q} = \mathbf{0}$ gives:

$$\mathbf{u}(\mathbf{q}) \approx 0 + \sum_{i=1}^{N_b} \left.\frac{\partial \mathbf{u}}{\partial q_i}\right|_{\mathbf{0}} q_i + \frac{1}{2}\sum_{i=1}^{N_b}\sum_{j=1}^{N_b} \left.\frac{\partial^2 \mathbf{u}}{\partial q_j \partial q_i}\right|_{\mathbf{0}} q_i q_j. \tag{31}$$

By substituting Eqs. (27) and (30) into Eq. (31), it then follows that the nonlinear response can be approximated as

$$\mathbf{u}(\mathbf{q}) \approx \sum_{i=1}^{N_b} \mathbf{v}_{b,i} q_i + \frac{1}{2}\sum_{i=1}^{N_b}\sum_{j=1}^{N_b} \boldsymbol{\theta}_{ij} q_i q_j. \tag{32}$$

Clearly, for linear systems the second term can be neglected, resulting in the well-known modal expansion approach. However, in geometrically nonlinear analyses, the modal derivatives span precisely the additional subspace needed to achieve an accurate reduction basis. Furthermore, the modal derivatives, as derived above, are symmetric with respect to the indices i and j, i.e. $\boldsymbol{\theta}_{ij} = \boldsymbol{\theta}_{ji}$.

It should be noted that the above derivation neglects the inertia terms and, thus, consider the static response of the geometrically nonlinear model. Accordingly, these modes are sometimes referred to as *static* modal derivatives. An alternative is to derive the modal derivatives based on the generalized eigenvalue problem (cf. Eq. (20)) as e.g. described in [10,16]. However, this approach is, arguably, less straightforward and, moreover, result in modal derivatives not being symmetric with respect to the indices i and j. Furthermore, the investigations presented in e.g. [13,16] indicate that the additional accuracy gained using this approach is fairly limited. In this study, we therefore consider only static modal derivatives (henceforth referred to as modal derivatives).

3.2.1. Non-intrusive calculation of modal derivatives

According to Eq. (30), the directional derivative of the tangent stiffness matrix along a mode $\mathbf{v}_{b,i}$ is required for computing the modal derivatives (i.e. $\left.\frac{\partial \mathbf{K}}{\partial q_i}\right|_{\mathbf{0}}$). This quantity can be computed analytically on the element level (see e.g. [6]). However, this requires specialized routines not available in most FE programs. An alternative, as e.g. proposed in [13,16], is to compute the derivative of the tangent stiffness matrix in a non-intrusive manner using numerical central differences, as:

$$\left.\frac{\partial \mathbf{K}}{\partial q_i}\right|_{\mathbf{0}} = \frac{\mathbf{K}(\mathbf{v}_{b,i}h) - \mathbf{K}(-\mathbf{v}_{b,i}h)}{2h}. \tag{33}$$

Hence, neither specialized routines nor detailed knowledge of the FE implementation are required; thus, the directional derivatives can be calculated using any FE program which releases the tangent stiffness matrix for nonlinear static problems (such as Abaqus, Nastran). Furthermore, note that only N_b evaluations of Eq. (33) is required for computing the N_b^2 modal derivatives $\boldsymbol{\theta}_{ij}$ (cf. Eq. (30)). Alternatively, if the tangent stiffness matrix is not available, the modal derivatives can be computed using numerical differentiation based on the reaction forces from prescribed displacement fields, as proposed in [13,19]. However, this approach is computationally more expensive.

3.2.2. Properties of modal derivatives for flat structures

For flat structures, it turns out that the modal derivatives associated to bending modes are in-plane modes. Furthermore, the bending modes $\mathbf{v}_{b,i}$, $i = 1, \ldots, N_b$ of flat structures are mass- and stiffness-orthogonal to all the modal derivatives $\boldsymbol{\theta}_{ij} = \frac{\partial \mathbf{v}_{b,i}}{\partial q_j}$, $i, j = 1, \ldots, N_b$. For nonlinear models using hyperelastic, St-Venant Kirchhoff materials this can be shown as follows (a similar proof can also be found in [19]):

First, note that a FE model can be fully represented in terms of modal coordinates. In particular, a transformation can be expressed as:

$$\mathbf{u} = \boldsymbol{\Phi}\boldsymbol{\eta} \tag{34}$$

where $\boldsymbol{\Phi} = \begin{bmatrix} \boldsymbol{\phi}_1 & \ldots & \boldsymbol{\phi}_n \end{bmatrix}$ is a $n \times n$ transformation matrix containing the full set of eigenmodes (cf. Eq. (20)). Hence, applying the basis result in a full-order transformed system which fully describe the original system.

Further, as discussed in Section 2, the reduced nonlinear restoring forces $\mathbf{f}_r$ can be expressed in terms of higher order stiffness arrays (cf. Eq. (4)). In particular, if including the higher order stiffness arrays $\mathbf{K}^{(2)}$ and $\mathbf{K}^{(3)}$, an exact expression is obtained for FE

models that uses St-Venant Kirchhoff materials (cf. Section 2). Furthermore, recall that all quadratic coefficients involving three bending coordinates are zero for flat beam and shell models, i.e $K^{(2)}_{ijk} = 0$ for all $i, j, k = 1, \dots, N_b$ (cf. Section 2.1). Based on this observation, let the set of eigenmodes for which this condition holds be defined as *bending* modes. Note that, by using this definition, the concept of in-plane and out-of-plane modes is generalized; thus, in addition to beam and shell models, it can be used for other FE models, such as flat structures modeled using solid elements.

Now, let $\boldsymbol{\Phi}$ be partitioned such that:

$$\boldsymbol{\Phi} = \begin{bmatrix} \boldsymbol{\Phi}_b & \boldsymbol{\Phi}_m \end{bmatrix} \tag{35}$$

where $\boldsymbol{\Phi}_b$ and $\boldsymbol{\Phi}_m$ contain the N_b bending modes and the N_m non-bending modes, respectively. Accordingly, the modal coordinate vector is partitioned such that $\boldsymbol{\eta} = \begin{bmatrix} \mathbf{q}^{\mathrm{T}} & \mathbf{p}^{\mathrm{T}} \end{bmatrix}^{\mathrm{T}}$, where $\mathbf{q}$ are the bending coordinates and $\mathbf{p}$ are the non-bending coordinates, respectively. Moreover, the reduced tangent stiffness matrix can be expressed according to Eq. (17) (restated here for convenience):

$$K_{r,iu} = K^{(1)}_{iu} + \left[K^{(2)}_{iju} + K^{(2)}_{iuj}\right]\eta_j + \left[K^{(3)}_{ijlu} + K^{(3)}_{ijul} + K^{(3)}_{iujl}\right]\eta_j\eta_l \tag{36}$$

where $\mathbf{K}_r$ is the $N \times N$ reduced tangent stiffness matrix. In this specific case, $N = N_b + N_m = n$, since the modal basis include the full set of eigenmodes.

Because the modal basis is orthogonal, prescribing a coordinate in Eq. (36), such that $\eta_j = h$ (with $\eta_i = 0\ \forall i = 1, \dots, N,\ i \neq j$), result in the following expression for the tangent stiffness matrix:

$$K_{r,iu}(\boldsymbol{\eta} = \mathbf{e}_j h) = K^{(1)}_{iu} + \left[K^{(2)}_{iju} + K^{(2)}_{iuj}\right]h + \left[K^{(3)}_{ijju} + K^{(3)}_{ijuj} + K^{(3)}_{iujj}\right]h^2 \tag{37}$$

where h is an arbitrary scalar and $\mathbf{e}_j$ is a $N \times 1$ unit vector in direction j. Then, by applying Eq. (37) to Eq. (33), an expression for the directional derivative of the tangent stiffness matrix along the unit vector $\mathbf{e}_j$ is obtained, namely:

$$\left[\frac{\partial K_r}{\partial q_j}\bigg|_{\mathbf{0}}\right]_{iu} = K^{(2)}_{iju} + K^{(2)}_{iuj}. \tag{38}$$

Moreover, for flat structures, where $\mathbf{K}^{(2)}_b = \mathbf{0}$ for the set of bending modes, the derivative of the tangent stiffness matrix can be written in partitioned form, as:

$$\frac{\partial \mathbf{K}_r}{\partial q_j}\bigg|_{\mathbf{0}} = \begin{bmatrix} \mathbf{0} & \left[\frac{\partial \mathbf{K}_r}{\partial q_j}\right]_{bm} \\ \left[\frac{\partial \mathbf{K}_r}{\partial q_j}\right]_{mb} & \left[\frac{\partial \mathbf{K}_r}{\partial q_j}\right]_{mm} \end{bmatrix} \tag{39}$$

where, the symbol $\bullet|_{\mathbf{0}}$ has been omitted on the right hand side to simplify the notation. Further, by using that

$$\begin{cases} \frac{\partial \mathbf{K}_r}{\partial q_j}\Big|_{\mathbf{0}} = \boldsymbol{\Phi}^{\mathrm{T}} \frac{\partial \mathbf{K}}{\partial q_j}\Big|_{\mathbf{0}} \boldsymbol{\Phi} \\ \mathbf{K}_0^{-1} = \boldsymbol{\Phi}\boldsymbol{\Lambda}^{-1}\boldsymbol{\Phi}^{\mathrm{T}} \\ \boldsymbol{\phi}_i = \boldsymbol{\Phi}\mathbf{e}_i \end{cases} \tag{40}$$

where $i, j = 1, \dots, N_b$, and $\boldsymbol{\Lambda} = \boldsymbol{\Phi}^{\mathrm{T}}\mathbf{K}_0\boldsymbol{\Phi} = \mathrm{diag}(\omega_1^2, \omega_2^2, \dots, \omega_N^2)$, Eq. (30) can be rewritten as:

$$\boldsymbol{\theta}_{ij} = -\mathbf{K}_0^{-1} \frac{\partial \mathbf{K}}{\partial q_j}\bigg|_{\mathbf{0}} \boldsymbol{\phi}_i = -\boldsymbol{\Phi}\boldsymbol{\Lambda}^{-1} \frac{\partial \mathbf{K}_r}{\partial q_j}\bigg|_{\mathbf{0}} \mathbf{e}_i = \sum_{k=1+N_b}^{N} \boldsymbol{\phi}_k \beta_k \tag{41}$$

where $\beta_k = -\frac{1}{\omega_k^2}\left[\frac{\partial \mathbf{K}_r}{\partial q_j}\Big|_{\mathbf{0}}\right]_{kj}$ are scalars. Hence, the modal derivatives associated to bending eigenmodes can be expressed as superpositions of the non-bending eigenmodes. It follows that, because the eigenmodes are mass and stiffness-orthogonal (cf. Section 3.1.1), the modal derivatives must be mass- and stiffness orthogonal to all the bending eigenmodes, thus

$$\begin{cases} \boldsymbol{\phi}_k^{\mathrm{T}}\mathbf{M}\boldsymbol{\theta}_{ij} = 0 \\ \boldsymbol{\phi}_k^{\mathrm{T}}\mathbf{K}_0\boldsymbol{\theta}_{ij} = 0 \end{cases} \tag{42}$$

for all $i, j, k = 1, \dots, N_b$.

For flat structures modeled using beam or shell elements, the linearized FE model can be formulated such that the in-plane and out-of-plane DOFs are uncoupled; thus, it is straightforward to separate the membrane and bending modes. However, the above derivation is valid for any structure where the condition $\mathbf{K}^{(2)}_b = \mathbf{0}$ holds for a set of N_b eigenmodes. Hence, as demonstrated in Section 5, the derivation can also be assumed valid for flat structures modeled using solid elements, for which the geometrical and material distribution as well as boundary conditions are symmetric with respect to the middle line/plane of the structure.

3.3. Reduction basis and orthogonalization

A reduction basis suitable for geometrically nonlinear, flat structures can be constructed using an appropriate set of out-of-plane linear modes and the corresponding modal derivatives. The basis can be partitioned such that

$$\mathbf{V} = \begin{bmatrix} \mathbf{V}_b & \mathbf{V}_m \end{bmatrix} \tag{43}$$

where

$$\mathbf{V}_b = \begin{bmatrix} \mathbf{v}_{b,1} & \dots & \mathbf{v}_{b,N_b} \end{bmatrix} \tag{44}$$

$$\mathbf{V}_m = \begin{bmatrix} \theta_{11} & \theta_{12} & \dots & \theta_{1N_b} & \theta_{22} & \theta_{23} & \dots & \theta_{2N_b} & \dots & \theta_{(N_b-1)(N_b-1)} & \theta_{(N_b-1)N_b} & \theta_{N_bN_b} \end{bmatrix}^{\mathrm{T}}. \tag{45}$$

Here, the linear modes $\mathbf{v}_{b,i}$ may be normal modes or force-dependent modes, as discussed in Section 3.1. Further, the symmetry property of the modal derivatives are considered, i.e. $\theta_{ij} = \theta_{ji}$, such that only the unique set of modal derivatives are included in the basis.

As shown in Section 3.2.2, the modal derivatives are in-plane (or non-bending) modes, being orthogonal to the out-of-plane bending modes. However, the modal derivatives may not be mutually orthogonal. Thus, the in-plane basis $\mathbf{V}_m$ consisting of the raw modal derivatives must generally be orthogonalized using e.g. the Gram–Schmidt method. Further, an in-plane basis being both mass- and stiffness-orthogonal, can be obtained by applying Eq. (23) to the set of in-plane modes.

3.4. Other non-intrusive basis selection methods

In addition to approaches using modal derivatives, other simulation-free, non-intrusive basis selection methods have been proposed, an extensive review can be found in [28]. In the following, two of the most popular methods are briefly introduced, namely, the ICE method [7] and basis selection strategies using *dual modes* [17].

The ICE method is a popular approach for establishing NLROMs, because it allows for analyzing flat as well as slightly curved shallow structures, in a fairly straightforward manner [7,8]. It uses a set of linear modes as input, e.g. a set of low-frequency normal modes, which would typically be used for analyzing the corresponding linearized system. Thus, additional, specialized basis vectors, such as modal derivatives, are not required. Instead, the statically condensed response of basis vectors not included in the basis are considered implicitly. Moreover, an enriched reduction basis (e.g. including in-plane modes) can be extracted in a second step, using the expansion process proposed in [7]. It turns out that the number of basis vectors generated in the expansion process equals to the number of unique model derivatives obtained for the same set of linear modes. Nonetheless, the techniques are fundamentally different; the ICE method uses a regression analysis, whereas the modal derivatives are derived using modal perturbations (cf. Section 3.2). Furthermore, using the ICE method, several full nonlinear static problems must be solved, which can be computationally expensive. Hence, even though the full-order solution of the dynamic problem is not needed, the ICE method can be interpreted as a type of data-driven method and, accordingly, the (static) training-simulations are of considerable importance. The magnitude as well as the distribution of the external load must be selected properly, generally requiring a trial and error process [8]. Following the procedure suggested in [8], the number of load cases for precomputing the NSCs and generating the in-plane modes is $2N_b + 2N_b(N_b-1) + 4N_b(N_b-1)(N_b-2)/3$. Here, it should noted that the condensed NSCs are obtained for the N_b linear modes. Hence, the additional modes generated in the expansion process are not considered explicitly in the dynamic response analysis.

Linear bases enriched by dual modes was introduced in [17] and has been further investigated by several researchers (see e.g. [9,27]). Similarly to the ICE method, several full-order static problems are solved for representative load configurations defined based on the linear basis (see [17] for further details). Then, in a second step, the displacement fields are orthogonalized with respect to the linear modes, which allows for extracting additional modes to be appended the linear basis. In contrast to the ICE method, the technique using dual modes only concerns the generation of the reduction basis. Thus, the NSCs are typically identified in a separate procedure using the ED or EED method. As e.g. indicated by the investigations presented in [13], the offline cost for constructing NLROMs using dual modes is generally larger, as compared to NLROMs constructed using modal derivatives.

4. Proposed methodology for efficient generation of NLROMs

As discussed in Section 2.3.3, the number of NSCs for flat structures can be significantly decreased by applying the ED method on out-of-plane (or master) DOFs, such that the statically condensed response of the non-bending coordinates are considered implicitly (cf. Sections 2.2 and 2.3.3). The drawback using this approach is that only the quasi-static response of the non-bending coordinates is considered and, furthermore, that several full-order nonlinear static problems must be solved because the in-plane (or slave) DOFs are allowed to move freely in the ED identification process.

In this section, we will investigate how these two issues can be addressed by utilizing the relationship between the NSCs and the modal derivatives. Thus, the aim is to formulate a methodology that allows for developing NLROMs that consider the in-plane dynamics, and, moreover, reduces the computational offline cost by both limiting the number of static load cases and avoiding iterative solution methods in the ED (or EED) identification process. Furthermore, we demonstrate that modal derivatives can be effectively used for recovering the in-plane (or slave DOFs) displacements for condensed NLROMs. Moreover, if the out-of-plane basis is constructed using normal modes, we show that the concepts extend also to curved structures.

The proposed methodologies for NLROMs including in-plane dynamics and condensed NLROMs are presented in Sections 4.1 and 4.2, respectively. A generalization of the concepts is introduced in Section 4.3.

4.1. Systems considering in-plane dynamics

If adopting the simplified form for flat structures, as described in Section 2.1, the only NSCs involving in-plane coordinates are the quadratic coupling coefficients $\mathbf{K}_{mb}^{(2)}$ and $\mathbf{K}_{bm}^{(2)}$, respectively (cf. Eq. (9)). Consequently, the modal derivatives provide all the information needed for precomputing the in-plane NSCs, which can be shown as follows:

First, by using that $\mathbf{K} = \frac{\partial \mathbf{f}}{\partial \mathbf{u}}$, the left hand side of Eq. (28) can be rewritten as:

$$\frac{\partial^2 \mathbf{f}}{\partial q_j \partial \mathbf{u}} \frac{\partial \mathbf{u}}{\partial q_i} + \mathbf{K} \frac{\partial^2 \mathbf{u}}{\partial q_i \partial q_j} = \frac{\partial^2 \mathbf{f}}{\partial q_i \partial q_j} + \mathbf{K} \frac{\partial^2 \mathbf{u}}{\partial q_i \partial q_j} = \mathbf{0}. \tag{46}$$

Then, evaluating Eq. (46) around $\mathbf{u} = \mathbf{0}$ gives:

$$\left. \frac{\partial^2 \mathbf{f}}{\partial q_i \partial q_j} \right|_{\mathbf{0}} + \mathbf{K}_0 \boldsymbol{\theta}_{ij} = \mathbf{0}. \tag{47}$$

Now, assume that an in-plane basis $\mathbf{V}_m$ is constructed using the full set of unique modal derivatives associated to the bending modes included in the out-of-plane basis $\mathbf{V}_b$ (cf. Eqs. (44) and (45)). Specifically, the in-plane basis vectors are given by $\mathbf{v}_{m,r} = \boldsymbol{\theta}_{ij} = \frac{\partial \mathbf{v}_{b,i}}{\partial q_j}$, for all $i, j = 1, \dots, N_b$, $j \geq i$, where the in-plane vectors are organized such that $r = N_b(i-1) + j - i(i-1)/2$ (thus, the total number of in-plane modes is $N_m = N_b + N_b(N_b - 1)/2$). Then, by pre-multiplying by the transpose of an in-plane basis vector $\mathbf{v}_{m,r}^{\mathrm{T}}$, Eq. (47) can be rewritten as:

$$\mathbf{v}_{m,r}^{\mathrm{T}} \left. \frac{\partial^2 \mathbf{f}}{\partial q_i \partial q_j} \right|_{\mathbf{0}} = -\mathbf{v}_{m,r}^{\mathrm{T}} \mathbf{K}_0 \mathbf{v}_{m,s} \quad \text{if} \quad j \geq i \tag{48}$$

where the indices $i, j = 1, \dots, N_b$, $r = 1, \dots, N_m$, and $s = N_b(i-1) + j - i(i-1)/2$. Moreover, note that the right hand side of Eq. (48) correspond to entries of the reduced linear stiffness matrix associated to in-plane coordinates, given by:

$$\mathbf{K}_m^{(1)} = \mathbf{V}_m^{\mathrm{T}} \mathbf{K}_0 \mathbf{V}_m. \tag{49}$$

Further, as indicated by the second Taylor coefficient in Eq. (4), the left hand side of Eq. (48) is related to the quadratic coupling coefficients $\mathbf{K}_{mb}^{(2)}$. Specifically, the following relations can be identified:

$$\begin{cases} K_{mb,rij}^{(2)} = \frac{1}{2} \mathbf{v}_{m,r}^{\mathrm{T}} \left. \frac{\partial^2 \mathbf{f}}{\partial q_i \partial q_j} \right|_{\mathbf{0}} & \text{if} \quad j \geq i \\ K_{m,rs}^{(1)} = \mathbf{v}_{m,r}^{\mathrm{T}} \mathbf{K}_0 \mathbf{v}_{m,s} \end{cases} \tag{50}$$

Thus, substituting Eq. (50) into Eq. (48) gives:

$$K_{mb,rij}^{(2)} = -\frac{1}{2} K_{m,rs}^{(1)} \quad \text{if} \quad j \geq i \tag{51}$$

where $s = N_b(i-1) + j - i(i-1)/2$.

Furthermore, it should be noted that the stiffness arrays are fully symmetric, thus $K_{mb,rji}^{(2)} = K_{mb,rij}^{(2)}$. Moreover, the nonlinear stiffness coefficients $\mathbf{K}_{bm}^{(2)}$ can be obtained by rearranging the elements of $\mathbf{K}_{mb}^{(2)}$. Now, as evident by Eq. (9), only the stiffness coefficients $\mathbf{K}_b^{(3)}$ remains to be identified, involving the N_b out-of-plane modes. Accordingly, the number of static load cases, if using the EED method, is of order $\mathcal{O}(N_b^2)$. Moreover, the static solutions already used for calculating the modal derivatives, i.e. using numerical differences according to Eq. (33), may be reused in the identification process.

As mentioned previously, the above procedure uses the raw modal derivatives in-plane basis. To ensure an accurate NLROM, the basis should be orthonormalized. This can be achieved by applying a transformation matrix $\mathbf{Z}$, e.g. calculated based on a small eigenvalue problem in accordance with Eq. (23). An orthogonal in-plane basis is then obtained as $\tilde{\mathbf{V}}_m = \mathbf{V}_m \mathbf{Z}$. The transformation can be applied either directly on the higher order stiffness array $\mathbf{K}^{(2)}$ or by replacing the in-plane basis vectors $\mathbf{v}_{m,r}^{\mathrm{T}}$ in Eq. (50) by the set of orthogonal vectors. This means that Eq. (51) will be replaced by:

$$K_{mb,rij}^{(2)} = -\frac{1}{2} \tilde{\mathbf{v}}_{m,r}^{\mathrm{T}} \mathbf{K}_0 \mathbf{v}_{m,s} \quad \text{if} \quad j \geq i \tag{52}$$

where, $s = N_b(i-1) + j - i(i-1)/2$.

Finally, since the higher order stiffness arrays are fully symmetric, the nonlinear system equations are commonly implemented such that non-unique NSCs are avoided, by assuming that the elements are zero unless the indices $j \leq l \leq k$. Specifically for flat structures, the system equations for the bending coordinates may be expressed as:

$$\sum_{j=1}^{N_b} \left[M_{b,ij} \ddot{q}_j + C_{b,ij} \dot{q}_j + K_{b,ij}^{(1)} q_j + \sum_{k=j}^{N_m} \tilde{\mathbf{K}}_{bm,ijk}^{(2)} q_j p_k + \sum_{k=j}^{N_b} \sum_{l=k}^{N_b} \tilde{\mathbf{K}}_{b,ijkl}^{(3)} q_j q_k q_l \right] = g_{b,i} \tag{53}$$

and for the in-plane coordinates:

$$\sum_{j=1}^{N_m} \left[M_{m,ij} \ddot{p}_j + C_{m,ij} \dot{p}_j + K_{m,ij}^{(1)} p_j \right] + \sum_{j=1}^{N_b} \sum_{k=j}^{N_b} \tilde{\mathbf{K}}_{mb,ijk}^{(2)} q_j q_k = g_{b,i} \tag{54}$$

where $\bar{\bullet}$ is introduced to distinguish the higher order stiffness arrays only including the unique elements from the corresponding full arrays. It follows that Eq. (51) must be adjusted accordingly, such that:

$$\bar{K}^{(2)}_{mb,rij} = \begin{cases} -K^{(1)}_{m,rs}/2 & \text{if} \quad i = j \\ -K^{(1)}_{m,rs} & \text{if} \quad i \neq j \end{cases} \tag{55}$$

Similarly, for an orthogonalized in-plane basis $\tilde{\mathbf{V}}_m$ one obtains:

$$\bar{K}^{(2)}_{mb,rij} = \begin{cases} -\frac{1}{2}\tilde{\mathbf{v}}^{\mathrm{T}}_{m,r}\mathbf{K}_0\mathbf{v}_{m,s} & \text{if} \quad i = j \\ -\tilde{\mathbf{v}}^{\mathrm{T}}_{m,r}\mathbf{K}_0\mathbf{v}_{m,s} & \text{if} \quad i \neq j \end{cases} \tag{56}$$

where $j \geq i$, and, again, the mapping between the elements are defined such that $s = N_b(i-1) + j - i(i-1)/2$.

4.2. Statically condensed systems

By using the methodology described in Section 4.1, an NLROM is obtained that considers the dynamics of the out-of-plane as well as in-plane coordinates. However, in some applications, it can be reasonable to neglect the dynamics of the in-plane modes to further decrease the system size. Then, if assuming that the external load on the in-plane coordinates is zero, and that $\mathbf{K}^{(1)}_m$, $\mathbf{K}^{(2)}_{mb}$, $\mathbf{K}^{(2)}_{bm}$, and $\mathbf{K}^{(3)}_b$ have already been determined using the procedure described in Section 4.1, the condensed stiffness coefficients can be obtained by using Eq. (12). Moreover, recall that the quasi-static response of the in-plane coordinates can be expressed in terms of the out-of-plane coordinates, i.e., in accordance with Eq. (10) (restated here for convenience):

$$p_j = -\left[K^{(1)}_m\right]^{-1}_{js} K^{(2)}_{mb,srl} q_r q_l. \tag{57}$$

Now, assume that the in-plane basis is defined by Eq. (45), and, moreover, that the set of raw modal derivatives are linearly independent (which should be checked for the specific application). Then, by using Eqs. (55) and (57), it can be shown that the quasi-static response of the in-plane coordinates $\mathbf{p}$ are in fact directly related to the out-of-plane coordinates $\mathbf{q}$, as:

$$p_s = \begin{cases} -q_i q_j/2 & \text{if} \quad i = j \\ -q_i q_j & \text{if} \quad i \neq j \end{cases} \tag{58}$$

where $j \geq i$, and $s = N_b(i-1) + j - i(i-1)/2$. Hence, the in-plane coordinate vector is given by:

$$\mathbf{p} = -\begin{bmatrix} q_1^2/2 & q_1 q_2 & \cdots & q_1 q_{N_b} & q_2^2/2 & q_2 q_3 & \cdots & q_2 q_{N_b} & \cdots & q^2_{N_b-1}/2 & q_{N_b-1} q_{N_b} & q^2_{N_b}/2 \end{bmatrix}^{\mathrm{T}}. \tag{59}$$

Thus, by using the above procedure, a condensed NLROM can be developed in a computationally efficient manner, which allows for recovering the physical displacements by applying Eq. (2) for the out-of-plane as well as in-plane coordinates.

4.3. Generalization for curved structures

The procedures described in Sections 4.1 and 4.2 are intended to be applied to flat structures which are symmetric with respect to the middle plane. However, the methodology can be generalized to consider curved structures and structures with non-symmetric stiffness distribution along the thickness. In this case, the modal derivatives are generally neither in-plane modes nor mass- and stiffness orthogonal to the out-of-plane modes. Nonetheless, if the linear basis is constructed using normal modes (cf. Section 3.1), a projector may be defined as:

$$\mathbf{P} = \mathbf{I} - \mathbf{V}_b\mathbf{V}_b^{\mathrm{T}}\mathbf{M} \tag{60}$$

which removes from a basis vector the part spanned by the linear modes $\mathbf{V}_b$. Specifically, the basis $\mathbf{V}_m$ given by Eq. (45), which include the set of unique modal derivatives can be orthogonalized to the linear modes:

$$\hat{\mathbf{V}}_m = \mathbf{P}\mathbf{V}_m \tag{61}$$

where the columns of $\hat{\mathbf{V}}_m$ are basis vectors being both mass- and stiffness orthogonal to the linear modes, i.e., $\hat{\mathbf{v}}_{m,r} = \hat{\boldsymbol{\theta}}_{ij} = \mathbf{P}\boldsymbol{\theta}_{ij}$ for all $i, j = 1, \ldots, N_b$, $j \geq i$. Further, the linear stiffness matrix projected onto $\hat{\mathbf{V}}_m$ can be expressed as:

$$\mathbf{K}^{(1)}_m = \hat{\mathbf{V}}^{\mathrm{T}}_m\mathbf{K}_0\hat{\mathbf{V}}_m = \hat{\mathbf{V}}^{\mathrm{T}}_m\mathbf{K}_0\mathbf{P}\mathbf{V}_m = \hat{\mathbf{V}}^{\mathrm{T}}_m\mathbf{K}_0\mathbf{V}_m - \hat{\mathbf{V}}^{\mathrm{T}}_m\mathbf{K}_0\mathbf{V}_b\mathbf{V}_b^{\mathrm{T}}\mathbf{M}\mathbf{V}_m = \hat{\mathbf{V}}^{\mathrm{T}}_m\mathbf{K}_0\mathbf{V}_m. \tag{62}$$

Now, by replacing $\mathbf{v}^{\mathrm{T}}_{m,r}$ in Eq. (48) with $\hat{\mathbf{v}}^{\mathrm{T}}_{m,r}$, and using the relation given by Eq. (62), it is clear that Eq. (55) holds also for non-flat structures. Moreover, if the external forcing is orthogonal to $\hat{\mathbf{V}}_m$, Eq. (58) is still valid. However, in contrast to the case of flat structures, the quadratic stiffness coefficients involving three bending coordinates $\mathbf{K}^{(2)}_b$ is not zero for curved structures and should therefore be added to the simplified form of the equation of motion (cf. Eq. (7)). Furthermore, by using the same procedure as described in Section 4.1, the orthogonalized modal derivatives $\hat{\boldsymbol{\theta}}_{ij}$ can be made mutually mass- and stiffness-orthogonal.

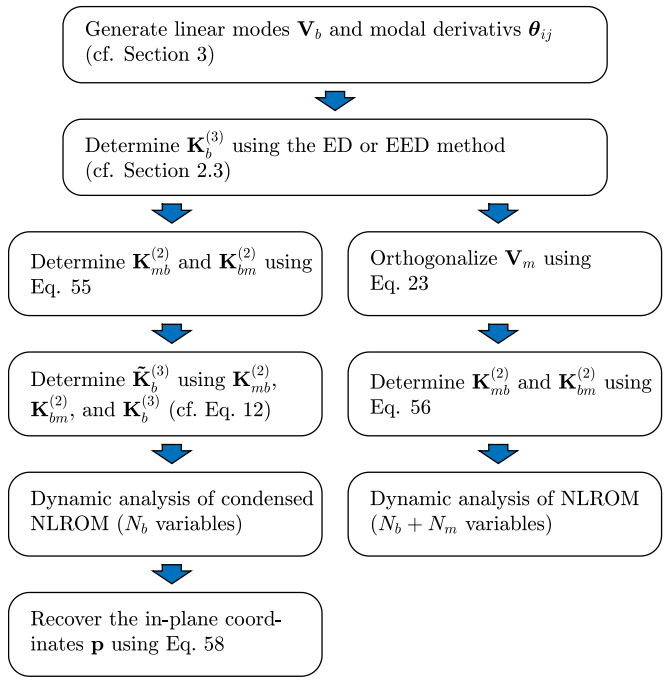

Fig. 3. Flowchart showing the proposed modeling procedures. Note that the NLROM can be analyzed using the full set of generalized coordinates or by means of the condensed system equations (cf. Eq. (11)) involving only the out-of-plane coordinates.

4.4. Remarks on the proposed methodology

The proposed methodologies, with and without non-bending inertia effects, are summarized schematically in Fig. 3. The decondensation technique for reducing the influence of numerical round-off errors, as discussed in Section 2.3.4, can be incorporated in the methodology by means of a small modification, namely, by computing the condensed stiffness coefficients $\tilde{\mathbf{K}}_b^{(3)}$ in the second step, and then applying Eq. (19) in the fourth step (right side) of the flowchart presented in Fig. 3. Furthermore, by means of the generalization introduced in Section 4.3, the methodology can be used for curved structures. However, a decondensation is then no longer possible.

The methodology allows for developing NLROMs without solving full-order static problems which necessitates iterative solution methods. Furthermore, if using the EED identification process, the number of static load cases for determining the NSCs is of order $\mathcal{O}(N_b^2)$. Thus, significantly smaller than in e.g. the standard EED method involving all NSCs or the ICE method, where the number of full-order static problems is of order $\mathcal{O}(N^2)$ and $\mathcal{O}(N_b^3)$, respectively.

In addition to reducing the number of full-order static problems in the offline stage, the computational online cost can also be decreased, as compared to systems considering the full set of NSCs. The NLROMs are solved using direct time-integration where the tangent stiffness matrix (cf. Eq. (17)) must be constructed in each iteration. By utilizing the symmetry of the tangent stiffness matrix, and noting that $K_{ijk}^{(2)}$ is zero if $j,k > N_b$ and $K_{ijkl}^{(3)}$ is zero if $i,j,k,l > N_b$, the computational cost for computing the tangent stiffness matrix can be significantly reduced. More specifically, only N_b rows (or columns) of the $N \times N$ reduced stiffness matrix $\mathbf{K}_r$ need to be updated, where the stiffness coefficients $K_{ijkl}^{(3)}$ are only involved in the update of $N_b \times N_b$ entries.

5. Numerical examples

The proposed modeling strategies were evaluated by means of numerical examples of beam structures (see Section 5.1) and a continuously supported panel structure (see Section 5.2). The beam structures were modeled with 2D solid elements using an FE code implemented in MATLAB, and the panel structure was modeled with shell elements using the commercial FE software Abaqus. The beam model was mainly used for investigating the proposed modeling procedures and, moreover, the properties of modal derivatives associated to out-of-plane bending modes, whereas the shell model is intended to represent a real-life application. NLROMs were established using the procedures presented in Section 4. Thus, the simplified system equations (cf. Eq. (9)) were considered. Moreover, statically condensed systems as well as the decondensation technique for mitigating the influence of numerical round-off errors were investigated (cf. Sections 2.2 and 2.3.4, respectively). Further, various support configurations were investigated. All

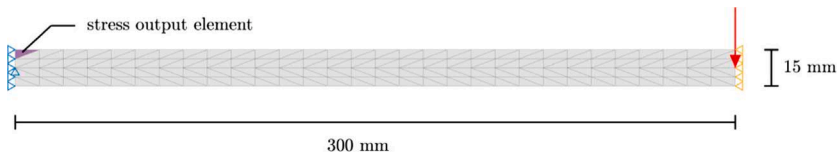

Fig. 4. Element mesh for solid 2D beam models. The displacement boundary conditions indicated by blue color are active for both the clamped–clamped and cantilever beam models and the orange boundary conditions are active only for the clamped–clamped model (thus, a symmetry model is considered). The position of the external point load is indicated by the red arrow. The horizontal stress component in the element marked with purple color is to be evaluated. (For interpretation of the references to color in this figure, the reader is referred to the web version of this article.).

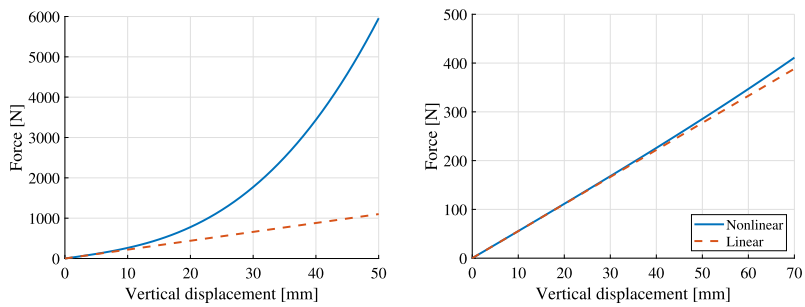

(a) clamped–clamped (b) cantilever

Fig. 5. Linear and nonlinear static response for clamped–clamped (a) and cantilever beam (b) models, respectively.

the developed NLROMs were solved in MATLAB using Newmark implicit time-integration, assuming constant average acceleration within time-increments. Equilibrium in each time increment was enforced by means of Newton–Raphson iterations. All the analyses were performed on a desktop PC with 16 GB RAM and Intel® Core™ i7-8700 CPU (3.2 GHz).

5.1. Solid beam model

The solid beam model, shown in Fig. 4, have a length of 300 mm and a height of 15 mm. The FE model was established using two-dimensional, triangular three-node elements assuming plain strain conditions. The thickness in the elements' out-of-plane direction was set to 10 mm. Further, a hyperelastic, St-Venant Kirchhoff material was used. The Young's modulus and Poisson's ratio was set to 10 GPa and 0.3, respectively, and the density was set to 1700 kg/m^3.

Two different support configurations were considered. Firstly, a symmetry model representing a clamped–clamped beam was obtained by prescribing the horizontal displacements at the beam ends, and the vertical displacement at the mid node at the left end (see Fig. 4). Secondly, a cantilever beam model was obtained by prescribing the horizontal displacements and the vertical displacement at the mid node at the left end. As demonstrated in Fig. 5, the static response of the systems differ significantly. In particular, the nonlinear response of the cantilever beam is close to the linearized response, whereas the clamped–clamped beam is characterized by a highly nonlinear response.

The dynamic response due to a triangular impulse applied at the right end of the beam models (see Fig. 4) were analyzed, having a peak force after 1 ms and a total duration of 2 ms. The impulse was adjusted for the respective cases; the peak forces were set to 5000 N and 1500 N for the clamped–clamped symmetry model and the cantilever model, respectively. To simplify the evaluations, both systems were assumed undamped. In practice, free vibration is studied, since the impulse duration is very short in comparison to the analysis time (see further Sections 5.1.1 and 5.1.2).

To provide a complete verification of the NLROMs, the response was also evaluated for a banded random excitation white noise applied at the load DOF (cf. Fig. 4). The random response was evaluated for the clamped–clamped beam and the cantilever beam. Furthermore, the response of a slightly curved clamped–clamped beam, as shown in Fig. 15, was evaluated. As shown in Fig. 15, the curved beam was generated using the same topology and boundary conditions as the clamped–clamped beam. The frequency range of the excitation was set to 0–2000 Hz for all the models. The response was calculated using direct time-integration with a fixed time-increment of 20 μs, and the total analysis time was 20 s. For the random response analyses a Rayleigh damping was adopted. The Rayleigh coefficients, α and β, were prescribed such that a modal damping ratio of 2% were obtained for the first and third linear mode. In the nonlinear analyses, the damping was proportional to the mass and tangent stiffness, i.e. $\mathbf{C} = \alpha\mathbf{M} + \beta\mathbf{K}$, thus, the damping was amplitude dependent. The displacement power spectral density (PSD) was estimated using a moving window of period 0.33 s. Note that the nonlinear responses are generally not stationary, although this is assumed when estimating the PSD. Nonetheless, several researchers have demonstrated that similar procedures for estimating the PSD for nonlinear models provide satisfactory results [8,13,17,18,38].

Table 1
Computational offline times using the ED method.

Model	Offline time [s]
4+10 Modes	0.4
4 Modes (Cond.)	0.4
4+10 Modes (All NSCs)	4.9
10+55 Modes	2.6
10 Modes (Cond.)	2.6
10+55 Modes (All NSCs)	428

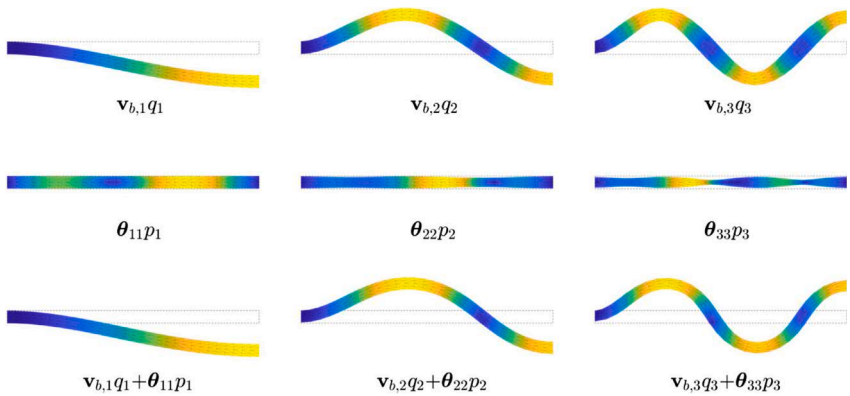

Fig. 6. First three linear modes and the associated modal derivatives θ_{ii} $(i = 1, 2, 3)$ for the clamped–clamped beam model. The amplitude of the modal derivatives are $p_i = -q_i^2/2$. Note that, for brevity, modal derivatives with different indices $(\theta_{ij},\ i \neq j)$ are not included in the figure.

The reduction bases for the flat beams were established using out-of-plane bending modes and the associated modal derivatives. Specifically, the bending modes were generated using the Krylov-subspace technique described in Section 3.1.2. The Krylov sequence was initiated using an external force at the right end of the beam, as shown in Fig. 4. Note that, in contrast to an approach using normal modes, this procedure ensures that any in-plane modes are excluded. The reduction basis for the curved beam was generated using the first four normal modes and the associated modal derivatives.

The computational offline cost using the proposed methodology and the standard approach considering the full set of NSCs are presented in Table 1 for NLROMs based on 4 and 10 linear modes. All the associated modal derivatives were considered such that a total of 4+10 and 10+55 modes, respectively, were included in the reduction bases. As shown in Table 1, the computational offline cost increases significantly if the number of basis vectors is increased. Particularly for dynamic analyses of short time frames, such as impulse analyses, the offline cost can be significantly larger than the online cost.

5.1.1. Clamped–clamped beam

The first three out-of-plane bending modes and the associated modal derivatives for the clamped–clamped model are shown in Fig. 6 (note that, for brevity, only the modal derivatives with equal indices $\boldsymbol{\theta}_{ii}$ are shown in the figure). In accordance with Section 3.2.2, the modal derivatives are non-bending modes, being orthogonal to the bending modes. Furthermore, the statically condensed response of the modal derivatives, being enslaved by the bending coordinates, are demonstrated in Fig. 6. Specifically, the amplitude of the modal derivatives are $p_i = -q_i^2/2$, where q_i is the associated bending coordinate (cf. Section 4.2).

The vertical displacement at the vertical DOF where the external load is applied, henceforth referred to as the *load* DOF, is presented in Fig. 7. The displacements are shown for the full-order model and NLROMs using various reduction basis sizes (Fig. 7a), as well as a linear ROM and NLROMs with/without inertia effects for the in-plane modes (Fig. 7b). As shown in the figure, a reduction basis including four bending modes and the associated modal derivatives (i.e. a total of 4+10 modes) provide a response close to the full-order model. Further, the condensed NLROMs are fairly accurate, meaning that the influence of in-plane inertia effects is small. In accordance with the results from the static analysis (cf. Fig. 5), the displacement from the linear analysis differ significantly.

The horizontal Cauchy stress at the top of the left support (in the element marked with purple color in Fig. 4) is shown in Fig. 8 for the full-order model and NLROMs developed using reduction bases of various sizes. As shown in the figure, up to six bending modes and the associated modal derivatives (i.e. a total of 6+21 modes) are required for an accurate response prediction. Moreover, it is notable that the magnitude of the max/min stresses differ significantly, which is due to that normal forces are induced in the geometrically nonlinear analyses. Accordingly, for the linearized system, this effect cannot be observed, i.e. the stress oscillates between approximately the same peak magnitudes.

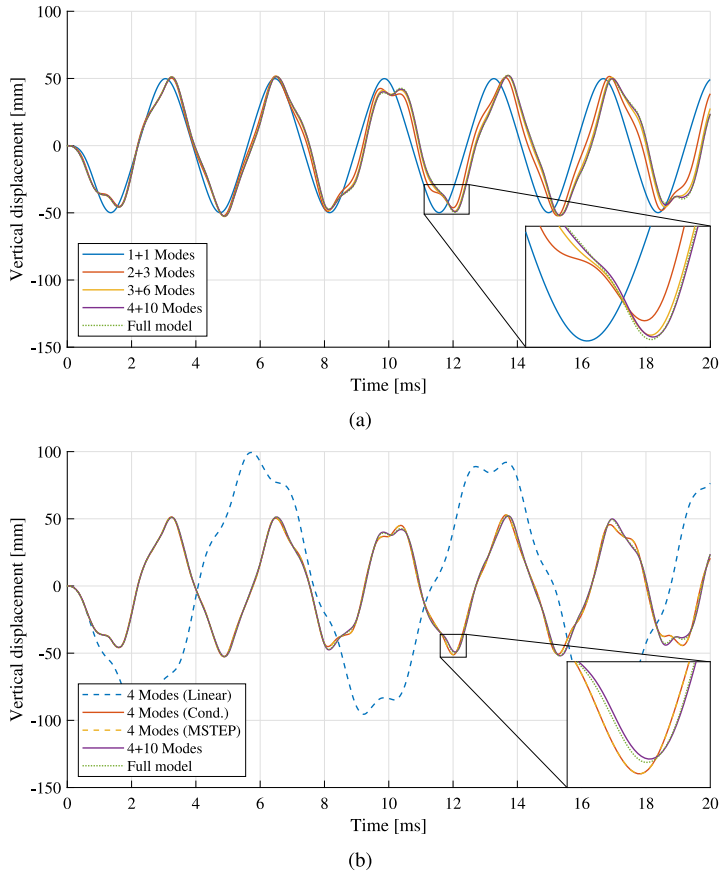

Fig. 7. Comparison of the vertical displacement at the load DOF for the full-order clamped–clamped model and NLROMs using various reduction basis sizes (a), and a linear ROM and NLROMs with/without inertia effects for the in-plane modes (b). The NLROMs were established using the method described in Section 4. The condensed NLROMs were established using both the MSTEP method [19] and the approach described in Section 4—as expected, these methods provide almost identical results.

Table 2
Computational online times for random excitation analyses.

Model	Online time [s]		
	Clamped–clamped	Cantilever	Curved beam
4+10 Modes	66	68	64
4 Modes (Cond.)	27	25	29
4+10 Modes (All NSCs)	681	715	683
Full model	73 248	77 066	72 928

The clamped–clamped beam was evaluated for a random excitation with a standard deviation of 300 N. The displacement PSD for the load DOF is shown for various models in Fig. 9. All the NLROMs are in fairly good agreement with the full-order model. As shown in Table 2, the computational online cost is decreased significantly as compared to the full-order model and the NLROM using the full set of NSCs.

5.1.2. Cantilever beam

The first three out-of-plane bending modes and the associated modal derivatives for the cantilever model are shown in Fig. 10. As shown, the modal derivatives are non-bending modes. Furthermore, the superposition of the bending modes and the statically condensed response of the modal derivatives indicate that the nonlinear response due to out-of-plane loading result in considerable in-plane displacements (i.e, in contrast to the clamped–clamped system).

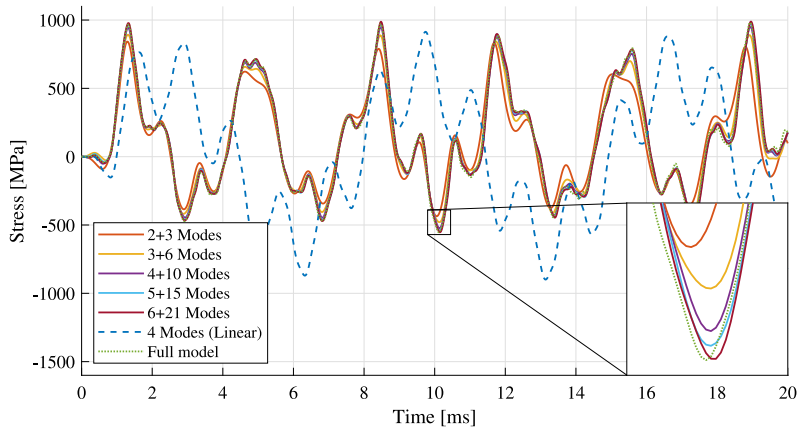

Fig. 8. Comparison of the horizontal Cauchy stress component in the element marked with purple color in Fig. 4 for the clamped–clamped full-order model and NLROMs established using various reduction bases. (For interpretation of the references to color in this figure legend, the reader is referred to the web version of this article.)

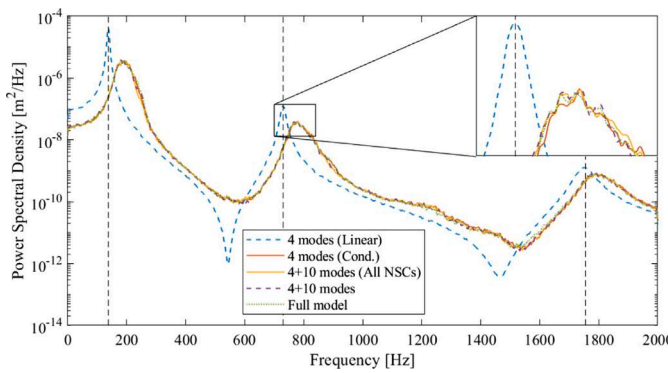

Fig. 9. Power spectral density of vertical displacement at the load DOF for the clamped–clamped beam given by the full-order model, linear ROM, NLROM considering all NSCs, and NLROMs with/without inertia effects for the in-plane modes (cf. Section 4). The black dashed lines mark the first three eigenfrequencies of the linearized system.

The vertical displacement at the load DOF are shown in Fig. 11, for the full-order model and NLROMs established using various reduction bases. As shown, the displacements are fairly close if including two bending modes and the associated modal derivatives (i.e. 2+3 modes). However, the response provided by the condensed NLROMs deviates from the full model. As indicated by the modal derivatives, shown in Fig. 10, the nonlinear response is characterized by a significant in-plane motion. However, the in-plane inertia is ignored in the condensed NLROMs, and, consequently, the systems oscillates at slightly higher frequencies. For this specific case, the displacements given by the linearized model are in fact more accurate than the condensed NLROMs.

Fig. 12 shows the horizontal displacement at the load DOF for the cantilever beam model given by a NLROM based on two bending modes and the associated modal derivatives (Fig. 12a), and a condensed NLROM based on to two bending modes (Fig. 12b). The response is fairly accurate, and adding additional basis vectors does not provide a notably increase of accuracy. However, as mentioned previously, the condensed NLROM ignores the in-plane inertia, which result in a periodicity error.

The horizontal Cauchy stress at the top of the left support (i.e. in the element marked with purple color in Fig. 4) are shown in Fig. 13 for the full-order model and NLROMs developed using reduction basis of various sizes. As shown in the Figure, a reasonable accuracy is obtained if including two bending modes and the associated modal derivatives. In contrast to the clamped–clamped beam, the stress oscillates between max/min values with approximately the same magnitudes, which is expected since the beam normal force is zero. Furthermore, it is notable that the linearized system provide a fairly accurate response.

The cantilever beam was evaluated for a random excitation with a standard deviation of 200 N. The PSD for the vertical displacement at the load DOF is shown for various models in Fig. 14. The NLROMs considering in-plane inertia effects are in good agreement with the full-order model. However, the displacement PSD clearly indicate that the condensed NLROM overestimates the resonant frequencies, thus, in accordance with the results obtained from the impulse analysis. As shown in Table 2, the computational online cost is decreased significantly as compared to the full-order model and the NLROM using the full set of NSCs.

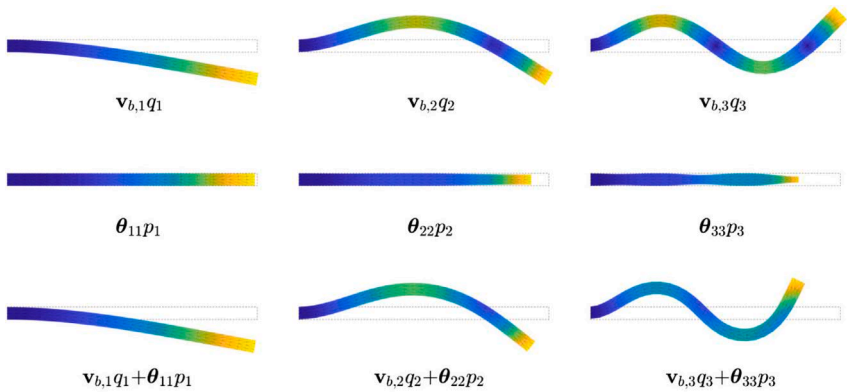

Fig. 10. First three linear modes and the associated modal derivatives θ_{ii} $(i = 1, 2, 3)$ for the cantilever beam model. The amplitude of the modal derivatives are $p_i = -q_i^2/2$. Note that, for brevity, modal derivatives with different indices $(\theta_{ij},\ i \neq j)$ are not included in the figure.

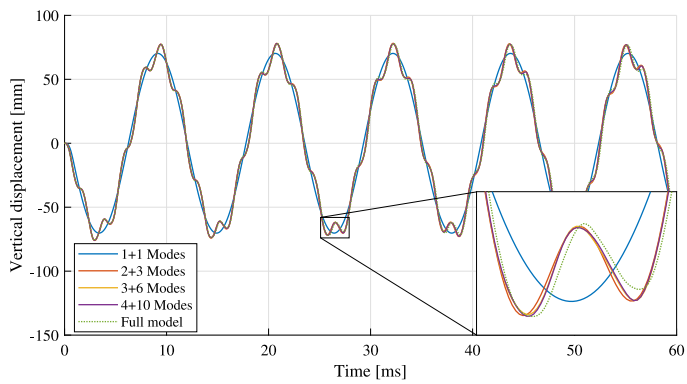

(a)

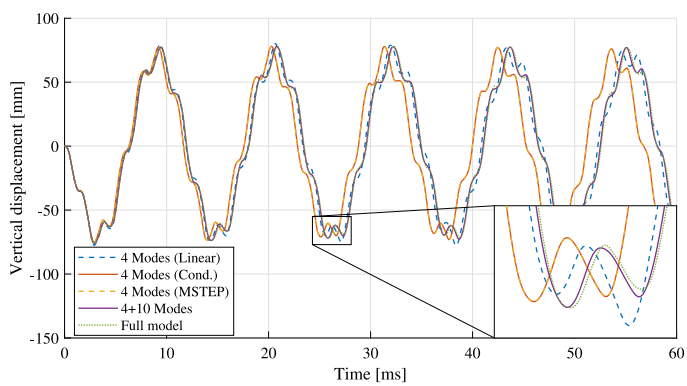

(b)

Fig. 11. Comparison of the vertical displacement at the load DOF for the full-order cantilever model and NLROMs using various reduction basis sizes (a), and a linear ROM and NLROMs with/without inertia effects for the in-plane modes (b). The NLROMs were established using the methodology described in Section 4. The condensed NLROMs were established using both the MSTEP method [19] and the approach described in Section 4—as expected, these methods provide almost identical results.

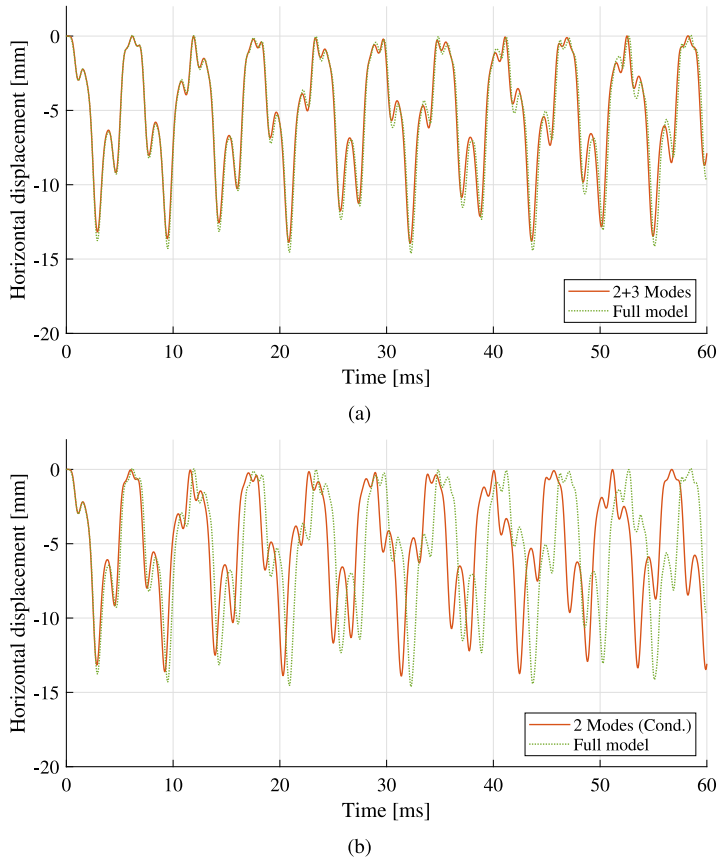

Fig. 12. Horizontal displacement at the load DOF for the cantilever beam model provided by a NLROM based on two bending modes and the associated modal derivatives (a), and a condensed NLROM based on to two bending modes (b).

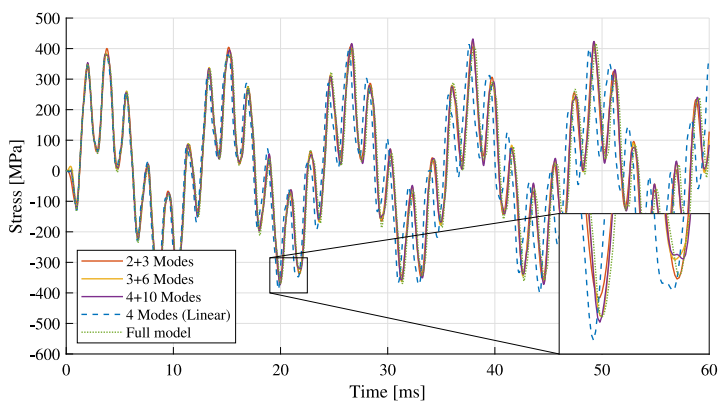

Fig. 13. Comparison of the horizontal Cauchy stress component at the top of the left support (i.e. in the element marked with purple color in Fig. 4) for the full-order cantilever model and NLROMs established using various reduction bases. (For interpretation of the references to color in this figure legend, the reader is referred to the web version of this article.)

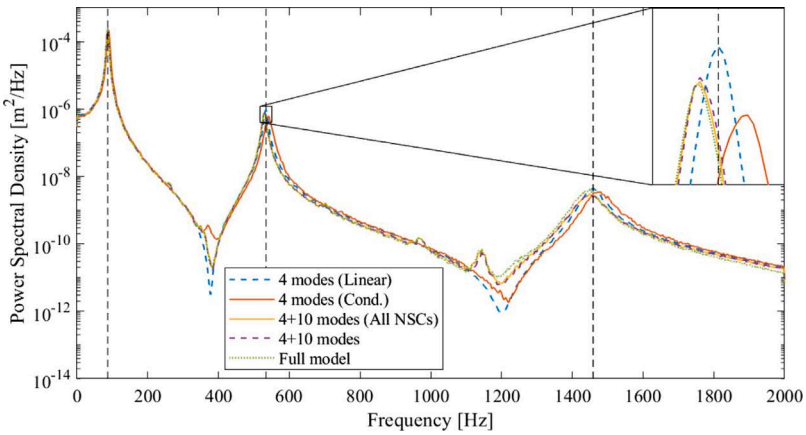

Fig. 14. Power spectral density of vertical displacement at the load DOF for the cantilever beam given by the full-order model, linear ROM, NLROM considering all NSCs, and NLROMs with/without inertia effects for the in-plane modes (cf. Section 4). The black dashed lines mark the first three eigenfrequencies of the linearized system.

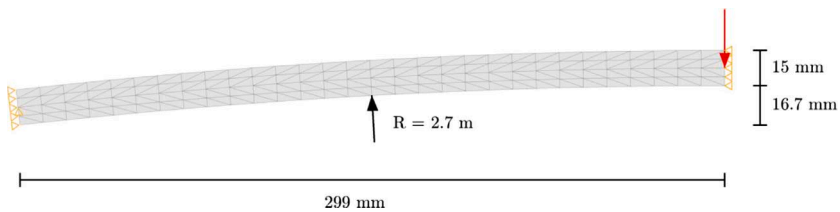

Fig. 15. Element mesh for curved solid 2D beam model. The position of the external point load is indicated by the red arrow.

5.1.3. Curved beam

The first three normal modes and the associated orthogonalized modal derivatives (cf. Section 4.3) for the curved beam model are shown in Fig. 16. The curved beam was evaluated for a random excitation with a standard deviation of 300 N. The PSD for the vertical displacement at the load DOF is shown for various models in Fig. 17. As shown, the NLROMs developed using the procedure described in Section 4, with/without in-plane inertia, provide a response close to the full order model as well as the NLROM using the full set of NSCs. Similar to the other beam models, the computational online cost is decreased significantly as compared to the full-order model as well as the NLROM using the full set of NSCs (cf. Table 2).

5.2. Continuously supported shell model

A four-sided, simply supported panel structure was studied (see Fig. 18). An FE model was established using four-node linear shell elements, denoted S4R in Abaqus. The panel height and width were 800 mm and 1000 mm, respectively, and the panel thickness was 8 mm. Further, the density was 2500 kg/m^3, the Young's modulus was 72 GPa, and Poisson's ratio was 0.23. This approximately correspond to the material properties of both glass and aluminum. Thus, the model can be representative for panel structures consisting of either of these materials. A small stiffness-proportional damping was prescribed, such that $\mathbf{C} = 5 \cdot 10^{-5}\mathbf{K}$. Hence, the damping is amplitude-dependent. The element mesh is shown in Fig. 18. The full-order models were analyzed in Abaqus. In addition, Abaqus was employed for generating the system matrices needed for generating the NLROMs, and for solving the static load cases in the NSC identification processes.

An out-of-plane reduction basis was generated by means of the Krylov-subspace approach, using a start vector corresponding to the static displacement of a uniform pressure (cf. Eq. (22)). The Krylov-subspace was generated using the modified Gram–Schmidt orthogonalization procedure—seven iterations were used, such that a total of eight basis vectors were obtained. Then, after the basis was orthonormalized according to Eq. (23), the first four modes, as shown in Fig. 19, were used in the reduction basis. Recall that the Krylov-subspace technique automatically excludes redundant modes that cannot be (explicitly) excited by the external pressure. Accordingly, any membrane modes or anti-symmetric bending modes, which cannot be excited by a uniform pressure, have been automatically excluded.

The panel structure was analyzed for two cases, where the in-plane displacement boundary conditions along the supports were free and fixed, respectively (see Fig. 18). As demonstrated in Fig. 21, both configurations result in models being geometrically

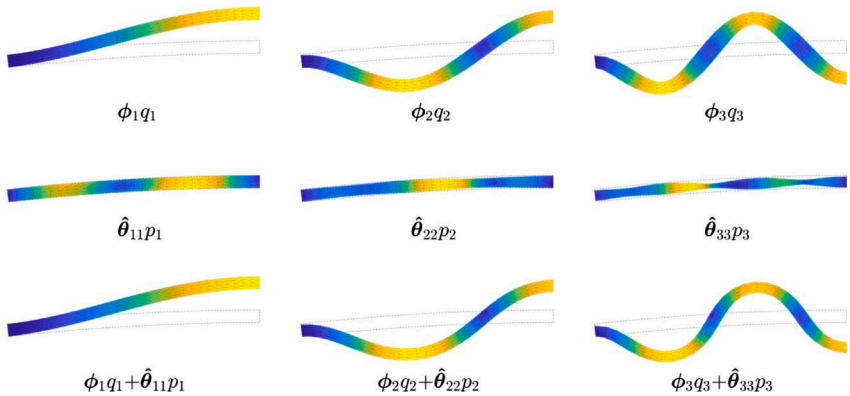

Fig. 16. First three normal modes and the associated orthogonalized modal derivatives $\hat{\theta}_{ii}$ $(i = 1, 2, 3)$ for the curved beam model. The amplitude of the modal derivatives are $p_i = -q_i^2/2$. Note that, for brevity, modal derivatives with different indices $(\theta_{ij},\ i \neq j)$ are not included in the figure.

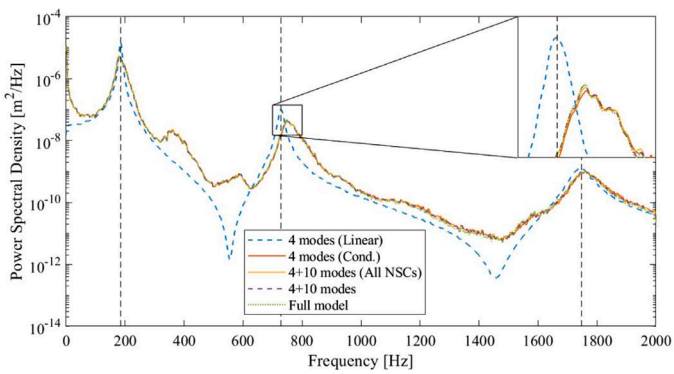

Fig. 17. Power spectral density of vertical displacement at the load DOF for the curved beam given by the full-order model, linear ROM, NLROM considering all NSCs, and NLROMs with/without inertia effects for the in-plane modes (cf. Section 4). The black dashed lines mark the first three eigenfrequencies of the linearized system.

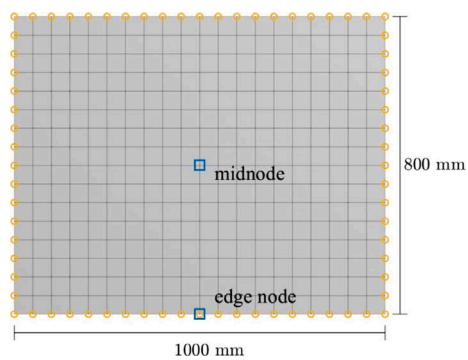

Fig. 18. Finite element mesh and output points (marked with blue squares), positioned at the center of the panel and at the midpoint of the bottom edge. Further, the displacement boundary nodes are marked with orange circles.

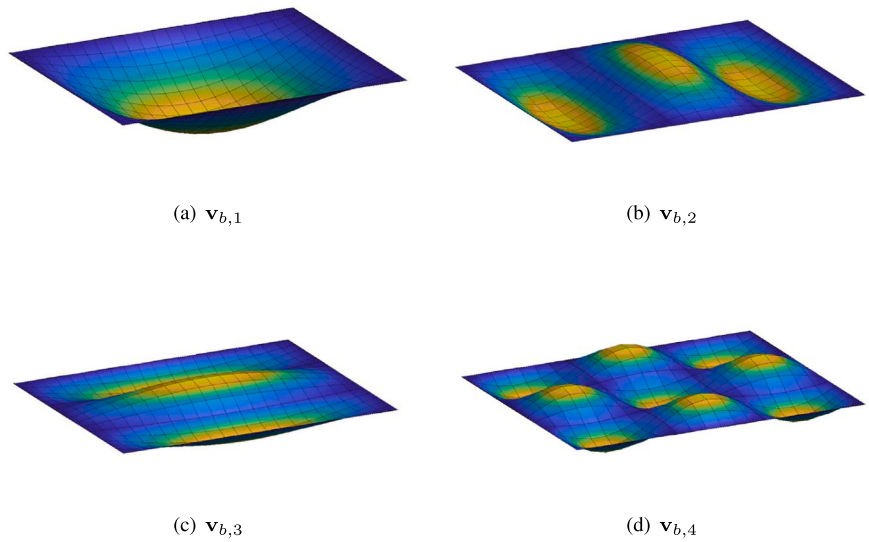

(a) $\mathbf{v}_{b,1}$ (b) $\mathbf{v}_{b,2}$

(c) $\mathbf{v}_{b,3}$ (d) $\mathbf{v}_{b,4}$

Fig. 19. First four bending modes generated using a Krylov-subspace approach, with a start vector corresponding to the static displacement due to a uniform pressure (cf. Section 3.1.2).

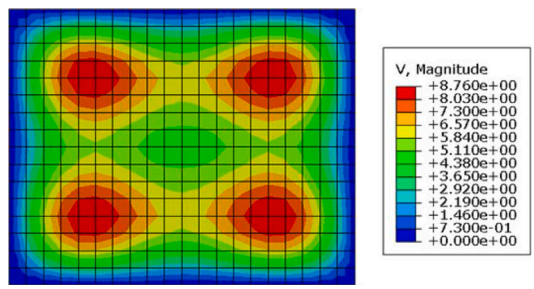

Fig. 20. Contour plot showing the initial velocity prescribed in Abaqus.

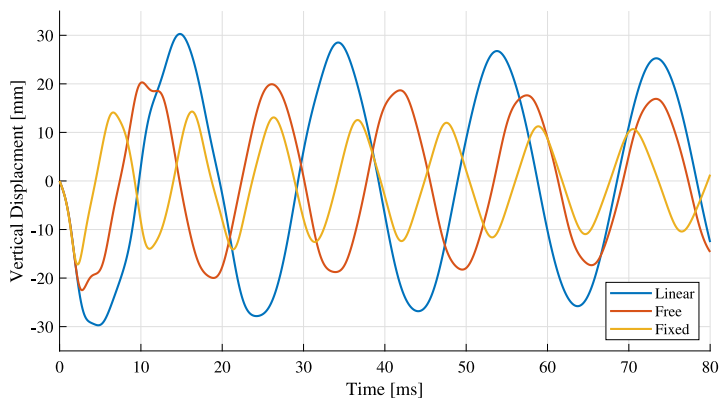

Fig. 21. Comparison of midpoint vertical displacement provided by the Abaqus model, for geometrically linear and nonlinear analyses, respectively. The nonlinear models are analyzed with free and fixed in-plane displacements along supports. Note that the in-plane displacement boundary conditions do not affect the linearized response.

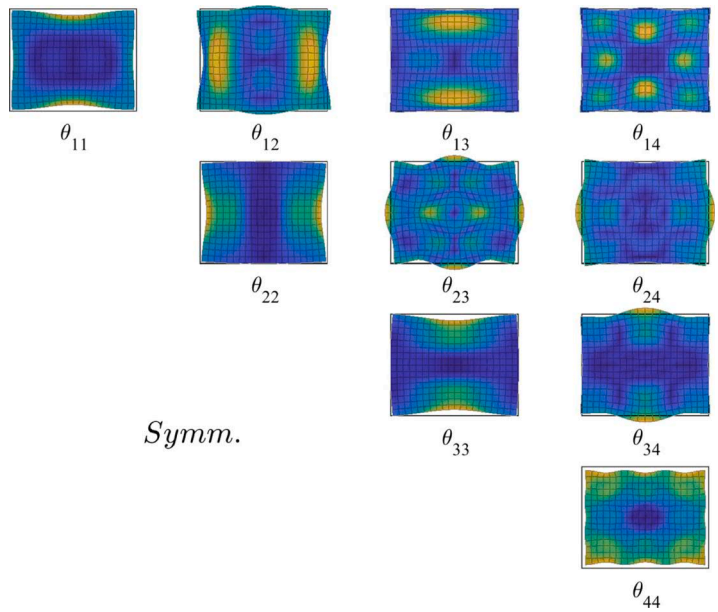

Fig. 22. Modal derivatives associated to the first four bending modes, computed with free in-plane displacements along supports. The contour plot colors correspond to displacement magnitude. (For interpretation of the references to color in this figure, the reader is referred to the web version of this article.).

nonlinear. Furthermore, the membrane bases were generated using the full set of modal derivatives associated to the linear modes. Note that the out-of-plane linear modes are not affected by the boundary conditions in the in-plane direction, thus, the same set of linear modes were used in both cases. However, the modal derivatives, which are in-plane modes, differ significantly (as demonstrated in Sections 5.2.1 and 5.2.2).

To evaluate the NLROMs, a uniformly distributed initial velocity was prescribed in the out-of-plane direction. Hence, the external forcing consist of a uniform impulse pressure with zero duration. Thus, free-vibration is studied. Furthermore, to make sure that the same load is applied in the NLROMs and the full-order Abaqus analyses, and thereby simplify the evaluation, the initial velocity field was projected onto the reduction basis, such that only the first four bending modes were explicitly excited in the initial phase. However, due to that the models are nonlinear, the modal responses are not decoupled (i.e., in contrast to linear models) and higher order modes can therefore be implicitly excited. The initial velocity field prescribed in the analyses is shown in Fig. 20.

5.2.1. Free in-plane displacements at supports

The modal derivatives for the model with free in-plane displacements along the supports are shown in Fig. 22. These were computed based on the linear modes (cf. Fig. 19), using the procedure described in Section 3.2. NLROMs were developed using the methodology in Section 4. Hence, the simplified system equations for flat structures were adopted (cf. Section 2.1). The cubic stiffness coefficient associated to bending coordinates were generated using the ED method, whereas the quadratic coupling coefficients were computed based on the modal derivatives (i.e., using the procedure proposed in Section 4.1). Moreover, a statically condensed model was developed, such that only the quasi-static response of the in-plane coordinates were considered. Here, the NSCs were generated by applying the ED method on the out-of-plane DOFs, while the in-plane DOFs were allowed to move freely, i.e., by using the approach described in Section 2.3.3. In addition, a NLROM was developed using the decondensation technique described in Section 2.3.4.

The vertical and horizontal displacements at the panel midpoint and bottom edge (cf. Fig. 18) for the NLROMs and the full-order Abaqus analysis are shown in Fig. 23. The displacements provided by the NLROMs are in good agreement with the displacements given by the full-order Abaqus analysis. Furthermore, the result from the statically condensed NLROM indicates that the influence of the in-plane inertia is small. Thus, it is sufficient to consider the quasi-static response of the in-plane modes. Moreover, the response provided by the condensed and the decondensed NLROMs are almost identical. Thus, the discrepancy between the NLROMs may be due to numerical round-off errors, which can be expected to be less pronounced for NLROMs that uses the condensed NSCs (as discussed in Section 2.3.4).

To allow for a more detailed comparison of the results, the vertical displacements were decomposed into the respective modal contributions. The decomposed displacements from the full-order Abaqus analyses were obtain from the physical displacement fields, using the expression:

$$\hat{\mathbf{u}}_{i,\mathrm{FE}} = \mathbf{v}_{b,i}\mathbf{v}_{b,i}^{\mathrm{T}}\mathbf{M}\mathbf{u}_{\mathrm{FE}} \tag{63}$$

where $\mathbf{u}_{\mathrm{FE}}$ is the displacement field given by Abaqus, and $\hat{\mathbf{u}}_{i,\mathrm{FE}}$ is the corresponding displacements projected onto $\mathbf{v}_{b,i}$.

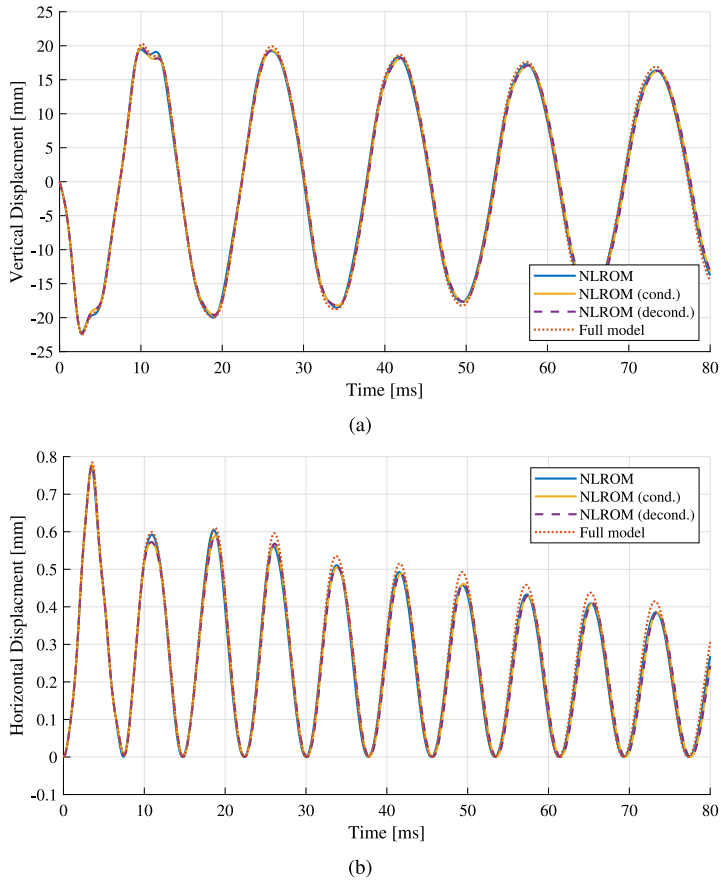

Fig. 23. Vertical displacement at midspan (a) and horizontal displacement at bottom edge (b) (see Fig. 18) for shell model with free in-plane displacements at the supports, provided by the full-order Abaqus model, and NLROMs established using a condensed, decondensed, and standard approach, respectively.

The decomposed responses are shown in Figs. 24 and 25, respectively. The results are in fairly good agreement. However, there are some discrepancies. In particular, the vertical displacements provided by the decondensed NLROM (which is very close to the results from the condensed NLROM) is closer to the full-order model. Thus, the results indicate that the decondensation technique can be used for mitigating the influence of numerical round-off errors.

5.2.2. Fixed in-plane displacements at supports

The modal derivatives for the model with fixed in-plane displacements along the supports are shown in Fig. 26. The midpoint vertical displacement for the NLROM and the full-order Abaqus analysis are shown in Fig. 27. Further, the decomposed displacements are shown in Fig. 28. As shown, the results from the NLROM correspond fairly well to the response provided by the full model. However, the discrepancies are larger than for the case where the in-plane displacements at the supports were allowed to move freely. Furthermore, the condensed and decondensed NLROMs provide almost identical results as the NLROM generated using the methodology in Section 4.1 (accordingly, these results are not included in the figures). One of the reasons for the deviations can possibly be due to a larger influence of the amplitude-dependent, stiffness-proportional damping. The panel structure having fixed in-plane boundaries are clearly stiffer than the corresponding model where the in-plane DOFs are allowed to move freely. Consequently, the amplitude dependency of the damping can be more pronounced, and, thus, the response can be more sensitive with respect to the specific implementation of the damping. In particular, the Abaqus manual does not provide sufficient information to ensure that our implementation is identical to the one used in Abaqus. However, by varying the damping level, it was indeed concluded that it had a fairly significant influence on the response magnitude and frequency.

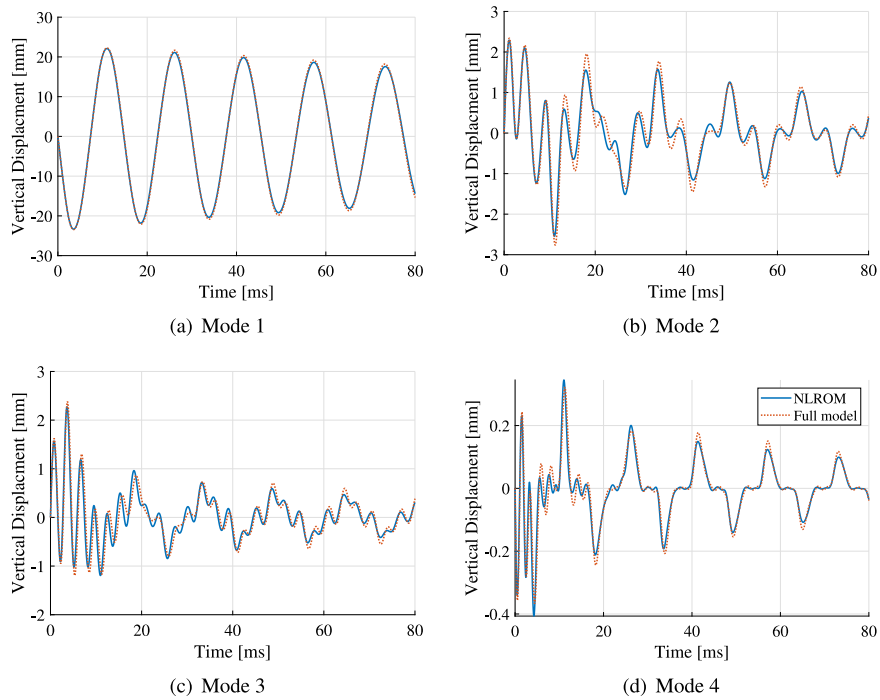

Fig. 24. Vertical displacement at midspan decomposed into the contributions from each bending mode for shell model with free in-plane displacements at the supports.

6. Discussion

The non-intrusive reduced order modeling techniques can be used effectively for developing NLROMs. However, with respect to computational efficiency, a bottleneck in the non-intrusive methods is typically the offline cost; in particular, the computational effort for identifying the NSCs. In this work, strategies were developed for reducing the offline cost of NLROMs applied to flat structures, as described in Section 4, and exemplified in Section 5. Furthermore, we showed that the concepts extend also to slightly curved structures.

The modal derivatives associated to out-of-plane bending modes essentially provide all the information needed for generating the NSCs for the in-plane coordinates. Consequently, NLROMs can be derived, that accurately represent both the out-of-plane and in-plane displacements in a computationally efficient manner. Moreover, the bending modes were generated using a Krylov-subspace approach, that considers the spatial distribution of the external load. Using this approach, redundant bending modes, which cannot be excited by the external load are automatically excluded. This is particularly important for limiting the number of modal derivatives which scales quadratically with the number of bending modes (cf. Figs. 22 and 26).

The proposed modeling strategies were evaluated using numerical examples, analyzed using both an FE code implemented in MATLAB and the commercial software Abaqus. The NLROMs generally show good agreement with the full-order models. Furthermore, in several of the studied cases, NLROMs that uses the statically condensed response of the in-plane modes provide accurate results (see Section 5). However, to accurately predict the response of cantilever structures, the numerical studies indicate that it can be important to consider the dynamics of the in-plane modes (see Section 5.1.2). For such cases, the NSCs involving in-plane coordinates can be generated with a small additional computational effort using the procedure described in Section 4.1.

In many engineering applications, it is of interest to compute the stresses and strains of the structure, which are typically required for evaluating the response. To accurately predict these quantities, the out-of-plane as well as in-plane displacements of the full model must be recovered. Hence, even though the dynamics of the in-plane modes may be negligible, an in-plane basis is needed. For such cases, modal derivatives can be effectively used for generating the in-plane displacements. More specifically, the quasi-static amplitudes of the modal derivatives are enslaved by the associated bending coordinates and, consequently, the in-plane displacements can be computed based on the bending coordinate amplitudes (see Section 4.2). It should be noted that this procedure does not involve the quadratic coupling coefficients $\mathbf{K}^{(2)}_{mb}$ and $\mathbf{K}^{(2)}_{bm}$. Thus, the in-plane coordinates can be recovered using Eq. (58) instead of Eq. (10), which would be required for a general in-plane basis. This is particularly convenient if the condensed NSCs $\tilde{\mathbf{K}}^{(3)}_{b}$ were explicitly determined using the procedures discussed in Section 2.3.3.

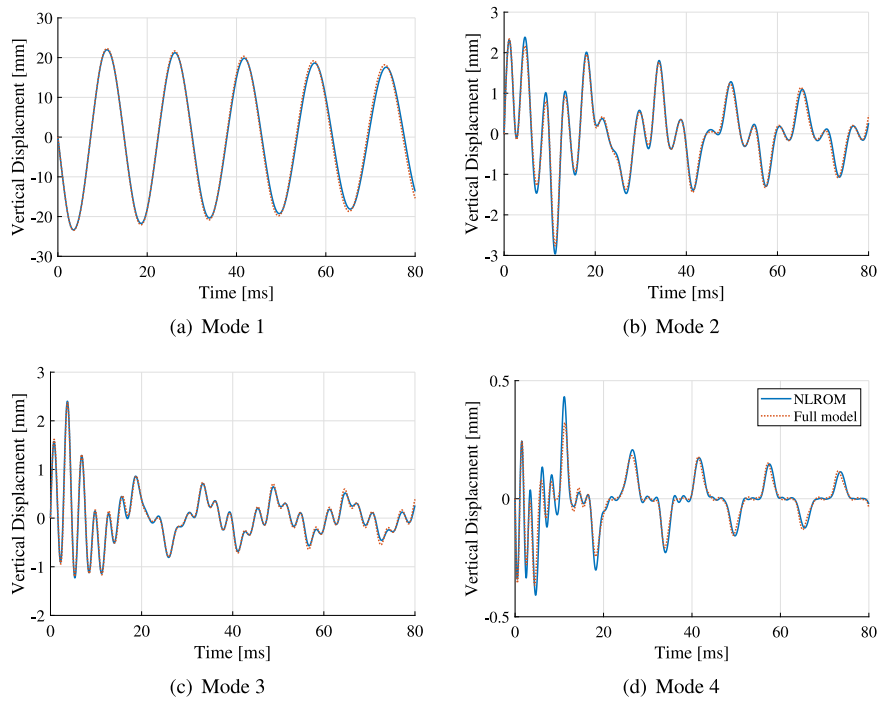

Fig. 25. Vertical displacement at midspan decomposed into the contributions from each bending mode for shell model with free in-plane displacements at the supports. The NLROM was establishing by means of the decondensation approach for mitigating the influence of numerical round-off errors, as discussed in Section 2.3.4.

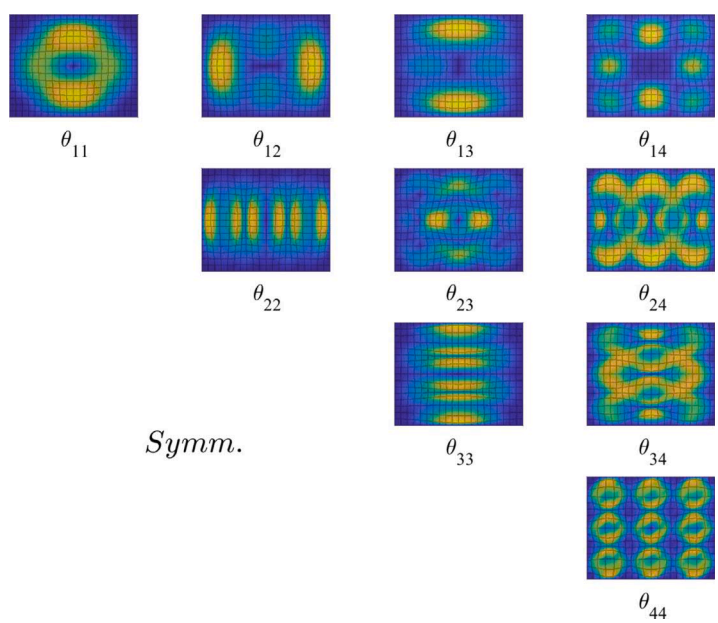

Fig. 26. Modal derivatives associated to the first four bending modes, computed with fixed in-plane displacements along supports. The contour plot colors correspond to displacement magnitude. (For interpretation of the references to color in this figure, the reader is referred to the web version of this article.).

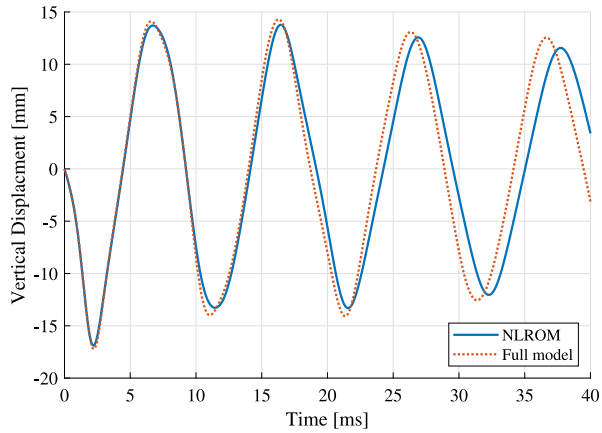

Fig. 27. Vertical displacement at midspan provided by the full-order Abaqus model and the NLROM for shell model with fixed in-plane displacements at the supports.

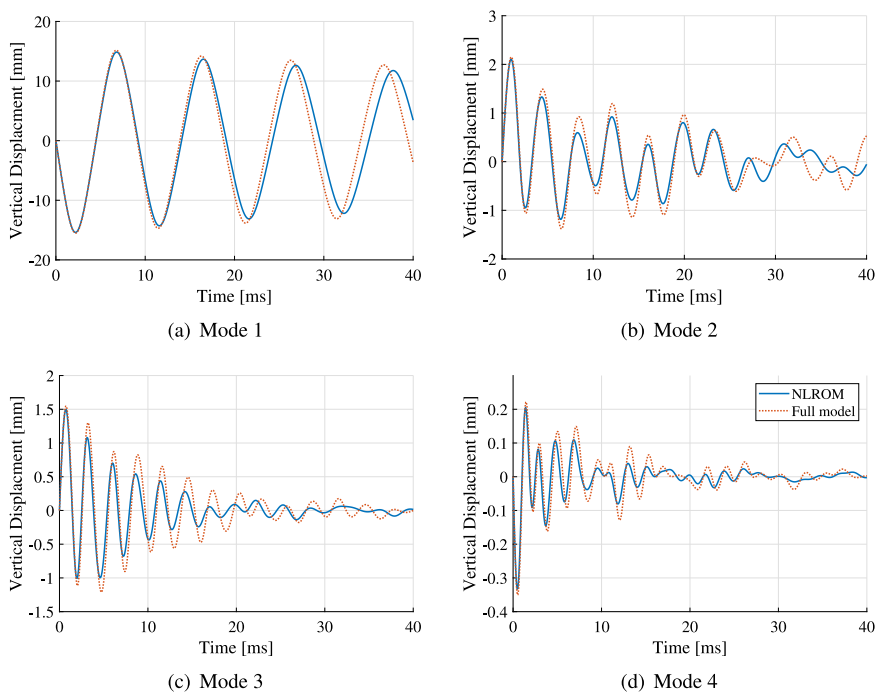

Fig. 28. Vertical displacement at midspan decomposed into the contributions from the bending modes for shell model with fixed in-plane displacements at the supports.

The influence of numerical round-off errors can be a significant problem when developing NLROMs using non-intrusive methods, affecting both the convergence and accuracy (cf. Section 2.3.4). To approach this problem, we investigated the decondensation method proposed by Wang et al. [18], which was originally developed and demonstrated using dual modes. The numerical investigations presented in Section 5.2.1 indicate that the accuracy can be increased using this approach for NLROMs established using modal derivatives. Furthermore, the technique can be combined with the M-STEP method [19] to allow for decondensation of solid models which are symmetric along the thickness. However, the computational offline cost can, in general, be expected to be larger due to that the solutions of several full-order nonlinear static analyses are required. Moreover, it was found that the

influence of numerical round-off errors were significantly larger for the FE models generated using Abaqus, as compared to the models implemented in MATLAB; thus, the decondensation technique was only applied to the Abaqus models.

The efficiency of the proposed method (cf. Section 4) can be compared to the ICE method (cf. Section 3.4) by evaluating the number of static solutions needed in the NSC identification process, which is strongly related to the computational offline cost. Using the ICE method, the number of static problems to be solved is $2N_b + 2N_b(N_b-1) + 4N_b(N_b-1)(N_b-2)/3$ (recall that N_b and N_m are the number of bending and membrane modes, respectively, whereas $N = N_b + N_m$ is the total number of basis vectors). On the contrary, if using the proposed methodology, the number of static load cases is $2N_b + 3N_b(N_b-1) + N_b(N_b-1)(N_b-2)/6$ if using the ED method and $2N_b + N_b(N_b-1)/2$ if using the EED method. Hence, by using the proposed method, the number of static load cases are decreased in either case. The numerical stability of the ED method was found to be somewhat better compared to the EED method, which was also observed in [13,27]. Thus, in applications where convergence and accuracy is problematic, the ED method can be the preferred choice. Finally, it should be noted that approaches using dual modes (cf. Section 3.4) are combined with the ED or EED method in a similar manner as for approaches using modal derivatives. However, as indicated by the investigations in [13], the total offline cost, including both the basis generation and NSC identification, is generally larger if using dual modes.

7. Conclusions

In the present paper, strategies for non-intrusive reduced order modeling of geometrically nonlinear flat structures were developed. The NLROMs were established by means of out-of-plane bending modes generated using a Krylov-subspace technique [31], which automatically excludes normal modes that are not explicitly excited by the external forcing. Modal derivatives were employed for generating in-plane reduction basis vectors. The proposed modeling strategies were validated and demonstrated using numerical examples. The following conclusion can be drawn:

- The computational offline cost for generating NLROMs of flat structures can be significantly reduced by using the method proposed in Section 4. Furthermore, we demonstrate that the method can be generalized to consider curved structures.
- By adopting the simplified form of the equation of motion, the modal derivatives provide all the information needed for generating the quadratic coupling coefficients required for considering the dynamic response of the non-bending coordinates.
- The number of linear modes can be effectively reduced by using a Krylov-subspace approach that considers the spatial distribution of the external load. It follows that the number of modal derivatives, which scales quadratically with the number of linear modes, is also significantly reduced.
- The developed NLROMs generally showed good agreement with the full-order models. Furthermore, in several of the studied load cases a reasonable approximation was obtained by condensed NLROMs, considering only the quasi-static response of the in-plane modes. However, for cantilever structures, the numerical investigations indicate that the in-plane inertia can have a significant influence on the response.
- Although the condensed NLROMs are expressed solely in terms of out-of-plane coordinates, an appropriate in-plane basis is still required for recovering the physical displacements of the full-order model. In particular, this is needed for computing stresses and strains, typically required in engineering applications for evaluating the response. In this context, an approach using modal derivatives turns out to be particularly useful because their quasi-static responses are enslaved by the amplitudes of the associated linear modes. Thus, the amplitudes of the modal derivatives are not involved in the reduced-order dynamic analysis and can, therefore, be computed in a post-processing procedure. In particular, the amplitude of the modal derivatives can be generated without knowledge of the quadratic coupling coefficients, i.e. by using Eq. (58) instead of Eq. (10).
- The numerical investigations suggest that the influence of numerical round-off errors for NLROMs developed using modal derivatives can be mitigated by use of the decondensation technique, proposed in [18]. However, the approach may result in a larger computational offline cost, because several full nonlinear static problems must be solved in the NSC identification process.

Declaration of competing interest

The authors declare that they have no known competing financial interests or personal relationships that could have appeared to influence the work reported in this paper.

Data availability

Data will be made available on request.

Acknowledgments

Financial support from the RecoNcile project, a part of the EU program Interreg IVA, and the Swedish glass associations: Glasbranschföreningen, Svensk Planglasförening and Balkongföreningen i Norden are gratefully acknowledged.

References

[1] K.J. Bathe, Finite Element Procedures, Klaus-Jurgen Bathe, 2006.
[2] M. Géradin, D.J. Rixen, Mechanical Vibrations: Theory and Application to Structural Dynamics, John Wiley & Sons, 2014.
[3] A.A. Muravyov, S.A. Rizzi, Determination of nonlinear stiffness with application to random vibration of geometrically nonlinear structures, Comput. Struct. 81 (15) (2003) 1513–1523.
[4] M.I. McEwan, J.R. Wright, J.E. Cooper, A.Y.T. Leung, A combined modal/finite element analysis technique for the dynamic response of a non-linear beam to harmonic excitation, J. Sound Vib. 243 (4) (2001) 601–624.
[5] J.J. Hollkamp, R.W. Gordon, S.M. Spottswood, Nonlinear modal models for sonic fatigue response prediction: a comparison of methods, J. Sound Vib. 284 (3–5) (2005) 1145–1163.
[6] J. Barbič, D.L. James, Real-time subspace integration for St. Venant–Kirchhoff deformable models, ACM Trans. Graph. 24 (3) (2005) 982–990.
[7] J.J. Hollkamp, R.W. Gordon, Reduced-order models for nonlinear response prediction: Implicit condensation and expansion, J. Sound Vib. 318 (4–5) (2008) 1139–1153.
[8] R.W. Gordon, J.J. Hollkamp, Reduced-Order Models for Acoustic Response Prediction, AFRL-RB-WP-TR-2011-3040, Air Force Research Laboratory, Dayton, OH, 2011.
[9] K. Kim, V. Khanna, X.Q. Wang, M. Mignolet, Nonlinear reduced order modeling of flat cantilevered structures, in: 50th AIAA/ASME/ASCE/AHS/ASC Structures, Structural Dynamics, and Materials Conference 17th AIAA/ASME/AHS Adaptive Structures Conference 11th AIAA No. 2009.
[10] S. Jain, P. Tiso, J.B. Rutzmoser, D.J. Rixen, A quadratic manifold for model order reduction of nonlinear structural dynamics, Comput. Struct. 188 (2017) 80–94.
[11] J.B. Rutzmoser, D.J. Rixen, P. Tiso, S. Jain, Generalization of quadratic manifolds for reduced order modeling of nonlinear structural dynamics, Comput. Struct. 192 (2017) 196–209.
[12] M.K. Mahdiabadi, A. Bartl, D. Xu, P. Tiso, D.J. Rixen, An augmented free-interface-based modal substructuring for nonlinear structural dynamics including interface reduction, J. Sound Vib. 462 (2019) 114915.
[13] M.K. Mahdiabadi, P. Tiso, A. Brandt, D.J. Rixen, A non-intrusive model-order reduction of geometrically nonlinear structural dynamics using modal derivatives, Mech. Syst. Signal Process. 147 (2021) 107126.
[14] R.R. Craig Jr, A.J. Kurdila, Fundamentals of Structural Dynamics, John Wiley & Sons, 2006.
[15] A.K. Chopra, Dynamics of Structures. Theory and Applications to Earthquake Engineering, fifth ed., Prentice Hall, NJ, 2016.
[16] J.B. Rutzmoser, Model Order Reduction for Nonlinear Structural Dynamics, Diss. Technische Universität München, 2018.
[17] K. Kim, A.G. Radu, X.Q. Wang, M.P. Mignolet, Nonlinear reduced order modeling of isotropic and functionally graded plates, Int. J. Non-Linear Mech. 49 (2013) 100–110.
[18] X.Q. Wang, V. Khanna, K. Kim, M.P. Mignolet, Nonlinear reduced-order modeling of flat cantilevered structures: Identification challenges and remedies, J. Aerosp. Eng. 34 (6) (2021) 04021085.
[19] A. Vizzaccaro, A. Givois, P. Longobardi, Y. Shen, J.F. Deü, L. Salles, C. Touzé, O. Thomas, Non-intrusive reduced order modelling for the dynamics of geometrically nonlinear flat structures using three-dimensional finite elements, Comput. Mech. 66 (6) (2020) 1293–1319.
[20] L. Wu, P. Tiso, Nonlinear model order reduction for flexible multibody dynamics: a modal derivatives approach, Multibody Syst. Dyn. 36 (2016) 405–425.
[21] L. Wu, P. Tiso, K. Tatsis, E. Chatzi, F. van Keulen, A modal derivatives enhanced Rubin substructuring method for geometrically nonlinear multibody systems, Multibody Syst. Dyn. 45 (2019) 57–85.
[22] O. Weeger, U. Wever, B. Simeon, On the use of modal derivatives for nonlinear model order reduction, Internat. J. Numer. Methods Engrg. 108 (13) (2016) 1579–1602.
[23] S. Jain, P Tiso, Simulation-free hyper-reduction for geometrically nonlinear structural dynamics: a quadratic manifold lifting approach, J. Comput. Nonlinear Dyn. 13 (7) (2018).
[24] H.S. Choi, J. An, S. Han, J.G. Kim, J.Y. Jung, J. Choi, G. Orzechowski, A. Mikkola, J.H. Choi, Data-driven simulation for general-purpose multibody dynamics using Deep Neural Networks, Multibody Syst. Dyn. 51 (4) (2021) 419–454.
[25] M.P. Mignolet, C. Soize, Stochastic reduced order models for uncertain geometrically nonlinear dynamical systems, Comput. Methods Appl. Mech. Engrg. 197 (45–48) (2008) 3951–3963.
[26] R. Perez, Multiscale Reduced Order Models for the Geometrically Nonlinear Response of Complex Structures (Ph.D. thesis), Arizona State University, 2012.
[27] R. Perez, X. Q. Wang, M.P. Mignolet, Nonintrusive structural dynamic reduced order modeling for large deformations: enhancements for complex structures, J. Comput. Nonlinear Dyn. 9 (3) (2014).
[28] M.P. Mignolet, A. Przekop, S.A. Rizzi, S.M. Spottswood, A review of indirect/non-intrusive reduced order modeling of nonlinear geometric structures, J. Sound Vib. 332 (2013) 2437–2460.
[29] J. Schneider, S. Schula, Simulating soft body impact on glass structures, Proc. Inst. Civ. Eng. Struct. Build. 169 (6) (2016) 416–431.
[30] L. Andersson, M. Kozłowski, P. Persson, P.E. Austrell, K. Persson, Reduced order modeling of soft-body impact on glass panels, Eng. Struct. 256 (2022) 113988.
[31] E.L. Wilson, M.W. Yuan, J.M. Dickens, Dynamic analysis by direct superposition of Ritz vectors, Earthq. Eng. Struct. Dyn. 10 (6) (1982) 813–821.
[32] N.S. Ottosen, H. Petersson, Introduction to the Finite Element Method, Prentice Hall, 1992.
[33] L.N. Trefethen, D. Bau III, Numerical Linear Algebra, SIAM, Philadelphia, 1997.
[34] R.R. Craig Jr., A.L. Hale, Block-Krylov component synthesis method for structural model reduction, J. Guid. Control Dyn. 11 (6) (1988) 562–570.
[35] L. Andersson, Reduced Order Modeling in Structural Dynamics - Consideration of Local Nonlinearities (Licentiate Dissertation), Lund University, 2021.
[36] L. Wu, P. Tiso, F. Van Keulen, A modal derivatives enhanced Craig–Bampton method for geometrically nonlinear structural dynamics, in: Proceedings of the 27th International Conference on Noise and Vibration Engineering, 2016.
[37] S.R. Idelsohn, A. Cardona, A load-dependent basis for reduced nonlinear structural dynamics, Comput. Struct. 20 (1–3) (1985) 203–210.
[38] S.A. Rizzi, A.A. Muravyov, Comparison of nonlinear random response using equivalent linearization and numerical simulation, in: Structural Dynamics: Recent Advances, Proceedings of the 7th International Conference, Vol. 2, 2000.

Paper E

Nonlinear Reduced Order Modeling of Glass Panels Subjected to Soft-body Impact

Linus Andersson*, Peter Persson, Kent Persson
Department of Construction Sciences, Lund University, Sweden
*linus.andersson@construction.lth.se

Abstract

In the paper, we propose a nonlinear reduced order model for dynamic analysis of glass panels subjected to soft-body impact. The aim is to determine the pre-failure elastic response of the glass panel in a computationally efficient manner, while maintaining sufficient accuracy of important output quantities. The response of glass panels, having a small thickness compared to the span width, are typically characterized by bending–stretching coupling effects, which result in a geometrically nonlinear behavior. To consider these effects, a reduction basis for the glass panel was established using out-of-plane bending modes and the associated modal derivatives, which span the additional subspace needed to adequately predict the geometrically nonlinear response. The reduced nonlinear restoring forces for the glass structure were expressed as cubic polynomials in modal coordinates. Consequently, the transient dynamic response can be effectively solved using direct time integration. The impacting body was modeled using a nonlinear, viscous single-degree-of-freedom system. Furthermore, a contact model was developed, allowing for approximating the contact pressure distribution using only a few time-dependent variables. For the studied load cases, the glass panel displacements as well as the principal tensile stresses predicted by the proposed model are in good agreement with the corresponding results provided by a detailed, full order finite element model.

Keywords: glass structures, dynamic analysis, model order reduction, geometrically nonlinear, nonlinear finite element model, modal derivatives, soft-body impact